STUDIES OF AEROSOL SAMPLER PERFORMANCE CHARACTERISTICS

Final report on research carried out under CDC Research Grant No. 5 RO1 OH02984-03

prepared by

Principal Investigator: James H. Vincent, Ph.D., D.Sc.*

Co-Investigator: Gurumurthy Ramachandran, Ph.D., CIH

Research Assistant: Avula Sreenath, MS (Ph.D. candidate)

Research carried out at: Division of Environmental and Occupational Health, School of Public Health, University of Minnesota, Box 807 Mayo, 420 Delaware Street S.E., Minneapolis, MN 55455.

*Address for correspondence: Department of Environmental and Industrial Health, School of Public Health, University of Michigan, 109 S. Observatory Street, Ann Arbor, MI 48109-2029

June 1998

Table of Contents

LIST OF TABLES AND FIGURES

Tables

Figures

LIST OF PRINCIPAL ABBREVIATIONS AND TERMINOLOGY

Abbreviations

ACGIH: American Conference of Governmental Industrial Hygienists
APS: Aerodynamic particle sizer (TSI Inc., St. Paul, MN)
CEN: Comité Européen Normalisation
CMAD: Count median aerodynamic diameter
FFT: Fast Fourier transformation
IOM: Institute of Occupational Medicine (Edinburgh, Scotland, U.K.)
ISO: International Standards Organisation
MMAD: Mass median aerodynamic diameter
NBS: National Bureau of Standards
OEL: Occupational exposure limit

Glossary of terms

Aspiration efficiency: The efficiency with which particles pass through the plane of the entry orifice of an aerosol sampler

Blunt sampler: An aerosol sampler where the body of the sampler imposes finite blockage to the flow.

Calm air: The scenario where the air velocity in the freestream is sufficiently small that the main agency bringing the particles into the vicinity of the sampler is gravitational settling.

Entry penetration efficiency: The efficiency with which particles pass through the entry nozzle of an aerosol sampler and reach the part of the flow where it has no 'memory' of the flow at the inlet itself.

Freestream: The undisturbed air flow, in this case the flow upwind of the aerosol sampler.

Moving air: The scenario where the air velocity in the freestream is sufficiently great that the main agency bringing the particle into the vicinity of the aerosol sampler is convection in the freestream.

Particle aerodynamic diameter (d_{ae}): The equivalent diameter of a spherical water droplet (density 10^3 kg/m^3) which has the same falling speed in air as the particle in question.

Reynolds' number (Re): A dimensionless parameter describing the relationship between inertial and viscous forces in fluid flow and so embodying much of the intrinsic nature of the flow.

Sampling efficiency: The efficiency with which particles pass to an appropriate region (e.g., the collecting filter, sensing region or some other region of interest) of an aerosol sampler.

Stokes' number (St): A dimensionless parameter embodying the effects of particle inertia in a given flow.

Strouhal number (Str): A dimensionless parameter embodying the effects of vorted shedding in a flow.

Thin-walled probe (or thin-walled sampler): An aerosol sampler comprising a thin-cylindrical tube that imposes minimal blockage to the air flow.

AIMS OF THE RESEARCH

The aims of the research were to: (a) develop laboratory models relevant to the study of aerosol sampling in industrial hygiene; (b) conduct experiments to evaluate basic aerosol sampling performance indices and the role of physical factors such as sampler size and shape, orientation, windspeed and sampling flowrate; (c) relate the results to existing theories and develop improved models for application by users and designers of practical aerosol samplers; and (d) propose physically-based guidelines for the development of new samplers meeting the new particle size-selective, health-related criteria.

SIGNIFICANT FINDINGS

The research generated a number of significant findings:-

1. We developed a novel experimental system, utilizing a small wind tunnel and direct-reading particle counting, which was able to rapidly provide very large amounts of sampling efficiency data for a range of sampler configurations. Such a system paves the way to future aerosol sampler research not previously possible, as well as new methods for developing and testing practical sampling devices.
2. A large number of experiments were performed, producing the largest and most reliable data set ever obtained for the basic performance characteristics of aerosol samplers. These data confirmed that aerosol sampler performance is a very complex function of particle size, sampler dimensions, windspeed, sampling flowrate and sampler orientation. It will provide a rich resource for the development of future, improved models for sampler performance.
3. The results of the research were compared with theoretical models for sampling efficiency developed in previous work. The models were found to be surprisingly consistent with these latest results, strongly supporting their potential for guiding the development and testing of practical sampling devices and systems.
4. We found that the physical act of sampling airborne particles is even more complex than we had anticipated. In particular, the role of particle transport in the region very close to the sampler - where the flow outside the sampler is coupled with the flow inside it, was found to be stronger than expected, and needs to be seriously considered in any future sampler design. Nonetheless, improved models were developed which look very promising for predicting the performances of practical aerosol samplers of the type used in the occupational setting.
5. The models for sampler efficiency that have evolved through previous work, and been extended during the present work, are largely semi-empirical, derived from physical considerations of the air flow and particle transport in the vicinity of the sampler. They are relatively simple, and accessible to industrial hygienists and aerosols scientists using modest computing resources. We found that they correlated quite successfully with the experimental results obtained in this work as well as those from the earlier studies. This experience provides considerable confidence to their continued use in the future in relation to aerosol samplers under realistic workplace and other environmental conditions.
6. Experimental studies of aerosol sampling under calm air conditions were found to be more difficult. As a result, definitive results were not forthcoming. However, a range of experimental challenges were identified and tackled. The results will now provide a good starting point for future research in this previously-neglected area.
7. A number of applications of the new knowledge gained have already been identified, leading towards the design and development of new aerosol samplers and testing them under relevant conditions. Central to these applications is the concept of the scaling of aerosol sampler performance, so that results obtained in experimental systems at small scale can be related to systems at full, 'real-life' scale.

USEFULNESS OF FINDINGS

The research has been quite basic in that relatively simple, idealized aerosol sampling systems have been investigated in a laboratory wind tunnel and in a calm air test chamber. The rationale for such research was that it would lead to knowledge about the factors influencing sampler performance which could not be obtained under less constrained and controlled conditions but which could easily be extended to understanding about the performances of real aerosol sampling systems under actual workplace conditions. At the end of the research, it is clear that such a link has been made. In particular, the behavior of actual aerosol samplers of the type used routinely by industrial hygienists, and as tested under full-scale conditions in the laboratory, has been elucidated by the new knowledge gained. This has reached the point where a clear understanding of the various facets of aerosol sampler performance has been achieved, and fair predictions of performance can be made both for current and new practical devices.

The usefulness of the research is best seen in the light of: (a) the general need for a new generation of aerosol samplers with performances meeting the latest particle size-selective criteria which will underpin aerosol occupational and environmental exposure standards worldwide; (b) the specific emerging need for a new generation of miniaturized personal samplers which, together with their pumps, can be worn by segments of the population to whom the current systems are inconvenient or even unacceptable (e.g., older workers, children); and (c) the need for experimental methods by which new samplers can be tested in a manner which in not only scientifically valid and reproducible but is simple, fast and cost-effective.

The research described here has paved the way for advances on all these fronts. It is timely in view of the current strong interest in all of the above, at home and abroad, as well as the anticipated publication of the new book by the American Conference of Governmental Industrial Hygienists (ACGIH) on particle size-selective aerosol exposure assessment in workplaces and the ambient environment. The latter is expected to generate even further impetus towards exposure standards based on the new criteria.

ABSTRACT OF THE REPORT

New criteria for health-related occupational exposure assessment have recently been agreed by prominent standards-setting bodies, and these will form the basis of future occupational exposure limits (OELs) for substances occurring as aerosols. This will require new knowledge about aerosol sampler performance upon which to base new, improved testing and design methods, as well as to aid in the interpretation of past and current occupational aerosol exposure data. With this in mind, the aim of the project was to investigate the factors influencing particle transport near aerosol samplers, and to express the results in forms that will facilitate their practical application.

Experiments were carried out in a small wind tunnel using simple, idealized samplers to provide new data against which to test some of the theoretical models that have been developed and to provide the basis of new ones. Novel experimental techniques were developed that allowed the rapid accumulation of large amounts of data, employing a direct-reading particle sizer/counter (the APS) and on-line computer control and data analysis. Experiments were carried out with cylindrical thin-walled probes and blunt samplers of simple shape (spherical and rectangular), and sampling efficiency was measured as a function of particle size, windspeed, sampling flowrate, sampler dimensions and geometry, and sampler orientation. The experiments were performed mostly under moving air conditions, but a small number of experiments were carried out in calm air.

A very large data set was obtained, revealing for the first time - and in a highly reproducible fashion - the complicated nature of the process of aerosol sampling. For moving air, the results drew attention to the need to account for the losses that occur as a direct result of the coupling between the external and internal air flows close to the sampler inlet. But, that notwithstanding, they showed that relatively simple models for aspiration efficiency generally provide a good first estimate of what might be expected for practical aerosol samplers. Such models are physically based but with coefficients obtained by fitting against experimental data. So they are at best semi-empirical. But they have the advantage that they are very accessible to industrial hygienists and aerosol scientists and require relatively modest computing resources. They have already been used in the preliminary development of scaling laws upon which new, small-scale, rapid and cost-effective aerosol sampler testing methods can be based. The demand for such methods derives from the growing interest worldwide on developing new samplers with performances consistent with the new particle size-selective criteria. Indeed, it has been learned that new research to be funded by the European Community will address such issues, based directly on the work described in this report.

Studies of aerosol sampling in calm air were less successful. But they were fruitful in that they enable identification of the requirements of experimental methods for testing under such conditions. Ironically, studies of aerosol sampling in calm air are more difficult than for moving air, both experimentally and - in some respects - theoretically. But now that the experimental challenges have been clearly identified, the path towards successful future work in this area is clear. Such work will be relevant to many indoor air situations.

1. INTRODUCTION

1.1 Introduction

Significance of the research

During the last two decades there has been great progress towards the setting of scientifically-based criteria for aerosol measurement in the workplace and elsewhere, led by the International Standards Organisation (ISO), the American Conference of Governmental Industrial Hygienists (ACGIH) and the Comité Européen Normalisation (CEN). All three bodies have moved during recent years towards international harmonization of particle size-selective criteria for health-related aerosol sampling, and these are summarized in the current ACGIH TLV booklet (ACGIH, 1998). The full background is given in the new ACGIH-sponsored book on particle size-selective sampling (Vincent, 1998). Such criteria are intended specifically as 'yardsticks' for the design of new sampling instrumentation. They focus attention firmly on the need for sampling to directly reflect the true physical nature of the human exposure. They identify firstly the *inhalability* of the human head itself, representing the efficiency, as a function of particle size, with which particles enter through the nose and/or mouth during breathing. This is the *inhalable fraction*. They then identify the *thoracic* and *respirable* fractions as **sub**fractions of that inhalable fraction. Here, the thoracic fraction describes the probability that an inhaled particle may penetrate into the lung below the larynx, and the respirable fraction the probability of penetration down to the alveolar region. Each of the three conventions is represented by a single curve describing it as a function of particle aerodynamic diameter (Vincent, 1995). It is expected that these will form the basis of future occupational exposure limits (OELs) for aerosols.

The inhalable fraction is the most relevant to the proposed research. This is mainly because it is expected that this fraction will apply to most OELs relating to so-called 'total' aerosol. In addition, the inhalable fraction is the starting point (or the 'envelope') for the other two fractions. Further, it is the most difficult to simulate in a sampling instrument since it is determined largely by physical (fluid and particle mechanical) factors outside the body of the sampler which are highly variable and largely uncontrolled.

The adoption of criteria like those described is stimulating the re-assessment of existing sampling instrumentation as well as the search for a new generation of aerosol sampling instruments with performances designed specifically to match those criteria. So far, just one personal sampler (Mark and Vincent, 1986) and one area sampler (Mark *et al.*, 1985) have been designed specifically to match the inhalability curve. Of these, only the personal sampler is currently available commercially to industrial hygienists (the so-called "*IOM sampler*", from SKC, Eighty-Four, PA). However a recent laboratory study of personal aerosol sampler performance in relation to the inhalability criterion, sponsored by the European Commission, has identified a number of other samplers that also appear to provide an adequate match (Kenny, 1995; Kenny *et al.*, 1997). This opens up the real possibility that a range of options is available to industrial hygienists for inhalable aerosol sampling.

The scientific problem

In general, the operation of aerosol samplers involves the aspiration of particle-laden air, selection of particles in the size range of health-related interest, and either collecting them onto a filter (for subsequent gravimetric or other assessment) or passing them through a sensing region (*e.g.*, for real-time assessment, optically or by some other means). The efficiency with which particles are aspirated and collected in this system depends mainly on a combination of inertial and gravitational forces. The physical fluid and particle mechanical scenario is complicated. It concerns the nature of the air flow outside a sampler which itself is aerodynamically blunt. It also involves the coupling between that air flow and the air flow inside the sampler (where the particles are ultimately collected or assessed), and the mechanics of the transport of particles in the highly distorted flow they encounter during the process of being sampled. In this scenario, both the fluid mechanics and the particle mechanics are still poorly understood. So, in relation to practical aerosol sampling (as applied for example in occupational and environmental hygiene), the performances of existing samplers cannot yet be predicted, and new samplers for collecting specific particle size fractions cannot be designed from first principles. This means, in turn, that the characterization, testing and development of aerosol samplers remains largely empirical, involving the use of facilities and procedures which are time-consuming, labor-intensive and costly.

Research like that described in this report provides important new insights into the factors that govern sampling efficiency, illuminating the path towards improved testing and development methods.

2. PREVIOUS RESEARCH

2.1 Background

The early background has been reviewed by the Principal Investigator (Vincent, 1989 and 1995). These describe how the performance of an aerosol sampler may be defined in terms of a number of indices. The primary one in the context of this project is *aspiration efficiency*, representing the effectiveness with which particles are taken from the atmosphere of interest and transferred into the body of the sampler. This may be expressed as

$$A = c_S/c_0 \qquad (2.1)$$

where c_S is the concentration of particles passing through the plane of the entry orifice and c_0 is that in the undisturbed air outside the sampler. In practice, however, overall sampler performance needs to take account additionally of other factors. These include particle rebound from external surfaces, the effects of the coupling between the air flow outside and inside the sampling orifice respectively, and particle losses between the plane of the sampler entry and the filter (or sensing zone) inside the instrument. In the body of the report that follows, the impact of these processes on the overall performance of the sampler - as distinct from just its aspiration efficiency - is discussed in detail.

Understanding of relevant performance characteristics and the factors that influence them is essential to the proper design and practical use of aerosol samplers. Most of the previous research effort has dealt with tube-shaped probes facing into the wind. Such simple devices have

been used for many years for sampling aerosols in stacks and ducts where the objective has been to obtain a 'representative' sample. Here, the ideal performance occurs when $A = 1$ for all particle sizes, and it is achieved when the velocity of air through the plane of the sampling orifice is the same as that in the undisturbed air. This is referred to as '*isokinetic sampling*'. Most of the research that has been reported has been aimed at understanding how performance is degraded when sampling is '*anisokinetic*'. In the large body of work for tube-shaped samplers in moving air (as reviewed by Vincent, 1989), theory usually assumes that the aspiration process is governed by inertial forces. That is, it depends on the ability of particles to follow the streamlines of the fluid motion, a function in turn of particle aerodynamic diameter, windspeed and sampling flowrate, sampler dimensions, and sampler orientation. Gravity has usually been neglected, except in the theories proposed by Ruping (1968) and, more recently, Grinshpun *et al.* (1993).

Two basic theoretical approaches have been taken to expressing the physics of the aerosol sampling process. The first - the so-called '*mathematical model*' – involves; (a) describing the flow in the vicinity of the sampler mathematically or numerically using the equations of fluid motion with appropriate boundary conditions; (b) computing the trajectories of particles moving in this flow field from the equations of particle motion; and (c) locating the limiting trajectories from which A can be determined. The second approach is the so-called '*impaction model*', based on considerations of changes in aerosol concentration as particles moving in a distorted airflow near a sampler inlet 'impact' into and out of regions of the flow. Such motions depend on the broad features of the flow pattern near the sampler.

Tube-shaped samplers described in the preceding paragraphs are just a limiting case of the wider family of aerodynamically '*blunt samplers*'. In a relatively small - but growing - body of work on blunt aerosol samplers, initial experiments and ideas first reported by Vincent *et al.* (1979) have been followed up by a few further basic experiments (Vincent and Mark, 1982; Vincent *et al.*, 1985; K.Y.K. Chung and Ogden, 1986). There is a much larger group of attempts to model the mechanics of blunt sampling (*e.g.*, Ingham, 1981; Vincent, 1984 and 1987; Dunnett and Ingham, 1986 and 1988, Ingham and Hildyard, 1991; I.P. Chung and Dunn-Rankin, 1992; Ingham and Wen, 1993; Erdal and Esmen, 1995). The theoretical models proposed have been of both the 'mathematical' and the 'impaction model' type, and suggest the general relation

$$A = f(St,\ U/U_S,\ \delta/D,\ \alpha,\ B) = f(St,\ \phi,\ R,\ r,\ \alpha,\ B) \qquad (2.2)$$

where $St = d_{ae}^2 \gamma^* U/18\eta\delta$, $\phi = \delta^2 U_S/D^2 U$, $R = U/U_S$ and $r = \delta/D$. In these relations, St is the Stokes' inertial parameter which embodies the main physics of the sampling process, reflecting the ability (or otherwise) of a particle to follow a diverging or converging airflow, d_{ae} the particle aerodynamic diameter, U the freestream air velocity, U_S the mean air velocity at the sampling inlet, δ the width of the sampling orifice, D the characteristic dimension of the sampler, α the sampling inlet orientation with respect to the wind, and B an aerodynamic shape factor (or 'bluntness'). In addition, γ^* is the density of water (10^3 kg/m^3) and η the viscosity of air. Physically, the quantity ϕ is the ratio of the sampled air volume to that which is geometrically incident on the sampling system. It is noted that, in Equation (1.2), neither the conditions of Reynolds' number or turbulence in the moving airstream are specified. These are discussed later.

Blunt samplers have also been investigated under so-called '*calm air*' conditions (again see Vincent, 1989). Here the only air movement in the system is that associated with the aspiration of air into the sampler; so gravity becomes the important agency in bringing particles

into the vicinity of the sampling inlet. Now the general functional form for aspiration efficiency is slightly modified from Equation (1.2), such that

$$A = f(St^*, v_S/U_S, \delta/D, \alpha, B) \quad (2.3)$$

where the new Stokes' inertial parameter (St^*) is given by $St^* = d_{ae}^2 \gamma^* v_S / 18 \eta\delta$. Here v_S is the gravitational settling velocity of particles of aerodynamic diameter d_{ae} and α is now the sampling inlet orientation with respect to the vertical. Such conditions may be relevant to some workplaces where air movements are relatively slow and particles relatively large. Indeed, whilst moving and calm air sampling have so far been treated as separate cases, it should in principle be possible to generate a general model which embodies both gravitational and inertial forces effects simultaneously. Only one attempt to develop such a model has so far been proposed, and that for thin-walled probes (Grinshpun *et al.*, 1993).

2.2 Recent research at the University of Minnesota

Extensive field studies of occupational aerosol exposures have been carried out by our group at the University of Minnesota during the past few years (*e.g.,* Tsai *et al.*, 1995a; Tsai *et al.*, 1996a and b; Werner *et al.*, 1996; Spear *et al.*, 1997; Wilsey *et al.*, 1996; and other papers). Many of these studies have been concerned with the effects of the application in aerosol standards of the new particle size-selective sampling criteria, and have involved the use of several different types of sampler. To support that effort, and to enable scientific interpretation of the results obtained using the different samplers, a body of work was conducted to extend our knowledge of how to model the aspiration efficiencies of blunt aerosol samplers. In turn, such models would be related to samplers of the type actually used in industrial hygiene practice. This was achieved by formulating physically-based models with empirical coefficients which were then estimated (using non-linear regression techniques) by reference to the experimental data that were available from previous research. Models were first generated for simple blunt samplers at large angles with respect to the wind (*i.e.*, 90° and 180° respectively) (Tsai and Vincent, 1993), taking account of R and r on the shape of the flow and particle transport near the sampling orifice, and yielding

$$A_{90} = 1 / [1 + 4 (2.21\ St) (R/r)^{1/2}]$$

and (2.4)

$$A_{180} = 1 / [1 + 4 (4.5\ St)\ \phi^{1/3}\ r^{-0.29}]$$

where R, r and ϕ are as defined earlier. These equations were subsequently incorporated into a model for the aspiration efficiency of a blunt sampler when orientation with respect to the wind (α) is averaged uniformly over the range 0° to 360° (Tsai *et al.*, 1995b). This is the situation appropriate to most industrial hygiene sampling. Firstly, it applies directly to the human head studies that led to the definition of inhalability. Secondly, it applies to some of the prototype new rotating-head omnidirectional samplers that have been developed for area sampling in the workplace and the ambient atmosphere. By correlating the orientation-averaged impaction model with data for the human head (from the mannequin studies reported by Vincent *et al.*, 1990) and for two rotating-head samplers (Mark *et al.*, 1985 and 1990), we obtained (Tsai *et al.*, 1995b)

$$A = 0.5 A_0 + [(A_{90}-A_0) / (181 R^{-2.31} r^{1.01} + 2)] + 0.5 A_{180}$$

(2.5)

for uniform averaging of A over the range $0 \leq \alpha \leq 180°$ where A_0 is calculated from the now well-established set of equations for the aspiration efficiency of a simple forwards-facing blunt sampler (Vincent, 1989) and A_{90} and A_{180} are as calculated from Equations (2.4). Equation (2.5) applies to samplers that are essentially symmetrical in terms of shape and of the location of the sampling orifice on the blunt sampler body. For personal sampling, however, the situation is more complicated still since not only is the body of the wearer asymmetric but so too is the position of the sampler on the body. We therefore extended the preceding model in order to reflect the effect of these asymmetries, and obtained (Tsai *et al.*, 1996c)

$$A = (0.4\,A_0 + 0.2\,A_{90} + 0.4\,A_{180}) - [\,0.4\,(A_0 - A_{90}) / (32\,St_0^{-0.97}\,R_0^{-0.75}\,r_0^{0.69} + 1)\,] + [\,0.1(A_0 - A_{90}) / (85\,St_0^{17.1}\,R_0^{8.53}\,r_0^{-1.12} + 1)\,] \quad (2.6)$$

where St_0, R_0 and r_0 are versions of the previously-used St, R and r adjusted to correspond to the situation when the sampling orifice is centrally located with respect to the axis of rotation.

Based on current knowledge, such models as those summarized above - although derived from physical ideas - are rather empirical. But, in the absence of other workable models, they may be useful in providing guidance about sampler performance under practical conditions, at least until improved models become available based on new research. They have the advantage (e.g., over numerical approaches developed by others) in that they can be applied using relatively modest desk-top computing resources, and so are highly accessible to occupational hygienists and aerosol scientists for applications in the practical world. As will be seen below, they have provided strong guidance to interpreting the results of the experimental study described in this report.

3. EXPERIMENTAL STUDY OF FLOW VISUALIZATION AND FLOW INSTABILITIES FOR BLUNT BODY SAMPLERS WITH SUCTION

3.1 Introduction

The study of the flow of air about bluff bodies is pertinent to many branches of science and engineering. There is an extensive literature on such flows which describes the nature of boundary layer formation and separation, vortex shedding, the role of the shape and size of the body, freestream turbulence, and many other fluid mechanical features. Much less is known about the case where the flow is accompanied by aspiration - that is, where the flow is further complicated by the removal of air by suction at one or more sinks on the surface of the body. Even so, this is a system relevant to many practical situations, including in environmental and occupational health. Aerosol sampling is just one area of particular current interest, where understanding the performance characteristics of sampling devices depends on knowledge about the nature of the airflow itself. With this in mind, we have conducted experiments aimed at further elucidating the basic nature of such flows. To achieve this, attention was focused on bluff bodies of relatively simple shape, both two and three-dimensional, containing single sampling orifices, and with orientations with respect to the freestream covering the full range from 0° to 180° (and hence 0° to 360°). Features of particular interest, and which have already been identified as helpful in describing the physics of aerosol sampling (Vincent, 1989), are the

locations of flow stagnation on the bluff body, dividing the aspirated airflow from the external flow which passes over the body. Also of interest is the nature of flow separation for such flows and, where appropriate, vortex shedding in the near wake.

3.2 Background

Cylindrical bodies

In principle, the full flow field about a bluff body with aspiration may be obtained by solving the Navier-Stokes equations. If the Reynolds number (*Re*) is high enough and the freestream turbulence is neglected, the flow outside the boundary layer on the sampler may be described to a good approximation by potential flow theory (Ingham, 1981; Ingham and Hildyard, 1991). Consider this applied to a cylindrical body of diameter D placed at right angles to the freestream, and containing a line sink along its length through which air is aspirated at the flowrate Q per unit length of cylinder. For this system, when the sink faces directly into the freestream, the tangential air velocity on the surface of the cylinder at the location identified by the angle θ from the forwards-facing is given by

$$V_\theta = 2U \sin\theta - \frac{Q}{\pi D} \cot\left(\frac{\theta}{2}\right) \tag{3.1}$$

where U is the freestream velocity. Here, the positions of stagnation on the cylinder surface (i.e., the locations on the body of the streamsurfaces separating the aspirated airflow from the external freestream) are defined by the condition $V_\theta = 0$ (Ingham, 1981). For the simplest case of uniform flow around a cylinder without aspiration ($Q = 0$), stagnation occurs at $\theta = 0°$ and 180°. When Q is increased, the stagnation position at 180° remains unchanged while that at the leading edge of the cylinder splits into two that move symmetrically away from the sink.

We now proceed to the solution for the location of stagnation points for the case where the slot is placed at an angle α with respect to forwards-facing (see Figure 3.1). The generalized equation for the positions of stagnation is now given by (Ingham and Hildyard, 1991)

$$\phi_C\, t\,(1+t^2) - 4\,t\cos\alpha - 2\,(1-t^2)\sin\alpha = 0 \tag{3.2}$$

where

$$\phi_C = \frac{Q}{\pi D U} \tag{3.3}$$

is the dimensionless aspiration flowrate (equivalent to the actual flowrate rate divided by the flowrate of air geometrically incident on the cylinder), and

$$t = \tan\left(\frac{\theta}{2}\right) \tag{3.4}$$

Equation (3.2) is cubic in t and so has three roots, indicating the existence of the three stagnation points. In Figure 3.1, S is the linear distance between the primary stagnation points P_1 and P_2, while P_0 identifies the sink at the angular location α. The calculated angular location of these

stagnation points, θ, is shown later for fixed Q (see Figure 3.6) as a function of the orientation of the sink (α) for the range up to 180°.

A boundary layer develops in the direction of the flow from a stagnation point and potential flow theory is not expected to hold beyond the position at which (for high enough Re) the flow separates. For the cylindrical geometry discussed here, it is very well known that - at least in the absence of aspiration - such separation is accompanied by boundary layer instability such that the near wake flow is characterized by strong, coherent periodic vortex shedding. The frequency of this vortex shedding (f) is usually expressed in terms of the dimensionless Strouhal number (Str), where

$$Str = \frac{f\,D}{U} \tag{3.5}$$

Roshko (1954), and many others, have shown experimentally that $Str \approx 0.21$ for a cylinder without aspiration and for Re in the range from about 400 to greater than $2\text{x}10^5$. But, to our knowledge, there has been no previous report of what happens to Str when aspiration is introduced at the surface of the body.

Spherical bodies

The three-dimensional flow at the surface of a sphere is more complicated, and needs to be characterized by the three components of velocity - the radial velocity V_r, the tangential velocity V_θ, and the azimuthal velocity V_φ. When there is aspiration from a point sink or circular orifice located on the spherical body, the positions of stagnation are defined as loci on the surface of the sphere where all these three components are identical to zero. However, the radial component of velocity on the surface of the sphere is always trivially zero, so that the stagnation zone loci can be determined by setting $V_\theta = V_\varphi = 0$. Partial solutions to this scenario have been obtained by Dunnett and Ingham (1988) by setting only $V_\theta = 0$, leading to

$$-\sin\theta\cos\alpha - \cos\theta\sin\alpha\cos\varphi + \frac{\phi_S}{3}\left[\frac{\sin\theta}{(2+2\cos\theta)^{3/2}} - \frac{1}{2\sin\theta}\left(1 - \frac{1+\cos\theta}{(2+2\cos\theta)^{1/2}}\right)\right] = 0 \tag{3.6}$$

in which the dimensionless aspiration flowrate is now

$$\phi_S = \frac{\delta^2 U_S}{D^2 U} \equiv \frac{Q}{D^2 U} \tag{3.7}$$

where δ is the orifice diameter and U_S is the sampling velocity (averaged over δ), and Q is now the actual sampling flowrate. In Equation (3.6), the angles θ and φ and the radial distance r relate to the spherical coordinate system shown in Figure 3.2, and α is the angular location of the orifice in the $\varphi = 0$ plane. From Equation (3.6), Dunnett and Ingham obtained the two 'diameters' characterizing the linear dimensions of the oblate stagnation region on the surface of the sphere enclosed by the condition of zero tangential velocity V_θ, thus

$$S_1 = D\left[\frac{\phi_S}{3\cos\alpha}\right]^{1/3} \tag{3.8}$$

$$S_2 = D\sin\left(\frac{\phi_S}{24}\frac{\left(1-\sin\frac{\alpha}{2}\right)}{\sin^2\frac{\alpha}{2}\cos\frac{\alpha}{2}} + \frac{1}{2}\sqrt{\frac{\phi_S}{3\sin\alpha}} + \frac{\alpha}{2}\right) \tag{3.9}$$

However, the true dividing line between the aspirated and external airflows (and which is relevant to our experiments described below) is the one where the additional condition $V_\varphi = 0$ is also satisfied. Since this was not taken into account by Dunnett and Ingham, only Equation (3.9) for S_2 is immediately relevant. For the specific case where $\alpha = 0°$, S_1 and S_2 are equal and an exact solution can be found from potential flow theory, thus

$$S_1 = S_2 = D\sin\left(\sqrt[3]{\frac{\phi_S}{3}}\right) \tag{3.10}$$

The near-wake vortex shedding mentioned earlier for the cylindrical body is also present for the flow about a sphere (without aspiration). However, as has been shown by Fuchs *et al.* (1979) and others, it is much less marked than for two-dimensional flows, and - for our purposes - can reasonably be neglected.

3.3 Experimental set-up for the air flow studies

Wind tunnel

Wind tunnels have been widely used for occupational hygiene-related aerosol research, where workplace atmospheres can be simulated with great precision and control. The wind tunnel used in this study was a small one, having a cross-sectional area of 0.3 m × 0.3 m at the test section. It is open-loop, with the discharge located in the same room. The test section was made of Plexiglas® and was 1.8 m in length. It is described in greater detail later in this report in Section 4. Here we discuss only those parts relevant to the aerodynamic inquiry.

Preceding the test section is a removable section that, for most of the experiments described later, holds a turbulence-generating grid. For the aerodynamic investigation of interest here, however, this grid was removed and replaced by a 'smoke wire' system (see Figure 3.3, see details below). In absence of the grid, the air flow in the test section is very stable and smooth.

Test samplers

Two test sampler models were built as the subjects of this part of the investigation. The first was a 3 cm-diameter, 25 cm-long cylinder with a 1.5 mm-wide slot. It was mounted horizontally between the walls of the tunnel, using support rods, in such a way that the sampler could be easily rotated about its axis (so allowing variation of α). End plates were deployed to reduce end and wall effects (as suggested by Cowdrey, 1962). Aspiration through the slot was maintained using a rotary vane pump with a calibrated rotameter to measure the air flowrate. With this system, the pressure drop across the slot was sufficient to ensure that the flow through the slot

was uniform along its length. The second body was a 6.35 cm-diameter sphere with a 4 mm-diameter circular orifice. This body was mounted centrally in the working section of the tunnel, using a support rod arranged such that the sphere could be rotated about its horizontal axis. The sphere was oriented such that the inlet orifice was always in the $\varphi = 0$ plane. It was necessary to provide an additional degree of freedom to allow movement of the sphere in the direction perpendicular to the walls of the tunnel. This was achieved by threading the support rod to allow the sampler to move along the axis of the rod (transversely to the tunnel), also incorporating a keyway on the support rod to prevent the entire assembly from rotating.

Flow visualization system

Smoke for flow visualization was generated using a variation of the well-known 'smoke-wire' method, employing a 0.003" (0.07 mm)-diameter stainless steel resistance wire mounted centrally and vertically at the entrance to the test section, held under tension by weights. This introduced minimal disturbance to the flow upstream of the bluff body under test. The wire was 'wetted' by dripping oil (of the type used in 'fog generators' and widely employed in flow visualization) continuously down the wire from a micro-pipette. The wire was heated by passing electric current through it, controlled by means of an auto-transformer. The generation of smoke was regulated by adjusting the current and hence the rate of evaporation of oil.

'Slit' illumination to enhance the flow visualization for the experiments with the cylindrical body was provided using a modified overhead transparency projector, where the open illuminated surface was covered by a black cardboard with a fine slit. Smoke traces were photographed using Tri-X Pan black-and-white film with a Nikon 6006 camera (with Nikon 60 mm f2.8D lens) whose settings were determined based on the results of preliminary exposures taken at various camera settings. The optimum settings were found to correspond to a shutter speed of 0.5 s with the aperture fully open (f/3.2) and an exposure compensation ranging from +1 to +3 EV.

Vortex shedding measurement system

The frequency of vortex shedding for the cylindrical body was determined using a capacitive micromanometer (Model FC014, Furness Controls Ltd., England, U.K.) to detect the pressure variations in the near wake. For this, a fine hypodermic needle was used as a probe to measure the pressure fluctuations behind the cylinder, so that minimum disturbance was created due to the physical presence of the probe itself. Several holes were drilled on the top of the tunnel so that an optimum location of the needle could be determined so that the noise to signal ratio is minimum. The probe was placed at approximately 7D from rear of the cylindrical sampler. The static pressure signal took the form of a 0-5 V analog output, which was acquired using a personal computer with an interface board (National Instruments Corp., Austin, TX, Model AT-MIO-16) driven by the software written in Lab Windows (National Instruments Corp., Austin, TX). Fast Fourier Transformation (FFT) of the collected data was performed off-line using MATLAB software (Mathworks Inc., Natick, MA), providing the full frequency spectrum. The vortex shedding frequency was studies over a wide range of Reynolds' number, sampler orientations

and sampling flowrates. The orientation of the sampling slot along the cylindrical sampler was rotated by simply rotating the sampler supports mounted on the walls of the tunnel along its axis.

3.4 Experimental procedures

Flow visualization

Measurement of stagnation points for a cylindrical body: Photographs were taken of the visualized flow around the cylinder (e.g., Figure 3.4). In the experiments, 24 photographs were obtained for each set of experimental conditions (inlet orifice orientation, freestream velocity, sampling flowrate). The negatives of these photographs were projected onto a plain white screen using a slide projector, and the streamlines were re-constructed by manually tracing the streamlines onto the screen. The locations of the positions of stagnation were thus easily identified by visually locating the point of intersection of the imaginary line drawn between the two closest streamlines that tend to move in opposite directions when they get close to the surface of the sampler. We were able to locate only two of the three stagnation points (P_1 and P_2) since the third stagnation point (P_3) was located towards the rear of the cylinder where the flow is unstable. Locating the center of the projected image of the cylindrical body was very critical in determining the precise location of the stagnation positions. To facilitate this; cross-wires were etched onto the end plates so that these appeared on the photographs at the center of the image.

Measurement of stagnation points for a spherical body: For the spherical body, the stagnation region was three-dimensional and so could not be located in exactly the same way as for the cylindrical body. So some modifications were made to the measurement technique. Firstly, in order to locate the maximum width of the stagnation region of the body of the sphere in the plane parallel to the freestream, the above technique of photographing the sheet of light to capture the two stagnation positions in the $\varphi = 0°$ plane was again applied. Secondly, however, for determination of stagnation in the plane transverse to the freestream, a direct visual observation method was applied. Here, the spherical sampler itself was moved linearly along the threaded support rod in this plane, and the position was noted at which the influence of a sink was seen to disappear. In this method, the two extremities of the stagnation region in the direction perpendicular to the freestream were identified by moving the sampler from one edge to another and noting the number of turns of the thread required to move that distance. Figure 3.5 illustrates a typical sequence of events in such a measurement. The example shown is for the orifice sampling at 90° to the freestream where, for the purpose of illustration, just one streamline is shown. The dotted lines indicate the positions of the sphere at the start and end of the measurement. It can be seen from Figure 3.5 that the sampler is gradually moved from right to left while the smoke lines from the heated wire remain at a fixed position. The influence of the orifice on the streamlines gradually decreases as the sampler moves to the left. The position where this influence ceases to occur where the streamlines are no longer deflected by the effect of the aspirating action (i.e., the streamline that just failed to be aspirated), determines the edge of the stagnation region. This procedure was repeated several times in order to obtain the mean extreme positions, and to reduce any backlash error associated with the threading. The number of turns required to travel from one edge of stagnation zone to the other was multiplied by the pitch

of the threading to calculate the linear distance moved. It should be noted that the linear distance measured in this way is, in reality, the width of the cross-section of the limiting streamsurface far upstream of the sampler (say s_1), and hence not directly the width of the stagnation region on the sampler body (S_1). For the forwards-facing case, however, Equation (3.10) yields

$$\frac{s_1}{S_1} = \frac{\sqrt{\phi_S}}{\sin\left(\frac{1}{3}\sqrt{\frac{\phi_S}{3}}\right)} \tag{3.11}$$

since $s_1 = D\sqrt{\phi_S}$ trivially. This expression was used to convert the measured s_1-values to the corresponding values for S_1, under the reasonable working assumption that the ratio s_1/S_1 remains invariant with the orientation of the sampler for a given value of ϕ_S. For $\alpha = 0°$, we know that

$$S_1 S_2 = D^2\left(\sin\left(\sqrt[3]{\frac{\phi_S}{3}}\right)\right)^2 \tag{3.12}$$

We can assume that for all other angles, Equation (3.12) has a similar form and we only need to determine the dependence on α. This means that we can relate s_1/S_1 to S_1/D as long as we assume that s_1/S_1 remains invariant. Then Equation(3.12) can be rewritten for all α as

$$S_1 S_2 = f(\alpha) D^2\left(\sin\left(\sqrt[3]{\frac{\phi_S}{3}}\right)\right)^2 \tag{3.13}$$

We can determine $f(\alpha)$ from experimental data by fitting a polynomial equation to S_1S_2/D^2. This polynomial equation turned out to be of third order in α and the resulting equation is given by

$$\frac{S_1 S_2}{D^2} = (0.61 + 0.55\alpha^2 - 0.2\alpha^3)\left(\sin\left(\sqrt[3]{\frac{\phi_S}{3}}\right)\right)^2 \tag{3.14}$$

Vortex shedding

Before any actual measurements were made, the sampling frequency and sampling time had to be determined so that the resulting frequency spectrum obtained using FFT would be reliable. The sampling frequency for each freestream velocity was chosen on the basis of Nyquist's theorem. This that states that the sampling frequency should be at least twice the frequency of the signal of interest in order to avoid 'aliasing'. With this in mind, the sampling time was chosen to be at least 30 seconds and each run was repeated five times. The five data sets were averaged and FFT was applied to the averaged data set. In some cases where the frequency spectrum was dispersed over a range of frequencies, seen most pronounced when the slot was oriented at angles greater than 90°, the software Mathematica® was used to fit a normal distribution to the dispersed primary mode. The median of this distribution was then taken as the vortex shedding frequency. The standard error in the data could also be calculated from the normal distribution.

3.5. Results and Discussion

Cylindrical bodies

Positions of stagnation: Initial experiments were performed with the slot facing the freestream (α = 0°) for ϕ_C at a very low value of 0.01. No significant changes in the locations of stagnation points were observed. This was as expected since the volume of air sampled relative to that geometrically incident on the body was very small. Results for the much higher value of ϕ_C = 0.25 are given in Figure 3.6, expressed in terms of the angular positions of stagnation. These show the forwards-facing stagnation point splitting symmetrically into two stagnation positions at about $\theta \approx \pm$ 12°. This result is quite close to the theoretical value of $\theta \approx \pm$15° predicted by the model of Ingham and Hildyard (1991).

Figure 3.6 shows what happens when α increases from zero. It is seen that the stagnation point P_1 moves around the body ahead of the slot, while the position of P_2 moves relatively slowly towards θ = 0°. The angular width of the stagnation region is therefore seen to increase sharply as α increases. For large angles with α upwards of about 140°, we were not able to identify the location of P_1 positions due to the interference arising from the effects of flow instability in the near wake flow region.

The experimental results are compared in Figure 3.6 with theoretical predictions based on the potential flow model of Ingham and Hildyard (1991). Agreement is good for α up to about 140° (and so, by symmetry, for the range from 220° to 360°). Figure 3.7 shows the same results in a different way, with the dimensionless linear width of the stagnation region (*S/D*) plotted as a function of α. Here, we again show the theoretical results based on the model of Ingham and Hildyard (1991), together with results using the earlier Dunnett and Ingham (1988) model. The difference between the two models is due to the fact that, in the Dunnett and Ingham model, the simplifying assumption was made that, at small ϕ_C, one stagnation position lies very close to the slot (i.e., $\theta = \alpha$) while the other lies close to θ = 0°. This was done to avoid the necessity of numerically solving the cubic form of Equation (3.2), and so provided a closed-form solution. As seen in Figure 3.7, agreement between our experimental results and the two models is quite good, except for small slot orientations ($\alpha \approx 0$), where the weakness of the simplifying assumption made in the Dunnett and Ingham model is clearly apparent. This notwithstanding, it is encouraging to note in general that a potential flow model can provide good agreement with experiment over such a wide range of α (at least up to 140°).

Vortex shedding frequency: Measurements of the frequency of vortex shedding were performed for flows both with and without aspiration. Figure 3.8 shows results for the cylinder without aspiration, and it is seen that the Strouhal number (*Str*) varies strongly with *Re*, falling from about 0.23 for *Re* = 880 to about 0.19 for *Re* = 12,600. The error bars shown represent one standard deviation, based on five separate measurements. For the purpose of comparison, Figure 3.8 also shows the envelope of experimental data from a range of other studies for rough and smooth cylinders (from Hammache and Gharib, 1991) and our results are broadly consistent with these. Qualitatively, this behavior may be explained in terms of changes that take place in the

boundary layer as it develops over the surface of the cylinder. For a cylinder without aspiration, the single stagnation point at $\theta = 0°$ gives rise to two boundary layers that grow on either side of the cylinder. A vortex on one side of the cylinder grows due to entrainment of fluid from the shear layer on the other side, bearing vorticity of opposite sign to that of the entraining vortex. The growing new vortex continues to be fed by circulation from the shear layer until it becomes strong enough to draw the opposite shear layer across the wake axis. Eventually, the approach of oppositely-signed vorticity cuts off further supply of circulation to the vortex, which is then 'shed'. The point where the growing boundary layer separates from the cylinder as a vortex is identified in terms of the separation angle, which corresponds to about $\theta = 104°$ (for $Re > 1000$) for a cylinder without aspiration. As Re increases, two opposing mechanisms come into play (Gerrard, 1966). On the one hand, the rate of entrainment increases, causing the forming new vortex to be weaker because fluid of opposite vorticity is being entrained more rapidly. So, as the size of the formation region subsequently shrinks, the frequency of shedding tends to increase. On the other hand, there is an opposing tendency due to the fact that, as turbulence in the shear layer increases, the shear layers become more diffuse, thus increasing the time taken for a concentration of vorticity to be carried across the wake axis. This tends to reduce the shedding frequency. For Re in our experimental range from 880 to 12,600, the second mechanism dominates somewhat, leading to the observed slow overall decrease of Str with Re.

The results for the case where there is aspiration at the surface of the cylinder are shown in Figure 3.9 (for the case where $\alpha = 60°$). Here, Str is seen to depend strongly not only on Re but also on ϕ_C. Explanation of this behavior may be related qualitatively to the positions of the two stagnation points which straddle the slot sink, each of which represents the starting point for boundary layer formation. As the sampling flow rate (and hence ϕ_C) increases, the two stagnation points located asymmetrically on either side of the slot move farther apart. Of particular interest is the position P_1. As this moves over the cylinder surface as ϕ_C increases, it tends to push further back the separation point (which, as mentioned above, had been close to $\theta = 104°$ for $\alpha = 0°$). This results in a separation region that is smaller, leading in turn to a higher shedding frequency.

Figure 3.10 shows experimental results for just one freestream condition with $U = 4.5$ m/s and $Re = 9450$, for the slot position varied from $\alpha = 0°$ to 180° and ϕ_C varied from 0.005 to 0.040 (corresponding to the sampling flowrate ranging from 10 to 80 Lpm). Here a very complex - but coherent - pattern emerges. Firstly, for given ϕ_C, Str remains fairly constant at first as α increases from zero. Then from about $\alpha = 45°$, Str rises steeply, reaching a peak for α around 90°. Thereafter, it suddenly falls back even more steeply, leveling off - at a value lower than that for $\alpha = 0°$ - as α approaches 180°. The magnitudes of both the rise and the fall in Str are seen to be greater as ϕ_C increases.

Again, the observed trends may be explained in terms of qualitative physical arguments similar to those advanced above. As α increases from 0°, the location of one stagnation point (P_2) remains roughly constant close to $\theta = 0°$ (see Figure 3.6). But the other stagnation point (P_1) moves ahead of the slot. So, as α increases, the angular location of the second stagnation point also increases. This pushes back the point at which the flow separates from the cylinder; however, the separation point does not move nearly as much as the second stagnation point, with the result that the angular separation between the stagnation and separation points decreases. As mentioned earlier, the boundary layer starts growing from the stagnation point and breaks off and

sheds at the separation point. The decrease in angular separation between these two locations leads to the formation of smaller vortices that are shed more frequently, and in turn a corresponding increase in *Str*. This trend proceeds for θ in the range up to about 90°. However, when α gets close to and beyond about 90°, conditions are no longer favorable for flow separation from the body itself. At this point, a sudden transition occurs in the nature of the flow, where the near-wake recirculation zone becomes detached and appears as a standing vortex just downstream from the cylinder. As suggested by the results in Figure 3.10, this is accompanied by a sudden marked reduction in vortex shedding frequency (and hence *Str*). It is reasonable to postulate that the boundary layer around the surface of the cylinder itself has now become essentially stabilized.

Spherical bodies

In the case of the spherical sampler, the stagnation region was characterized by the end-to-end linear widths of the two sides of the oblate stagnation region. We have already referred to these as S_1 and S_2 respectively, and the experimental results (obtained using the methods described earlier) for just one value of $\phi_S = 0.31$ are shown in Figure 3.11. Here it is seen that S_1 (see Figure 3.11a) decreases as α increases in the range up to about 140° (beyond which measurements were not possible). On the other hand, it is seen that S_2 (see Figure 3.11b) increases steadily over the same range of α.

Theoretical values for S_1 and S_2 were calculated from the potential flow model of Dunnett and Ingham (1988). For S_1 it is seen that agreement with the experimental data is poor, not surprisingly since the mathematical definition of stagnation in that earlier study did not match what we measured. Whereas Dunnett and Ingham has set just $V_\theta = 0$, both V_θ and V_φ need to be equated to zero in order to be consistent with our experiments. By contrast, the original analytical expression for S_2 generally agrees quite well with our experimental results, as expected since this does not depend on the additional assumption about V_φ. There is, however, some disagreement at smaller values of α, arising from the underlying simplifying assumption by Dunnett and Ingham that one of the stagnation points (corresponding to P_1 in our notation for the cylinder) is always relatively close to the orifice. This of course is true only at larger values of α.

In general these results for the spherical body suggest that a potential flow model can be quite adequate for predicting the dimensions and locations of stagnation zones on the surface of the body.

3.6 Conclusions from this part of the research

The nature of airflow around cylindrical and spherical bluff bodies with aspiration (i.e., suction) has been studied. A simple but effective means of flow visualization for studying such flows was developed, involving photographing the flow patterns generated using a modified version of the 'smoke-wire' method. This method not only helped in visualizing the flow patterns but also in locating the positions of flow stagnation on the surfaces of the two bluff bodies studied. The experimental results for the cylinder were found to agree quite well with the results of the potential flow models of Dunnett and Ingham (1988) and Ingham and Hildyard (1991). From the

comparison between experiment and theory, we may conclude that, at least when sampling in the regime of relatively low ϕ_C (where all our experiments were performed), potential flow theory for describing the flow field in the vicinity of this body holds quite well for slot orientations (α) up to at least about 140°. For angles larger than this, reliable data could not be obtained due to the presence of flow instabilities in the near wake of the cylinder. So we cannot yet claim with certainty that our conclusion extends to these extreme orientations.

For the cylinder, the experiments also helped identify conditions where the aspiration flowrate modifies the nature of the near wake instability. In particular, we observed the interesting phenomenon associated with the strong dependence of vortex shedding frequency (and hence Strouhal number, *Str*) on aspiration flowrate and slot angle (α). So we were able to qualitatively relate the observed behavior with plausible physical arguments about the nature of the development of the boundary layer over the cylinder surface. This behavior may have a significant bearing on the transport of airborne contaminants - during, for example, the sampling of particulates at large angles with respect to the wind.

For the spherical body, the location of the positions of flow stagnation of stagnation were mapped visually by determining the extremities of this region along two perpendicular axes, using the same photographic approach as for the cylinder for one direction, and a direct-visualization approach for the other. A good match between the experimental results and the mathematical theory of Dunnett and Ingham (1988) was obtained for S_2, again for α up to about 140°. The fact that the comparison was less satisfactory for S_1 arises directly from the difference in how stagnation was defined in our experiments (i.e., the line on the surface of the sphere which divides the aspiration from the non-aspirated air) in comparison to the Dunnett and Ingham theory.

This body of experimental research has increased our knowledge about the nature of airflows about bluff bodies with aspiration, in particular providing insights into the possible extended range of applicability of relatively simple potential flow models. The bluff bodies studied were of very simple geometry, thus enabling us to identify easily the most important physical features of such flows which may be generalizable to bodies of more complex shape. The work is particularly relevant to aerosol sampling where, for many years, our progress towards understanding the factors which govern sampler performance (in particular aspiration efficiency) has been our inability to satisfactorily describe the flow, particularly for large sampler orientations. By describing the nature of the flow, largely by reference to the locations of positions of stagnation, links up with the use of such information in particle aspiration efficiency models, as described for example by Dunnett and Ingham (1988) and Vincent (1989). In such models, the positions of stagnation - in particular the size of the stagnation region on the sampler body - define the distortion of the flow in the region of the sampling orifice which in turn governs particle transport in that region and hence their ability to enter the sampling orifice.

4. EXPERIMENTAL SET-UP AND PROCEDURES FOR THE WIND TUNNEL STUDIES OF SAMPLER EFFICIENCY IN MOVING AIR

4.1 Introduction

A major objective of the overall project was to provide a rich data bank on the effects of various parameters on the aspiration characteristics of blunt body aerosol samplers. This required an elaborate experimental setup that would be flexible enough to rapidly acquire copious amounts of data but does not require major modifications when the focus of the study changes from one parameter to the other. As already pointed out, sampler aspiration efficiency is a complex parameter influenced by freestream velocity, sampling flow rate, orientation of the sampling orifice and sampler geometry. The experimental set-up should enable us to study any combination of such parameters with ease. In this section, we describe the experimental system that was used in the major part of the research, namely that concerning the sampling efficiencies of aerosol samplers in moving air.

4.2 The wind tunnel

The same wind tunnel was used for the main aerosol sampling part of the research as was used for the aerodynamic inquiry. It has a test section with cross-sectional area of 0.3 m × 0.3 m and length 1.8 m (see Figure 4.1). Clean air entered through an inlet HEPA filtration bank, drawn through the wind tunnel by a centrifugal fan coupled to a variable-frequency, transistor-inverter speed controller, exiting through another HEPA filter bank (to prevent aerosol generated in the wind tunnel from contaminating the laboratory area), and finally through a silencer. The blower was connected to the test-section through bellows that dampened and prevented the vibrations from the blower from being transferred to the test section.

This system provided mean air velocities in the test section ranging from 0.15 to about 20 m/s with low levels of freestream turbulence with intensity about 0.25%. The test chamber was preceded by a dispersion chamber, the purpose of which was to accommodate square lattice grids to provide well-defined turbulence in the test section. In addition to the turbulence-generating grid, the dispersion chamber also accommodated the aerosol injection nozzle and the distribution plate that ensured adequate mixing of the injected aerosol. Adequate sampling ports were provided along the test section to enable measurement of concentration and velocity profiles along the tunnel cross-section. The top section of the wind tunnel could be completely removed in order to clean the internal walls of the tunnel or to mount the blunt body sampler. The exit filter bank was also easily accessible for maintenance.

To ensure adequate mixing of the aerosol and to test the dependence of aspiration efficiency on turbulence intensity, experiments to measure aspiration efficiency were performed using two different lattice-type screens, capable of generating freestream turbulence with well-defined intensity and length scale. The characteristic turbulence intensity I_f and length scale ℓ_f at a distance z downstream of the screen can be estimated from (Baines and Peterson, 1951)

$$I_f = 1.12\left(\frac{z}{b}\right)^{-5/7} \tag{4.1}$$

and

$$\ell_f = 0.075\left(\frac{z}{b}\right)^{0.54} \tag{4.2}$$

where b is the width of the screen bars. Two different lattice screens were used, the first with b = 0.2 cm and the second with b = 1.7 cm. The freestream turbulence parameter Λ_f, which may be regarded as the dimensionless turbulent diffusivity of the freestream approaching the sampler, is given by (Humphries and Vincent, 1976)

$$\Lambda_f = \left(\frac{I_f\,\ell_f}{D}\right) \tag{4.3}$$

For the spherical test sampler used with diameter D = 6.35 cm placed at a distance z = 119.4 cm, we obtained Λ_f = 0.004 (I_f = 0.011 and ℓ_f = 2.36 cm) and Λ_f = 0.006 (I_f = 0.053 and ℓ_f = 0.745 cm) respectively.

4.3 Aerosol generation and injection system

The NBS-type mechanical dust feeder (BGI Inc., Boston, MA) was used to inject aerosol into the tunnel. It could deliver powdered material at rates ranging from 10 mg/min to 1000 mg/min. For the experiments described here, the aerosol was generated from polydisperse glass bead powders (Cataphote Inc., Jackson, MS), comprising individual particles with density about 1500 kg/m^3. The diameters of the spheres ranged from 1 to 37 μm and the mass median aerodynamic diameter for the resultant aerosol as measured by the APS (see below) was found to be 26 μm with a geometric standard deviation of 2.5. In preparation for each experiment, the glass beads were heated in an oven to reduce the moisture content and so reduce agglomeration during aerosolization. Immediately prior to aerosolization, the glass beads were sieved through a 74 μm mesh to remove any large agglomerates. An infrared lamp was used to heat the dust in the disperser to reduce subsequent moisture adsorption, agglomeration and clogging of the dust hopper. A 2-mCi Kr^{85} aerosol neutralizer (TSI Inc., Saint Paul, MN; Model 3012) was used in-line, and the neutralized aerosol was then injected into the tunnel in the direction opposite to the freestream flow in the region of the wind tunnel just downstream of the contraction. A distribution plate was placed just behind the injection nozzle to create enough turbulence to uniformly mix the injected dust. This dust generation system could consistently produce uniform aerosol concentration over the working section cross-section stable to within about 1% over periods of up to three hours.

4.4 Description of the test samplers

For the major part of the aerosol aspiration efficiency experiments, we employed a very simple blunt aerosol sampler of spherical shape. Such a sampler has no direct relation to aerosol samplers of the types used in practical industrial and environmental hygiene but have a common physical basis. But it is simple enough to allow the physical mechanisms associated with the aspiration process to be identified and studied in relation to accessible theoretical models. The spherical

sampler used in the main part of the study comprised an orb of diameter (D) 6.35 cm, with a single entry orifice of diameter (δ) 0.635 cm. A steel tube (I.D. = 0.635 cm) was embedded inside the sphere such that the entrance to this tube was flush with the spherical surface. The sampled aerosol entered and exited the spherical sampler through this tube. A similar sampler was made with $D = 3.14$ cm and $\delta = 0.635$ cm.

As mentioned in §3, the performance of thin-walled probes at orientations greater than 90° from the freestream has not previously been studied in detail. So in the present work, a simple thin-walled probe with an inlet diameter of 0.635 cm was also investigated, not only to determine aspiration efficiency as a function of orientation to the freestream, but also to study the effect of inlet losses on the aspiration efficiency. The length and configuration of the thin-walled probe was identical to the tube used in the spherical samplers mentioned above.

The effect of asymmetry on aspiration efficiency was also studied using a rectangular sampler of dimensions 80 mm × 80 mm × 30 mm, with the sampling inlet mounted offset from the center. The performance of this sampler was studied with respect to another identical sampler with the inlet mounted at the geometric center of the sampler. The use of such a sampler is a step closer to the realistic personal samplers used in industrial hygiene. Figure 4.2 shows schematic diagrams of all samplers used.

4.5 Aerosol sampling and measurement systems

Air velocity measurements

Measurements of air velocity were made using a velocimeter (VelociCheck, TSI Inc., St, Paul, MN, Model 8330). This has a range of from 0.13 to 20 m/s with an accuracy of ±0.03 m/s. Velocity profiles in the wind tunnel working section were determined by making measurements with the probe at intervals along the horizontal and vertical axes of the wind tunnel cross section. They were normalized by reference to the centerline velocity.

Aerosol concentration measurements

The aspirated aerosol passed through the sampling tube described above and was delivered to an Aerodynamic Particle Sizer (APS, Model 3310, TSI Inc., St. Paul, MN). As shown in Figure 4.1, for experiments where the sampler orientation was varied only in the horizontal plane, this involved transporting the aerosol through one 90° bend. As will be described later, some experiments were also carried out with the sampler orientation varied in the vertical plane, for which the sampling tube was similar but now required transporting the aspirated aerosol through two 90° bends. The APS is a 'time-of-flight' instrument calibrated to operate at 5 Lpm. For sampling flowrates equal to this, the APS was connected directly to the sampling tube. For sampling flowrates less than or greater than 5 Lpm, by-pass air was either added or subtracted so that the APS was always receiving 5 Lpm. This was achieved using the conical coupling shown in Figure 4.3, designed to minimize aerosol losses during the transition (Sreenath, 1998). This involved numerically modeling the diverging flow inside the coupling, choosing the dimensions to ensure that the entry to the APS always aspirated air from the main flow in the cone at the desired 5 Lpm and sampled particles isokinetically. In the use of the APS, sampled particles were

detected and counted into 1024 bins representing particle aerodynamic diameter (d_{ae}) in the range from 0.5 to 30 μm. This information was stored in a personal computer that also controlled the APS operation. It is important to note here that the upper end of the useful range of the APS is really about 25 μm, since above this APS inlet losses (as opposed to the other losses and biases which are the primary focus of this report) become large and uncontrollable.

Unless stated otherwise, the surfaces of the test samplers were cleaned and sprayed with silicone grease (Bostik, Middleton, MA) prior to each individual run to prevent particle bounce and, thus, secondary aspiration (e.g., of the type identified by Vincent and Gibson, 1981 and Mark *et al.*, 1982). Further, to reduce the likelihood of unwanted electrostatic effects, all wind tunnel surfaces were sprayed with anti-static fluid (Static Guard, Alberto-Culver Inc., Melrose Park, IL) at the beginning of each experiment. Additionally, the tunnel, test sampler and all instruments were electrically grounded.

Sampling efficiency (E_α) for the sampler described was determined experimentally as a function of α as measured in the horizontal (equatorial) plane (as shown in Figure 4.1). It was found indirectly by referring all measured particle number concentrations to those obtained for the forwards-facing case (i.e., α = 0°), and then normalizing with respect to the sampling efficiency calculated for that orientation from elementary blunt sampler theory (Vincent, 1989; 1995). In this scenario

$$E_\alpha = \frac{c_\alpha}{c_0} = \frac{c_\alpha}{c_{\alpha=0}} \cdot \frac{c_{\alpha=0}}{c_0} = \frac{c_\alpha}{c_{\alpha=0}} \cdot E_0 \qquad (4.4)$$

where c_α is the concentration actually measured at orientation α and $c_{\alpha=0}$ is that at orientation α = 0°, c_0 is the freestream concentration, and E_0 is the sampling efficiency for α = 0°. For each measurement of E_α, the particle number concentration was measured eleven times: six times at the forwards-facing orientation to provide an average value of $c_{\alpha=0}$, and five times at orientation α to provide an average value of c_α. To ensure that any count differences between the positions were not caused by any temporal shifts in the aerosol generation rate, the concentrations were measured at the two positions in the '0-α-0-α-0-α-0-α-0-α-0' sequence. Thus, in Equation (4.4), the part we actually measured is the ratio $c_\alpha/c_{\alpha=0}$.

In the preceding, it is noted that we have used the term "*sampling efficiency*" as distinct from the "*aspiration efficiency*" that was mentioned earlier (see Section 2). The research described in this report has drawn attention to the importance distinction between these terms, as elaborated in more detail later in this section.

4.6 Use of the Aerodynamic Particle Sizer (APS)

The APS determines the aerodynamic diameters of particles by measuring the velocities of the particles relative to the air flow in an accelerating nozzle. Such velocity is measured as a function of particle transit time between two laser beams. As the particle passes through the laser beams, it generates two distinct light pulses that are detected by a photodetector that in turn generates proportionate electronic pulses which trigger a timer that measures the transit time. By calibration using 'unit' density spheres (that is, a density of 1000 kg/m^3), the transit time provides a direct measure of aerodynamic particle diameter (Wang and John, 1987).

The advantages and limitations of the APS have been well documented in the published literature (Baron, 1986; Ananth and Wilson, 1988; Brockmann *et al.*, 1988; Brockmann and Rader, 1990; Chen *et al.*, 1985, 1986 and 1989; Cheng *et al.*, 1990; Griffiths *et al.*, 1984; Heitbrink *et al.*, 1991; Heitbrink and Baron, 1992; Rader *et al.*, 1990; and Wang and John, 1987). The relative velocity between the particle and the accelerating flow is a function of particle diameter only so long as the Reynolds' number (Re_p) of the particle is in the Stokes regime (i.e., $Re_p < 0.1$). The APS is usually calibrated using monodisperse polystyrene latex particles. The advantages of the APS include its high resolution, wide detection range (0.5 to 30 μm), near real-time measurement, insensitivity to changes in refractive index or scattering fluctuations, and monotonic calibration over its entire range. Baron (1986) also pointed out the excellent calibration stability of APS, rapid readout and its data manipulation capabilities.

Any instrument, however, has its limitations. The major parameters that influence the accuracy of the APS are particle density, particle coincidence, particle shape factor and particle deformation. Since the APS was so critical to the success of the work described in this report, it was appropriate to investigate the nature of relevant such limitations and to explore what corrections to the raw data are appropriate.

Coincidence effects

Since the APS is a 'time-of-flight' instrument, accurate detection of a particle in the sensing zone of APS requires full detection of two pulses from the same particle. Hence, the transit time is the time difference between the two pulses of light. For the APS version used in the present research, this time is measured by one of the two timers.[8] The two timers, also called the "small particle processor" (SPP) and the "large particle processor" (LPP), are specifically designed to count small particles (that have small transit times) and large particles (that have large transit times) respectively. Coincidence can occur if a second particle crosses the first laser beam before the first particle crosses the second laser beam. This has a complex effect on the measured aerosol particle size distribution. Due to the coincidence, the real particle size is replaced by a spurious or "phantom" particle size. This coincidence error occurs when a pulse is generated by the second particle when the timer is open, hence these particles are also called "open timer phantom particles". Such coincidence effects in the APS have previously been mathematically modeled using Monte Carlo simulation techniques (Heitbrink *et al.*, 1991).

In general, coincidence can be encountered in three possible ways. In Case 1, the first particle's second pulse is too small to be detected such that the timer waits for a certain time that defines the largest particle that can be sized. But before the timer is turned off, a second particle arrives at the first laser beam, creating a second pulse. Hence, the first pulse of the first particle and the first pulse of the second particle are used to determine the transit time. Hence two real particles are replaced by one phantom particle. In Case 2, the second particle arrives at the first laser beam during the timer's dead-time period (750 ns) when no pulses are detected. If the second pulse of the first particle is below the detection threshold and the second pulse of the second particle is detected before the timer switches itself off (at the end of maximum transit time), a larger size phantom

[8] It should be noted that a new version of the APS is now available from TSI in which the two processors are replaced by a single processor, so that problems like those outlined below in this report are thought to be eliminated.

particle is created that replaces the two real particles. In Case 3, phantom particle generation occurs when the first pulse of the second particle is generated before the second pulse of the first particle. The net result is the generation of two smaller size phantom particles. Heitbrink and Baron (1992) recommended either reduction of particle concentration (to not more than 100 particles/cm^3) for small diameter particles or reduction of photomultiplier (PMT) gain as possible remedies.

Of the two processors in the APS circuitry, the SPP and the LPP respectively, the SPP tends to create phantom particles along the lines indicated above, while the LPP is designed to prevent creation of phantom particles. These two processors have an overlap range of 5.2 μm to 15.4 μm. Heitbrink and Baron (1992) used the difference in counts in the overlap range to estimate the phantom particle count. This approach has been tested in relation to current data and will be discussed later.

Minimizing coincidence

The traditional approach to minimizing phantom counts is to determine the difference between the counts in the SPP and the LPP for the overlap region and use this as a measure of phantom counts in this overlap range. There are four different ways (Maynard, 1997) in which the phantom counts can be removed from the raw data file. One way is to take an average of the difference between the SPP (which has more counts than the LPP) and the LPP and to subtract this average count from the SPP for all channels in the overlap region. In the second approach, instead of taking an average, a linear fit is fitted to the difference in counts between the SPP and the LPP, and this is used to deduce counts from the SPP in the overlap region. In the third approach, a polynomial fit is applied to represent the difference in counts. The fourth method is that described in the manufacturer's Advanced Software Manual. Here, TSI has recommended a series of correction factors or "extrapolation factors" to be applied to the counts in the SPP and LPP channels in the overlap region. This is done in such a way that there is progressively increasing weight given to the LPP data and progressively decreasing weight given to the SPP data. Before going into the details of analyzing the APS output files using the above approaches, however, it is appropriate first to describe the way in which the APS stores the raw data.

.The APS stores data from the photodetector output pulses in terms of channel numbers which in turn are related to d_{ae} by means of calibration against known standard. These are channels 0 to 78. Channels 0 to 50 correspond to the SPP that has a 2-ns timer. Channels 51 to 62 correspond to the LPP that has a 66.67-ns timer. Channels 63 to 78 also represent LPP data, but in the overlap region that corresponds to channels 36 to 50 of the SPP data. Hence, channels 63 and 36 correspond to the same particle diameter, channels 64 and 37 correspond to the same particle diameter, and so on. It should be noted that, while the SPP contains phantom particles, the LPP underestimates the counts for small diameter particles in the overlap region. Hence, looking at the channels of corresponding d_{ae}, it is possible to predict the phantom counts, and eventually to deduce the phantom counts in the corresponding SPP channels in the overlap region. Another approach requires the use of correction factors to downgrade the total SPP counts (including phantom counts) and so enhance the LPP counts. One may use both the above methods simultaneously to reduce phantom counts. Reducing phantom particle counts can also be achieved by extending the range of the LPP to sizes below 5 μm. In order to do this, the gain of

the LPP is lowered using an external potentiometer. In this case, only the LPP data are used and the SPP data are usually discarded.

Our new approach (see below) is to correct the SPP and LPP data for the particular case of sampling by a thin-walled probe in wind tunnel. Here, the relationship between theory and experiment is well known (i.e., $\alpha = 90°$), and so we may obtain correction factors that should apply for all other sampling conditions and samplers. It will be shown in the course of the discussion that such correction factors are independent of the sampling conditions and the sampler used, but are instrument-specific and dependent on the type of aerosol used. It is aerosol-dependent because, if the aerosol contains too many small-diameter particles, the number of phantom particles would also increase. For this reason, some investigators are recommending the use of a virtual impactor at the APS inlet to reduce entry of small particles and enhance the concentration of large particles that have extremely low entry efficiency at the inlet of the APS (Maynard, 1997).

The correction factors developed by TSI are shown in Table 5.1. These were derived purely from statistical analysis of the probability of phantom counts occurring in the SPP in the overlap region, and to our knowledge no specific experiments were carried out to confirm their validity. The APS software does not provide any routine for merging the SPP and LPP data, nor indeed does it warn the user about phantom counts.

The earliest studies on phantom counts (Heitbrink *et al.*, 1991) recommended using the APS only at very low concentrations (less than 100 particles/cm^3 against the TSI recommendation of 300 particles/cm^3). Heitbrink *et al.* performed an experiment using an aluminum oxide aerosol with known mass median aerodynamic diameter having 90% of all particles less than d_{ae} = 15 μm. The aerosol at a concentration of 120 particles/cm^3 was sampled for 47 min. It is appropriate to discuss their experimental results here since those results were found to be very similar to those obtained in our own experiments for the aspiration efficiency of thin-walled tube sampling at 90° with respect to the freestream. An approximate replication of their graph is shown in Figure 4.4. It is worth noting that their y-axis represents number counts while the y-axis in our graphs (see Figures 4.5 and 4.6) represent sampling efficiency. In other words, Figure 4.4 is effectively a plot of the efficiency of the SPP and LPP respectively whereas our results depict effects of these processor efficiencies on sampling efficiency. What is more interesting (and will soon become evident from the discussion) is the fact that when a ratio of two raw data sets (that contain coincidence effects) are taken to estimate aspiration efficiency, the coincidence effects do **not** cancel out.

In Figure 4.4, Curve 1 represents the counts of the SPP, Curve 2 represents the counts of the LPP, and Curve 3 represents actual counts of particles injected into the APS inlet nozzle. The errors in the SPP and LPP are divided in to four different types. Type A error occurs as a result of the SPP threshold, and affects data for d_{ae} between 0.5 to 1.5 μm. Type D error occurs due to the LPP threshold. But this error is masked by the correction factors if the raw data are converted using the factors suggested in the APS Advanced Software Manual. Type B and E occur due to the coincidence of two fully-detected particles by the SPP and LPP respectively. While the SPP generates a small phantom particle relative to the coincident particles, the LPP completely eliminates the two coincident particles. Hence, the efficiency of the LPP drops with increasing particle size. Again, this depends on the aerosol characteristics, particularly the concentration. Type B and E errors are thought to be reduced by reducing the aerosol concentration, although no suggested values appear in published literature, and - in any case - are probably dependent on the

type of aerosol used. Type C error corresponds to the phantom particle counts that exist throughout the size range but become apparent only at the tail end of the particle size distribution where there are more phantom counts than real particles.

It is evident from Figure 4.4 that using only the SPP or only the LPP in the overlap region will either overestimate or underestimate particle counts and hence the aspiration efficiency. Therefore, for the present research, there has to be a reliable method by which the SPP and the LPP data can be merged. Heitbrink *et al.* discuss possible ways to reduce coincidence effects and also ways to analyze the data, but did not recommend any specific procedure to analyze the raw data. Further.we have discussed the matter with several experienced APS users. From all this, it would appear that there is no hard-and-fast rule as to how the SPP and LPP data from this version of the instrument may be merged in the overlap region. So long as the aerosol concentration is low and there is a way to compare the output from the APS with an known standard, the SPP and LPP data can be merged reasonably accurately within the range of experimental error. One such possibility has been examined, and a method to correct SPP and LPP data reliably and consistently for all sampling conditions has been developed.

Our new approach to minimizing coincidence errors

In order to study the effect of phantom particle counts on aspiration efficiency in aerosol sampler research, a thin-walled tube was used as a sampler for which the aspiration efficiency was determined in the wind tunnel. The major advantage of this procedure lies in the fact that thin-walled probes have been studied over a long period of time, and well-proven theories exist for predicting their performances, both facing the freestream and for angles up to 90°. The theory is particularly solid for α = 90°. Hence, the trend in aspiration efficiency determined using APS should be similar to that predicted by theory.

Figure 4.5 compares the sampling efficiency obtained experimentally with that calculated from theory for α = 90° (see Section 5 for a description of the distinction between this and actual aspiration efficiency). It should be noted here that, in the theory, we make use of the fact that for α = 90° there is zero loss in the sampler entry associated with boundary layer effects (i.e., $P_{entry}(\alpha)$ = 1, see Sections 4.9 and 5.2). Theory predicts that sampling efficiency should fall with increasing particle diameter or Stokes' number (St). But, this does not seem to be the case looking at the sampling efficiency data obtained on the basis of the measurement from APS without applying any correction to raw data. Sampling efficiency seems to suddenly increase in the d_{ae} range from about 5.0 to 15 μm, followed by a sharp cut beyond this point where the efficiency suddenly drops to zero. The sudden increase with St is physically unrealistic unless particles are being added externally during the aspiration process. Such addition would be possible only due to particle bounce or electrostatic effects. But, as has been mentioned earlier, all samplers were thoroughly greased and electrically grounded to reduce the possibility of such effects. Hence, we believe that the observed increase in aspiration efficiency can be attributed only to spurious counts in the SPP.

In order to merge the SPP and LPP data, we first used the corrections given by TSI in the APS Advanced Software Manual. Figure 4.6 clearly illustrates the effect of using the correction algorithm in the overlap region. The sampling efficiency thus obtained appears more realistic with respect to the existing theory than when compared with aspiration efficiency obtained using raw data. However, it is apparent that these factors are not adequate since the deviation from

theory still persists. It may be noted that the TSI correction factors are linear, a smooth way to include contributions from SPP and LPP in the overlap zone. This method of interpolation also assumes that the efficiency curves for the SPP and LPP are monotonic, in the sense that the SPP efficiency steadily increases (due to phantom counts) and the LPP efficiency also increases from a very low value to a reasonably high value with increasing particle size. The TSI correction factors are supposed to compensate for these inefficiencies by suppressing the SPP counts and boosting the LPP counts to predict the actual concentration.

What the efficiencies are for SPP and LPP in reality depend on a number of factors. The photomultiplier tube (PMT) voltage and gain play a major role in influencing the efficiencies of the processors. Since the APS does not have individual controls for SPP and LPP gain, the gain has to be adjusted for both processors simultaneously. Since the SPP requires a low gain and LPP requires a high gain, the user must look for an optimum value. Having a low gain is usually preferred since the low gain will help the APS to avoid counting too many small diameter particles that are a major source of phantom counts. But at the same time the LPP counting efficiencies may be too low for smaller diameter particles. Having a high gain will result in the SPP becoming too sensitive, thereby skewing the measured size distribution and also increasing phantom particle counts. Another approach to reducing phantom counts and so increasing the reliability of the SPP is to use the APS at low particle concentration. But for experiments where the entire range of APS is crucial, reducing the concentration of the aerosol sampled by the APS will increase Poisson-type counting errors, especially for large diameter particles that are difficult to transport through the inlet of the APS.

The above discussion leads us to the question about whether the TSI factors are adequate and universal: that is, are they applicable for all APSs? We believe that the correction factors in the overlap region are dependent on the aerosol particle size distribution, inlet concentration, PMT voltage and gain and - last but not least - the number of phantom counts as a consequence of the above factors. Hence, a better approach would be to develop correction factors for APS data with respect to a known particle size distribution or any other known outcome - for instance, the sampling efficiency of a thin-walled probe for which the theory is well established.

Before introducing our new correction factors, we also explore the method suggested by Heitbrink and Baron (1992). In this approach, the difference in counts between the SPP and the LPP in the overlap region is used as a basis to estimate phantom counts. The difference in this region for all the ten runs at a reference aerosol concentration was used to determine either an average concentration of phantom counts or to develop a function (by curve fitting) that defines the phantom counts with respect to particle aerodynamic diameter (Maynard, 1997). This function, defining the mean phantom count, may be of any order, although a quadratic or linear form should be adequate. It is then subtracted from all SPP channels, thereby minimizing the effect from the phantom counts. The corrected SPP data are then blended with the LPP data using the TSI correction factors for the overlap region. This approach is adopted for both reference concentration and the condition for which the sampling efficiency needs to be determined. Figure 4.7 compares the different methods of reducing phantom counts and their consequent effect on the measured aspiration efficiency. It is evident from the graph that all these methods tend to over-estimate the coincidence effects, as a result of which the measured sampling efficiency is much sharper than the theory. One might argue that the difference between the obtained sampling efficiency and the theory may occur due to the sampling losses which do not cancel out while taking the ratio between the reference concentration (tube facing the freestream) and the tube oriented at an arbitrary angle.

As discussed later, these losses include entry losses very close to the inlet associated with the coupling between the external and the internal flow. However, it has been shown that such entry losses can be estimated reasonably well for tubes oriented at angles up to 90° and for St up to 0.2 (Hangal and Willeke, 1990). For the range of conditions in which our experiments were conducted, these losses were estimated as being negligible.

As already mentioned, our approach to correcting the APS data was to compare the APS raw data for a thin-walled probe oriented at 90° to the freestream with a theory (Vincent, 1989) that has been well tested. The experiments are described in greater detail in Section 5 of this report. The raw data and the corrected APS data using new correction factors are shown in Figure 4.8. The new correction factors were developed by comparing the raw APS data with theory. This too is shown in Figure 4.8. The new correction factors were then used to correct the raw data for all other conditions. An example for such a correction is shown in Figure 4.9 (for $\alpha = 180°$). This correction is for a spherical sampler with experimental conditions entirely different from that of the thin-walled tube experiments. These correction factors seem to work well for all the other conditions as well in that the error bars are also significantly reduced and are of the same magnitude as that in the rest of the regions.

Effect of particle density and shape factor

The effect of particle density on APS performance was probably one of the earliest parameters to be studied (Wilson and Liu, 1980; Baron, 1983; Wang and John, 1987). It was identified that large diameter particles (that is with d_{ae} greater than 1 μm) were accelerated in the APS such that the particle velocity placed it beyond the Stokes' regime, leading in turn to a dependence on particle density. In the non-Stokesian regime, particle acceleration, and hence particle velocity are dependent not only on particle aerodynamic diameter but also on the physical diameter which may be expressed in terms of aerodynamic diameter and particle density. The Reynolds' number in the APS nozzle ranged from 0.001 to 100 for particles in the range of d_{ae} from 0.1 μm to 15 μm. It was reported that, even for densities in the range 800 kg/m^3 to 2000 kg/m^3, 5% underestimation to 10% overestimation may occur if no density correction were incorporated. In general, particles with densities greater than 1000 kg/m^3 were oversized and so required a correction factor less than unity, while particles with densities less than 1000 kg/m^3 were undersized, requiring a correction factor greater than unity. With this in mind, an analytical formula was derived (Wang and John, 1987) and was incorporated into the software provided with the APS used in the present research.

Marshall *et al.* (1991) and Cheng *et al.* (1990) employed a similar approach but also took the particle shape factor and particle density into account. The equations were hence modified to include the influence of particle shape factor and density on particle acceleration. The same equations hold good except that the particle Reynolds' number was modified. However, by choosing spherical-shaped uniform-density glass spheres, such problems were not encountered relevant to our experiments.

Summary

It is evident from the above that the APS is a very sensitive instrument but that the data need to be interpreted with great caution. The APS is sensitive to the particle size distribution of the aerosol,

particle concentration, particle density and the particle shape factor. Of all these, phantom particle generation is the least studied and is dependent on the PMT voltage and gain, making it very instrument-specific as well. Hence, calibrating the APS is not the only thing the user needs to be concerned about. The user has to actually verify the output from the APS using a known aerosol particle size distribution or devise ways to characterize the error in order to come up with suitable correction factors that are appropriate only for that set of experiments. With all this in mind, an innovative approach to correct and characterize APS data has been developed.

4.7 Uniformity of air velocity and particle concentration profiles

Aspiration efficiency defines the effectiveness with which particles are transported from the air outside the sampler through the plane of the entry orifice. By starting from the most fundamental definition of aspiration efficiency based on particle fluxes, we will show - for the first time - that aspiration efficiency is strongly dependent on the spatial distributions of air velocity and particle concentration. Then we will discuss how uniformity of velocity and concentration are maintained in the wind tunnel.

To aid this discussion, Figure 4.10 shows the air flow near an arbitrarily-shaped, blunt aerosol sampler at arbitrary orientation with respect to the wind (after Vincent, 1989). The streamline pattern represents the mean air motion. The limiting streamsurface divides the air between the portion that is aspirated and the portion that passes around the sampler body. The incident plane is the transverse plane far upstream of the sampler where the flow pattern is undistorted by the presence of the sampler. The sampling plane is the plane tangential to the sampler orifice. Aspiration efficiency for this system is described at its most fundamental level in terms of the ratio of aerosol fluxes in the aspirated air passing through the incident and aspiration planes respectively.

Let $N_0(t)$ be the number per unit time of particles of a given size passing through the area, S_0, of the incident plane contained within the dividing the stream-surface (which, for the sake of generality, is taken to be a function of time, t). Due to inertia, gravity and (possibly) other forces, not all of these particles actually enter the sampler. So, let $N_a(t+<\Delta t>)$ be the number per unit time of the same particles which enter the sampler by crossing the aspiration plane, where $<\Delta t>$ is the average time for the particles to travel from the incident plane to the aspiration plane. Thus for a proper accounting of all the particles, the variation in $N_a(t)$ is time-shifted by $<\Delta t>$ from $N_0(t)$. Then the most basic definition of aspiration efficiency (A) is given by

$$A(t) = \frac{N_a(t + <\Delta t>)}{N_0(t)} \tag{4.5}$$

The dividing particle trajectory surface divides the particles between those that enter the sampler directly without touching the sampler body and those that either strike the sampler body or pass around it. This encloses an area S_p in the incident plane. If the cross-sectional area of the sampler orifice (in the sampling plane) is S_a, then

$$A(t) = \frac{\int_{S_a} c_a\left(x,y,t+<\Delta t>\right)\cdot v_{pa}\left(x,y,t+<\Delta t>\right)dy\,dx}{\int_{S_0} c_0\left(x,y,t+<\Delta t>\right)\cdot v_{p0}\left(x,y,t+<\Delta t>\right)dy\,dx} \tag{4.6}$$

where v_{pa} and c_a describe the local particle velocity and concentration profiles respectively in the sampling plane, and v_{p0} and c_0 are the corresponding quantities in the incident plane. Again, we note that the variations in v_{pa} and c_a are time-shifted by $<\Delta t>$. Since the limiting particle trajectory surface encloses all particles that enter the sampler, conservation of particle number yields

$$A(t) = \frac{\int_{S_p} c_p\left(x,y,t+<\Delta t>\right)\cdot v_{pp}\left(x,y,t+<\Delta t>\right)dy\,dx}{\int_{S_0} c_0\left(x,y,t+<\Delta t>\right)\cdot v_{p0}\left(x,y,t+<\Delta t>\right)dy\,dx} \tag{4.7}$$

If it is now assumed that there are no spatial variations in particle concentration and velocity in the incident plane, then $c_p(x, y, t) = c_0(x, y, t)$, and $v_{pp}(x, y, t) = v_{p0}(x, y, t)$, so that Equation (4.7) reduces to

$$A(t) = \frac{S_p}{S_0} \tag{4.8}$$

Since in the incident plane, the particle velocity is the same as the wind velocity there (U), then

$$A(t) = \frac{U(x,y,t)S_p}{U(x,y,t)S_0} = \frac{U\,(x,y,t)S_p}{U_S\,S_a} = \frac{U\,(x,y,t)S_p}{Q_s} \tag{4.9}$$

in which Q_S is the sampling flowrate. If the wind velocity is assumed to be constant, both spatially and temporally, then Equation (4.9) provides the direct (or trajectory) method (see Vincent, 1989) for defining aspiration efficiency which is the basis of most theoretical determinations and some experimental ones (Belyaev and Levin, 1974; Lipatov *et al.*, 1986). Alternatively, if Equation (4.9) is re-written as $A = Q_p/Q_S$ (where $Q_p = U\,S_p$), and since N_a is the flux of particles passing through the area S_p, then we have

$$A(t) = \frac{N_a(t)/Q_S}{N_a(t)/Q_p} = \frac{c_s(t)}{c_p(t)} = \frac{c_s(t)}{c_0(t)} \tag{4.10}$$

This equation, expressing the ratio of the concentration of the aspirated aerosol to that in the undisturbed freestream, provides the indirect (or comparison) method (again see Vincent, 1989) for defining aspiration efficiency which is the basis of most experimental determinations and underlies most assumptions about practical sampler performance. In Equation (4.10), even if both the numerator and denominator in Equation (4.10) are time-varying quantities, the ratio of the two is not. So, provided that U is time-independent, so too is A.

From the above discussion, it is clear that experimental determinations of aspiration efficiency using Equation (4.10) hinge crucially on assumptions of spatial uniformity of velocity and aerosol concentration profiles in the incident plane. If these assumptions are not met, then a more fundamental relation such as Equation (4.6), which takes into account the velocity and aerosol concentration profiles in the incident plane, needs to be used in calculating aspiration efficiency. Using Equation (4.10) in such circumstances might lead to significant errors.

In the wind tunnel, the velocity and concentration profiles were maintained uniform and constant by employing a variety of techniques. The aerosol was injected against the wind tunnel flow so that sufficient mixing occurred. Further, a mixing plate was placed immediately behind the aerosol injection nozzle to disperse the aerosol effectively. Downstream of this plate, a turbulence-generating grid was used to reduce the flow disturbances caused by the presence of the disk so that both good mixing of the aerosol as well as flat velocity profile could be attained simultaneously. This arrangement was very effective throughout the range of wind velocities for which the experiments were performed.

4.8 Experimental procedure for sampling efficiency measurements

A standard operating procedure was adopted for testing the various samplers. The wind tunnel velocity was first fixed and the aerosol concentration mapped. The position of the injection nozzle and the distribution plate were adjusted using positioning screws on the sides of the wind tunnel until the concentration profile across the test section were flat to within ±5%. The glass beads were heated in an oven to a temperature of about 70° C. The entire wind tunnel section was cleaned and sprayed with anti-static and also silicon spray to prevent electric charge build-up and particle bounce. The APS was switched on and warmed up for about 2-3 hrs by which time the PMT voltage displayed on the instrument panel would have reached a steady value. The sampling flowrate and the sheath air flowrate were checked against the calibration values. All flowrates were measured using the bubble flowmeter. The sampler was greased and the inside of the sampling lines flushed with compressed air.

The temperature and humidity of the air in the wind tunnel were recorded. In case the humidity was too low (< 30%), the compressed air passing through the dust feeder was humidified using a bubbling column containing distilled water. Water traps were used to remove any water from entering in to the neutralizer. The neutralizer was flushed and cleaned with either water (done once a day) or air (done as often as possible) to prevent the accumulation of dust.

The sampler was mounted in the wind tunnel supported by the sampling lines. The sampling flowrate was again measured with the sampler in line with the APS to check for any leaks in the sampling system. Dust was injected into the wind tunnel and APS was used to monitor the aerosol concentration. It usually took about 15 minutes for the aerosol injection to stabilize, after which a steady output of aerosol is achieved. The concentration measured using the APS remained constant with number concentrations to within ±1% for up to three hours. Now the experimental setup was ready for sampling.

As already mentioned, each individual experiments was performed as a series of 11 runs (6 runs with sampler facing the freestream alternating with 5 runs with sampler placed at the desired orientation), after which the sampler was cleaned, sampling lines flushed and sampler regreased, ready for the next sequence.

Raw data files generated by the APS were analyzed using simple software routines written in Qbasic (Microsoft Corp. 1990 Ver.4.5).

4.9 What are we measuring?

The experimental procedures adopted here are significantly different from all other aerosol sampling experiments cited in the literature. The more common approach would involve using a set of monodisperse aerosols whose referfence concentration would be measured by isokinetic sampling. The concentration collected by the sampler of interest would be compared with that collected using the isokinetic probe, and the ratio would give aspiration efficiency directly. This procedure would be repeated for a range of particle sizes. Any aerosol deposited on the walls inside the sampler and the isokinetic probe would be accounted for by recovering the internal wall deposit from the sampler after each experiment. The whole process is very laborious and time-consuming.

Our experiments were markedly different, exploiting the advantages of the APS time-of-flight instrument. A polydisperse aerosol with a wide particle size distribution was used as test aerosol so that each run would produce aspiration efficiencies simultaneously for a whole range of particle sizes. But it is important to note that, in these experiments, the wall losses were not measured directly. The significance of this is elaborated in what follows below.

Discussion of what was actually measured in our experiments is based on Figure 4.11. From this, the aspiration efficiency (A_α) of the sampler for the given orientation of interest (α) is given by

$$A_\alpha = \frac{{}_1c_\alpha}{c_0} = \frac{c_\alpha}{{}_1c_{\alpha=0}} \cdot \frac{{}_1c_{\alpha=0}}{c_0} = \frac{{}_1c_\alpha}{{}_1c_{\alpha=0}} \cdot A_{\alpha=0} \tag{4.11}$$

where ${}_1c_\alpha$ is concentration in the plane of the inlet for the sampler oriented at an angle α to the freestream, ${}_1c_{\alpha=0}$ is the concentration there for the sampler facing the freestream, c_0 is the freestream concentration, and $A_{\alpha=0}$ is the aspiration efficiency of the sampler facing the freestream.

Although primary interest is in aspiration efficiency (since it is the most fundamental index of aerosol sampler performance), the basis of our measurement was in fact the *sampling efficiency* given, from Equation (4.4), by

$$E_\alpha = \frac{{}_{APS}c_\alpha}{c_0} \tag{4.12}$$

where ${}_{APS}c$ is the particle concentration reaching the APS for the orientation indicated. Since c_0 could not be determined directly in our experimental system, what was actually measured was the *sampling ratio* (H_α) given by

$$H_\alpha = \frac{{}_{APS}c_\alpha}{{}_{APS}c_{\alpha=0}} = \frac{E_\alpha}{E_{\alpha=0}} \tag{4.13}$$

The losses in the tube including the bend may be represented by the penetration P_{tube}, which - in the way in which the experiment was designed - remains constant for any value of α. So, again by reference to Figure 4.11, we have

$$H_\alpha = \frac{{}_2c_\alpha P_{tube}}{{}_2c_{\alpha=0} P_{tube}} = \frac{{}_1c_\alpha P_{entry}(\alpha)}{{}_1c_{\alpha=0} P_{entry}(\alpha=0)} \tag{4.14}$$

where ${}_2c$ is the particle concentration inside the sampler at the point where the flow has reached equilibrium (i.e., it does not 'remember' the external flow). In the above expression, unlike P_{tube}

that remains constant for all angles, P_{entry} depends on α since it depends on the coupling between the external and the internal flow. As a consequence, using Equation (4.11), we get

$$H_\alpha = \frac{{}_1c_\alpha \cdot P_{entry}(\alpha)}{{}_1c_{\alpha=0} \cdot P_{entry}(\alpha=0)} = \frac{A_\alpha c_0 \cdot P_{entry}(\alpha)}{A_{\alpha=0} c_0 \cdot P_{entry}(\alpha=0)} = \frac{A_\alpha \cdot P_{entry}(\alpha)}{A_{\alpha=0} \cdot P_{entry}(\alpha=0)} \tag{4.15}$$

so that

$$A_\alpha \cdot P_{entry}(\alpha) = H_\alpha \cdot A_{\alpha=0} \cdot P_{entry}(\alpha=0) \tag{4.16}$$

In this expression, we measure H_α and we may calculate both $A_{\alpha=0}$ and $P_{entry}(\alpha=0)$ for the samplers of interest based on current knowledge of sampling theory. This means that, what we have at the end are values for the combination $A_\alpha \cdot P_{entry}(\alpha)$. Since it is A_α which is of primary interest, then understanding the nature of the quantity $P_{entry}(\alpha)$ becomes of vital importance. This will become apparent in later sections of this report.

d_{ae} (μm)	SPP channel #	SPP correction factor	LPP channel #	LPP correction factor
5.42	36	15/16	63	1/16
5.83	37	14/16	64	2/16
6.26	38	13/16	65	3/16
6.73	39	12/16	66	4/16
7.23	40	11/16	67	5/16
7.77	41	10/16	68	6/16
8.35	42	19/16	69	7/16
8.98	43	8/16	70	8/16
9.65	44	7/16	71	9/16
10.4	45	6/16	72	10/16
11.1	46	5/16	73	11/16
12.0	47	4/16	74	12/16
12.9	48	3/16	75	13/16
13.8	49	2/16	76	14/16
14.9	50	1/16	77	15/16

Table 5.1 Table of correction factors recommended by TSI

d_{ae} (μm)	SPP channel #	SPP correction factor	LPP channel #	LPP correction factor
5.42	36	15/32	63	1/6
5.83	37	14/32	64	2/6
6.26	38	13/32	65	3/6
6.73	39	12/32	66	4/6
7.23	40	11/32	67	5/6
7.77	41	10/32	68	6/6
8.35	42	19/32	69	7/6
8.98	43	8/32	70	8/6
9.65	44	7/32	71	9/6
10.4	45	6/32	72	10/6
11.1	46	5/32	73	11/6
12.0	47	4/32	74	12/6
12.9	48	3/32	75	13/6
13.8	49	2/32	76	14/6
14.9	50	1/32	77	15/6

Table 5.2 Table of correction factors developed in our new approach

5. EXPERIMENTAL STUDY OF THIN-WALLED PROBES AT VARYING ANGLES TO THE WIND

5.1 Introduction

The thin-walled probe is the simplest form of aerosol sampler. Although it is the most extensively studied of all aerosol samplers (e.g., Belyaev and Levin, 1974; Durham and Lundgren, 1980; Jayasekara and Davies, 1980; Davies and Subari, 1982; Tufto and Willeke, 1982; Okazaki *et al.*, 1987; Wiener *et al.*, 1988; Hangal and Willeke, 1990; Grinshpun *et al.*, 1993; and many others, as reviewed by Vincent, 1989), relatively little data exist for the case where it is placed at large angles to freestream (> 90°). Most are limited to probes sampling at small orientations to the freestream (that is up to 90°). In the case of cylindrical thin-walled probes, the focus of research was on *isokinetic* sampling - that is, where $R = U/U_S = 1$ for which the sampling velocity and freestream velocity are the same - and the consequence of *anisokinetic* sampling ($R \neq 1$). Anisokineticity also occurs when the probe is oriented at an angle to the freestream, even with $R = 1$. It is this which is the primary subject subject of the part of our research described here, particularly in view of the insights it brings to blunt samplers which are the primary subjects of our inquiry.

5.2 Losses in thin-walled probes

In a general aerosol sampling system, sampling errors arise from a number of sources. With this in mind, overall sampling efficiency (E) may be described in general as a product of three terms, thus

$$E = A\ P_{entry} P_{tube} \tag{5.1}$$

where, as before, A is the aspiration efficiency, P_{entry} is the penetration efficiency for the entry (relating to the region close to the sampler inlet) and P_{tube} is the penetration efficiency for the rest of the the particle transport inside the sampler before collection. The main purpose of conducting experiments with thin-walled probes in the present study was to elucidate the nature of those internal losses, particularly P_{entry}. Whereas particle losses along the main length of the

tube (P_{tube}) in our blunt sampler experiments may be regarded as constant for all sampler orientations, P_{entry} will be strongly dependent on sampler orientation (α). By studying the thin-walled probe, where we have good knowledge of aspiration efficiency for α varying up to 90°, it was hoped to shed more light on the nature of P_{entry} which could then be applied to blunt samplers.

We begin the discussion of these losses by referring back to what was measured during the present research. From §4, it is seen that the primary measurement is the ratio between what is detected by the APS at sampler orientation α and that which is detetced by the APS when α = 0°. In this report, this is referred to as the *sampling ratio* (H_α)

$$H_\alpha = \frac{{}_{APS}C_\alpha}{{}_{APS}C_{\alpha=0}} \tag{5.2}$$

where ${}_{APS}C_\alpha$ is the number concentration of particles detected by the APS when the sampler is oriented at an angle α to the freestream, and ${}_{APS}C_{\alpha=0}$ is the concentration detected when the sampler is facing the freestream.

The particle concentrations at different parts of the sampling system are as shown earlier in Figure 4.11. So, reiterating Equation (4.16), we have

$$A_\alpha \cdot P_{entry}(\alpha) = H_\alpha \cdot A_{\alpha=0} \cdot P_{entry}(\alpha = 0) \tag{5.3}$$

Since P_{tube} in Equation (5.1) is constant, it is convenient for the purpose of the rest of this report to refer to $A_\alpha \cdot P_{entry}(\alpha)$ as E_α - that is, the sampling efficiency. Equation (5,3) then becomes the basis of our analysis. For simple blunt body samplers like thin-walled probes or spherical sampler like the one used in our experiments, $A_{\alpha=0}$ can be determined using Vincent's model (Vincent *et al.* 1986; Vincent, 1987 and 1989) for thin-walled probes or blunt samplers facing the freestream. In addition, the model of Okazaki and Willeke (1987) can be used to estimate $P_{entry}(\alpha=0)$. This means that, in order to determine A_α, the only remaining unknown is $P_{entry}(\alpha)$.

5.3 Rationale for new experiments with thin-walled samplers

The main objective of our new experiments with thin-walled samplers was to investigate the entry loss as a function of *St* and α. The new experimental data for H_α - as described by Equation (5.2) - were compared with theoretical values obtained using the existing theory for thin-walled probes (Vincent *et al.*, 1986; Vincent, 1989 for the aspiration efficiency; Okazaki and Willeke, 1987 for the entry loss when α = 0°). This enables the entry loss to be determined for a wide range of α-values. The new knowledge about entry loss may then be extended to the case of blunt samplers which was the main focus of the research as a whole. More specifically, re-arranging Equation (5.3), we get

$$P_{entry}(\alpha) = H_\alpha \frac{A_{\alpha=0} \cdot P_{entry}(\alpha = 0)}{A_\alpha} \tag{5.4}$$

where, for thin-walled probes, all the terms on the right hand side are either measured or can be calculated on the basis of current knowledge. Then, under the assumption that $P_{entry}(\alpha)$ is

controlled primarily by inertial effects, we look to fit the values obtained from Equation (5.4) in terms of an empirical function of just St and α.

5.4 Results and discussion

The new experiments for thin-walled probes were conducted at a single freestream velocity of 4 m/s and for a single sampling flowrate of 5 Lpm corresponding to an R-value of 1.52. The sampler was oriented in the horizontal plane at α ranging from 0° to 180° in steps of 15°. The sampler was also tested in the vertical plane where the effect of gravity either aids gravitational deposition on to the inner walls of the sampler or lowers it based on whether the sampler is facing up or down. This is discussed separately later in this report.

For fixed U and Q, the aspiration efficiency and the entry losses of the thin-walled probe sampling system are influenced by two independent parameters, namely α and St. Since, it is difficult to visualize the influence of both these parameters on two-dimensional graphs, the effects are discussed in terms of two separate sets of graphs; $E_\alpha = A_\alpha \cdot P_{entry(\alpha)}$ versus St and E_α versus α.

Sampling efficiency for angles up to 90°

The measured sampling efficiency ($E_\alpha = A_\alpha \cdot P_{entry(\alpha)}$, as in the modified definition given in Section 5.2) is plotted in Figure 5.1 as a function of St for α ranging from 15° to 180° in steps of 15°. On this graph, consider first the experimental data. For all cases, for $St < 0.1$, E_α decreases with increasing St. But as St increases beyond 0.1, and for all $\alpha < 90°$, E_α reverses its trend and increases. Hence, a minimum is introduced around $St = 0.1$, relatively independently of α. However, as the tube is oriented farther away from the freestream, the depth of the minimum increases. The recovery in E_α beyond the minimum depends strongly on the orientation of the sampler from the freestream and tends approximately towards $R\cos\alpha$ for large St. At this point we reiterate the expression for aspiration efficiency (Vincent, 1989)

$$A_\alpha = 1 + \left[1 - \frac{1}{1 + G(\alpha)\cdot St\cdot\left(\cos\alpha + 4\cdot R^{1/2}\cdot\sin\alpha\right)^{0.5}}\right]\left(R\cos\alpha - 1\right) \qquad (5.5)$$

where it is seen that A_α is a strong function of $R\cos\alpha$. It is therefore useful to consider E_α in this light. For angles less than 45°, $R\cos\alpha$ is greater than 1. Hence, beyond the minimum, E_α tends to increase towards $R\cos\alpha$ with increasing St. For angles greater than 45°, $R\cos\alpha$ is less than 1 and hence E_α rises just past the minimum. But it then falls back towards $R\cos\alpha$ with increasing St. Equation (5.5) shows that, if St is large, the aspiration efficiency, A_α, will also tend towards $R\cos\alpha$. So it is very reassuring to observe from our experiments that E_α too tends towards $R\cos\alpha$. This implies that the entry losses do not play a strong role at large St.

One feature of the results is the sudden disappearance of the minimum when $\alpha = 90°$. That is E_α does not recover as St is increased further. This is related to the fact that, at this orientation, there is no part of the internal wall that presents itself to the freestream for impaction. So here the mechanism of particle entry loss is suddenly different, as also noted by Tufto and

Willeke (1982) and Okazaki *et al.* (1987). In turn, any expression used to describe entry penetration at small angles will not hold good for 90°.

Yet another way of presenting the results is to plot E_α as a function of α for a range of *St*. As shown in Figure 5.2, this portrays how the influence of α becomes stronger as St increases. For small *St*, the influence of α is very weak, as might be expected since the particles are sampled easily even at large orientations from the freestream. But as particle size increases in the range up to $St = 0.2$, E_α falls with α increasing up to about 90°. Beyond 90° for this range of *St*, there is a small recovery in E_α. But for $St > 0.2$, there is no such rise. For larger *St*-values, E_α increases for α between 15° to 45°, a trend that corresponds to the $R\cos\alpha$ effect discussed earlier.

In Figures 5.1 and 5.2, the experimental results are also compared with existing theory (Vincent *et al.*, 1986) for thin-walled probes sampling at α up to 90°. It is seen that the experimental data agree best with theory only at 90°. But it is noted that what is shown also includes the entry losses.

The entry losses may be extracted empirically from the data by the application of Equation (5.4), using the Vincent *et al.* model for A_α and the Okazaki and Willeke model for $P_{entry}(\alpha = 0)$. Figure 5.3 shows the results of this exercise, in the form of P_{entry} versus *St* for α up to and including 90°. It is evident that P_{entry} is close to unity for all angles for *St* up to about 0.04. But beyond $St \approx 0.04$, P_{entry} drops with increasing *St*, more steeply the greater the value of α. This trend continues for all angles for *St* up to about 0.1. Beyond this, however, P_{entry} rises back up again to a value close to one. As already noted, this trend is broken sharply when $\alpha = 90°$. But for all $\alpha < 90°$, the observed non-monotonic behavior suggests that the entry loss is a result of two competing mechanisms. Although the exact nature of these mechanisms remains unclear, for present purposes they can be well characterized by fitting two monotonic empirical expressions. With this in mind, a mathematical function for P_{entry} was sought, using our experimental data, along with Tablecurve3D software (ver. 3.0, SPSS Inc., Chicago, IL). Using the data for α up to and including 75°, we obtained

$$P_{entry} = \left(1 - \left(c_1 \cdot \left(1 - \exp(-c_2\alpha)\right) \cdot \exp\left(-0.5 \cdot \ln\left(\left(\frac{St}{c_3}\right)\right)\right)\right)\right) \qquad (5.6)$$

where c_1, c_2, c_3 and c_4 are constant coefficients that need to be determined by non-linear regression. Best-fit was achieved with an R^2-value of 0.55.

It has emerged from this part of the research that the particle losses that occur close to the inside of the sampler are a significant feature which need to be better understood. At present we have only a qualitative knowledge of the mechanisms by which particles are deposited as a result of the coupling between the air flow outside the sampler and that inside the sampler. Consequently, it is realistic that we can only propose an empirical relationship to account for the roles of impaction and the *vena contracta* of the flow just inside the entry.

To support the qualitative reasoning which has been given above, it is appropriate to describe the actual patterns of the flow that might be expected. This is achieved by means of the sketches shown in Figure 5.4. An ideal condition where the coupling between the external flow

and the internal sampling flow is perfect is for isokinetic sampling where $R = 1$. Entry losses in this case are negligible since the flow remains undisturbed and the stagnation points separating the sampled for the un-sampled air flow lie at the tip of the sharp edged probe. On the other hand, for $R > 1$, the stagnation points lie inside the entry, as a result of which no *vena contracta* is formed inside the tube. Although, as suggested, the flow might separate **outside** the sampling orifice, this does not affect P_{entry}. For $R < 1$, however, separation does occur at the leading edge of the sampler entry and a *vena contracta* does form inside the entry. It is likely to be unstable. If the sampling flow rate is high so that $R << 1$, the stagnation point will move further over the external surface of the sampler, as a result of which the separated air volume in the *vena contracta* will be larger. Such a flow pattern will almost certainly play a significant role in particle deposition. But, at this stage, the nature of that role must remain speculative.

Orientation of the sampler to angles other than facing the freestream further complicates the flow picture, as shown in Figure 5.5. As the sampler orientation increases, the shape of the *vena contracta* will become increasingly asymmetric (and probably unstable). Impaction onto the inside wall will increase at first as the area of the inside projected to the upstream flow increases, then will decrease as that area falls back to zero when α approaches 90°.

Sampling efficiency beyond 90°

For α greater than 90°, our results show that E_α decreases sharply and monotonically with increasing St and does not recover (see Figure 5.6). Indeed, we see that particles are only sampled when St is small. The influence of α is slight, and the general pattern of behavior suggests that the entry losses should remain nearly constant for all $\alpha > 90°$.

5.5 Conclusions from this part of the research

It has been shown that the losses of particles to the internal walls of the sampler close to the entry are an important component of overall sampling efficiency. Such losses relate to the nature of the air flow in the region near the sampler entry associated with the coupling between the flow outside and inside the sampler respectively. Based on our new experimental results for the thin-walled sampling probe, an empirical expression for penetration through the entry regions of thin-walled probes has been developed. Important new insights have been gained into the factors influencing overall sampling efficiency, beyond aspiration efficiency itself. Although the situation is expected to be quantitatively different for the blunt samplers that are of primary interest in this research, it is expected that the same qualitative trends will pertain. So what has been learned in this part of the work will be valuable in discussing the overall sampling efficiencies of blunt samplers.

6. EXPERIMENTAL STUDY OF A SIMPLE BLUNT SPHERICAL SAMPLER AT VARYING ANGLES TO THE WIND

6.1 Introduction

An extension of a thin-walled sampler more realistic to the field of industrial hygiene is the simple symmetric spherical sampler that is the primary focus of our experimental research. Interest in understanding the performance of blunt samplers stems from the fact that most of the samplers used in industrial hygiene are indeed blunt samplers and, with a growing interest in occupational aerosol exposure assessment, understanding the physics behind the blunt body sampling would help design better samplers or help characterize the bias of existing samplers in relation to established health-based criteria.

As discussed earlier, aspiration of particles by a blunt sampler is much more complex than that using a thin-walled probe because the presence of the blunt sampler itself distorts the external flow around the sampler. An idealized spherical sampler was chosen for our experiments due to its simplicity in geometry and its symmetry. The experiments focussed on sampling at large angles to the freestream, something that has not been widely studied before for blunt samplers but very relevant to typical workplace sampling.

6.2 Preliminary results and discussion

Before moving on to the main body of the research, preliminary tests were conducted to investigate the possible roles of electrostatic effects, freestream turbulence and particle bounce/blow-off. In addition, the effect of freestream velocity profile on the concentration of the aerosol and its subsequent influence on the aspiration efficiency were also studied.

Effects of air velocity and aerosol concentration profiles

Measurements were carried out for two cases: (a) when the velocity and concentration profiles were uniform, and (b) when the velocity and concentration profiles were intentionally made non-uniform by misaligning the test aerosol injection nozzle. Figure 6.1 shows the velocity profiles along the horizontal axis of the wind tunnel cross section for the two cases, in which the '+' and '-' designations represent distances on either side of the center-line. Figure 6.2 shows a three-dimensional plot of the aerosol concentration profile for uniform conditions, in which the spatial distribution is shown also as a function of particle aerodynamic diameter. Here, the aerosol was measured using the APS as already described. However, the spherical sampler was replaced by a simple thin-walled probe, placed facing into the wind.

In order to draw the distinction between uniform and non-uniform conditions, Figures 6.3 and 6.4 show the measured concentration profiles for those conditions respectively at ± 5 cm (from the wind tunnel centerline). The error bars denote one standard error from the mean. If the velocity and concentration profiles had been uniform, irrespective of particle size, then there should be no significant difference between the aspiration efficiency at $\alpha = +30°$ and $-30°$ in the horizontal plane. Figure 6.5 contains results for E_α for the spherical sampler for conditions

corresponding to uniform velocity and aerosol concentration distributions, and these show no significant differences between the two orientations. The situation is markedly different, however, for non-uniform conditions, for which Figure 6.6 shows E_α again for $\alpha = \pm 30°$ under non-uniform conditions. Here, while the differences in E_α for the two positions are insignificant for small particles, they become substantial as particle diameter increases.

From Figure 6.1, it is seen that the velocity profile has a gradient such that higher velocities are found in the positive direction (from the center-line) than in the negative direction. At ± 5 cm from the centerline, the normalized velocities are $v_+/v_{center} = 1.04$ and $v_-/v_{center} = 0.95$ respectively. From Figure 6.3 we see that higher concentrations are found in the negative direction than in the positive. For particles with $d_{ae} = 15$ μm, the normalized concentrations are $c_+/c_{center} = 1.04$ and $c_-/c_{center} = 1.28$ respectively. From Figure 6.6 we see that E_α is higher for $\alpha = +30°$ than for $\alpha = -30°$. For $d_{ae} = 15$ μm, the E_α-values at those locations are 1.4 and 0.8 respectively.

In order to qualitatively explain these results, we go back to the basic definition of aspiration efficiency given by

$$A = \frac{c_a U_a S_a}{c_0 U S_0} \tag{6.1}$$

where it is assumed that the particle velocity is equal to the air velocity, and that c_0 and U are averages over the area S_0 where the limiting streamsurface intersects the incident plane. When there are concentration and velocity gradients in the incident plane, then for different orientations of the sampler, the area S_0 occupies different regions in space, leading to different values of c_0 and U. Thus $A_{\alpha=30}$ and $A_{\alpha=0}$ must be defined as

$$A_\alpha = \frac{c_a U_a S_a}{c_{0x} U_x S_{0x}} = \frac{c_a Q_s}{c_{0x} U_x S_{0x}} \tag{6.2}$$

and

$$A_{\alpha=0} = \frac{c_{a=0} Q_s}{c_{0centre} U_{centre} S_{0centre}} \tag{6.3}$$

where Q_s is the sampling flowrate and the subscript "x" refers to the position in the incident plane. Dividing Equation (6.2) by (6.3) and rearranging, we obtain

$$\frac{c_a}{c_{\alpha=0}} = \left(\frac{A_a}{A_{\alpha=0}}\right) \Big/ \left(\frac{c_{0x}}{c_{0centre}} \frac{U_x}{U_{centre}} \frac{S_{0x}}{S_{0centre}}\right) \tag{6.4}$$

Since all streamlines within the limiting streamsurface enter the sampling orifice, $U_{center}S_{0center} = U_xS_{0x}$, so that

$$\frac{c_a}{c_{\alpha=0}} = \left(\frac{A_a}{A_{\alpha=0}}\right) \Big/ \left(\frac{c_{0x}}{c_{0centre}}\right) \tag{6.5}$$

Thus the greater the value of $c_{0x}/c_{0center}$, the lesser is the value of $c_a/c_{\alpha=0}$. For example, when $c_{0x}/c_{0center} = 1.28$ (at $x = -5$ cm from the center line), then $c_{\alpha=-30}/c_{\alpha=0} = 0.8$, and when $c_{0x}/c_{0center} = 1.04$ (at $x = +5$ cm from the centerline), then $c_{\alpha=+30}/c_{\alpha=0} = 1.4$. Only if the concentration gradient in the incident plane is uniform is the relationship given by Equation (4.4) valid. Otherwise Equation (6.5) should be used.

Overall from the preceding, the message is that, in wind tunnel experiments to investigate the performances of aerosol samplers, careful attention should be given to ensure that the air velocity and test aerosol concentration profiles over the working region are as uniform as possible.

Effect of aerosol charge

Measurements were performed for two electrical conditions: (a) with the aerosol neutralized to close to Boltzmann equilibrium before injecting it into the wind tunnel, and (b) with the aerosol injected directly into the wind tunnel without neutralization. For the first case, the aerosol sampler and the wind tunnel were grounded. For the second case, they were not. Figure 6.7 shows measured results for E_α for the spherical sampler oriented at 30° to the freestream, with and without the aerosol being neutralized. It is seen that there is no detectable difference between the two cases for small particles (d_{ae} < 10 μm). For larger particles, however, E_α tends to be slightly - but consistently - lower when the aerosol is not neutralized. This tendency is consistent with previous experimental results (Johnston *et al.*, 1987) and modeling (Vincent, 1989) which show that the net effect of electrostatic forces between charged particles and a charged sampler is to cause a lowering in sampling efficiency.

In general, it is considered prudent that, in laboratory studies of aerosol sampler performance like those reported here, the test aerosol should be neutralized.

Effect of freestream turbulence

It is inevitable that, in virtually all practical aerosol sampling situations, the motion of the surrounding air will be turbulent. Further, the intensity and scale will vary greatly and, in general, will not be known. Therefore, while conducting laboratory experiments to investigate aspiration efficiency, it is usually not feasible to try to match freestream turbulence conditions to those that would be met in practice. However, there is some evidence that, within certain limits, the effect of freestream turbulence on aspiration efficiency is small (Vincent *et al.*, 1985). Nevertheless, in wind tunnel studies of aerosol sampler performance, it is important to maintain freestream turbulence at conditions that are clearly defined.

In our present experiments, we considered the possibility that freestream turbulence might influence aspiration efficiency. As described earlier, turbulence with well-defined intensity and length scale were generated by the use of two lattice-type screens providing values of Λf = 0.004 and 0.006 respectively, where Λf is the freestream turbulence parameter. These conditions represent ranges of conditions of turbulence intensity and length scale that, although not as wide as might be encountered in practical sampling situations (since they are inevitably limited by the size of the small wind tunnel used), are sufficient to reveal any significant effects of turbulence.

Figure 6.8 shows results for E_α for the spherical sampler for the two cases, and these indicate that there are no significant differences. This is broadly consistent with the earlier experimental results of Vincent *et al.*

Effect of particle bounce and blow-off

The possibility of effects due to secondary aspiration was investigated in this research, to examine whether there were any unwanted contributions to aspiration efficiency from particle bounce or blow-off from the external surfaces of the sampler. This was achieved by conducting experiments to determine E_α for the spherical sampler both with and without the external surfaces of the sampler being coated with silicone grease. The results are shown in Figure 6.9, and it is seen that there are no significant differences. This is generally reassuring. In general, however, as for the interfering factors discussed in the preceding, it is considered prudent to grease the external surfaces of aerosol samples for the purpose of research studies where the question of secondary aspiration is not the subject of the investigation.

6.3 Sampling efficiency measurements for the spherical blunt sampler

The data

We now move on to describe the main results from this part of the study. The matrix of test conditions studied is shown in Table 6.1. Once again, it is emphasized that what was measured is

$$E_\alpha = A_\alpha \cdot P_{entry}(\alpha) \qquad (6.6)$$

However, unlike thin-walled probes where we had a valid, well-tested theory for blunt samplers for all orientations up to and including 90°, the theory for blunt body sampler is well-tested only for α = 0°, 90° and 180°. In turn, therefore, we cannot so easily extract $P_{entry}(\alpha)$ from our experimental results.

E_α is plotted against St for a range of α and each set of graphs correspond to a particular value of R. Figure 6.10 shows a set of graphs for R = 0.38 and r = 0.1, where the error bars correspond to the calculated standard error. Comparison is made with the theory of Tsai *et al.* (1995b) and the earlier model of Vincent (1987) (see Section 2). It is noted again that the Tsai *et al.* model is an interpolation of what has been well-established for A_0, A_{90} and A_{180} (Tsai and Vincent, 1993) for all α up to and including 180°. From Figure 6.10 it is seen that agreement between the Tsai *et al.* model and the experimental data is surprisingly good, even though (it should be stressed) we are comparing the calculated aspiration efficiency (A_α) with the measured sampling efficiency (E_α). Qualitatively, the agreement is best at 30° and worst at 60°. It is also evident that the α greater than 90°, the difference between theory and experimental data increases with increasing St. For small St, there is a very good agreement with theory and E_α is close to 100%.

Figures 6.11a and b illustrate the effect of α on E_α over a range of St for R = 0.76 and r = 0.1. It is evident that entry losses seem to be significant in this case, and are responsible for the non-monotonic behavior of E_α. There is good agreement with both models only for small St. Beyond 90°, the measured dependence of E_α on α is weak, and the agreement between the measured E_α and the Tsai *et al.* model for A_α is very good. It is notable that both the data and the Tsai *et al.* model show constant A_α for $\alpha > 90°$ and beyond. Similar trends were also observed for R = 1.52, as seen in Figures 6.12a and b.

Figures 6.13a and b and Figure 6.14 show the dependence of E_α on α over a range of St for R = 2.28 and r = 0.1. Agreement with the Tsai *et al.* model is good for small α and for α close to 90°. But the departure from theory first increases with increasing α and then decreases back down again as α approaches 90°. Beyond 90°, the effect of α is negligible.

Figure 6.14 illustrates the dependence of E_α on α over a range of St for R = 3.8 and r = 0.1. The observed trends are similar to those for R = 2.28. Figure 6.15 shows the trends for R = 1.52, this time with r = 0.2. In comparison with Figure 6.12 for R = 1.52 and r = 0.1, the non-monotonic behavior indicative of entry losses is less apparent. From this, it would appear that P_{entry} is dependent on r, and hence that the value of r influences the coupling between external flow and the internal flow near the sampler entry.

Figures 6.16 to 6.21 show the same data replotted in the form of E_α versus α for various R-values and St-values and for the two r-values. The general trend for all values of R is that, for small St, E_α remains close to 1 for all sampler orientations. For larger St, E_α falls with increasing α up to about 90°. But beyond 90°, E_α rises again. As St increases further, the magnitude of the observed 'dip' in E_α increases, while the corresponding rise beyond 90° decreases. Eventually, as St increases still further, the inertial forces become strong enough that E_α falls rapidly to zero as α approaches 90° and does not rise again. This may be viewed as a consequence of the removal of larger particles by impaction onto the leading face of the blunt body of the sampler. In this event, it is not surprising that E_α is not strongly dependent on α, and it makes little difference whether the inlet is close to 90° or close to 180°. It is evident from Figures 6.19 and 6.20 that the value of R also plays a significant role. In fact, for large St there is a tendency for $E_\alpha \rightarrow R\cos\alpha$, consistent with the Tsai *et al.* model. For large values of R (2.28 and 3.8), and small values of α, $R\cos\alpha$ is greater than 1.

From the above discussion it is evident that the effects of orientation and St on E_α are strongest at relatively small angles to the freestream. It is therefore worth noting that the entry loss is most significant at small angles and gradually becomes less significant for α close to 90° (Okazaki and Willeke, 1987).

It has been identified from thin-walled probes studies (Tufto and Willeke, 1982) and blunt body sampler studies (Tsai and Vincent, 1993) that A_{90} is a strong function of $St \cdot R^{0.5}$. If this is true, then all the A_{90} data should collapse towards a single curve represented by $St \cdot R^{0.5}$. With this in mind, Figure 6.22 shows a plot of all the E_{90} data plotted in this way, and a good collapse is obtained confirming that E_{90} is indeed a unique function of $St \cdot R^{0.5}$. This in turn suggests that the entry losses are small (and hence $P_{entry} \approx 1$) for α = 90° - otherwise there would have been strong other dependences clearly visible. Similarly, Tsai and Vincent identified that A_{180} should be a unique function of the combination $St \cdot r^{-1.29} \cdot \phi^{0.33}$. Figure 6.23 shows all the new E_{180} data plotted against $St \cdot r^{-1.29} \cdot \phi^{0.33}$. Again a very good general collapse was obtained, even though some departure from the Tsai and Vincent model is evident at large St.

Another approach is to compare our measured E_α with the Tsai and Vincent model, for α = 90° and 180° and different values of R. In Figures 6.24 and 6.25, E_α is plotted against St for different values of R. The trends for E_α are consistent with the results of Okazaki *et al.* (1987) for thin-walled probes at α = 90°, which showed that A_{90} decreases as R increases.

Discussion

As has emerged from the preceding, all our new measurements pertain to E_α while what we would really like to know is A_α. In the case of thin-walled probes (see the preceding §5), P_{entry} was determined empirically from the experimental measurements of E_α using well-tested theory for aspiration efficiency. But, in the case of the blunt spherical sampler, both P_{entry} and A_α are unknown over the range of α of interest. In order to overcome this difficulty, we use knowledge gained from our study with thin-walled probes, and apply it judiciously to the blunt sampler results.

In our approach, it was assumed that the general form of the expression for P_{entry} obtained for the thin-walled probe should hold for the blunt spherical sampler, but with modified coefficients reflecting the different geometry. The may be obtained by non-linear least-squares regression. In addition, it was assumed that $P_{entry(\alpha=0)}$ can also be modelled using the Okazaki and Willeke model as we did for the thin-walled probe. With this in mind, the starting point for modelling these data is to apply the form of the original simple blunt body sampler model (Vincent, 1987) together with the form of the expression for P_{entry} developed for thin-walled probes. For the first part, we have

$$A_\alpha = \left(1+\left(1-\frac{1}{1+G_1\cdot St\cdot\frac{\delta}{S}\left[\cos(\alpha)+4\phi^{0.5}\frac{S}{D}(\sin(\alpha))^{0.5}\right]}\right)\left[\frac{S^2}{D^2\phi}\cos(\alpha)-1\right]\right)\times \left(1+\left(1-\frac{1}{1+G_2\cdot St\cdot\phi\cdot\frac{D^2}{S^2}}\right)\left[\frac{\delta^2}{S^2}-1\right]\right) \tag{6.7}$$

For the second part, we have from Equation (5.8)

$$P_{entry} = \left(1-r^{c1}R^{c2}\alpha^{c3}\left(c_4*\left(1-\exp(-c_5\alpha)\right)\times\exp\left(-0.5\cdot\ln\left(\left(\frac{\left(\frac{St}{c_6}\right)}{c_7}\right)\right)\right)\right)\right) \tag{6.8}$$

It is recalled in Equation (6.7) that S is the width of the stagnation region on the surface of the blunt sampler, separating the sampled from the un-sampled air flow. For the spherical blunt sampler, Vincent (1987) proposed

$$S = B\phi^{1/3}Df(\alpha) \tag{6.9}$$

where B is the sampler bluntness and its variation with α is unknown. However S can be estimated from the measurements of S_1 and S_2 obtained during the flow visualization experiments described in §3. Thus, from the empirical relationship given by Equation (3.14), we have

$$S = \sqrt{S_1 S_2} = \left\{ \left(\sin\left(\frac{\phi}{3}\right)^{1/3} \right)^2 \cdot \left(0.61 + 0.55\alpha^2 - 0.2\alpha^3\right) \right\} \cdot D \qquad (6.10)$$

Combining Equations (6.7) to (6.10), the unknown coefficients c_1, c_2, c_3, c_4, c_5, and c_6 were found by non-linear regression to be $c_1 = 0.608$, $c_2 = 0.127$, $c_3 = -0.02$, $c_4 = 1.122$, $c_5 = 0.602$ and $c_6 = 2.11$. Hence, an empirical equation for E_α was developed and is applicable within the range of experimental conditions for which experimental data exists. It is evident from the empirical fit that the losses are a complex function of St, R, r and α.. The comparisons of the model with experimental data are shown in Figures 6.26 to 6.31.

$R = 0.76$ $r = 0.1$ $\delta = 0.635$ cm	$2 \times 10^{-4} < St < 0.9$ $Q_S = 5$ lpm $U = 2$ m/s	$R = 1.52$ $r = 0.1$ $\delta = 0.635$ cm	$4 \times 10^{-4} < St < 1.8$ $Q_S = 5$ lpm $U = 4$ m/s
$R = 0.38$ $r = 0.1$ $\delta = 0.635$ cm	$4 \times 10^{-4} < St < 1.8$ $Q_S = 20$ lpm $U = 4$ m/s	$R = 2.28$ $r = 0.1$ $\delta = 0.635$ cm	$6 \times 10^{-4} < St < 2.7$ $Q_S = 5$ lpm $U = 6$ m/s
$R = 3.8$ $r = 0.1$ $\delta = 0.254$ cm	$4 \times 10^{-4} < St < 1.8$ $Q_S = 5$ lpm $U = 4$ m/s	$R = 1.52$ $r = 0.2$ $\delta = 0.635$ cm	$4 \times 10^{-4} < St < 1.8$ $Q_S = 5$ lpm $U = 4$ m/s

Table 7.1 Test Matrix for Current Experiments

7. STUDIES OF THE EFFECT OF GRAVITY ON SAMPLING EFFICIENCY

7.1 Results and discussion for sampling in the vertical plane

Sampling efficiency for the spherical sampler ($r = 0.1$) was measured along the vertical plane to study the effect of gravity on the inlet losses. Measurements were made at three different freestream velocities (corresponding to $R = 0.76$, 1.52 and 2.28) for α covering the entire range up to 180°. The sampling protocol was identical to the experiments along the horizontal plane. The experimental results for $R = 0.76$ are shown in Figure 7.1a for the sampler facing downwards and Figure 7.1b for the sampler facing upwards. They may also be compared with the corresponding results for the horizontal plane (from Figure 6.11a). From this it is evident that, for the sampler facing downwards, E_α is comparable with that for the sampler with its entry always in the horizontal plane. But there is a marked difference for the sampler facing upwards, suggesting an effect associated with the entry losses described earlier. These results are in broad agreement with Hangal and Willeke for thin-walled probes, who found that losses for the thin-walled probe facing downwards was consistently lower than for thin-walled probe facing upwards. For the sampler facing upwards, the maximum in sampling efficiency obtained at $St \approx 0.4$ was found to be much more pronounced than for the sampler facing downwards or for the experimental data for the sampler entry moving through the horizontal plane. E_α is also seen to be lower for large St for the sampler facing upwards than for facing downwards. The minimum at $St \approx 0.1$, however, remains unchanged for a given α for sampler facing both upwards or downwards, and is also comparable with the results for horizontal plane. Hence, it can be

inferred that the minimum for E_α is caused by a component of inlet losses that depends only on α and does not depend on gravity. Similarly, the maximum at $St \approx 0.4$, is strongly depend on both α and gravity. For $\alpha = 90°$, there is no difference for the sampler facing either upwards or downwards, and is comparable with the sampler placed at $\alpha = 90°$ for the horizontal plane. This confirms that the inlet losses are strongly dependent on whether or not the sampler is facing into the freestream (which is not the case when $\alpha = 90°$).

Similar trends were observed for results for $R = 1.52$ (Figure 7.2a and b). $E_\alpha > 1$ for large St when the sampler was facing downwards. It is recalled that $A > 1$ for this case as $St \rightarrow \infty$. But the reason why $E_\alpha > 1$ for increasing St, especially for small α, may be due to the fact that inlet losses may be greater when the sampler is facing the freestream ($\alpha = 0°$), as a result of which H_α and hence E_α will be greater than 1. For the sampler facing upwards and for correspondingly increasing St, E_α is seen to decrease with increasing St. It is interesting to note that, for $\alpha \geq 90°$ (Figure 7.3a and b), there is no difference between sampling up or down or on the vertical or horizontal plane at a given α. The only mechanisms whose effects change over all these conditions are direct wall impaction and gravitational settling. Based on the comparisons with the horizontal and vertical plane data for identical conditions of α and R, it is evident that only particles corresponding to large St are influenced by inlet losses. This trend is dominant only for small orientations from the freestream. Similar trends were also observed for $R = 2.28$ and orientations up to 90° and up to 180° respectively (Figures 7.4a and b and Figures 7.5a and b). For all cases along the vertical plane, the deviation from existing models for A is considerably greater. The agreement is good for small St, but deteriorates with increasing St. This provides further evidence that the deviation of E_α from A is due to the influence of inlet losses. Further, the standard errors for data along the vertical plane are larger than for the sampler entry moving in the horizontal plane for the same conditions.

Similar experiments were carried out for the thin-walled sampler, and the results are shown in Figures 7.6a and b. These show that, unlike for the blunt spherical sampler, there was **no** difference between upwards and downwards facing.

7.2 Conclusions

In summary, there is a marked difference between sampling efficiency for the spherical sampler facing upwards and facing downwards respectively. Such a difference was not observed for thin-walled probes sampling up or down. These difference make it clear that sampling losses are significantly influenced by the flow distortion created by the presence of the blunt sampler body. In the case of thin-walled probes, even when sampling anisokinetically, the external flow around the sampler is not as distorted as it would be by the spherical sampler. So particles close to the sampling inlet of the thin-walled probe are not subjected to the same degree of deceleration arising from the presence of the sampler, and so are not as susceptible to the influence of gravity. Consequently, E_α is more sensitive to changes in α along the vertical plane for spherical sampler than for thin-walled probes.

8. STUDIES OF THE EFFECT OF ASYMMETRY ON SAMPLING EFFICIENCY

8.1 Results and discussion

As mentioned earlier, spherical sampler is highly idealized sampler and the only sampler that closely matches a sphere is a human head. Although the purpose of this research involved understanding the influence of different parameters on sampling efficiency, and not so much simulating real-life samplers, some experiments were conducted to mimic one such case. To idealize this situation, the human body was considered to be a three-dimensional flat rectangular body, and the sampler mounted asymmetrically on the lapel of the human body as a sampling orifice on this idealized rectangular body. With this in mind, the 80 mm x 80 mm x 30 mm sampler, with the offset entry, as described earlier in Section 4.4 was used.

For the sake of comparison, the performance of this sampler was compared with that of a rectangular body with sampling orifice located symmetrically at the geometric center of the face of the largest rectangle. It is noted that the aspiration efficiency of a rectangular sampler cannot yet be calculated from theory. So only the sampling ratio ($E_\alpha / E_\alpha = 0$) is accessible.

Measurements were made for orientations up to and beyond $\alpha = 90°$ (Figures 8.1a and b respectively). It is evident that there is little difference between the sampling ratios for the two cases.

Although it is hard to infer the nature of sampling losses from sampling ratio alone, it is evident, from the appearance of the minimum and maximum in the data as plotted in Figure 8.1a, that sampling losses are significant in both the cases. But for the limited sampling conditions studied (R = 1.52), the losses seem to be less than for the spherical sampler. As expected, the sampling ratio does not change significantly for $\alpha > 90°$, where the trends for both the symmetric and asymmetric samplers also continue to be identical.

8.1 Conclusions

The results of this limited investigation into the importance of asymmetry on sampler performance suggest that the performance of a personal in a real-life personal sampling situation would not be significantly influenced by where the sampler is mounted on the worker.

9. STUDIES OF AEROSOL SAMPLING EFFICIENCY IN CALM AIR

9.1 Introduction

As is apparent from much of what has gone before in this report, most of the previous studies into the mechanics of aerosol sampling have concentrated on the performance of aerosol sampling devices in moving air. This is because it has long been held that the ambient air in workplaces and elsewhere is in motion. Indeed, in most situations this is a reasonable assumption. The question at low windspeeds pertaining to many workplaces is: how low does the windspeed have to be in order for the assumption of 'calm air' to hold? Ogden (1983) examined this theoretically, and provided some useful quantitative guidelines, from which it may be

deduced that the widespread use of the 'calm air' assumption is indeed reasonable much of the time. However, as has recently been pointed out, there are some situations, perhaps more widespread that had previously been thought, where windspeeds are of the order of a few 10s of cm/s, and where the assumption of 'calm air' is therefore more appropriate (e.g., Aitken *et al.*, 1998).

In an aerosol sampling situation where there is relatively little air movement, the theoretical models developed for the moving air case may not hold. Here, because there is no external air movement, particles are brought into the region of the sampler not by convection in the freestream (as is assumed in the moving air scenario) but by gravitational settling. Sampling efficiency is now governed by a combination of inertial forces (in the airflow caused by the aspiration action of the sampler itself) and, importantly, gravitational forces.

A number of theories have been proposed for calm air sampling, but there is a lack of experimental evidence against which to validate them. Only a small number of such experimental studies have been reported. Indeed, the studies reported by Kaslow and Emerich (1973 and 1974) and Yoshida *et al.* (1978) appear to be the only ones that have been carried out, and neither of those has been published in the western peer-reviewed literature. This is surprising in the light of the potential importance of calm air sampling to aerosol measurement, especially in indoor air situations.

One of the reasons for the lack of experimental enquiry into this aspect of aerosol sampling may be the degree of difficulty of the experiments that are needed. There are two main problems. The first is in finding a means of measuring the reference concentration in the calm air environment since the concept of isokinetic sampling (which has been widely used for making reference aerosol measurement sin moving air) has no meaning in the calm air scenario. The second relates to the fact that, in studies of aerosol sampling in moving air, compressed air may be used to disperse the test aerosol with minimal agglomeration, and the effects of the injection of the compressed air itself can be minimized by appropriate aerodynamic design. In the case of calm air, such use of compressed air is severely restricted since no disturbance to the calm air conditions in the test chamber can be tolerated. Such difficulties as those alluded to impose significant challenges to the conduct of experiments into the physics of calm air sampling.

With the preceding in mind, the goals of the part of the study concerned with calm air were limited to (a) developing an experimental objective which would eliminate the need for a direct reference concentration measurement, and (b) introducing a well-defined test aerosol with the minimum of disturbance. Thus the study reported in this report therefore became primarily an exploratory experimental investigation to develop methods by which to examine how the various factors mentioned above effect sampler performance in a calm air environment.

9.2 Background

In the case of a moving air environment, the predominant influence on particle motion is assumed to be inertia, and the effects of gravity are usually minimal in comparison and so are often neglected entirely. In the calm air case, however, the only air movement is that provided by the suction of the sampling device itself. Here, a velocity gradient occurs around a sampler, where the local velocity far away from the suction will tend towards zero, but will progressively increase as the distance to the sampler decreases. In this system, the force of gravity on airborne particles exhibits a much greater effect on particle motion, in particular in bringing particles into

the region of the sampler where they can come under the influence of the aspirating air flow. Thus particles far away from the sampler will fall vertically purely under the influence of gravity, undisturbed by the suction, But in the immediate vicinity of the sampler, they will be drawn towards the inlet, and so inertial forces will also become influential. As a result of these forces, a gradient of particle trajectories will occur, with the *limiting particle trajectory* separating the trajectories of all particles that enter the inlet directly from those that do not. As shown in Figure 9.1, this limiting particle trajectory encloses an area, $a = a''$, above the sampler where the particles are undisturbed by the suction of the sampler. For a downwards-facing cylindrical nozzle, this area is circular in cross-section, and has a circular inner boundary corresponding to the 'shadow' created by the presence of the nozzle itself (Vincent, 1989). The measure of aspiration efficiency is the extent of the difference in a associated with inertial forces. Thus, if the inertial effects on the particles are negligible, $a = a_0$. Aspiration efficiency (A) is defined for calm air as (Vincent, 1989)

$$A_C = c_S/c_0 = a''/a_0 \tag{9.1}$$

where c_0 is defined as the particle concentration at a large distance from the sampler and c_S is that entering the sampler. This leads

$$A_C = v_S a''/Q \tag{9.2}$$

where v_S is the particle settling velocity and Q is the sampling flowrate.

Levin (1957) derived an expression of aspiration efficiency for calm air sampling by considering a simplified case in which the sampler is treated as an infinitesimally small point sink. This approach eliminates the problems of the geometry and orientation of the sampler, and allows for an analytical k_L solution from potential flow theory. Levin introduced the dimensionless quantity, given by

$$k_L = (\tau v_S)/l_S \tag{9.3}$$

where l_S is the distance to the point on the limiting trajectory where the settling velocity of a particle is just balanced by the upwards suction induced by the point sink (also called the "saddle point"), and τ is the particle relaxation time (see Figure 9.2). Levin's expression for aspiration efficiency is

$$A_C \sim 1 - 0.8k_L + 0.008k_L^2 \text{ for } k_L << 1. \tag{9.4}$$

This expression shows that aspiration efficiency is a function of the effects of inertia; in particular, A_C decreases as inertial effects increase.

The application of this formula is limited because the effects of particle impaction on a sampler body have not been considered. The expansion of this theory to a tube with a finite width requires consideration of the flow distortion around the sampler as well as the particle characteristics. These factors are embodied in the Stokes' number, which is expressed here in a form relevant to the calm air situation: thus

$$St_C = (\tau U_S)/\delta \tag{9.5}$$

where U_S is the velocity at the entry of the sampler and δ is the dimension of the sampler inlet. This quantity is equivalent to the k_L in Levin's theory. The other important parameter for determining aspiration efficiency in calm air sampling is the equivalent velocity ratio (R_C) which accounts for the particle settling velocity and also includes the entry velocity, thus

$$R_C = v_S/U_S \tag{9.6}$$

Kaslow and Emerich (1973 and 1974) calculated the aspiration efficiency of a thick-walled tube for three different sampler orientations (i.e., vertically downwards, vertically upwards, and horizontally sideways). They found in general that small particles were sampled efficiently over a wide range of sampling conditions, whereas larger particles with greater inertia and gravitational effects were sampled less efficiently. They also conducted experiments in which particle trajectories were viewed and photographed under intense flash lighting from a carbon arc, and successfully executed one of only two calm air sampling experiments ever reported.

Yoshida *et al.* (1978) performed the only other calm air experiments. They also conducted both theoretical (numerical) studies for two sampler orientations (facing up and facing down), two particle sizes and two sampler sizes. They obtained good agreement between the experimental and theoretical values of aspiration efficiency. In addition, the efficiency was higher when the sampling probe was facing downwards than when it was facing upwards. Increases in inertial and gravitational effects were again seen to cause decreases in sampling efficiency.

Agarwal and Liu (1980) carried out a numerical simulation of the problem of aspiration for an upwards-facing thin-walled tube. They showed that the aspiration efficiency depended on St_C and R_C. Aspiration efficiency was found to decrease with an increase in the product of these two dimensionless parameters. From this, they were able to determine that aspiration efficiency was 100% ± 5% provided that

$$St_C \cdot R_C < 0.05 \qquad (9.7)$$

This so-called "*Agarwal-Liu criterion*" for representative sampling in calm air is less restrictive than the earlier "*Davies criterion*" (Davies, 1968) which, based on semi-quantitative considerations of the role of inertia and gravity, required

$$St_C < 0.016 \text{ and } R_C < 0.04 \qquad (9.8)$$

In order to locate the position immediately below the entrance to the downward-facing tube where the particles are just sampled (labeled as the "saddle point" in Figures 9.1 and 9.2), we may consider the flow velocity on the axis of the tube entry imparted from the suction of the sampler. From Dallavalle (1952), the axial velocity varies according to

$$v_x = Q / (10x^2 + A) \qquad (9.9)$$

where Q is the sampler flowrate, A is the area of the sampler orifice, and x is the distance from the tube inlet. By applying this to calm air sampling, this is equal to the point where the particle settling velocity is just balanced by the suction of the sampler. If x is now placed equal to l_S, then

$$v_S = Q / (10l_S^2 + A) \qquad (9.10)$$

leading to

$$12.7 (l_S/\delta)^2 = U_S/g\tau - 1 \qquad (9.11)$$

From this is clear that a plot of $(l_S/\delta)^2$ versus $(U_S/g\tau)$ should be a straight line. Equation (9.11) therefore should serve as the theoretical basis by which the validity of the current study will be determined.

9.3 Experimental

The test chamber

The experiment was conducted in a purpose-built enclosed calm air chamber of rectangular cross section, approximately 1.5 m long, 1.1 m wide and 1.5 m high (see Figure 9.3). The chamber had a narrow slit on one side to allow for the illumination of the dust, and another at the top for dust injection. A thin-walled probe of diameter (δ) 0.635 cm was mounted in the chamber, where it could be arranged to be facing directly upwards or directly downwards as desired. The flow through the sampler was provided by a vacuum pump, and a precision rotameter was placed in line to measure sampling flowrate.

Test aerosol generation

The dusts used in the experiment were relatively monodisperse fused alumina powders of varying average particle diameters. The average particle diameters and standard deviations for aerosols generated from these powders are given in Table 9.1 (taken from Gomes, 1994).

One of the biggest challenges in performing calm air sampling studies is the introduction of the aerosol into the test environment. The aerosol must be generated in such a way that the air in the chamber is not disturbed (i.e., no extraneous motions are introduced), the degree of agglomeration and electric charge effects are minimized, and the particles fall vertically parallel to one another immediately after dispersion. Several approaches were tried, but in the end a very simple method was considered to be the most promising and was adopted. In this method, the dust was simply allowed to fall under gravity from the top of the chamber. When introduced in this manner, the dust was given minimal initial velocity, and would have sufficient time and distance to reach the terminal settling velocity before encountering the flow field created by the suction of the sampling probe. In an effort to eliminate particle agglomeration, the dust was placed in an 70°F oven for 2-3 hours to remove moisture, then was lightly brushed across a 74-μm sieve placed at the top of the chamber and allowed into the vicinity of the sampler under gravity. In addition, the sampling probe was grounded to reduce electric charge effects in the system.

Dust #	MMAD (μm)	σ_g	CMAD (μm)	γ (g/cm^3)	d_{ae} (μm)
295	47.0	1.3	38.2	1.0	38.2
200	30.0	1.3	24.4	1.0	24.4
145	22.0	1.3	17.9	1.0	17.9
95	13.9	1.3	11.3	1.0	11.3

MMAD = mass median aerodynamic diameter
CMAD = count median aerodynamic diameter
σ_g = geometric standard deviation
γ = particle density
d_{ae} = particle aerodynamic diameter

Table 9.1 Average particle diameters and standard deviations for aerosols generated from fused alumina powders (Gomes, 1994).

Measurements of particle trajectories

Measurements of aspiration and of the position of the 'saddle point' were made directly from visualization of particle trajectories in the calm air chamber. This involved illuminating the aerosol, photographing the resultant visible particle trajectories, and using the photographs to determine the relevant indices, most notably a'' and l_S as outlined above.

To accurately measure the parameters associated with the limiting particle trajectory, it was necessary to visually observe the trajectories surrounding the sampling orifice in a single plane. To enable this, it was necessary to illuminate the system so that only a single plane of aerosol was visible. The lighting arrangement also had to be chosen so that it would not impart heat, and therefore unwanted air movement by virtue of thermal convection, to the calm air system. This was achieved by the use of an overhead project located outside the chamber and to one side, and the two-dimensional sheet of light obtained by the use of a slotted overhead transparency, was admitted to the chamber through a narrow slot in the chamber side wall. This method was effective in illuminating the aerosol in the plane of the sampler, and the amount of light reflected by the aerosol was sufficient to be recorded photographically.

Particle trajectories visualized in this way were photographed using Fuji 1600-speed color film with a Nikon 6006 SLR camera (with a Nikon 180-mm f5.6 lens) whose settings were determined based on the results of preliminary exposures taken at various settings. The optimum camera setting was determined to be a shutter speed of 2 seconds with an aperture of f5.6. A very short depth of field was necessary to ensure that the particles being photographed were in the same plane as the sampling tube. In addition, the magnification settings were chosen to provide the largest possible image while still capturing sufficient area around the sampling head to identify the effects of turbulence. The photographs were taken with the camera placed just outside the front chamber wall. The developed film negatives were mounted in slide mounts and projected onto a screen to provide for greater accuracy and ease in measuring the sampling parameters.

The photographs clearly showed the trajectories of the particles as they approached the sampling probe and were either drawn into the probe or passed by and fell to the chamber floor. The area enclosed by the critical trajectory, a'', was measured by locating the point below the nozzle inlet where the particles were just sampled (the 'saddle point') and tracing this particle trajectory up to a point where the particles were falling vertically parallel to one another. The distance from this trajectory to the centerline of the sampling probe was taken as the radius corresponding to the area a''. The value of this radius was determined for each photograph, and used to calculate aspiration efficiency. The distance from the saddle point to sampler inlet, defined as l_S, was also measured for each photograph.

Because the technique used in determining both a'' and l_S was dependent, to some degree, on the accuracy and judgment of the observer, an evaluation was made of inter-observer variability to identify any potential measurement bias. Twenty-five photographs were chosen at random from the total set of photographs, and the measurements of the radius and l_S were made by four different observers and evaluated for bias, using ANOVA statistical methods. There was found to be no statistically significant difference in these measured values between observers.

9.4 Results and discussion

In the experiments that were conducted, each of the test aerosols was sampled at five different flowrates, and measurements were made for each for both the upward and downwards-facing tube orientations. Five photographs were taken for each set of conditions, for a total of 200 photographs. Two typical examples are shown by way of illustration in Figure 9.4. The limiting particle trajectory, as identified in such photographs, was used to measure a'' and l_S. These parameters, in turn, were used to calculate aspiration efficiency, A_C, for various conditions and to evaluate the validity of the study.

Particle size

In order to determine whether a satisfactory experimental method has been achieved, Equation (9.11) provides a useful basis. With this in mind, the results for the downwards-facing tube are plotted in the form $(l_S/\delta)^2$ versus $(U_S/g\tau)$ in Figure 9.5. Also shown in this graph is the straight line that represents the prediction based on the theory outlined. The values of each of the calculated and measured experimental parameters are shown in Table 9.2.

If the particle size has been correctly determined and the experiment was otherwise done correctly, the data should fall along the predicted line. However, Figure 9.5 shows that all of the data points lie consistently and significantly below the line. Although the data follow the same trend as the line, over most of the range of the $U_S/g\tau$-axis has been overestimated by a factor of about 10x. The only variable within this expression that is not explicitly known is τ, the particle relaxation time, so it is assumed that this is the primary source of the error. Therefore, it follows that τ has been underestimated by approximately 10x. Since this quantity depends on the square of particle aerodynamic diameter, the results strongly suggest that we have underestimated the particle aerodynamic diameter by about a factor of about 3x.

In an attempt to explain this finding, the aerosols generated in these experiments were examined more closely for agglomeration. For this, microscope slides were placed on the floor of the chamber during dust injection, and the deposited particles were then viewed under a microscope. It became apparent that agglomeration had occurred for all particle sizes with, qualitatively, the greatest degree of agglomeration apparent for the smaller diameter dusts. This is broadly consistent with the trend shown in Figure 9.5, where the degree of particle size underestimation appears to increase with decreasing particle size.

Aspiration efficiency

Since inertia is considered to be an important mechanism in calm air sampling, the results for aspiration efficiency in the form of A_C versus St_C are shown in Figure 5 for the downwards-facing probe. Here the value of St_C is calculated from the assumed particle size. There is clearly a relationship between A_C and St_C, with A_C increasing as St_C increases. But, unfortunately, the observed relationship is in the opposite direction from what is expected on the basis of previous work - both Kaslow and Emerich (1973 and 1974) and Yoshida *et al.* (1978) showed that aspiration efficiency should decrease as the contribution from inertia increases. This dichotomy is almost certainly associated with an error in the assumed particle size, although - it should be

noted - A_C is also a complex function of R_C (as well as St_C), so that the conclusions that can be made about the observed relationship are limited.

From photographs like those shown in Figure 9.4, it is seen that clear particle trajectories can be identified, without cross-over and therefore unambiguously. This provides a means to estimate particle size from the location of the 'saddle point', using Equation (9.11). However, since this comes from the same experiment in which A_C is determined, it is not strictly an independent measure of particle size. So this approach was not adopted.

9.5 Conclusions

In the end, this part of the research became an exploratory investigation of experimental techniques for measuring aspiration efficiencies in a calm air chamber, aimed at overcoming the multitude of obstacles inherent to calm air experiments. Such obstacles reflect the degree of difficulty involved in performing such experiments, and probably explain why so little such research has been carried out in the past, despite the fact - as we now know - that it is an area of aerosol sampling research which has important practical implications.

This study was successful in several aspects of the development of experimental techniques for the studying of aerosol sampling in calm air. A system for illuminating the aerosol was developed, allowing for the capture of the image of the particle trajectories on film. In addition, the methodology for measuring the sampling efficiency parameters from the photographs was developed and shown to be free from observer bias. But the difficult problem of aerosol generation and characterization was not solved, in particular the generation of an agglomerate-free aerosol without disturbing the desired calm-air conditions.

Since this project was completed, research carried out under separate auspices has led to an improved aerosol generation and delivery system. In this system, the particles are again generated from a powder, but are injected under compressed air into an auxiliary chamber that is located inside and near the top of the calm air chamber itself. This chamber is separated from the main chamber by a fine honeycomb screen. The compressed air injection provides enough force to break up any agglomerates, and the auxiliary chamber is designed such that the aerosol thus generated is uniformly dispersed inside it. The honeycomb screen is such that that air movement inside the auxiliary chamber is not imparted to the main test chamber. So, after injection, the particles fall under gravity through the screen and emerge into a region of the main chamber where the air remains calm. Through this method, it appears that the final obstacle to this experiment, proper aerosol characterization, has been overcome and may be applied to future research.

It is clear that much more work in the area of calm air sampling is needed, and that the present research in that area has done no more than to ease the path towards such future work.

10. ACHIEVEMENTS, IMPLICATIONS AND APPLICATIONS OF THE RESEARCH

10.1 Achievements

The research described in this report was successful in nearly all of the goals it set out to achieve, and in many regards exceeded our expectations. It may be measured against the original aims as follows:-

Aim (a): To develop laboratory models relevant to the study of aerosol sampling in industrial hygiene.
Achievement: We developed a novel experimental system, utilizing a small wind tunnel and direct-reading particle counting and sizing instrumentation, which was able to rapidly provide very large amounts of data about the sampling efficiency for a range of sampler configurations chosen. The sampler systems studied were simple and idealized, since the intention was to identify the basic physical functional relationships which would lead to a fundamental understanding of the factors influencing sampler performance (which could in turn be applied to more complex systems more immediately application to the real world). The experimental system and procedures that were developed were shown to be capable of generating very accurate and reproducible data about sampler performance. The techanical challenges involved in developing such methodology were very difficult, involving problems not only in aerosol science and engineering fluid mechanics but also data handling and analysis. They were completely solved for the more important moving air case considered to be the most representative of most workplace situations.

Aim (b): To conduct experiments to evaluate basic aerosol sampling performance indices and the role of physical factors such as sampler size and shape, orientation, windspeed and sampling flowrate.
Achievement: A very large number of experiments were performed, producing the largest and most reliable data set ever obtained for the basic performance characteristics of aerosol samplers. These experiments were carried out for a range of particle size, sampler dimensions, windspeed, sampling flowrate and sampler orientation which, after scaling (see below), can be related to the whole range of conditions relevant to the occupational and outdoors environment. Such data will continue to provide a rich resource for the future study of the physics of aerosol sampling.

Aim (c): To relate the results to existing theories and develop improved models for application by users and designers of practical aerosol samplers.
Achievement: The results of the research were compared with theortical models for sampling efficiency developed in previous work. Those earlier models were found to be surprisingly consistent with these latest results, and strongly support the potential of such semi-empirical, physically-based models for guiding the development and testing of practical sampling devices and systems. The results did, however, highlight the fact that the physical act of sampling airborne particles is very complicated. In fact, we found that it was even more complex than we had anticipated. Much of this perception is the result of the new insights we have gained into the

role played by particle transport in the region very close to the sampler inlet. This is the region where the flow outside the sampler is coupled - aerodynamically - with the flow inside the sampler. The resultant distortions are such that significant particle losses can occur under certain conditions of particle flowrate, windspeed and sampler orientation.

Aim (d): To propose physically-based guidelines for the development of new samplers meeting the new particle size-selective, health-related criteria.
Achievement: The models for sampler efficiency are largely semi-empirical, derived from physical considerations of the air flow and particle transport in the vicinity of the sampler, but with coefficients obtained by fitting the models against the new experimental data. Early on the research we did explore the possibility of applying computed-based numerical models. But it soon became clear that such models are not yet at the stage where even the air flow in a system as complex as that studied can be described in this way. So this was dropped. The search for alternative physical models was much more successful. The ones we have developed and examined are relatively simple, and certainly accessible to industrial hygienists and aerosols scientists using modest computing resources. The success in this work in comparing experimental sampler performance data with results calculated from the models, together with the success obtained in earlier studies, is such that we now have high confidence that such models can be effective in providing good estimates of sampler performance under realistic conditions.

10.2 **Implications**

This research has cleared the way for the application of relatively simple theoretical models to blunt aerosol sampler systems of the type found in most industrial hygiene situations. Previously we had good knowledge only about the simple thin-walled samplers of the type used for collecting aerosols in stacks and ducts. Our confidence in the various blunt sampler models that had been proposed was limited by the fact that good experimental data against which to test such models were not available. Such paucity of basic sampling data has frustrated industrial hygiene-based aerosol researchers for many years (bearing in mind that the first blunt sampler models were proposed as long ago as 1979).

Considerable interest has been generated by this work. For example, scientists working under the auspices of the European Community (led by Dr. Lee C. Kenny of the United Kingdom Health and Safety Laboratory) are planning a new international, multi-laboratory study to examine new aerosol sampling standardized testing procedures. This will be based on direct application of the models validated during this work (see below). A new grant has been requested by our group for similar work to be conducted in the United States. Elsewhere, Dr. Sarah Dunnett of the University of Loughborough in the United Kingdom, herself an active researcher in this field for more than 10 years, has been awarded a NATO Fellowship to enable her to continue to work on problems relating to this work. It is explicitly intended that this will facilitate continued interactions with our group. Her primary interest will be in using the large data set we have generated as a starting point for still further improved predictive models.

Meanwhile, the continuing worldwide interest in implementing the new particle size-selective sampling criteria in new occupational exposure standards is fueling the mounting

interest in further improved methods for developing and testing new sampling devices, as well as in interpreting results obtained in the field using samplers of the previous generation.

10.3 Applications

Sampler design and development

As mentioned previously, aerosol samplers are important to industrial hygiene through their role in the measurement (and hence regulation) of workers' exposures to airborne particles. Proposed new health-related aerosol standards (as reviewed in Vincent, 1998) require that such measurement should reflect the true physical nature of human exposure (i.e., the manner in which they are inhaled and penetrate into the respiratory tract). This, in turn, has stimulated the search for new generations of practical sampling devices. The development of these will be facilitated by the improved knowledge about their basic performance characteristics derived from the research described in this report. Models like those described will be very useful in guiding the design of new samplers.

One area of considerable interest is in the development of miniaturized sampling systems. While it is recognized that the current generation of personal aerosol sampling systems are adequate for most industrial hygiene purposes, they do involve sampling flowrates requiring the use of relatively large and cumbersome pumps. There is now emerging interest in assessing the aerosol exposures of people to whom such systems are inconvenient or even unacceptable. In the occupational setting these may include older workers and some female workers. In the non-occupational setting these may include children or infirm people. In such situations, the use of compact and lightweight low-flowrate pumps (e.g., even as low as 0.1 Lpm) would greatly facilitate aerosol exposure assessments for such groups of individuals. Bearing in mind that most personal sampling for aerosols is currently carried out at about 2 Lpm, it is clear - on the basis of research like that described in this report - that the actual sampling heads themselves will need to be modified. This is to ensure that their performances can continue to be consistent with the particle size-selective criteria pertaining to their use. This is where what has been learned in the present research may be directly applied. Most notably, the newly validated models for sampling efficiency can be used as the basis of scaling laws by which the parameters for modified samplers of the type sought can be determined. The approach to this is outlined below. It should be noted, however, that the question of miniaturizing aerosol samplers goes beyond the matching of the particle size-selective performance of the sampling head. Since it means that smaller amounts of sampler particulate material will be collected, even greater demands will be placed on the analytical procedures by which such samples will be analyzed. This will provide new scientific challenges, this time at the interfaces between industrial hygiene, aerosol science and analytical chemistry, and will doubtless be the subject of future work.

Towards new standardized testing methods for aerosol samplers

The construction of scaling laws, based on reliable models for sampler efficiency, is relevant not only to the development of new samplers (as mentioned in the preceding) but also in the testing of both existing and new sampling devices. At present, such testing can be reliably carried out only for full-scale sampling systems in large wind tunnels (e.g., large enough to accommodate

personal samplers mounted on life-sized mannequins) and for particles with aerodynamic diameter in the range up to and exceeding 100 μm (*i.e.*, the range typical of many workplace aerosols). But such tests are very difficult because of the problems of achieving uniform aerosol spatial and temporal distributions in the working sections of such large facilities. They are also very time-consuming and laborious, as has been borne out by previous studies (e.g., Vincent and Mark, 1982; Mark and Vincent, 1986; Vincent and Mark, 1990; Kenny, 1995; Kenny *et al.*, 1997; and others). Inevitably, therefore, the cost is also very high, so much so that it is unlikely that such methods can be routinely applied for the testing of such intrinsically low-cost devices. In any case, the availability of resources and expertise to carry out such experiments is severely limited (where only about four laboratories in the world are presently suitably equipped). It is therefore clear that an alternative approach to sampler design, development and testing is essential if progress towards the full implementation of the new aerosol standards is to be maintained.

With this in mind, we seek scaling laws by which the testing of aerosol samplers can be carried out in a meaningful way in smaller and more manageable facilities. Here it is important to recognize that it is not only the physical dimensions and airflows that may be scaled but also - within the natural principles of physics and engineering - the particle size itself. Thus, experiments or tests carried out for particles of small size (say, up to just 25 μm - which happens to be the range of the APS) can be used to directly infer knowledge about what would happen for particles of large size (say, up to 100 μm or beyond). This concept opens the door to practical application of the very sophisticated and rapid testing methods that were developed during the project described in this report.

The objective is to establish a framework by which results for aerosol sampler aspiration efficiency obtained in a model system can be related to those obtained in a full-scale, real system. Specifically, what ranges of sampler dimensions, sampling flowrate and windspeed, and - importantly - particle size are required in a small-scale (e.g., 1/5-scale) wind tunnel model to provide aspiration efficiency data which correspond directly to the equivalent full-scale sampler system over particle size ranges and windspeeds relevant to actual workplaces? This requires knowledge of the inter-relationships between the large number of variables that can influence aerosol sampler performance. It involves classical engineering dimensional analysis together with inspection of physical models for the air flow characteristics and particle transport. In what follows, all the terms introduced (unless stated otherwise) have been defined above.

The air flow in the vicinity of an aerosol sampler is very complicated. The Reynolds' number (*Re*) governs the intrinsic nature of the air motion, and the vortex shedding-like instabilities are embodied in the Strouhal number (*Str*). In previous theories, *Re* has not usually been considered a major influence since it has been assumed to be large enough that inertial fluid forces predominate over viscous forces. This has been the basis of the assumption - widely made by aerosol scientists - that potential flow mathematical models are adequate descriptors of the fluid flow. Further, *Str* has never previously been considered at all in relation to aerosol sampling. However, the present research (see §3) has shown that *Str* depends strongly on the sampling flowrate, windspeed and sampling orientation and can affect the size of the wake cavity. This, in turn, can affect the sampling efficiency of aerosol samplers, especially when they are oriented away from the wind and sampling, in effect, from the near wake. In addition to these parameters (which apply to all bluff body flows), consideration needs to be given to additional

parameters that relate to the shape and magnitude of the distortion of the flow near the sampler due to its aspirating action. These are described by the individual parameters, R ($=U/U_S$) and r ($=\delta/D$), which together form the parameter ϕ ($= r^2/R$). Further, if freestream turbulence is present, consideration is required of the scaling of turbulent kinetic energy (k) and length scale (ℓ), as may be embodied in the non-dimensional mixing parameter, $\Lambda_f = k^{1/2}\ell/DU$ (Humphries and Vincent, 1976; Vincent *et al.*, 1985).

For particle transport, additional parameters are required which reflect the ability (or otherwise) of the particles to follow the motion of the air near the sampler. In general, these may involve considerations of inertial, gravitational, electrostatic, diffusive and phoretic forces. But, in reality, it may safely be assumed that inertia and gravity are the only ones likely to be significant. The parameter that governs inertial forces is Stokes' number, St. In addition, the role of gravitational forces is embodied in the gravitational parameter, G ($= v_S/U$, where v_S is the particle settling velocity). The relative contributions of inertial to gravitational forces is determined by the Froude number, $Fr = St/G$.

In general, it may be assumed that dynamic similarity exists when all of the dimensionless groups identified above are held constant. But, as rapidly becomes apparent, the fluid-particle system described is dauntingly complicated. However, as is usual in such cases, some simplifications may be justified. For present purposes, for example, we are justified in assuming that the dependencies of aspiration efficiency (A) on Re, Str and Λ_f are weak. Similarly, gravity may be neglected for most moving air situations, and so the dependence on G is weak. Then, for a fixed configuration A remains invariant with scaling with respect to just St, R, r and - additionally - α. Now, in a scaling exercise, we can set the condition that, after scaling of all the relevant variables, the model-scale and full-scale aerosol samplers should have the same aspiration efficiency for a given St.

To begin with, we need to identify one or more equations that describe sufficiently well the aspiration efficiency of an aerosol sampler as a function of the various parameters identified above. Then we need to scale down the characteristic dimension of the sampler by a desired factor, and adjust all the other factors accordingly. It does not matter whether the function is physically rigorous or is empirical, so long as it is expressed in terms of the controlling parameters and is reasonably representative of the available experimental data. So, for present purposes, Equations (2.4) and (2.5) provide a suitable starting point, and are expected to apply for all samplers that are essentially symmetrical in terms of shape and location of the sampling orifice on the blunt sampler body. One practical sampler that comes into this category is the 3 Lpm static inhalable aerosol sampler proposed by Mark *et al.* (1985). It is characterized by a rotating cylindrical sampling head (D = 127 mm) and rectangular sampling entry 15 mm long and 3 mm high (and hence having an effective circular orifice diameter, δ, of 7.57 mm). This instrument matches the inhalability criterion quite well for d_{ae} from 10 μm to 90 μm and for windspeeds up to 2.5 m/s. Equation (2.5) describes the aspiration efficiency of this sampler as a function of St. The results are shown in Figure 10.1 for a typical windspeed of 1 m/s (see results for "Full-Scale"). This corresponds to R = 0.9, r = 0.06, ϕ = 0.004, and U_S = 1.11 m/s. The corresponding experimental conditions and sampler design for testing an equivalent system in a small-scale wind tunnel can be determined by setting the aspiration efficiency of model (small-scale) equal to the aspiration efficiency of the full-scale sampler. That is, $A_M = A_{FS}$, where the subscripts M and FS refer to model and full-scale respectively. Thus

$$0.5\,A_{0M} + [(A_{90M} - A_{0M}) / (181\,R_M^{2.31}\,r_M^{1.01} + 2)] + 0.5\,A_{180M} = 0.5\,A_{0FS} + [(A_{90FS} - A_{0FS}) / (181\,R_{FS}^{2.31}\,r_{FS}^{1.01} + 2)] + 0.5\,A_{180FS} \quad (10.1)$$

In this approach, however, a number of constraints must be included. Firstly, while the full-scale device is used for practical sampling of particles up to about 100 μm in aerodynamic diameter, it may be feasible to sample only smaller particles - say, up to only 25 μm - in the model-scale system. In general, such a constraint may be imposed, for example, by the aerosol handling capability of the test facility and by the range of capability of the aerosol detection instrumentation used. Secondly, scaling should take account of the range of actual windspeeds relevant to the practical applications of the various samplers. Thus, for personal samplers of the type used in workplaces, actual windspeeds will range from about 20 cm/s to about 3 m/s. For samplers of the type used in ambient air sampling, actual windspeeds may be as high as 10 m/s.

In the scaling exercise itself, it is noted that, for each value of St, the values of A_M and A_{FS} should be equal. The values of R_{FS}, r_{FS}, St_{FS}, ϕ_{FS} and D_{FS} are known (since they represent an existing aerosol sampler). Now we wish to design a model sampler of the same overall geometrical shape whose characteristic dimension, D, is scaled down by a factor x (that is, $D_M = D_{FS}/x$) while at the same time keeping St the same. The aim now is to determine appropriate values for R_M, r_M and ϕ_M such that the difference between the aspiration efficiency for the model and full-scale system is less than some small value ε (representing the experimental uncertainty). Thus we have a multi-dimensional minimization problem, where

$$|A_M(R_M, r_M, \phi_M) - A_{FS}(R_{FS}, r_{FS}, \phi_{FS})| \leq \varepsilon \quad (10.2)$$

subject to the constraints $St = k$, $R_{M1} < R_M < R_{M2}$, $r_{M1} < r_M < r_{M2}$ and $\phi_{M1} < \phi_M < \phi_{M2}$, where k is the defined value of St at which the minimization is carried out and R_{M1}, R_{M2}, r_{M1}, r_{M2}, ϕ_{M1} and ϕ_{M2} are the lower and upper limits of each of those parameters that will be set based on considerations of "good" engineering design. For example, the diameter δ of the entry orifice cannot be made too small and U_S cannot become too large, since these may lead to an unacceptably high pressure-drop across the orifice. This consideration in turn imposes limits on r and R.

There are a number of numerical methods in the literature for solving such constrained, multi-dimensional minimization problems. Since we have to match the aspiration efficiency curves for the full-scale and model samplers over a wide range of values of St, this constrained minimization procedure should be performed for all the values of St in this range. There will be many combinations of R, r and ϕ satisfying the above minimization problem for each value of St. In turn there will be many different sets of combinations for different values of St. However, some of these combinations will be common to all values of St. Each such combination represents a different scaled-down design that has the same set of aspiration efficiency characteristics as the full-scale model over the range of St considered. By way of illustration, we show here two examples of how, using a preliminary analysis along the lines suggested above, such scaling might be achieved.

For the 3 Lpm static inhalable sampler example described above, we may design a scaled-down (geometrical scaling factor = 5:1) version by setting D = 25.4 mm and δ = 1.51 mm. If it assumed that the aerosol sizing instrument we might wish to use in our experimental system

has an upper particle aerodynamic diameter limit of 25 μm, this imposes a constraint on the size of aerosols that can be used in the small scale wind tunnel. By setting U = 5 m/s, and sampling flow rate Q = 0.6 Lpm, we can obtain an aspiration efficiency curve (in the form of *A vs. St*) which is identical to that for the full-scale sampler (see Figure 10.1, "Small-Scale A"). The values of R, r, and ϕ are the same as for the full-scale. Another solution can be obtained by setting D = 25.4 mm, δ = 2.52 mm, U = 3 m/s, and Q = 1 Lpm (see Figure 10.1, "Small-Scale B"). It becomes clear that there are an infinity of such solutions, and one can choose any one them based on engineering constraints. For example, while both the solutions presented here are technically feasible, the sampler with δ = 2.52 mm is easier to machine and has a smaller pressure drop across it, and may therefore be consider to be a "better" design. Thus, testing any of these scaled-down samplers in a small wind tunnel with a smaller range of particle sizes is equivalent to testing the static inhalable sampler in a large wind tunnel.

As a second example, consider a small personal sampler mounted on the lapel of a life-sized mannequin placed in a large (2.5 m x 1.5 m) wind tunnel. This is highly relevant to industrial hygiene aerosol sampling. Here the sampling configuration is inherently asymmetric because the mannequin (and the human body) presents a different profile to the freestream flow as the orientation is changed, and the sampler itself is asymmetrically located on the lapel of the mannequin. As a result, Equation (2.5) developed for symmetric configurations is not directly applicable for such cases. So the extended model embodied in Equation (2.6) is more appropriate.

One such personal sampler is the so-called "*IOM sampler*", first proposed for collecting the inhalable aerosol fraction by Mark and Vincent (1986). This device has dimensions of δ = 15 mm, and operates at a sampling flowrate of 2 Lpm. When it is worn on the body, the body itself becomes part of the sampling system.

So, for modeling purposes, we also need to prescribe D_1 and D_2 as the width and the thickness respectively of the body's cross-section (which for present purposes we take to be rectangular). We assume that, typically at full-scale, $D_1 \approx 400$ mm and $D_2 \approx 150$ mm. The aspiration efficiency curve for this system, for up to d_{ae} = 90 μm and for a windspeed of 1 m/s, is shown in Figure 10.2 (see "Full-Scale"), and it is seen to be well within the ±10% tolerance bounds originally defined for the inhalability curve (ACGIH, 1985). As in the previous example, we seek a 5:1 scaled-down sampler design to test in a small wind tunnel. Two solutions are shown in Figure 10.2. The first solution (see "Small-Scale A") has dimensions of δ = 3 mm, D_1 = 80 mm and D_2 = 30 mm. The sampler should operate at a flow rate of 10 Lpm, and be tested at a windspeed of 5 m/s. The second solution (see "Small-Scale B") prescribes dimensions of δ = 3.2 mm, D_1 = 80 mm and D_2 = 30 mm. This sampler should operate at a flow rate of 5 Lpm, and be tested at a freestream velocity of 3 m/s. Both these designs lead to almost exactly the same aspiration efficiency curve (in the form A vs. St). This example shows that an inhalable personal sampler can indeed be tested in a small-scale wind tunnel after suitable scaling of sampler dimensions and particle size.

Although the two examples given are based on the scaling with respect to aspiration efficiency, A, it is seen from the research described in this report that the link with actual sampling efficiency, E, is strong and can be predicted relatively easily using models like those shown. The examples show very clearly the practical feasibility of achieving scientifically-based scaling of the factors influencing sampler performance, not only with respect to physical

dimensions and air flows but also with respect to particle size. The latter is particularly important in that it opens the door to experiments and testing at small scale using direct-reading instruments such as the APS, leading in turn to very rapid acquisition of test data.

While the two examples shown in Figures 10.1 and 10.2 describe a scaling-down process, the real practical benefits of using the scaling approach will accrue when one uses it to design and test a sampler exhaustively in a small wind tunnel, and then scale it up for full scale applications. This should lead to substantial savings in the time and cost associated with the testing of aerosol samplers, especially as currently tested in large wind tunnel facilities. The further development and validation of the approach outlined will be the subject of future work. Indeed, it has been learned that it will be the subject of a European Community-sponsored project directly based on the wrok described in this report. Further, new work has been proposed in the United States by the present investigators.

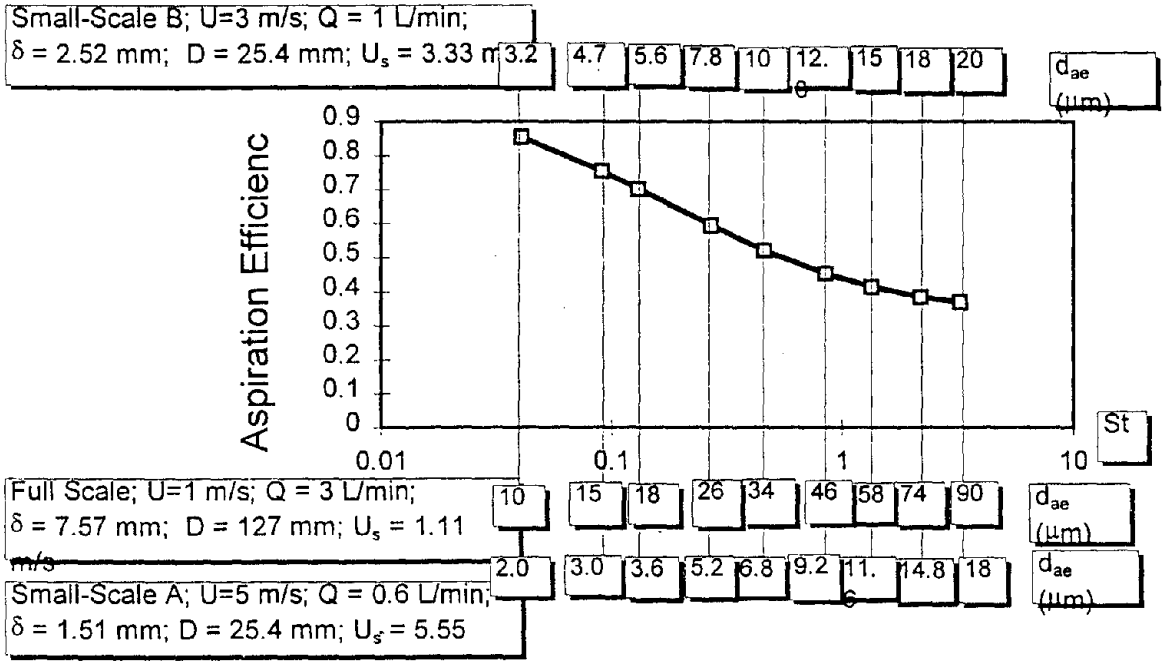

Figure 10.1. Two scaled-down (5:1) sampler designs and experimental conditions dimensionally equivalent to the 3 Lpm IOM static inhalable aerosol sampler (tested at full-scale in a wind tunnel at a windspeed of 1 m/s).

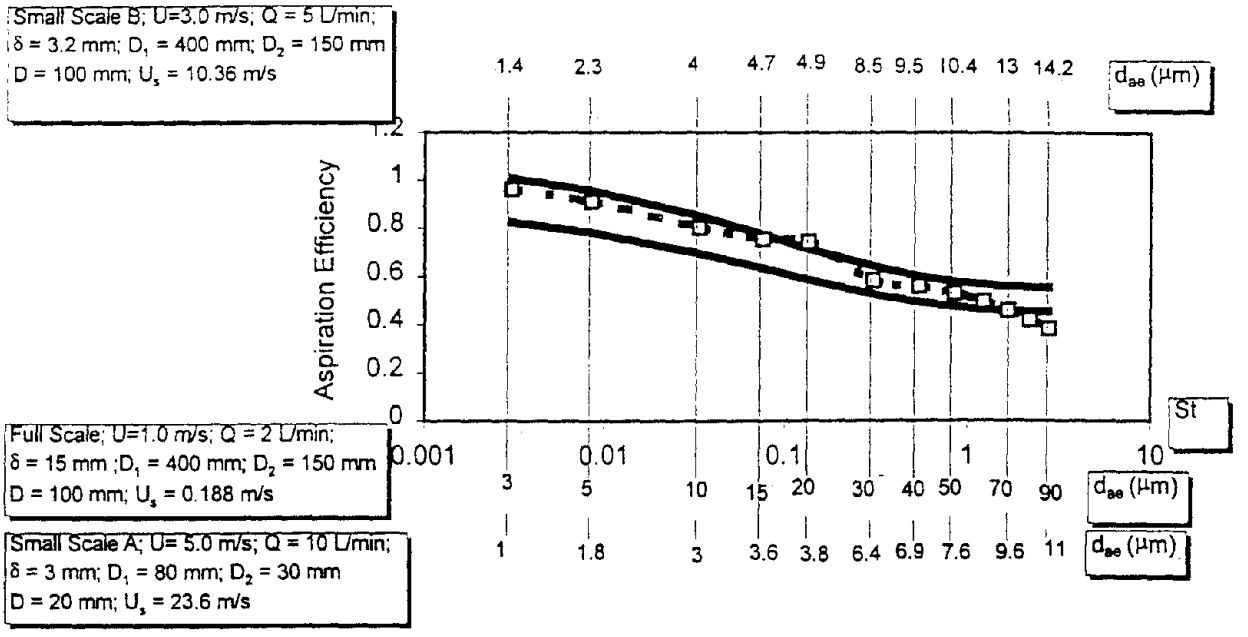

Figure 10.2. Two scaled-down (5:1) sampler designs and experimental conditions dimensionally equivalent to the 2 Lpm IOM personal inhalable aerosol sampler (tested at full-scale in a wind tunnel at a windspeed of 1 m/s)

REFERENCES

Agarwal, J.K. and Liu, B.Y.H. (1980), A criterion for accurate aerosol sampling in calm air, *Am. Ind. Hyg. Ass. J.*, 41, 191-197.

Aitken, R.J., Baldwin, P.E.J., Beaumont, G.C., Kenny, L.C., and Maynard, A.D. (1998), Aerosol inhalability in very low winds, *J. Aerosol Sci.*, in press.

American Conference of Governmental Industrial Hygienists (ACGIH) (1985), Particle size-selective sampling in the workplace, Report of the Air Sampling Procedures Committee (Ed. R.F. Phalen), ACGIH, Cincinnati, OH.

American Conference of Governmental Industrial Hygienists (ACGIH) (1998), Threshold limit values for chemical substances and physical agents, ACGIH, Cincinnati, OH.

Ananth, G. and Wilson, J.C. (1988), Theoretical analysis of the performance of the TSI aerodynamic particle sizer: the effect of density on response, *Aerosol Sci. Tech.*, 9, 189-201.

Baines, W.D. and Peterson, E.G. (1951), An investigation of flow through screens. *Trans. A.S.M.E.*, 73, 467-480.

Baron, P.A. (1983), Sampler evaluation with an aerodynamic particle sizer, *Aerosols in the Mining and Industrial Work Environments* (Eds. V.A. Marple and B.Y.H. Liu), Ann Arbor Science, Ann Arbor, MI, pp861-877.

Baron, P.A. (1986), Calibration and use of the APS (APS 3300), *Aerosol Sci. Tech.*, 5, 55-69.

Belyaev, S.P. and Levin, L.M. (1974), Techniques for collection of representative aerosol samples, *J. Aerosol Sci.*, 5, 325-338.

Brockmann, J.E., Yamano, N. and Lucero, D. (1988), Calibration of the aerodynamic particle sizer 3310 (APS 3310) with polystyrene latex monodispersed spheres and oleic acid monodispersed particles", *Aerosol Sci. Tech.*, 8, 279-281.

Brockmann, J.E. and Rader, D.J. (1990), APS response to non-spherical particles and experimental determination of dynamic shape factor", *Aerosol Sci. Tech.*, 13, 162-172.

Chen, B.T., Cheng, Y.S. and Yeh, H.C. (1985), Performance of a TSI aerodynamic particle sizer, *Aerosol Sci. Tech.*, 4, 89-97.

Chen, B.T. and Crow, D.J. (1986), Use of an aerodynamic particle sizer as a real-time monitor in generation of ideal solid aerosols, *J. Aerosol Sci*, 17, 963-972 .

Chen, B.T., Cheng, Y.S. and Yeh, H.C. (1989), An experimental approach to studying particle density effects in the TSI aerodynamic particle sizer (3300), *J. Aerosol Sci.*, 20, 1489-1492.

Cheng, Y.S., Chen, B.T. and Yeh, H.C. (1990), Behavior of isometric non-spherical aerosol particles in the aerodynamic particle sizer, *J. Aerosol Sci.*, 21, 701-710.

Chung, K.Y.K. and Ogden, T.L. (1986), Some entry efficiencies of disklike samplers facing the wind, *Aerosol Sci. and Tech.*, 5, 81-91.

Chung, I.P. and Dunn-Rankin, D. (1992), Numerical solution of two-dimensional blunt body sampling in viscous flow, *J Aerosol Sci.*, 23, 217-232.

Cowdrey, C.F. (1962), A note on the use of end plates to prevent three-dimensional flow at the ends of bluff cylinders, U.K. National Physical Laboratory - Aerodynamics Division, NPL AERO REP. 1025.

Dallavalle, J.M. (1952), *Exhaust Hoods, Second Edition*, Industrial Press, New York, NY.

Davies, C.N. (1968). The entry of aerosols into sampling tubes and heads, *Br. J. Appl. Phys.*, 25, 921-32.

Davies, C.N. and Subari, M. (1982), Aspiration above wind veloecity of aerosols with thin-walled nozzles facing and at right angles to the wind direction, *J. Aerosol Sci.*, 13, 59-71.

Dunnett, S.J. and Ingham, D.B. (1986), A mathematical theory to two-dimensional blunt body sampling, *J. Aerosol Sci.*, 17, 839-853.

Dunnett, S.J. and Ingham, D.B. (1988), An empirical model for the aspiration efficiencies of blunt aerosol samplers oriented at an angle to the oncoming flow, *Aerosol Sci. and Tech.*, 8, 245-264.

Durham, M.D. and Lundgren, D.A. (1980), Evaluation of aerosol aspiration efficiency as a function of Stokes' number, velocity ratio and nozzle angle, *J.Aerosol Sci.*, 11, 179-188.

Erdal, S. and Esmen, N.A. (1995), Human head model as an aerosol sampler: calculations of aspiration efficiencies for coarse particles using an idealized human head model, *J. Aerosol Sci.*, 26, 253-272.

Fuchs, H.V., Mercker, E. and Michel, U. (1979), Large-scale coherent structures in the wake of axisymmetric bodies, *J. Fluid Mech.*, 93, 185-207.

Gerrard, J.H. (1966), The mechanics of the vortex formation region of vortices behind bluff bodies, *J. Fluid Mech.*, 25, 401-413.

Gibson, H., Vincent, J.H. and Mark, D. (1987), A personal inspirable dust spectrometer for applications in occupational hygiene research, *Ann. Occ. Hyg.*, 31, 463-479.

Gomes, M.S.P. (1994). On the dispersion of particles in the near wake of a blunt obstruction. Ph.D. Thesis, University of Minnesota.

Griffiths, W.D., Patrick, S., and Rood, A.P. (1984), An aerodynamic particle size analyser tested with spheres, compact particles and fibers having a common settling rate under gravity, *J. Aerosol Sci.*, 15, 491-502.

Grinshpun, S., Willeke, K and Kalatoor, S. (1993). A general equation for aerosol aspiration by thin-walled sampling probes from calm and moving air. *Atmos. Environ.*, 27A, 1459-1470.

Hammache, M. and Gharib, M. (1991), An experimental study of the parallel and oblique vortex shedding from circular cylinders, *J. Fluid Mech.*, 232, 567-590.

Hangal, S. and Willeke, K. (1990), Overall efficiency of tubular inlets sampling at 0-90 degrees from horizontal air flows, *Atmos. Environ.*, 24A, 2379-2386.

Heitbrink, W.A., Baron P.A. and Willeke, K. (1991), Coincidence in time-of-flight aerosol spectrometers: phantom particle creation, *Aerosol Sci. Tech.*, 14, 112-126.

Heitbrink, W.A. and Baron, P.A. (1992), An approach to evaluating and correcting aerodynamic particle sizer measurements for phantom particle count creation, *Am. Ind. Hyg. Ass. J.*, 53, 427-431.

Hinds, W.C. (1982), *Aerosol Technology*, Wiley and Sons, New York, NY.

Humphries, W. and Vincent, J.H. (1976), Experiments to investigate transport processes in the near wakes of disks in turbulent air flow, *J. Fluid Mech.*, 75, 737-749.

Ingham, D.B. (1981), The entrance of airborne particles into a blunt sampling head, *J. Aerosol Sci.*, 12, 541-549.

Ingham, D.B. and Hildyard, M.L. (1991), The fluid flow into a blunt aerosol sampler oriented at an angle to the oncoming flow, *J. Aerosol Sci.*, 22, 235-252.

Ingham, D.B. and Wen, X. (1993), Disklike body sampling in a turbulent wind, *J. Aerosol Sci.*, 24, 629-642.

International Standards Organization (ISO) (1983 and 1992), Air quality - particle size fraction definitions for health-related sampling, Technical Report ISO/TR/7708-1983 (E), ISO, Geneva (revised 1992).

Jayasekera and Davies, C.N. (1980), Aspiration below wind velocity of aerosols with sharp-edged nozzles facing the wind, *J. Aerosol Sci.*, 11, 535-547.

Johnston, A.M., Vincent, J.H. and Jones, A.D. (1987), Electrical charge characteristics of dry aerosols produced by a number of laboratory mechanical generators, *Aerosol Sci. Tech.*, 6, 115-127.

Kaslow, D.E. and Emrich, R.J. (1973), Aspirating flow pattern and particle inertia effects near a blunt, thick-walled tube entrance, Technical Report No. 23, Department of Physics, Lehigh University, PA.

Kaslow, D.E. and Emrich, R.J. (1974), Particle sampling efficiencies for an aspirating blunt, thick-walled tube in calm air, Technical Report No. 25, Department of Physics, Lehigh University, PA.

Kenny, L.C. (1995), Pilot study of CEN protocols for the performance testing of workplace aerosol sampling instruments, Report of work carried out under EC Contract MAT1-CT92-0047, September 1995, U.K. Health and Safety Executive, Sheffield, England, U.K.

Kenny, L.C., Aitken, R., Chalmers, C., Fabries, J.F., Gonzales-Fernandez, E., Kromhout, H., Liden, G., Mark, D., Riediger, G. and Prodi, V. (1997), A collaborative European study of personal inhalable aerosol sampler performance, *Ann. Occup. Hyg.*, 41, 135-153.

Levin, L.M. (1957), The intake of aerosol samples, *Izv. Akad. Naik SSSR Ser. Geofiz.*, 7, 914-25.

Lipatov, G.N., Grinshpun, S.A., Shingarov, G.L. and Sutugin, A.G. (1986), Aspiration of coarse aerosol by a thin-walled sampler, *J. Aerosol Sci.*, 17, 763, 769.

Mark, D., Vincent, J.H. and Witherspoon, W.A. (1982), Particle blow-off: a source of error in blunt dust samplers, *Aerosol Sci. Tech.*, 1, 463-469.

Mark, D., Vincent, J.H., Gibson, H. and Lynch, G. (1985), A new static sampler for airborne total dust in workplaces, *Am. Ind. Hyg. Ass. J.*, 46, 127-133.

Mark, D. and Vincent, J.H. (1986), A new personal sampler for airborne total dust in workplaces, *Ann. Occup. Hyg.*, 30, 89-102.

Mark, D., Vincent, J.H., Aitken, R.J., Botham, R.A., Lynch, G., van Elzakker, B.G., van der Meulen, A. and Zierock, K.H. (1990), Measurement of suspended particulate matter in the ambient atmosphere, Final Report on CEC Contracts B6611-44-89, 45-89 and 47-89, Institute of Occupational Medicine, 8 Roxburgh Place, Edinburgh, U.K.

Mark, D., Upton, S.L., Hall, D.J., Lyons, C.., Douglass, E.J., Marsland, G.W. and Walker, S. (1995), Improvements to the design and performance of an ambient inhalable aerosol sampler, AEA Technology Report AEA-TPD-0299, Harwell, UK.

Marshall, I.A., Mitchell, J.P. and Griffiths, W.D. (1991), The behavior of regula-shaped non-spherical particles in a TSI aerodynamic particle sizer, *J. Aerosol Sci.*, 22, 73-89.

Maynard, A.D. (1997), personal communication.

Ogden, T.L. (1983), Inhalable, inspirable and total dust, In: *Aerosols in the Mining and Industrial Work Environments* (Eds. V.A. Marple and B.Y.H. Liu), Ann Arbor Science, Ann Arbor, MI, pp185-204.

Okazaki, K. and Willeke, K. (1987), Transmission and deposition behavior of aerosols in sampling inlets, *Aerosol. Sci. Tech.*, 7, 275-283.

Okazaki, K., Wiener, R.W. and Willeke, K. (1987), The combined effect of aspiration and transmission on aerosol sampling accuracy for horizontal isoaxial sampling, *Atmos. Environ.*, 21, 181-185.

Rader, D.J., Brockmann, J.E., Ceman, D.L. and Lucero, D.A. (1990), A method to employ the aerodynamic particle sizer factory calibrated under different operating conditions, *Aerosol Sci. Tech.*, 13, 514-521 .

Ramachandran, G., Sreenath, A. and Vincent, J.H. (1997), Towards a new method for experimental determination of aerosol sampler aspiration efficiency in small wind tunnels, *J. Aerosol Sci.*, in press.

Roshko, A. (1954), On the development of turbulent wakes from vortex streets, *NACA Report* 1191.

Ruping, G. (1968), The importance of isokinetic suction in dust flow measurement by means of sampling probes, *Staub-Reinhalt. Luft* (English trans.), 28(4), 1-11.

Spear, T.M., Werner, M.A., Bootland, J., Harbour, A., Murray, E.P., Rossi, R. and Vincent, J.H. (1997), Workers' exposures to inhalable and 'total' lead and cadmium-containing aerosols in a primary lead smelter, *Am. Ind. Hyg. Ass. J.*, 58, 893-899.

Sreenath, A. (1998), The physics of aerosol sampling by blunt samplers at an angle to the wind. Ph.D. Thesis, University of Minnesota.

Tsai, P.-J. and Vincent, J.H. (1993), Impaction model for the aspiration efficiencies of aerosol samplers at large angles with respect to the wind, *J. Aerosol Sci.*, 24, 919-928.

Tsai, P.-J., Vincent, J.H., Wahl, G.A. and Maldonado, G. (1995a), Occupational exposure to inhalable aerosol in the primary nickel production industry, *Occup. Environ. Med.*, 52, 793-799.

Tsai, P.J., Vincent, J.H., Mark, D., and Maldonado, G. (1995b), Impaction model for the aspiration efficiencies of aerosol samplers in moving air under orientation-averaged conditions, *Aerosol Sci. and Tech.* 22, 271-286.

Tsai, P.-J., Werner, M.A., Vincent, J.H. and Maldonado, G. (1996a), Exposure to nickel-containing aerosol in two electroplating shops: comparison between inhalable and 'total' aerosol, *Appl. Occup. Environ. Hyg.*, 11, 484-492.

Tsai, P.-J., Vincent, J.H., Wahl, G.A. and Maldonado, G. (1996b), Worker exposure to inhalable and 'total' aerosol during nickel alloy production, *Ann. Occup. Hyg.*, 40, 651-669.

Tsai, P.-J, Vincent, J.H. and Mark, D. (1996c), Semi-empirical model for the aspiration efficiencies of personal aerosol samplers of the type widely used in occupational hygiene, *Ann. Occup. Hyg.*, 40, 93-114.

Tufto, P.A. and Willeke, K. (1982), Dependence of particulate sampling efficiency on inlet orientation and flow velocities, *Am. Ind. Hyg. Ass. J.*, 43, 436-443.

Vincent, J.H., Wood, J.D., Birkett, J.L. and Gibson, H. (1979), External flow effects on personal sampling, IOM Report No. TM/79/18, Institute of Occupational Medicine, 8 Roxburgh Place, Edinburgh, U.K.

Vincent, J.H. and Gibson, H. (1981), Sampling errors in blunt dust samplers arising from external wall loss effects, *Atmos. Environ.*, 15, 703-712.

Vincent, J.H. and Mark, D. (1982), Application of blunt sampler theory to the definition and measurement of inhalable dust, In: *Inhaled Particles V* (ed. W.H. Walton), Pergamon Press, Oxford, pp3-19.

Vincent, J.H. (1984), A comparison between models for predicting the performances of blunt dust samplers, *Atmos. Environ.*, 18, 1033-1035.

Vincent, J.H., Emmett, P.C. and Mark, D. (1985), The effects of turbulence on the entry of airborne particles into a blunt dust sampler, *Aerosol Sci. and Tech.*, 4, 17-29.

Vincent, J.H., Stevens, D.C., Mark, D., Marshall, M. and Smith, T.A. (1986), On the aspiration characteristics of large-diameter, thin-walled aerosol sampling probes at yaw orientation with respect to the wind, *J. Aerosol Sci.*, 17, 211-224.

Vincent, J.H. (1987), Recent advances in aspiration theory for thin-walled and blunt aerosol sampling probes, *J. Aerosol Sci.*, 18, 487-498.

Vincent, J.H. (1989), *Aerosol Sampling: Science and Practice*. Wiley, London.

Vincent, J.H., Mark, D., Miller, B.G., Armbruster, L. and Ogden, T.L. (1990), Aerosol inhalability at higher windspeeds, *J. Aerosol Sci.*, 21, 577-586.

Vincent, J.H. and Mark, D. (1990), Entry characteristics of practical workplace aerosol samplers in relation to the ISO philosophy, *Ann. Occup. Hyg.*, 34, 249-262.

Vincent, J.H. (1995), *Aerosol Science for Industrial Hygienists,* Pergamon/Elsevier, Oxford.

Vincent, J.H., Ramachandran, G., Pui, D.Y.H., Gomes, M.S.P., Sato, S. and Sreenath, A. (1997), Experimental studies of particle transport in air flows near bluff bodies with and without aspiration, *Proceedings of the 1997 ASME Fluids Engineering Division Summer Meeting (FESM'97)*, American Society of Mechanical Engineers, Paper 3634 (CD-ROM).

Vincent, J.H. (Ed.) (1998), *Particle Size-Selective Sampling of Particulate Air Contaminants*, American Conference of Governmental Industrial Hygienists (ACGIH), Cincinnati, OH, in press.

Wang, H.-C. and John, W. (1987), Particle density correction for the aerodynamic particle sizer, *Aerosol Sci. Tech.*, 6, 191-198.

Werner, M.A., Spear, T.M. and Vincent, J.H. (1996), Investigation into the impact of introducing workplace aerosol standards based on the inhalable fraction, *The Analyst*, 121, 1207-1214.

Wiener, R.W. et al. (1988), Influence of turbulence on aerosol sampling efficiency, *Atmos. Environ.*, 22, 917-928.

Wilson, J.C. and Liu, B.Y.H. (1980), Aerodynamic particle size measurement by laser-doppler velocimetry, *J. Aerosol Sci.*, 11, 139-150. Exposures to inhalable and 'total' oil mist aerosol by metal machining shop workers, *Am*

Wilsey, P.W., Vincent, J.H., Bishop, M.J., Brosseau and I.A. Greaves (1996),. *Ind. Hyg. Ass. J.*, 57, 1149-1153.

Witschger, O., Willeke, K., Grinsphun, S., Aizenberg, V., Smith, J. and Baron, P.A. (1997), Simplified method for testing personal aerosol samplers, *J. Aerosol Sci.*, in press.

Yoshida, H., Uragami, M., Masuda, H., and Iinoya, K. (1978), Particle sampling efficiency in still air, *Kagaku Kogaku Ronbunshu*, 4, 123-8 (HSE translation No. 8586).

PRESENT AND EXPECTED FUTURE PUBLICATIONS ARISING FROM THE RESEARCH

Published

Sreenath, A., Ramachandran, G. and Vincent, J.H. (1996), Experimental studies of the aspiration efficiencies of blunt aerosol samplers at large angles to the wind, *J. Aerosol Sci.*, 27, Supplement 1, S677-S678.

Sreenath, A., Ramachandran, G. and Vincent, J.H. (1997), Experimental investigations into the nature of airflows near bluff bodies with aspiration, with implications to aerosol sampling, *Atmos. Environ.*, 31, 2349-2359.

Vincent, J.H., Ramachandran, G., Pui, D.Y.H., Gomes, M.S.P., Sato, S. and Sreenath, A. (1997), Experimental studies of particle transport in air flows near bluff bodies with and without aspiration, *Proceedings of the 1997 ASME Fluids Engineering Division Summer Meeting (FESM'97)*, American Society of Mechanical Engineers, Paper 3634 (CD-ROM).

Ramachandran, G., Sreenath, A. and Vincent, J.H. (1998), Towards a new method for experimental determination of aerosol sampler aspiration efficiency in small wind tunnels, *J. Aerosol Sci.*, 29, 875-891.

In press

Vincent, J.H. (1998), Advances in aerosol sampling science and its applications, *J. Aerosol Sci.*, in press (invited plenary lecture to the International Aerosols Conference, Edinburgh, U.K., September 1998)

Submitted

Sreenath, A., Ramachandran, G., and Vincent, J.H. (1998), Experimental measurements and development of improved physical models for aerosol sampler aspiration efficiency, *Appl. Occup. Environ. Hyg.*, submitted.

In preparation

Sreenath, A., Ramachandran, G., and Vincent, J.H. (1998), Correction of APS particle counts from ex perimental studies with thin-walled probes, in preparation

Sreenath, A., Ramachandran, G., and Vincent, J.H. (1998), Angular dependence of the sampling efficiency of thin-walled aerosol sampling probes, in preparation.

Sreenath, A., Ramachandran, G., and Vincent, J.H. (1998), Wind tunnel studies of the sampling efficiency of a simple blunt aerosol sampler at various angles to the wind, in preparation.

Sreenath, A., Ramachandran, G., and Vincent, J.H. (1998), Experimental studies of the roles of attitude and asymmetry on the sampling efficiency of blunt aerosol samplers, in preparation.

Vincent, J.H., Ramachandran, G. and Thomassen, Y. (1998), Applications of recent advances in aerosol sampling science towards the development of improved sampling devices: the way ahead, in preparation (invited paper to the AirMon '99 Symposium in Geilo, Norway, February 1999, to be published by the Royal Society of Chemistry, U.K.).

FIGURES

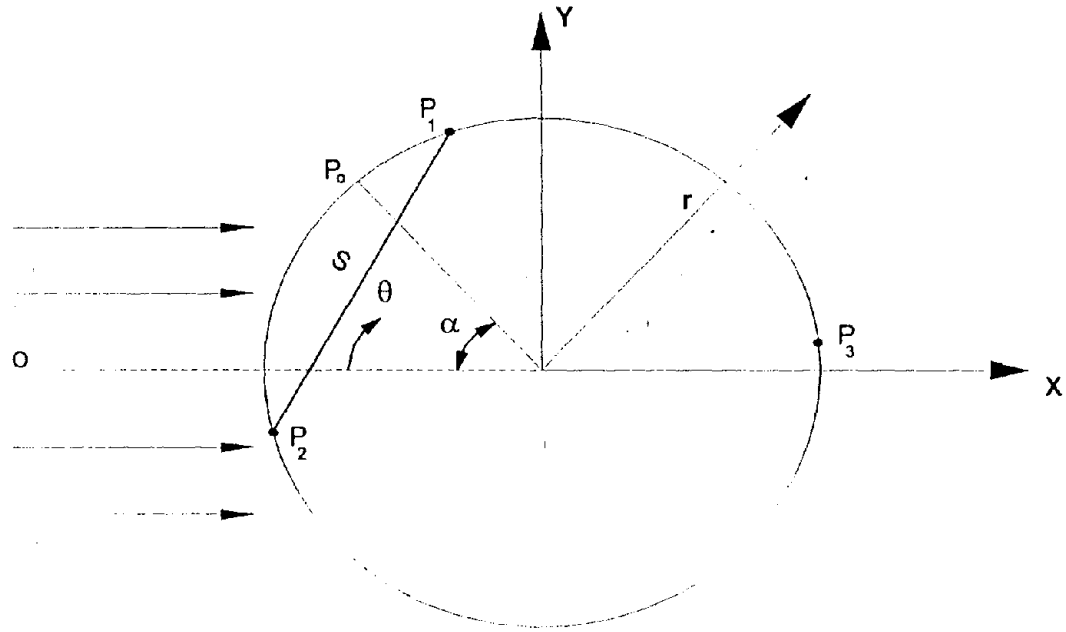

Figure 3.1 Coordinate system for the cylindrical body with aspiration

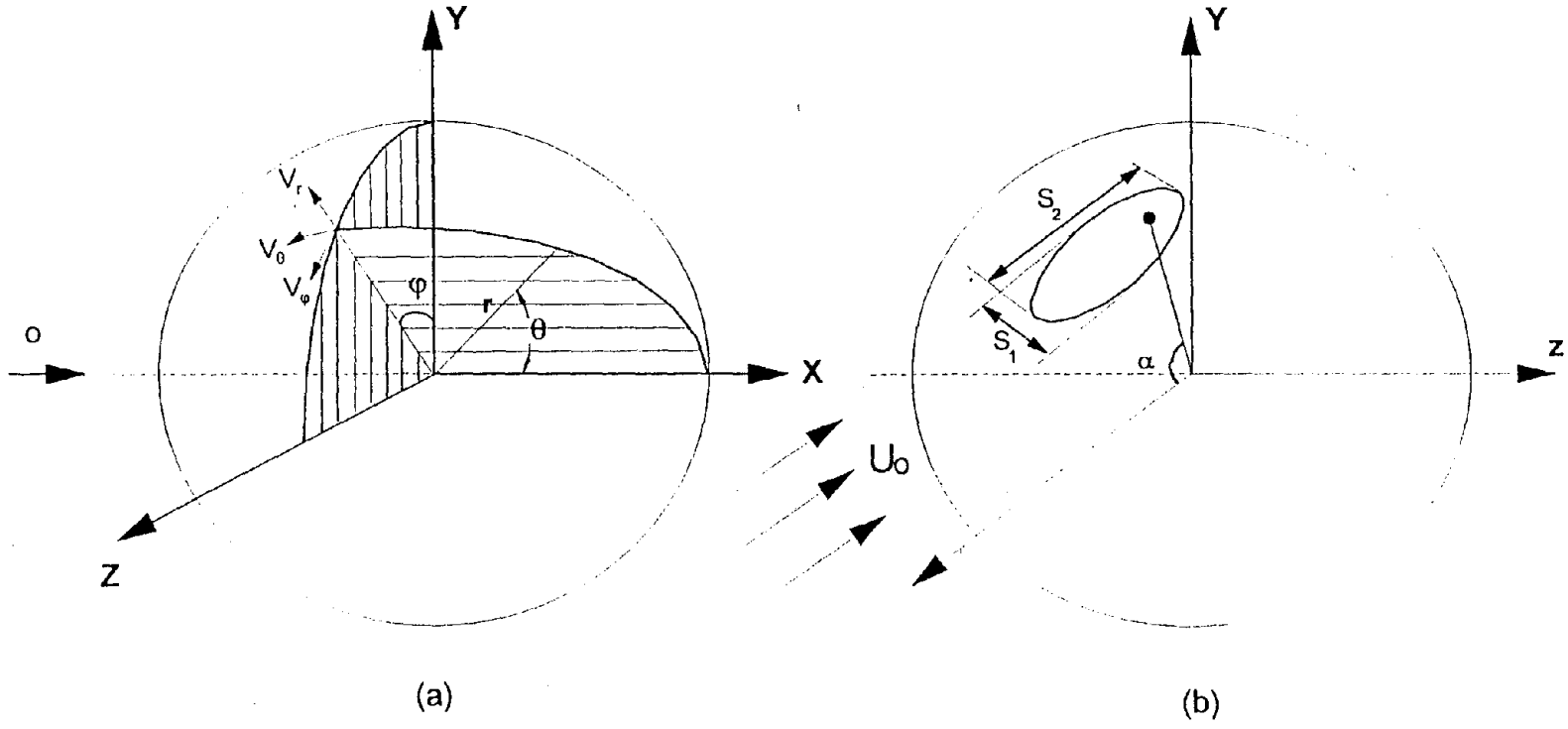

Figure 3.2 (a) Coordinate system for the spherical body with aspiration, where α is the angle of the orifice with respect to the forwards facing orifice
(b) Diagram indicating the stagnation zone

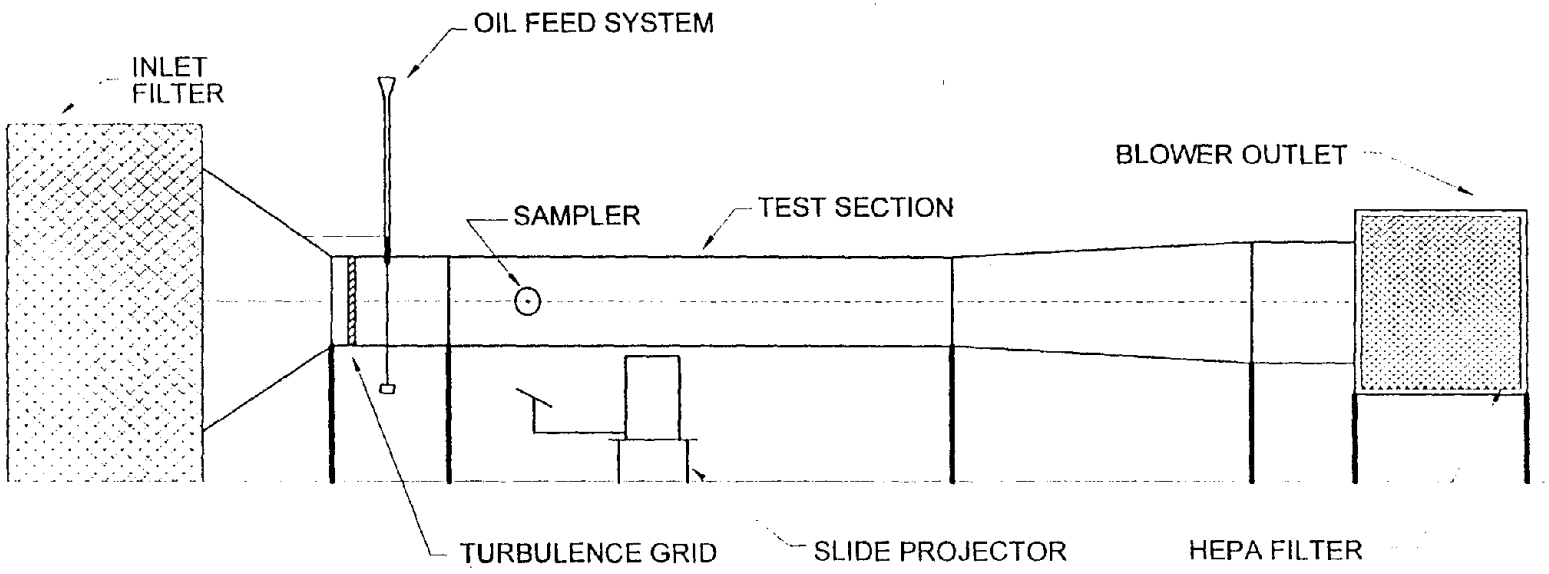

Figure 3.3 Schematic of the wind tunnel

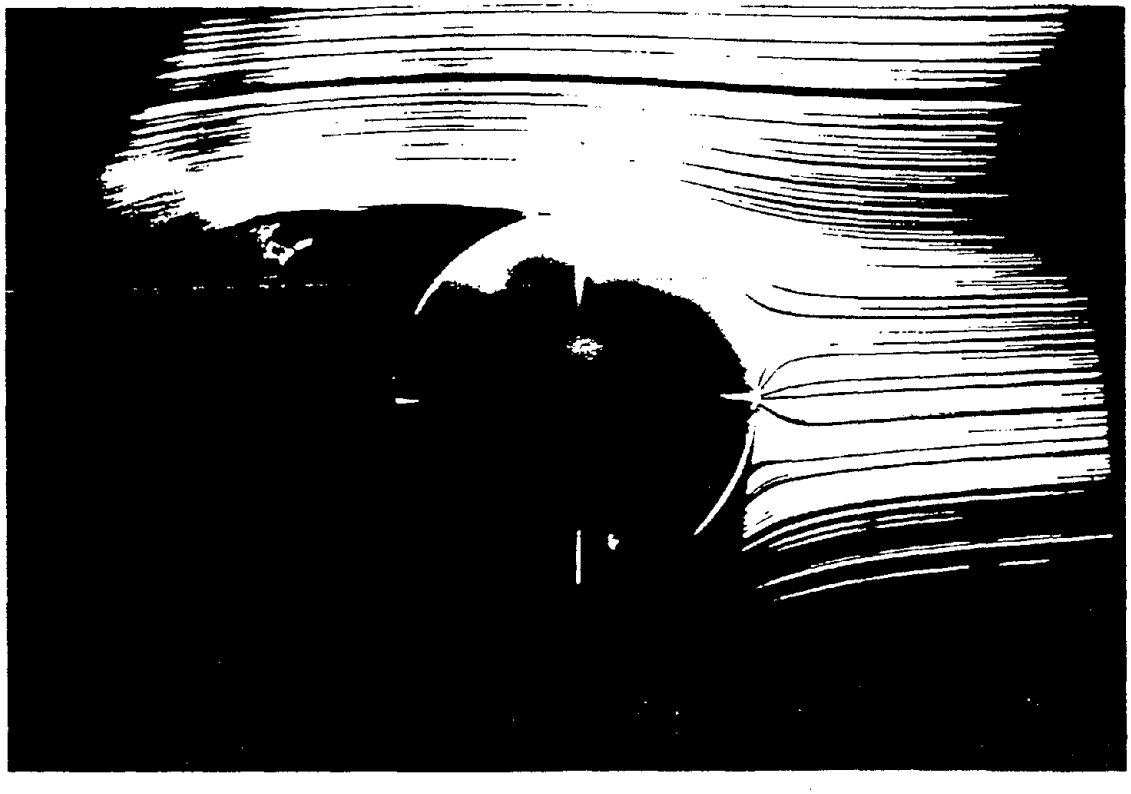

Figure 3.4 Photographs of flow visualizations

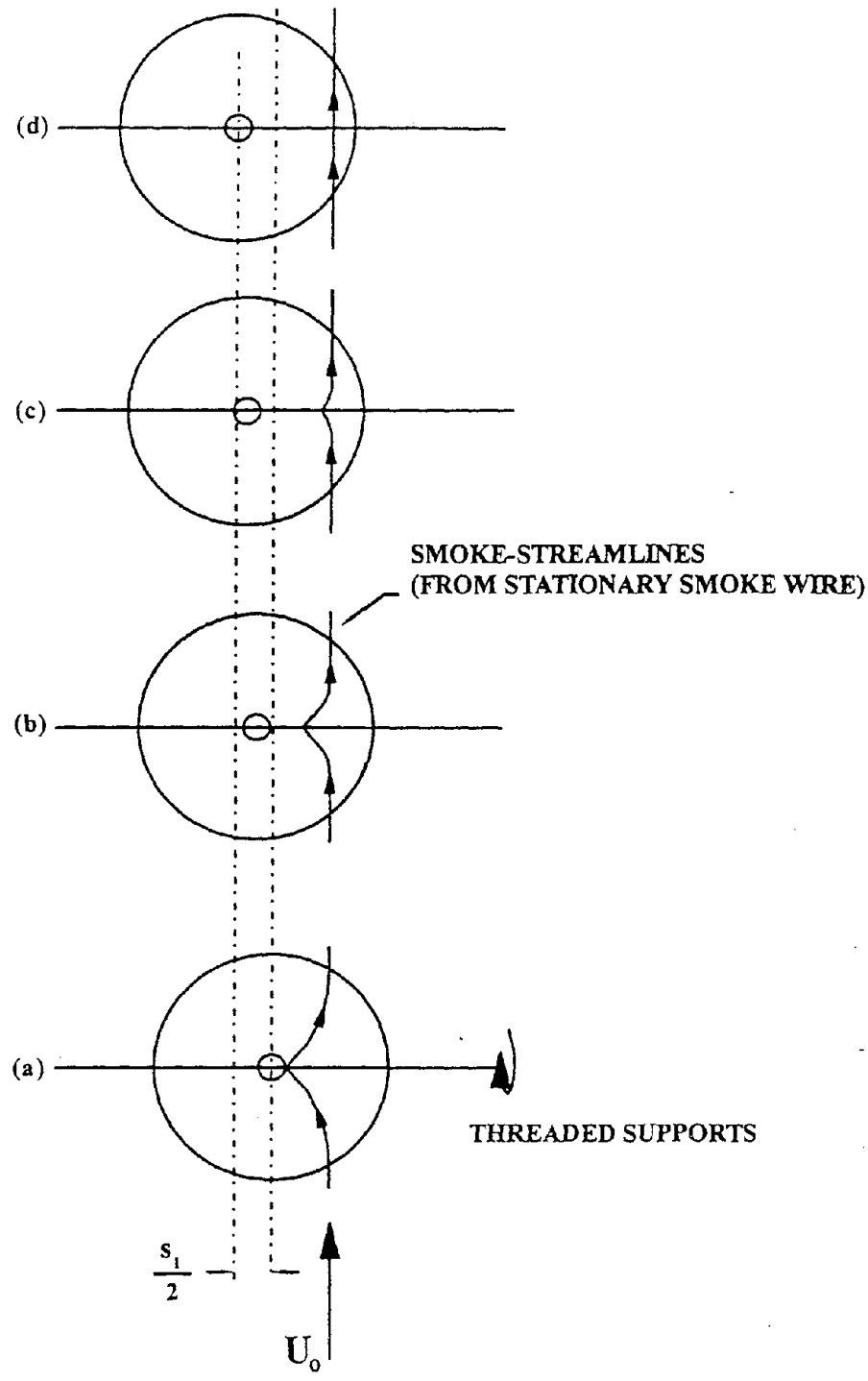

Figure 3.5 Diagram to indicate sequence of events in measuring the width S_1 of the upstream projected stagnation region transverse to the freestream for a spherical sampler with aspiration

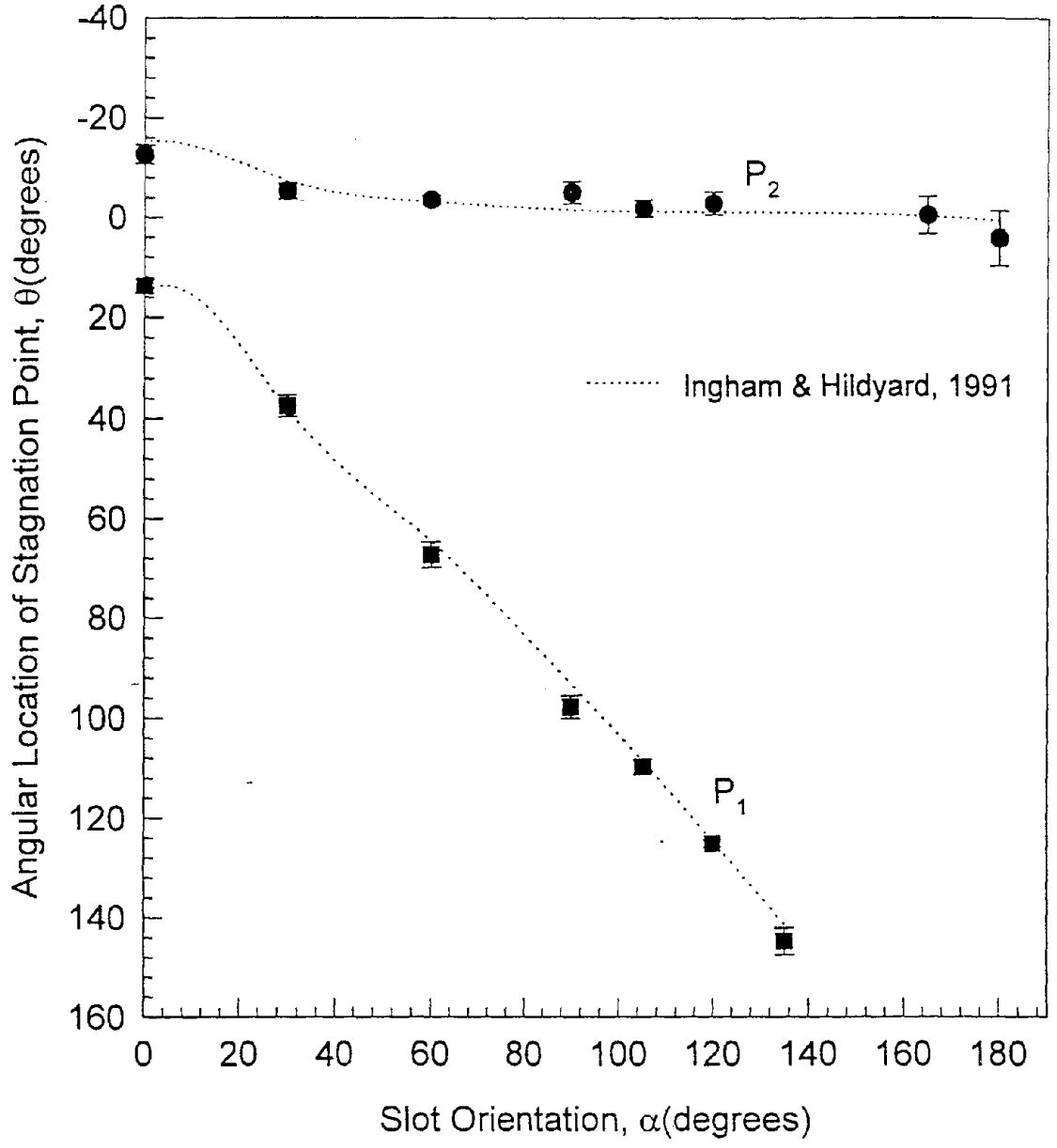

Figure 3.6 Experimental results for the angular position (θ) of the stagnation points at various slot orientations (α) for $\phi_c = 0.25$ and $U = 0.76$ m/s

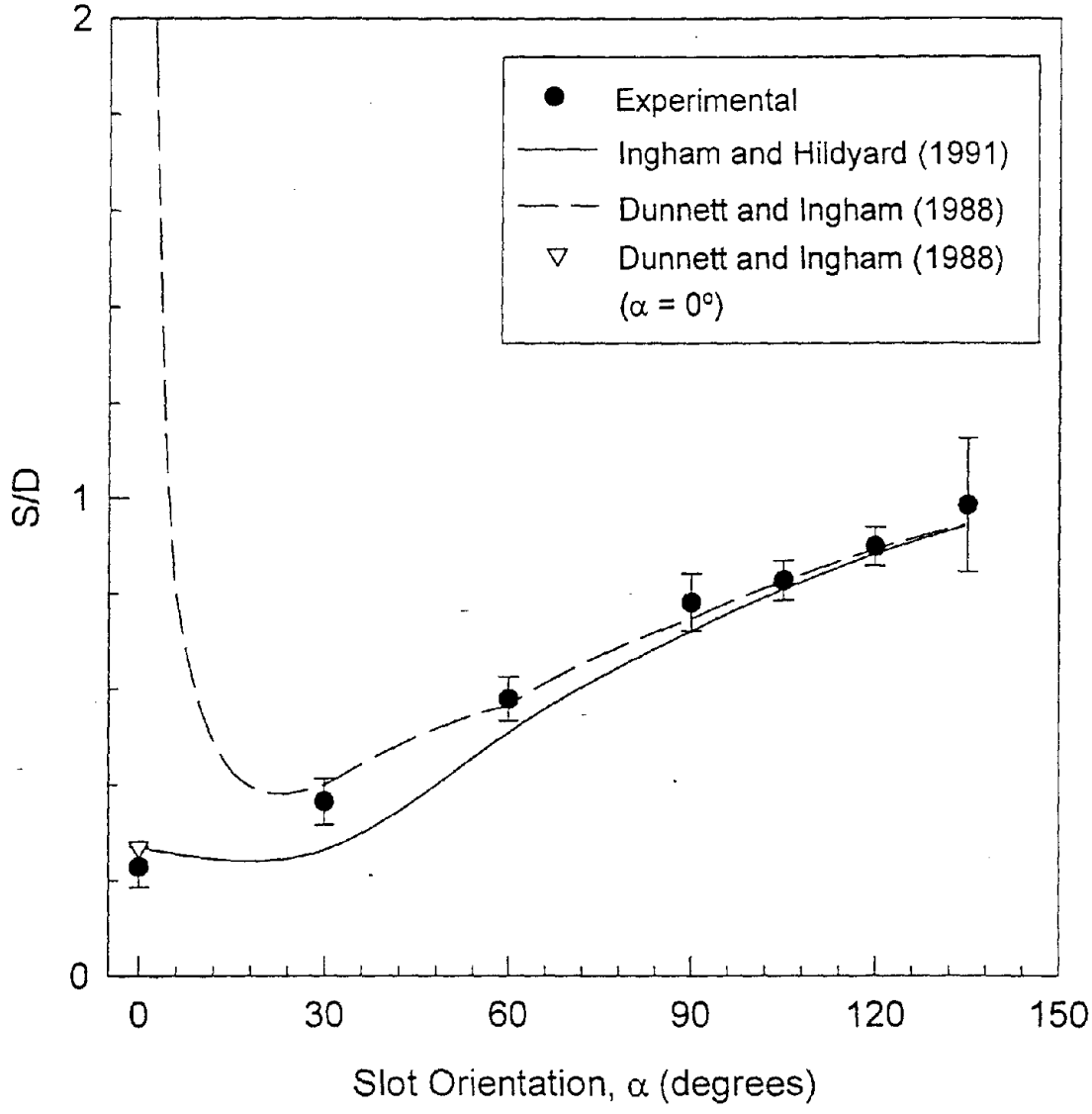

Figure 3.7 Dimensionless linear width of the stagnation zone (*S/D*) for a circular cylinder with aspiration, comparison of experimental data with Dunnett and Ingham (1988)

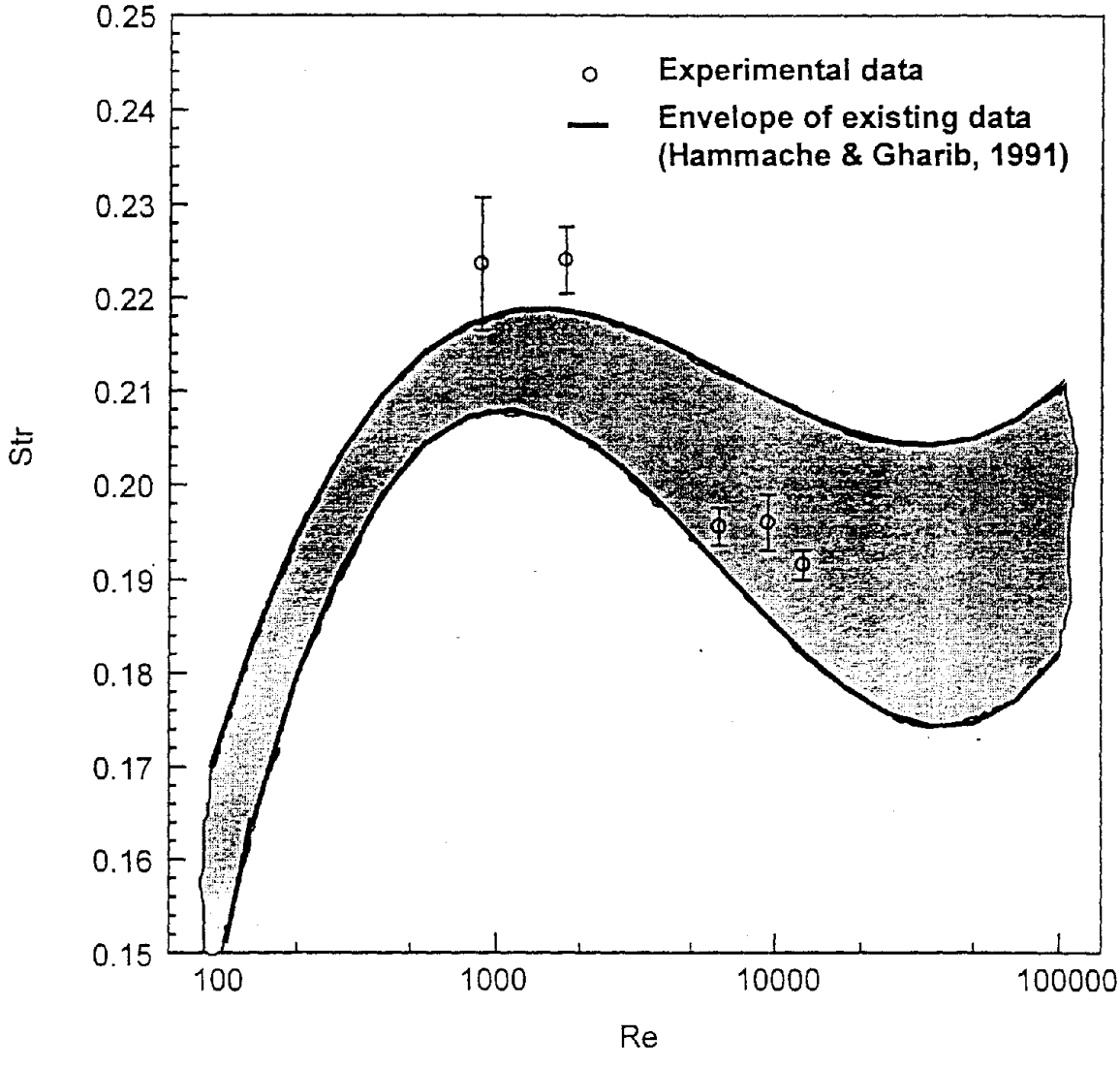

Figure 3.8 Experimental results of *Str* as a function of *Re* for a cylinder without aspiration;data from current study and envelope of data from literature (Hammache and Gharib, 1991)

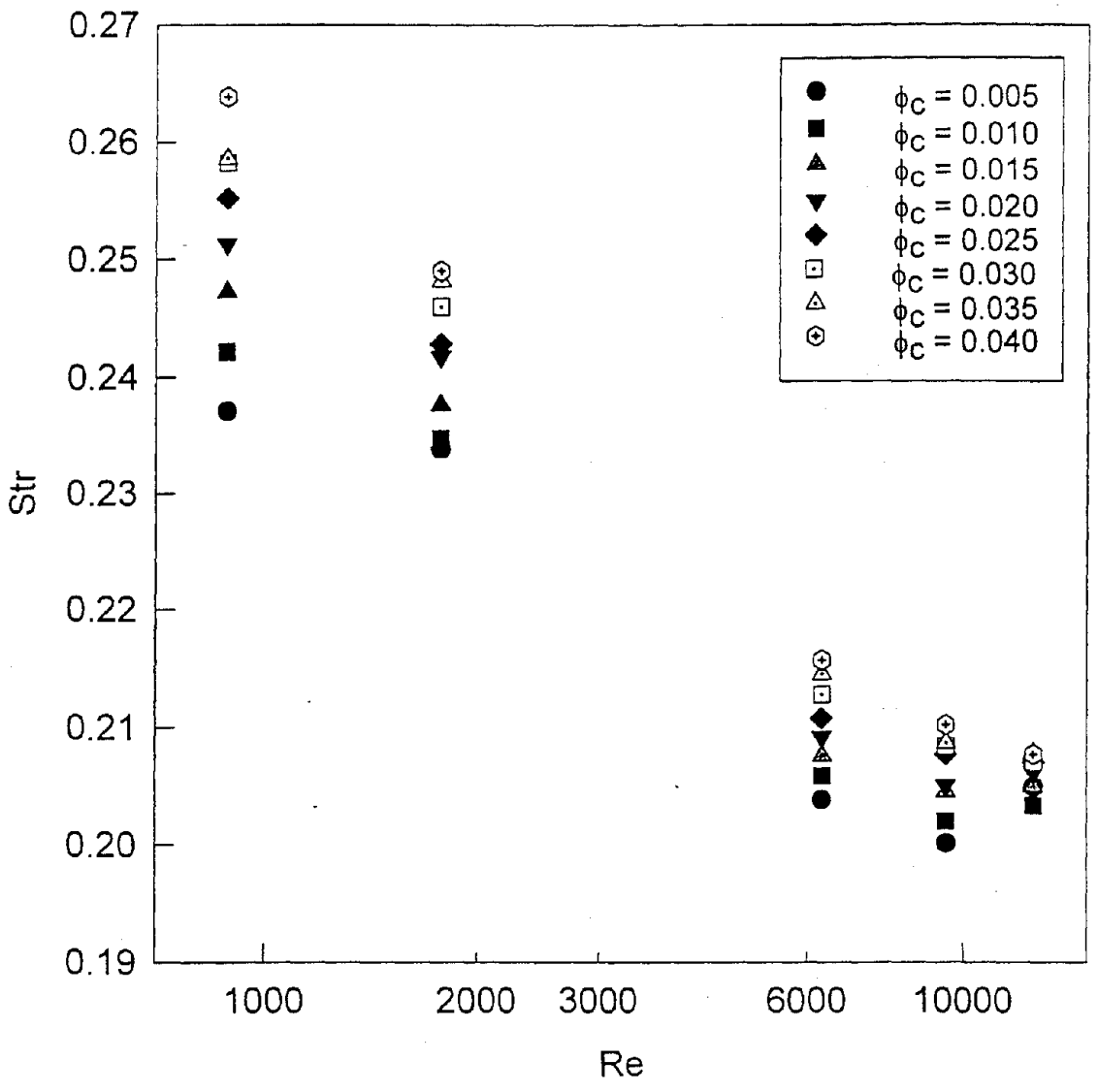

Figure 3.9 Experimental results of *Str* as a function of *Re* for a cylinder with aspiration for various values of ϕ_c for $\alpha = 60°$

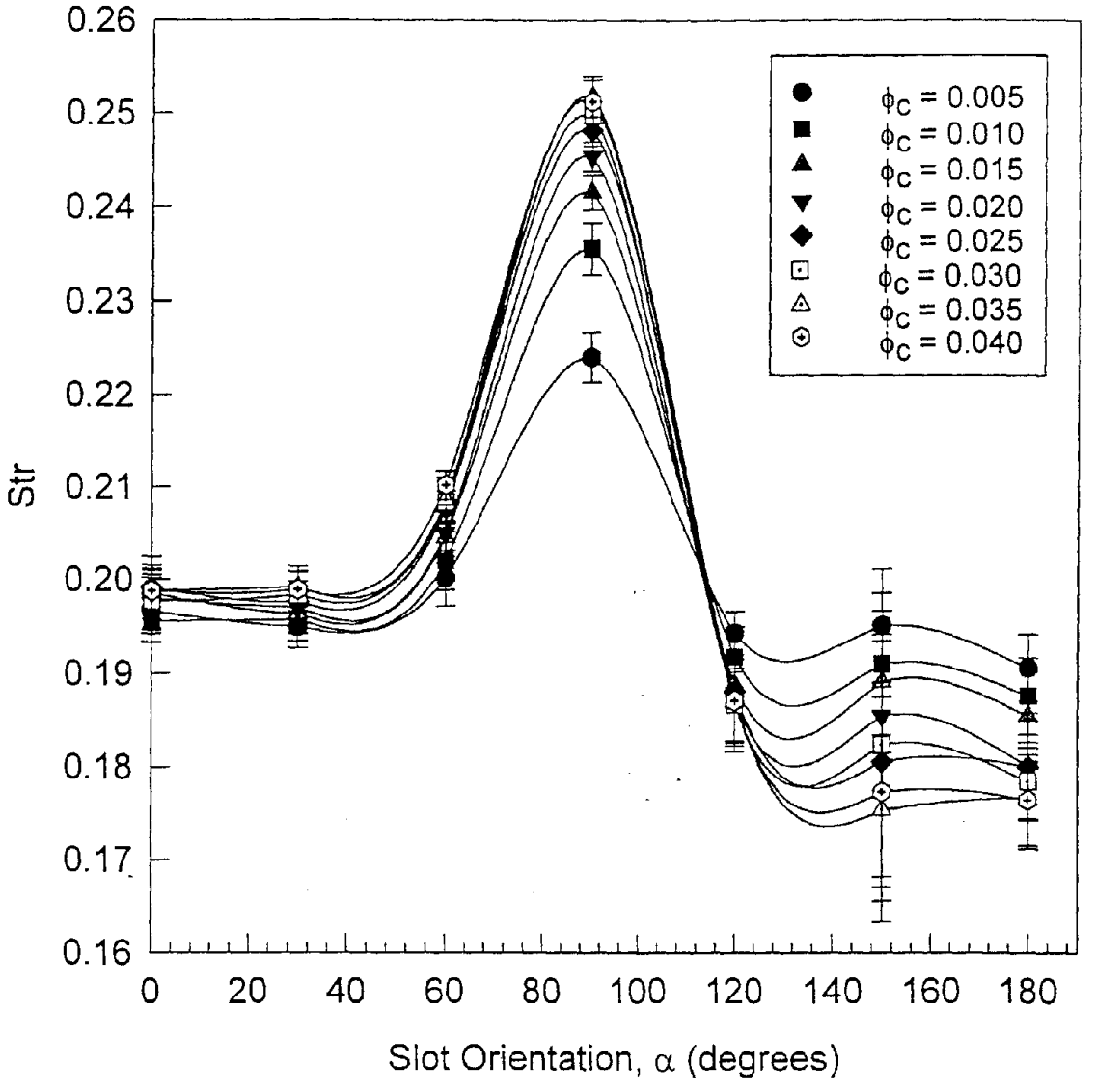

Figure 3.10 Experimental results for *Str* as a function of angular position of the orifice (α) for a cylinder with aspiration for various values of ϕ_c for $U = 4.5$ m/s and $Re = 9450$

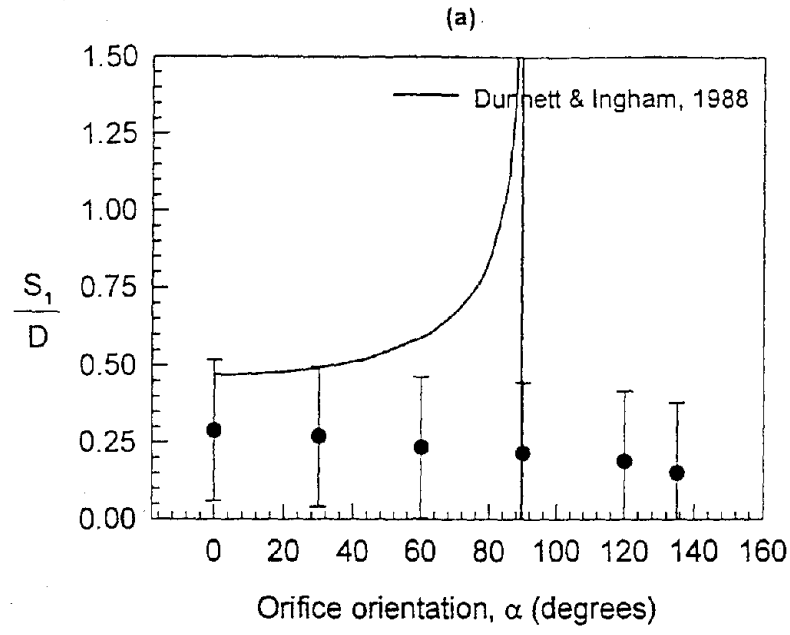

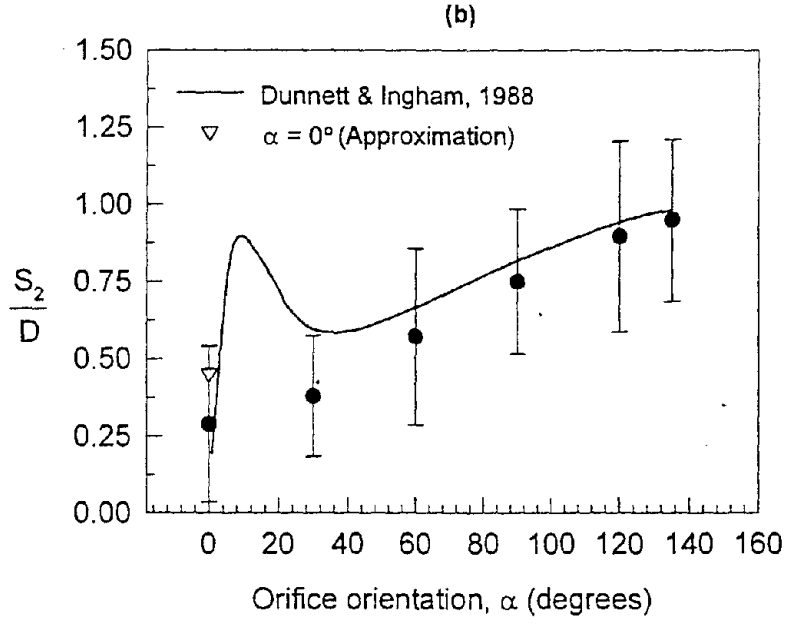

Figure 3.11(a) and (b) Experimental results for the linear widths of the stagnation region, S_1 and S_2 for a spherical body with aspiration, as functions of α; comparison with the potential flow model of Dunnett and Ingham (1988) for $\phi_s = 0.31$ and $U = 0.76$ m/s

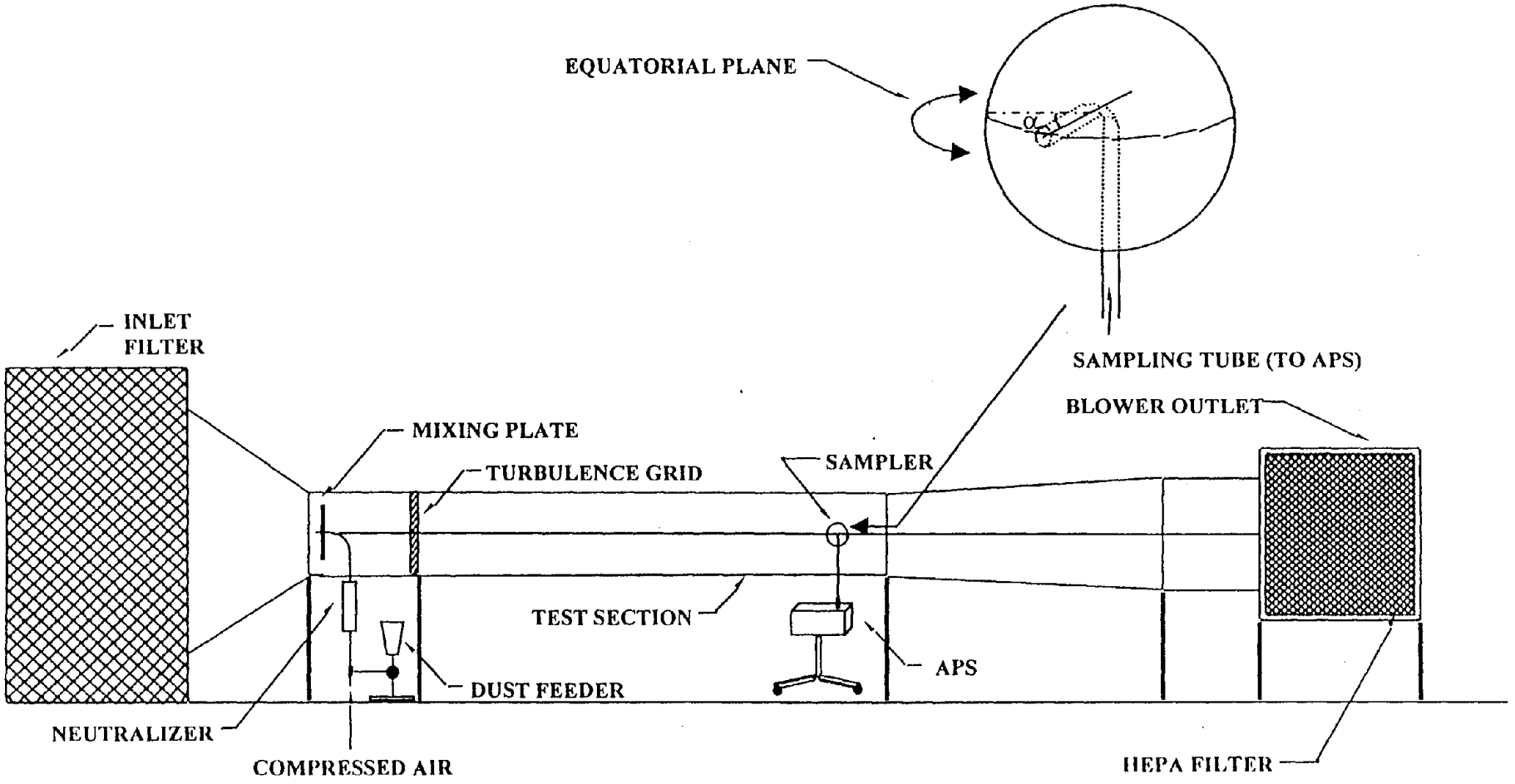

Figure 4.1 Schematic of the Wind Tunnel

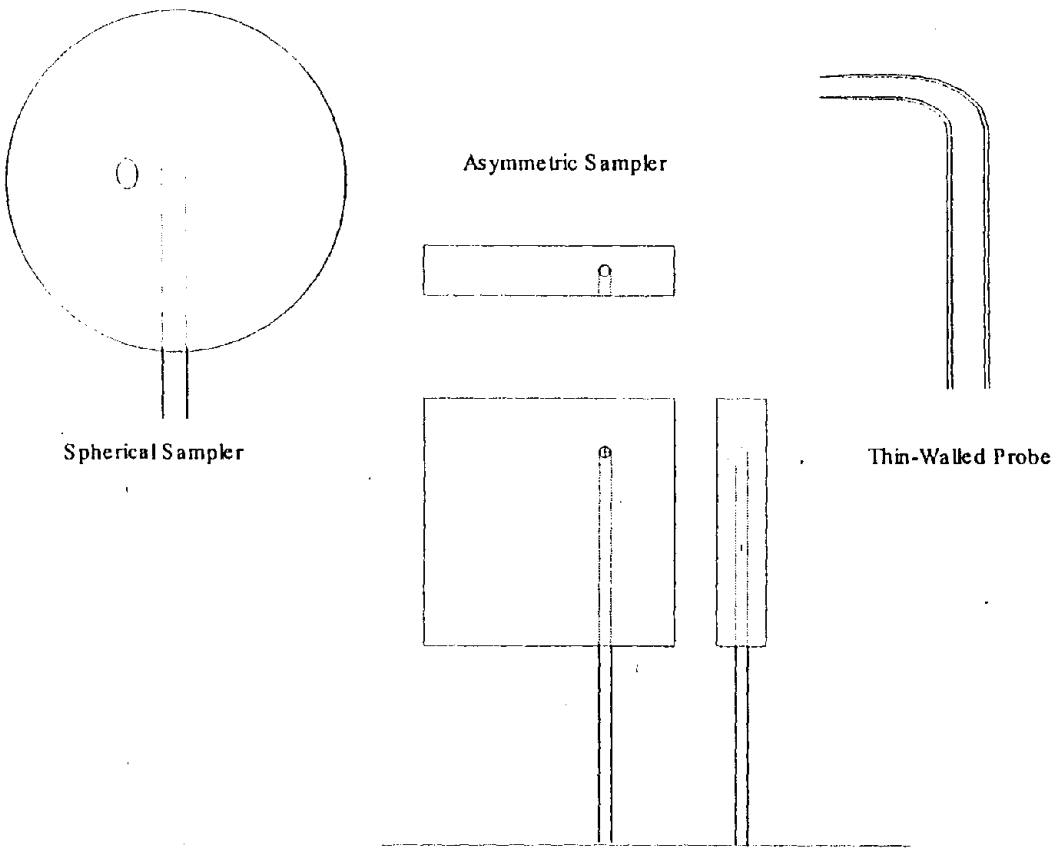

Figure 4.2 Description of the Samplers

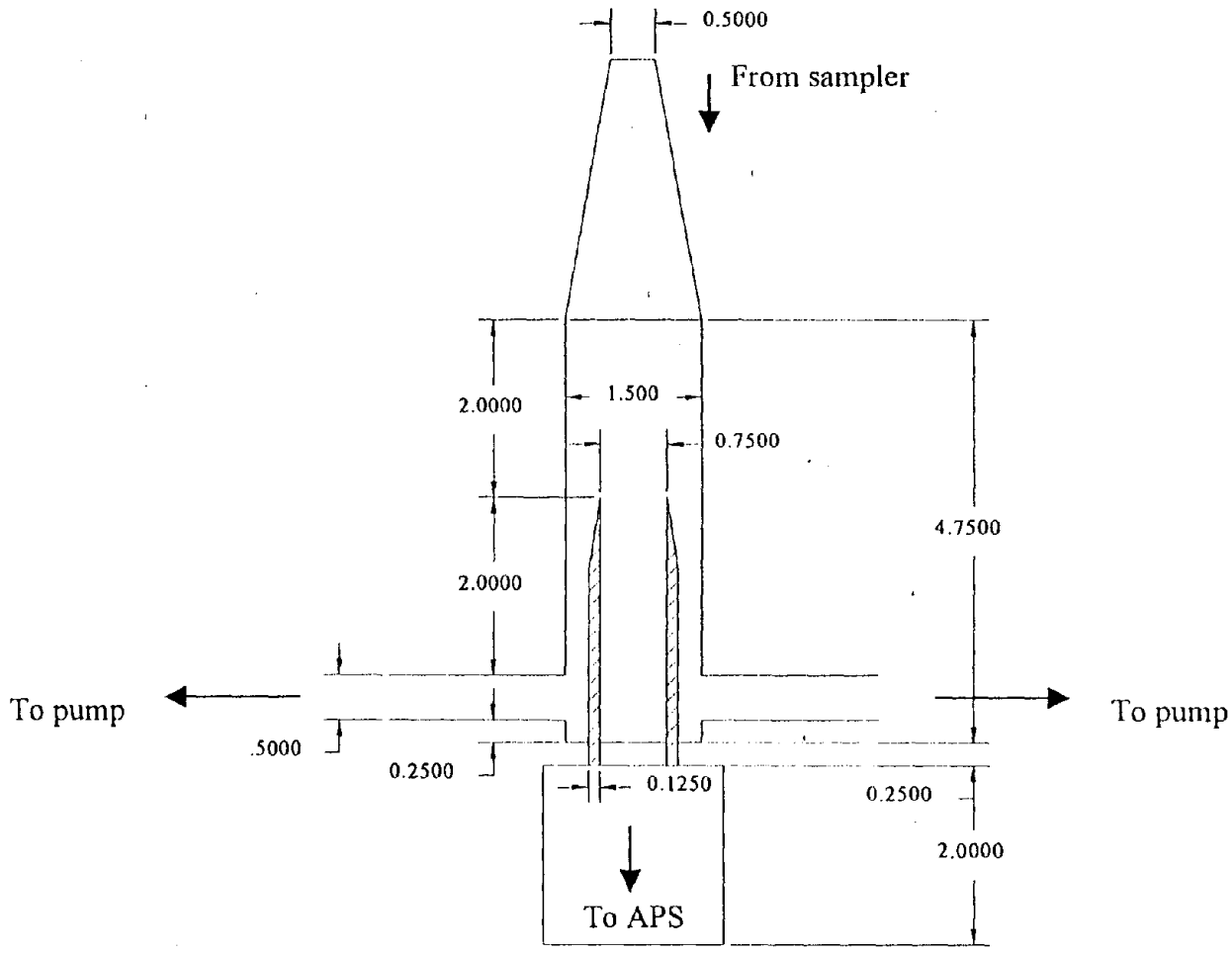

Figure 4.3 Schematic of the APS Inlet Adaptor for Variable Flow

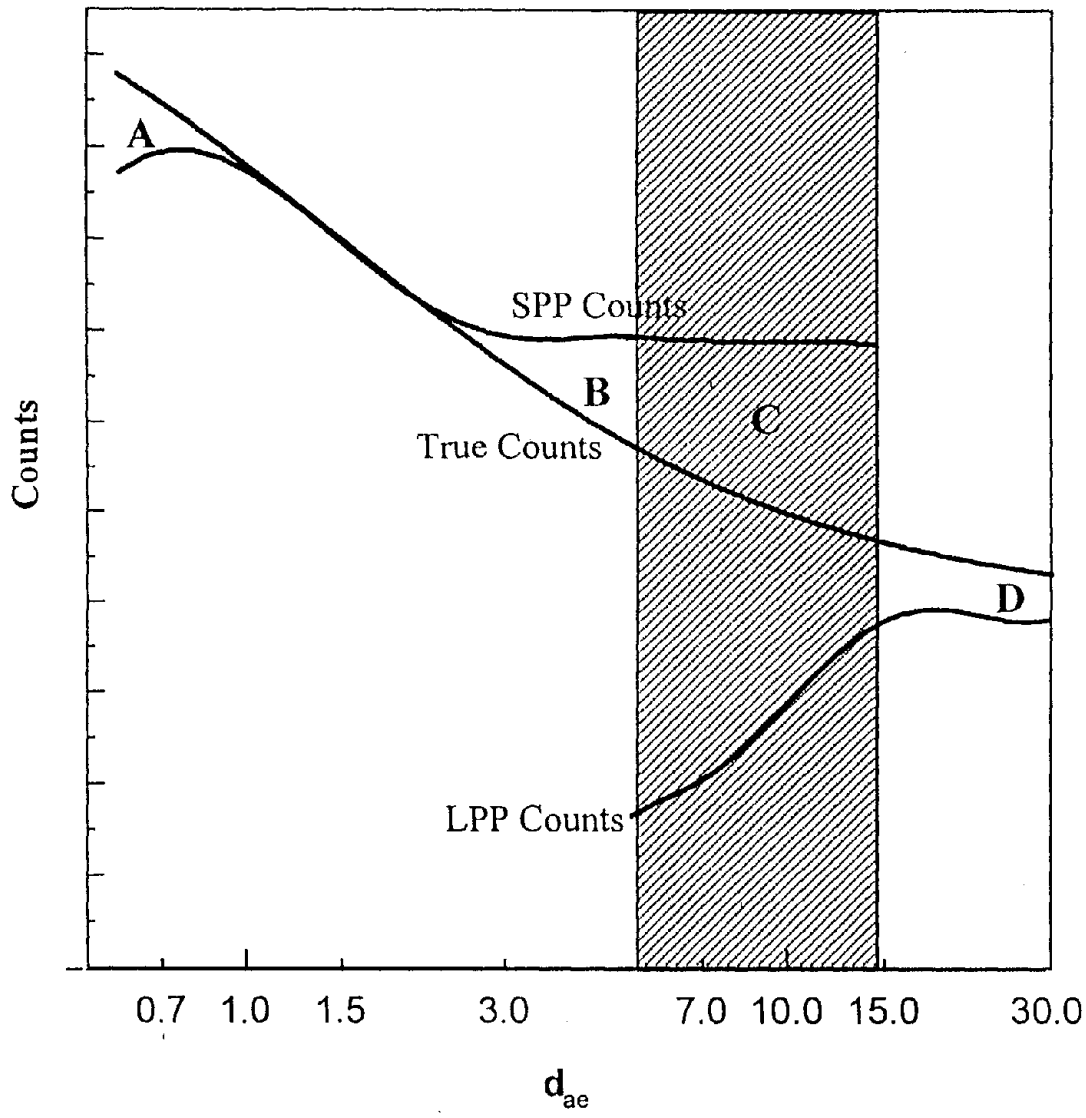

Figure 4.4 Counting Efficiency of the Small Particle Processor and the Large Particle Processor

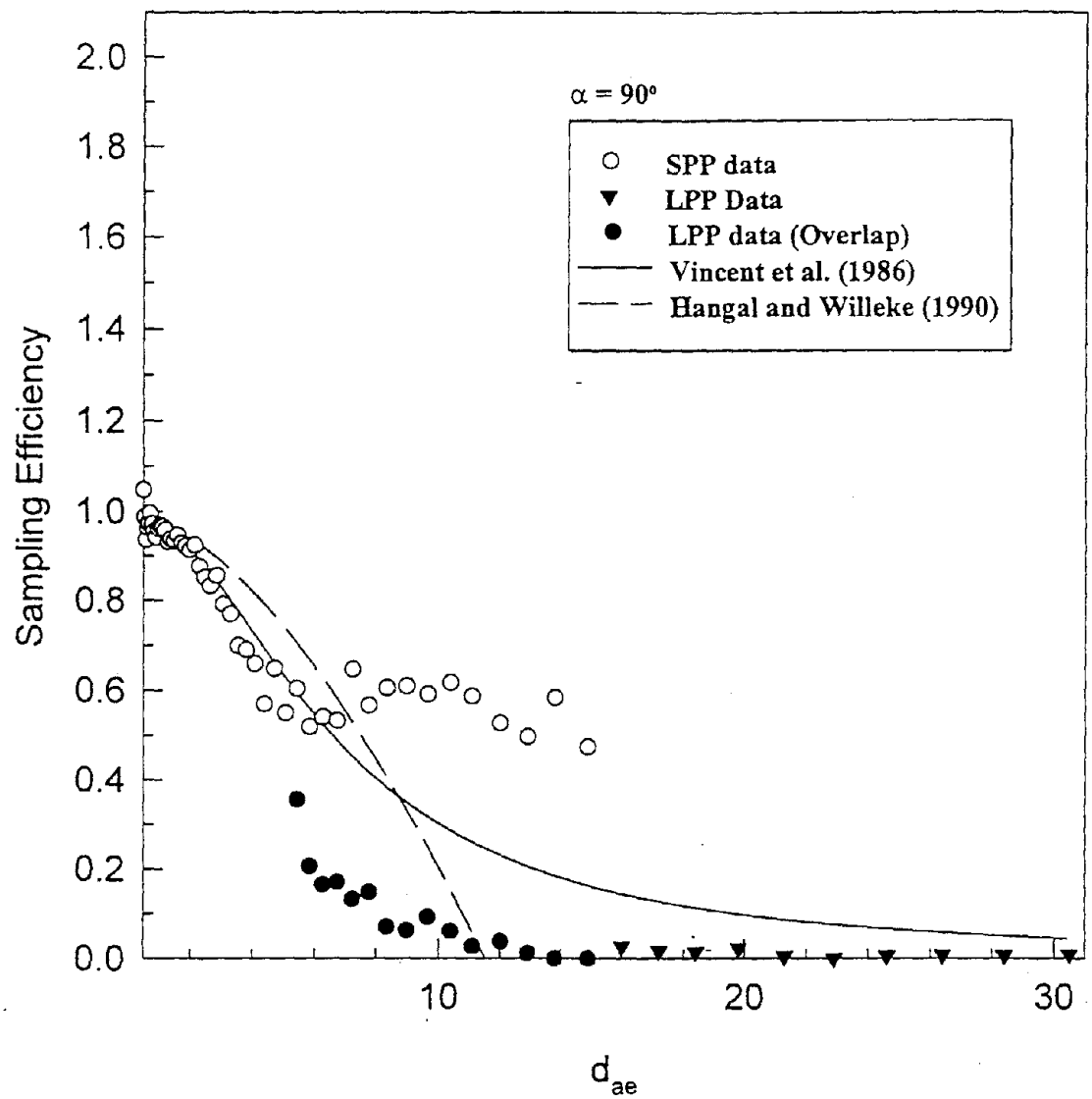

Figure 4.5 Plot of Sampling Efficiency Versus *St* for Thin-Walled Probe at $\alpha = 90°$ Compared with Theory

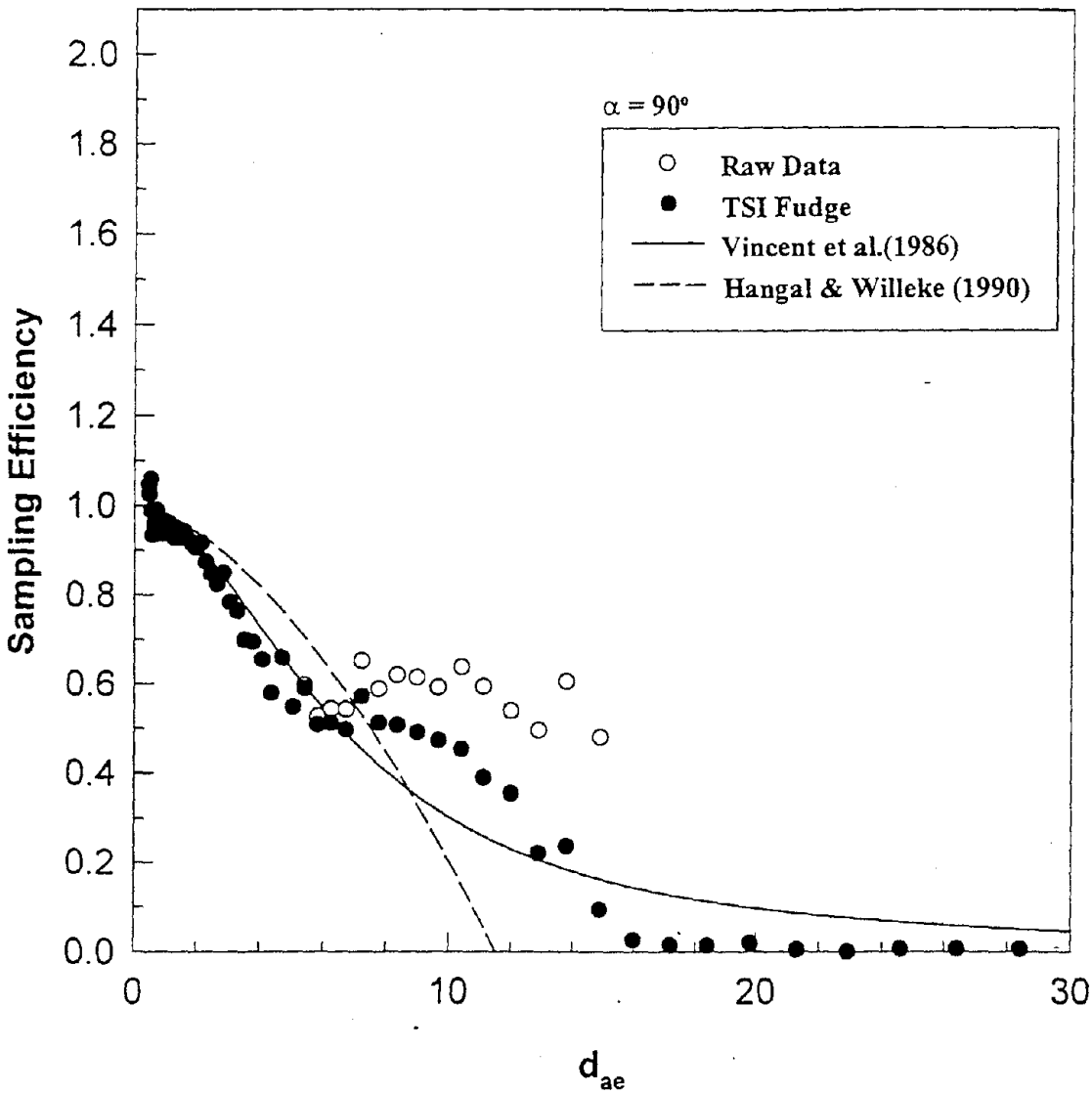

Figure 4.6 Plot of Sampling Efficiency Versus *St* for Thin-Walled Probe at $\alpha = 90°$ Derived Using TSI Correction Factors

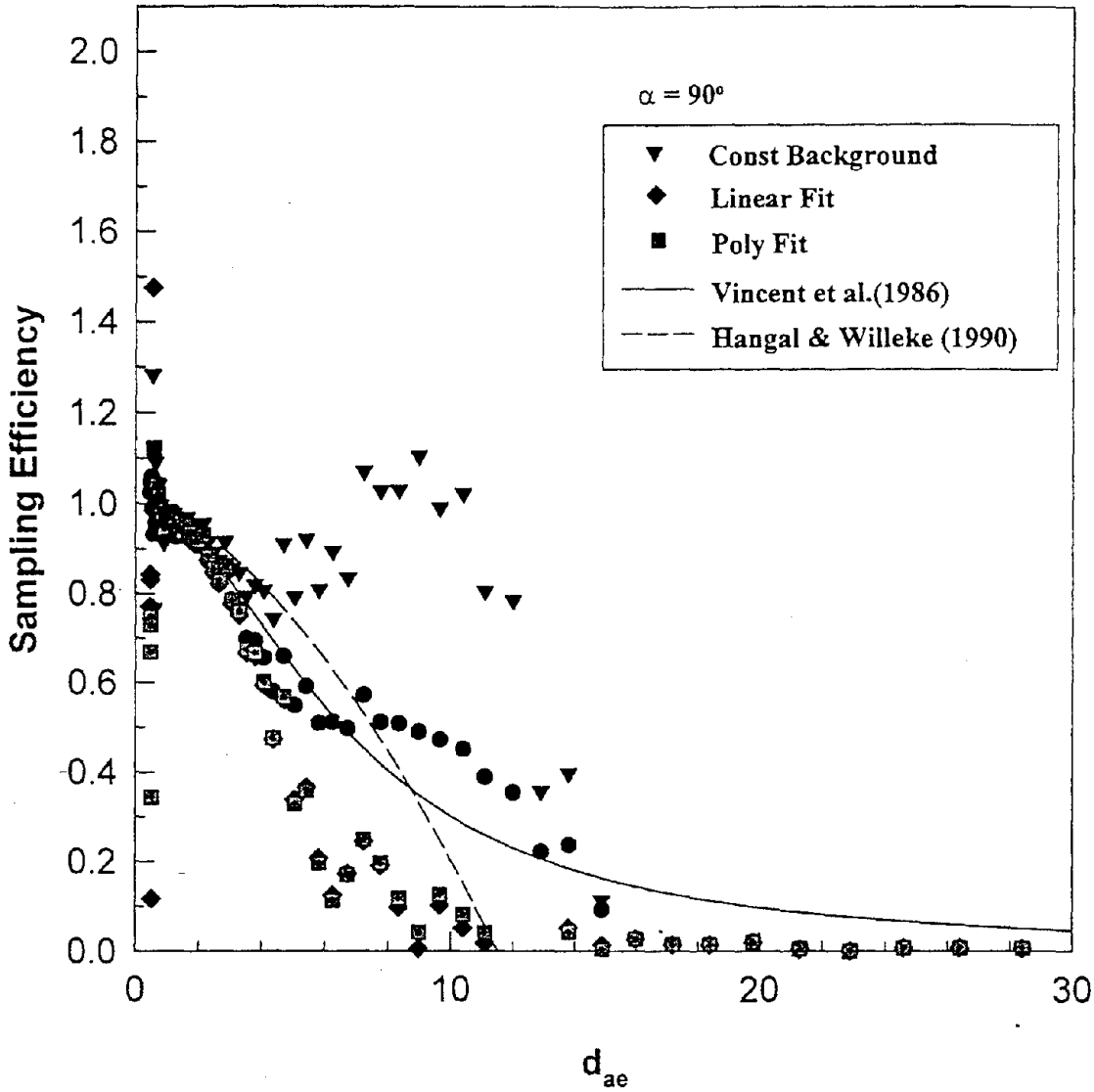

Figure 4.7 Comparison of Different Correction Factors for Sampling Efficiency of Thin-Walled Probe at $\alpha = 90°$

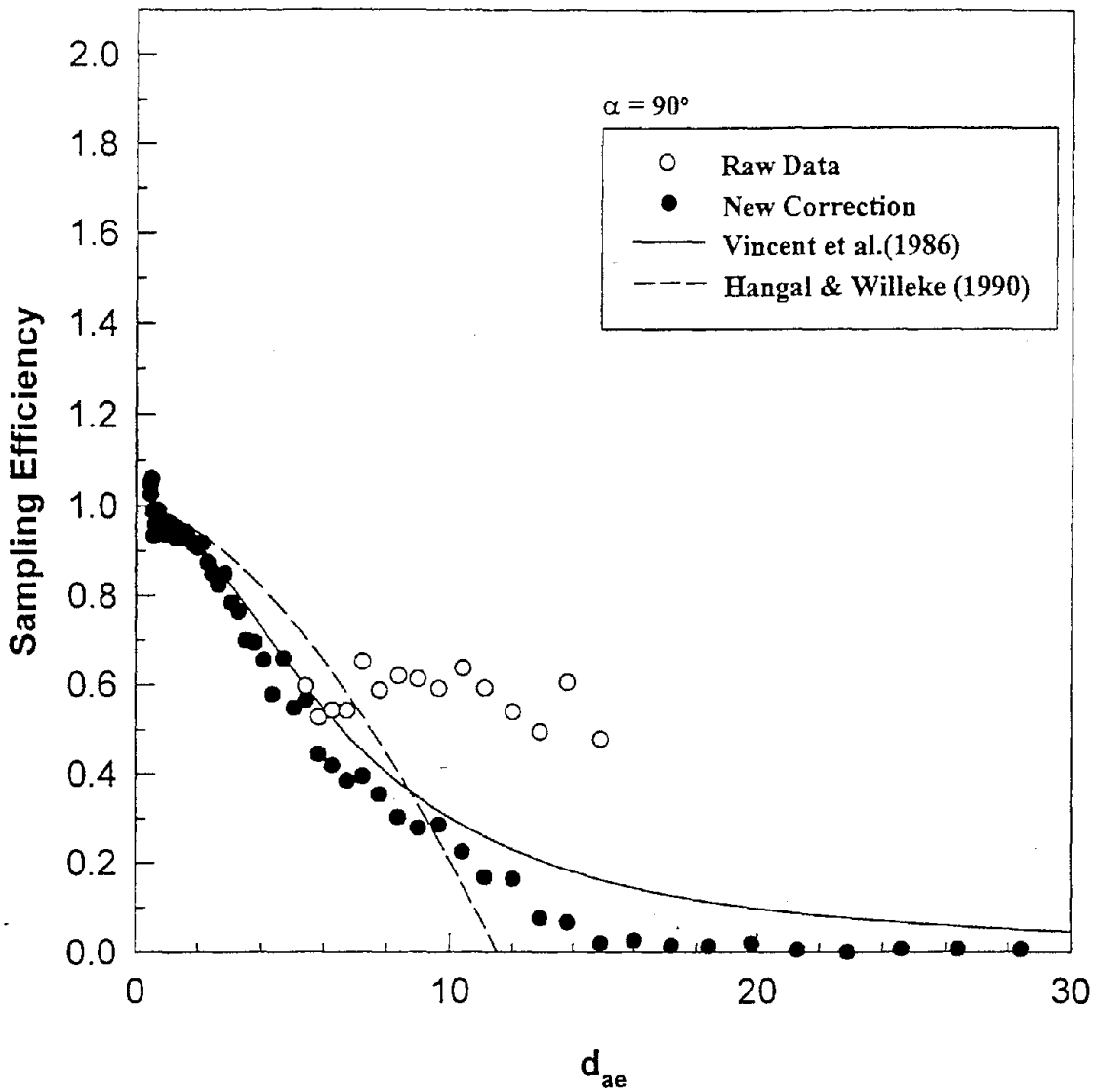

Figure 4.8 Comparison of our Correction Factors with Raw Data and Theory for Thin-Walled Probe at $\alpha = 90°$

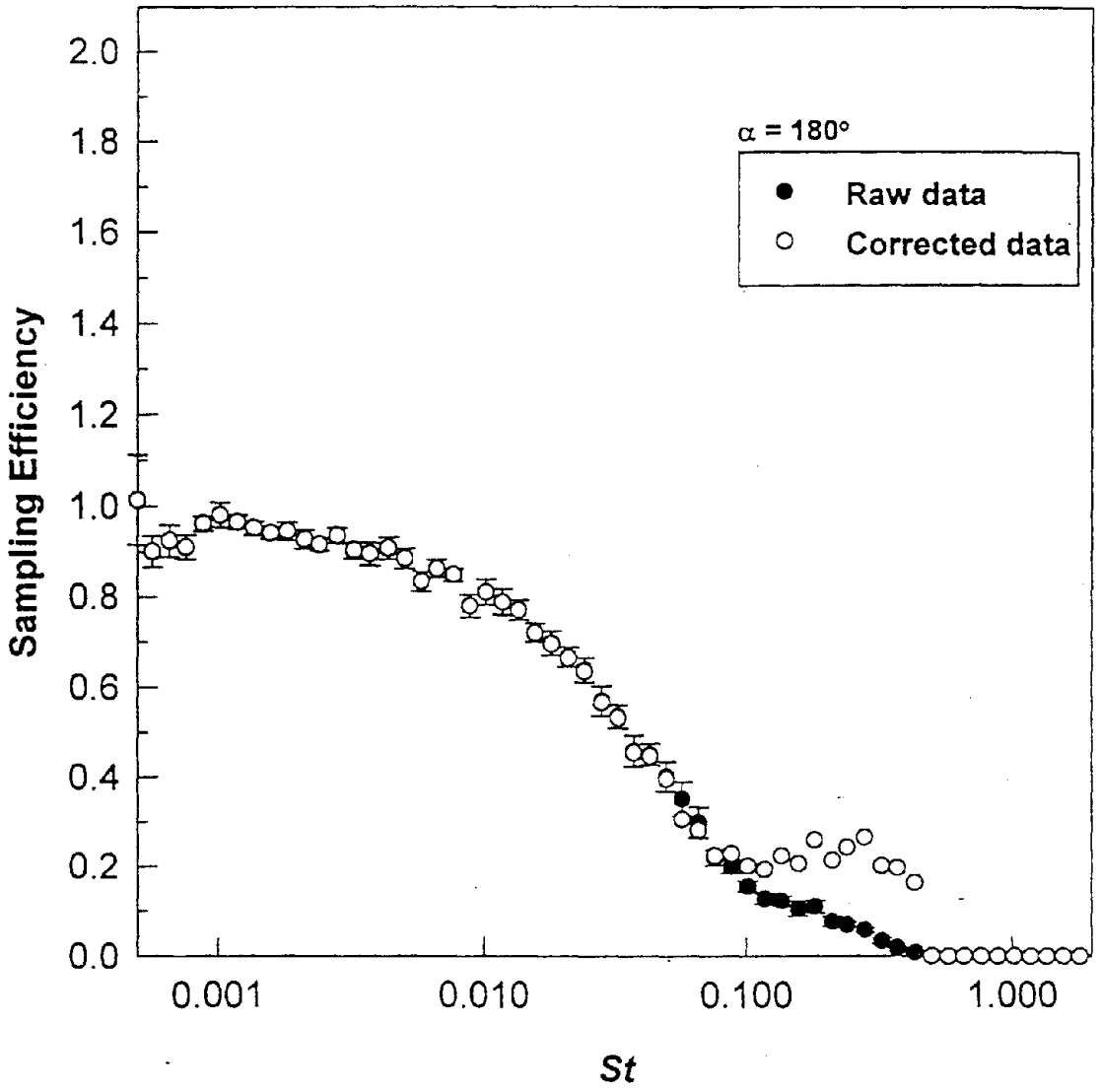

Figure 4.9 An Example of New Correction Factors Applied to Thin-Walled Probe at $\alpha = 90°$

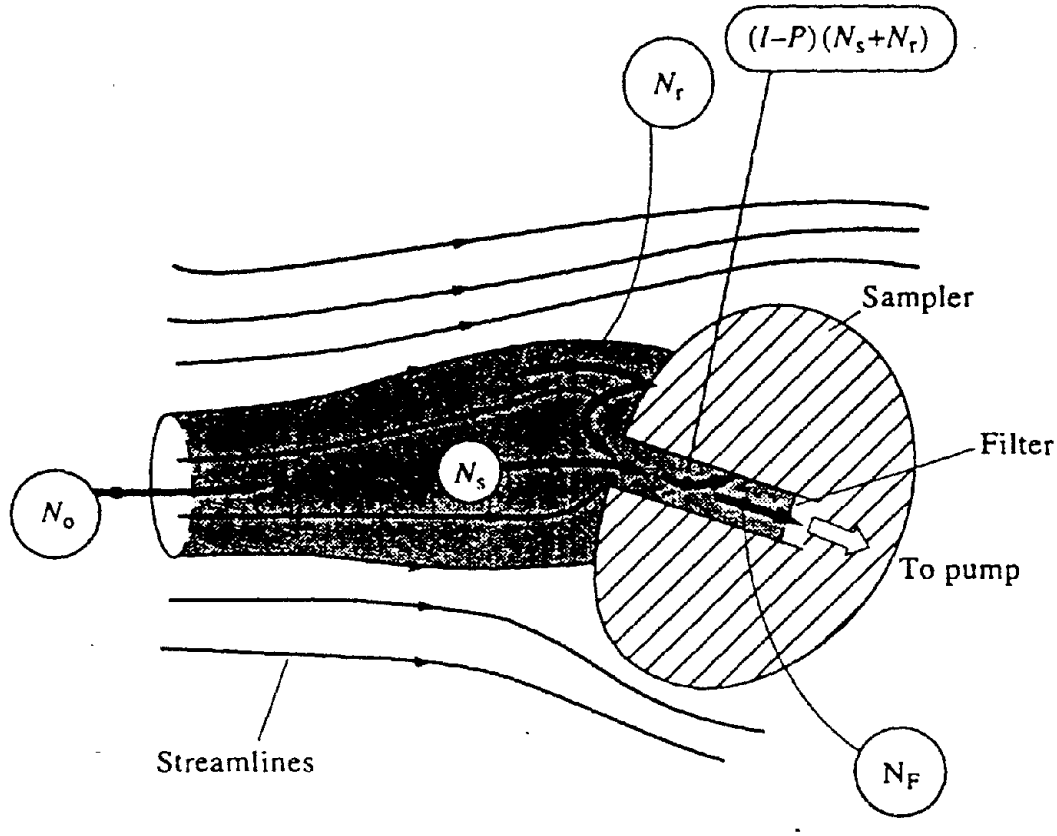

Figure 4.10: Air and particle flow near a blunt aerosol sampler of arbitrary shape And orientation, on which to base considerations of sampler performance (from Vincent, J.H., Aerosol Sampling: Science and Practice, Copyright 1989, adapted by permission of John Wiley and Sons Limited.)

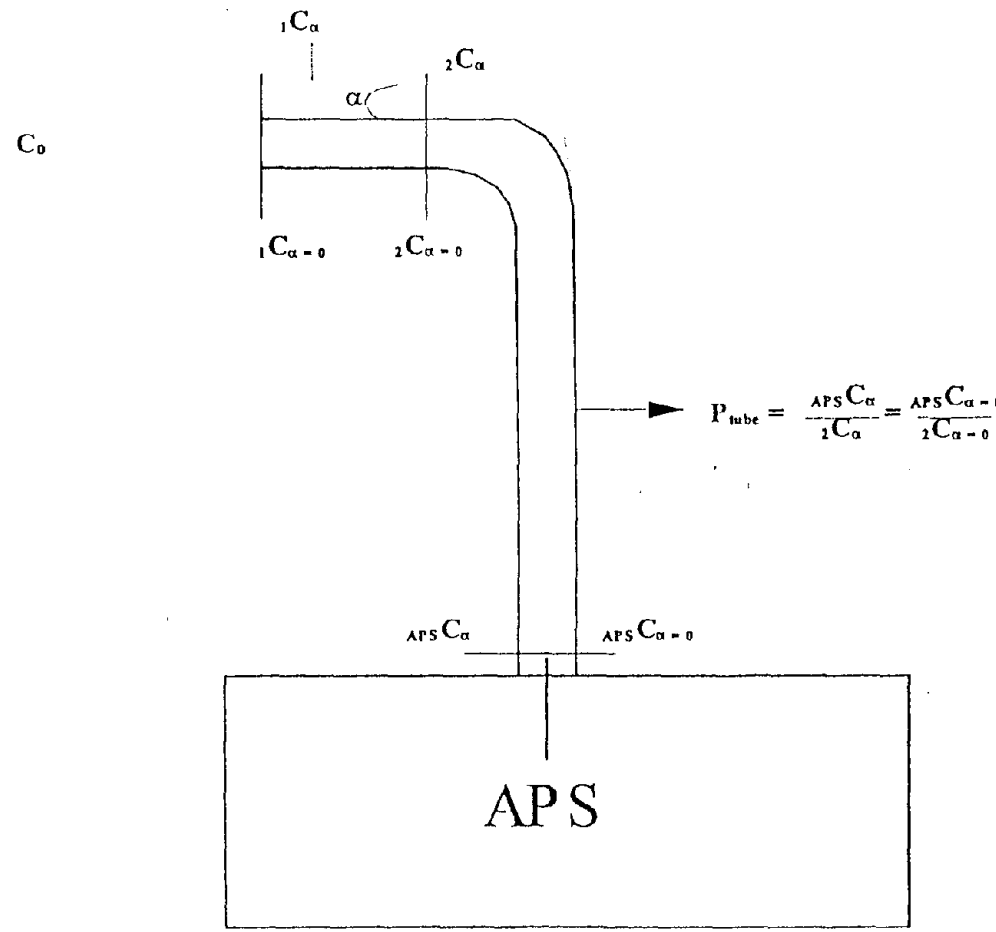

Figure 4.11 Schematic of the Sampling System

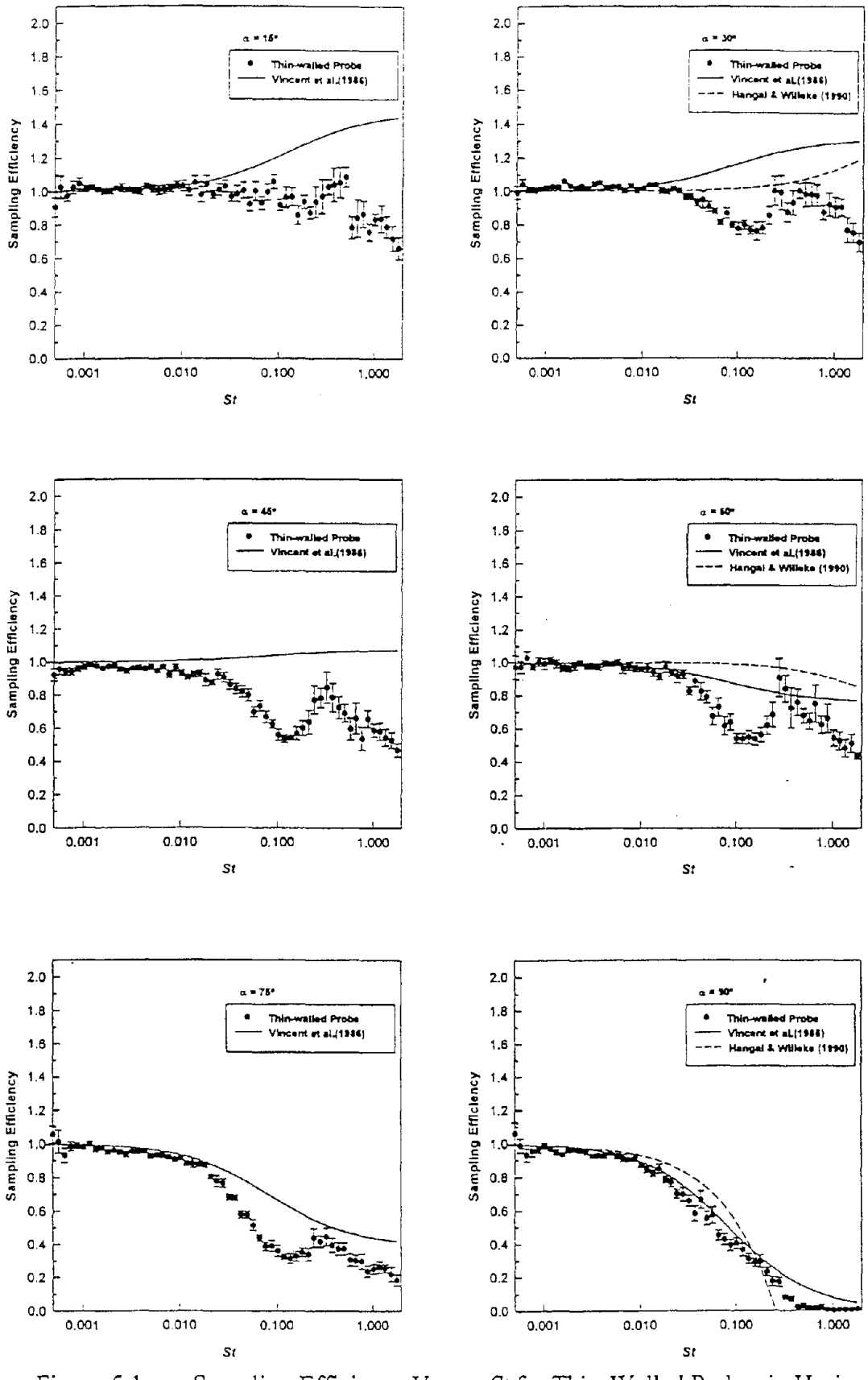

Figure 5.1 Sampling Efficiency Versus *St* for Thin-Walled Probes in Horizontal Plane for Angles up to 90°

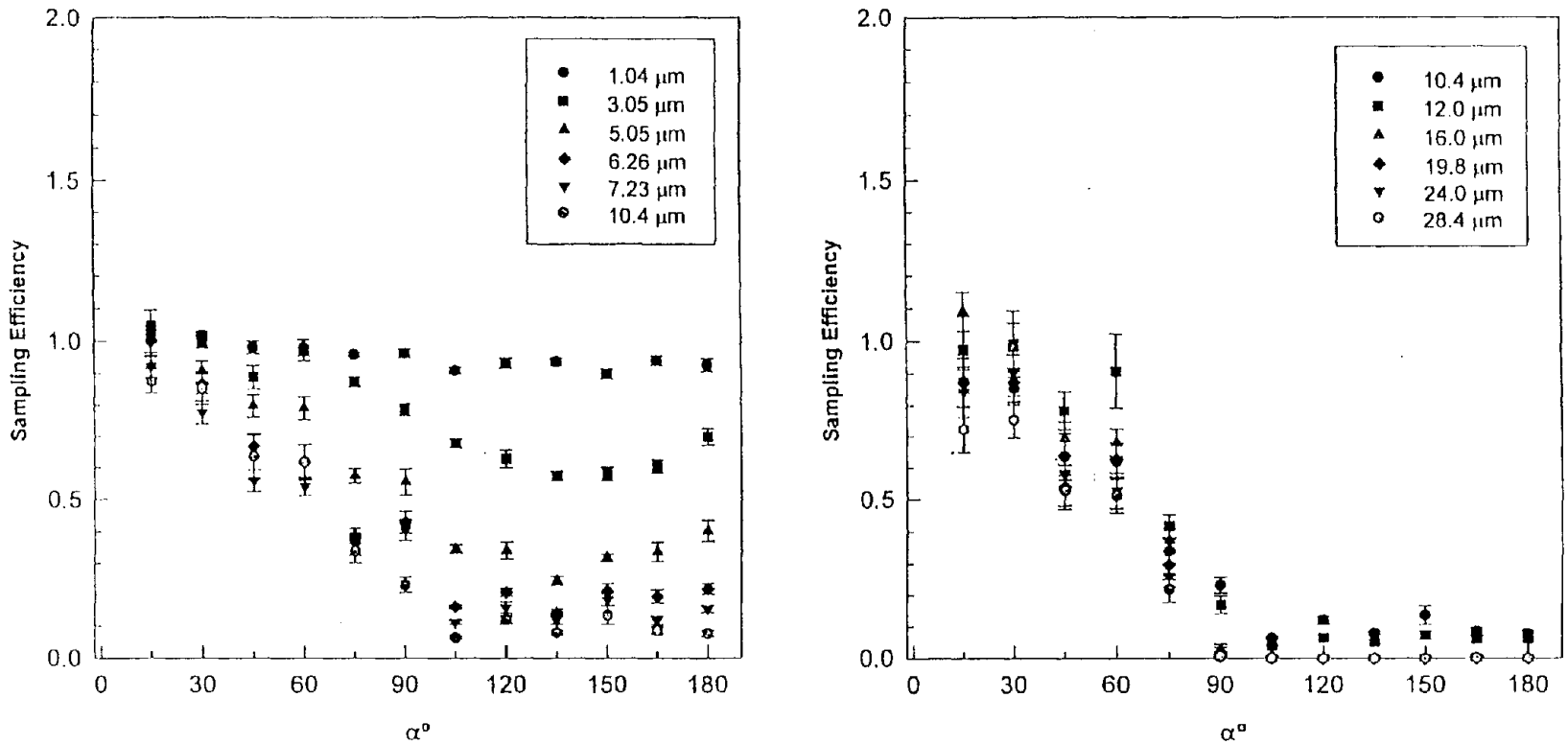

Figure 5.2 Effect of Orientation on the Sampling Efficiency for Various Particle Sizes for Thin-Walled Probes Along the Horizontal Plane for $R = 1.52$

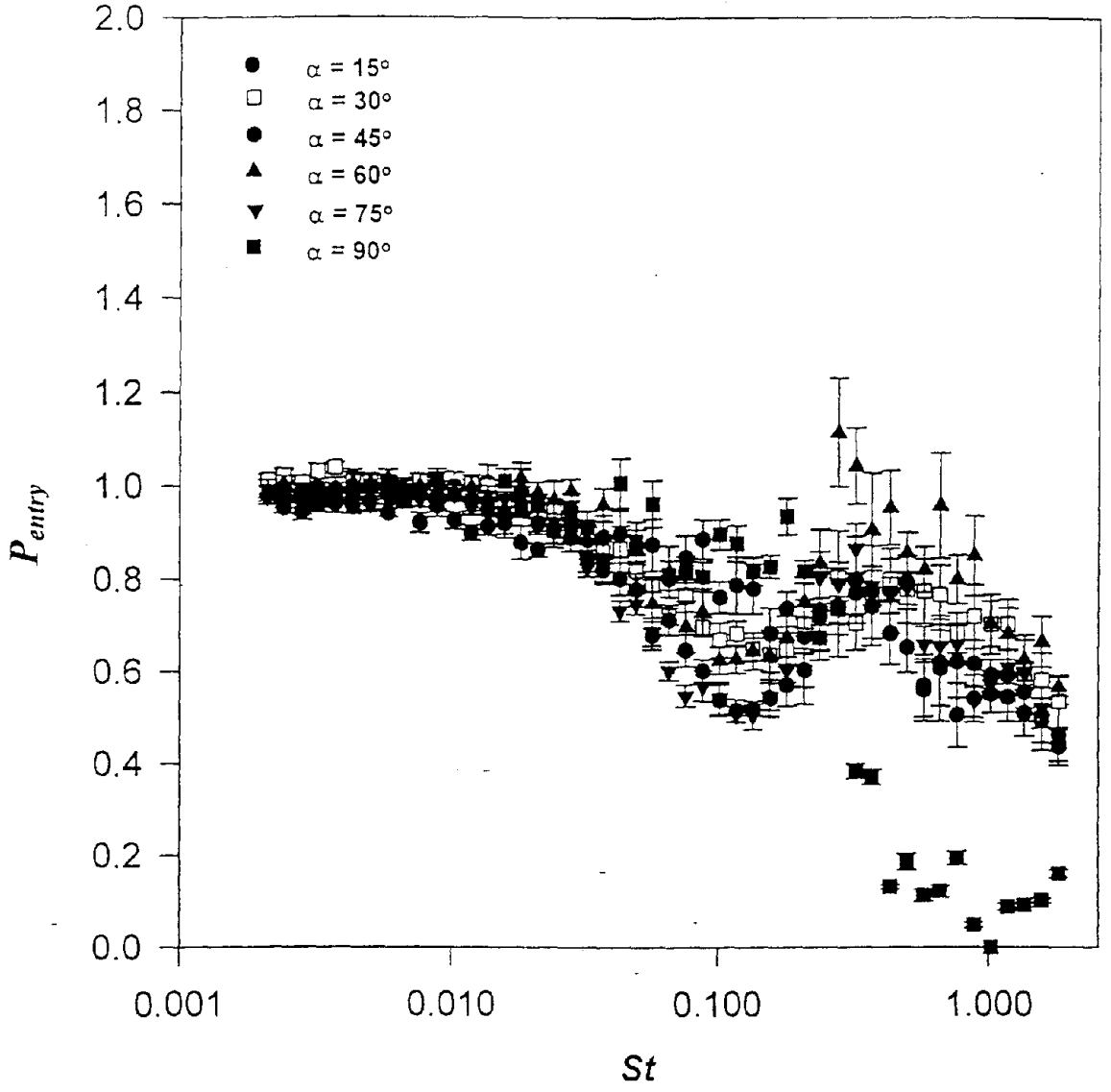

Figure 5.3 Entry penetration Vs *St* for orientations up to 90°

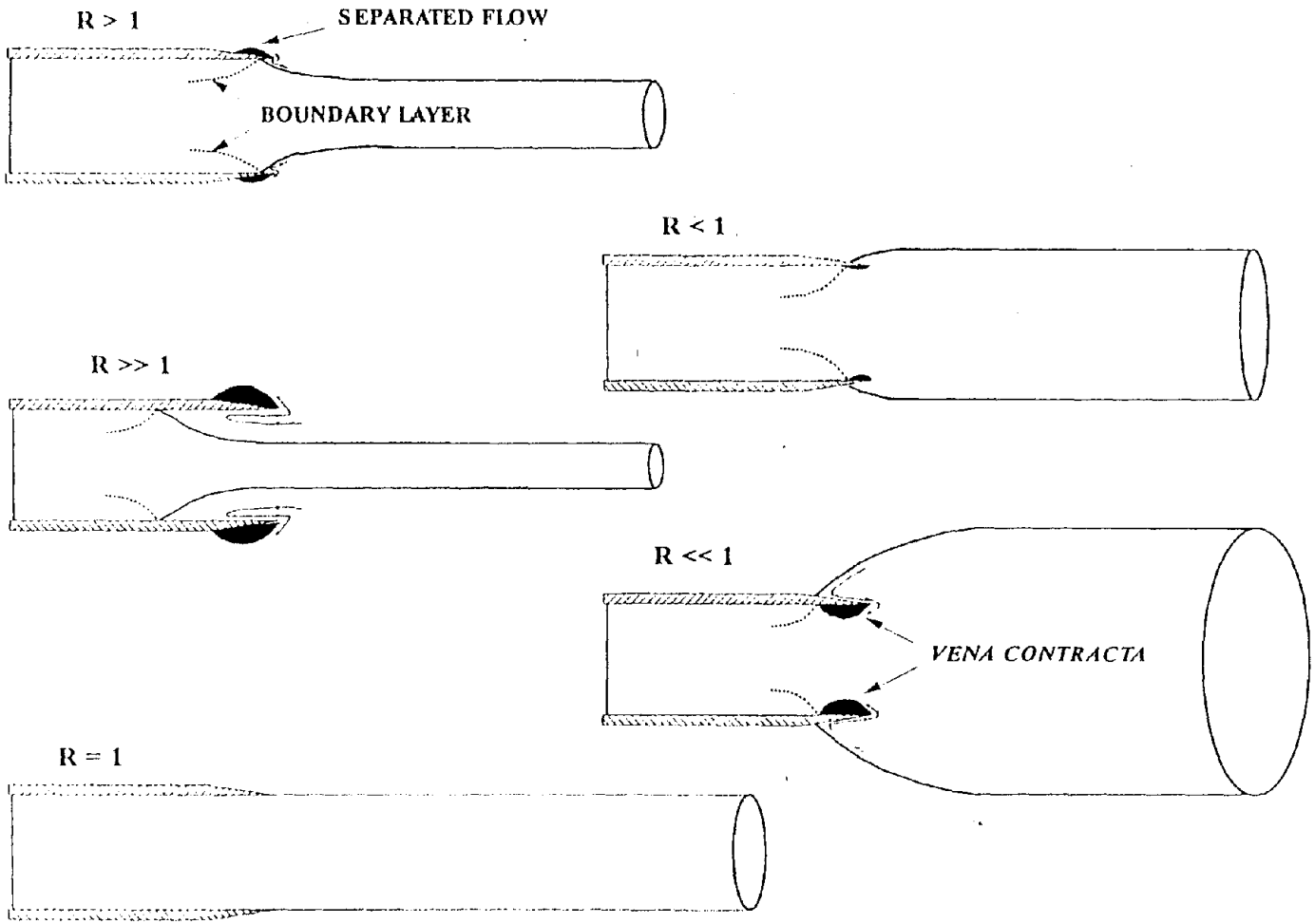

Figure 5.4 Limiting Streamlines for a Variety of Sampling Conditions for Thin-Walled Probe Entries

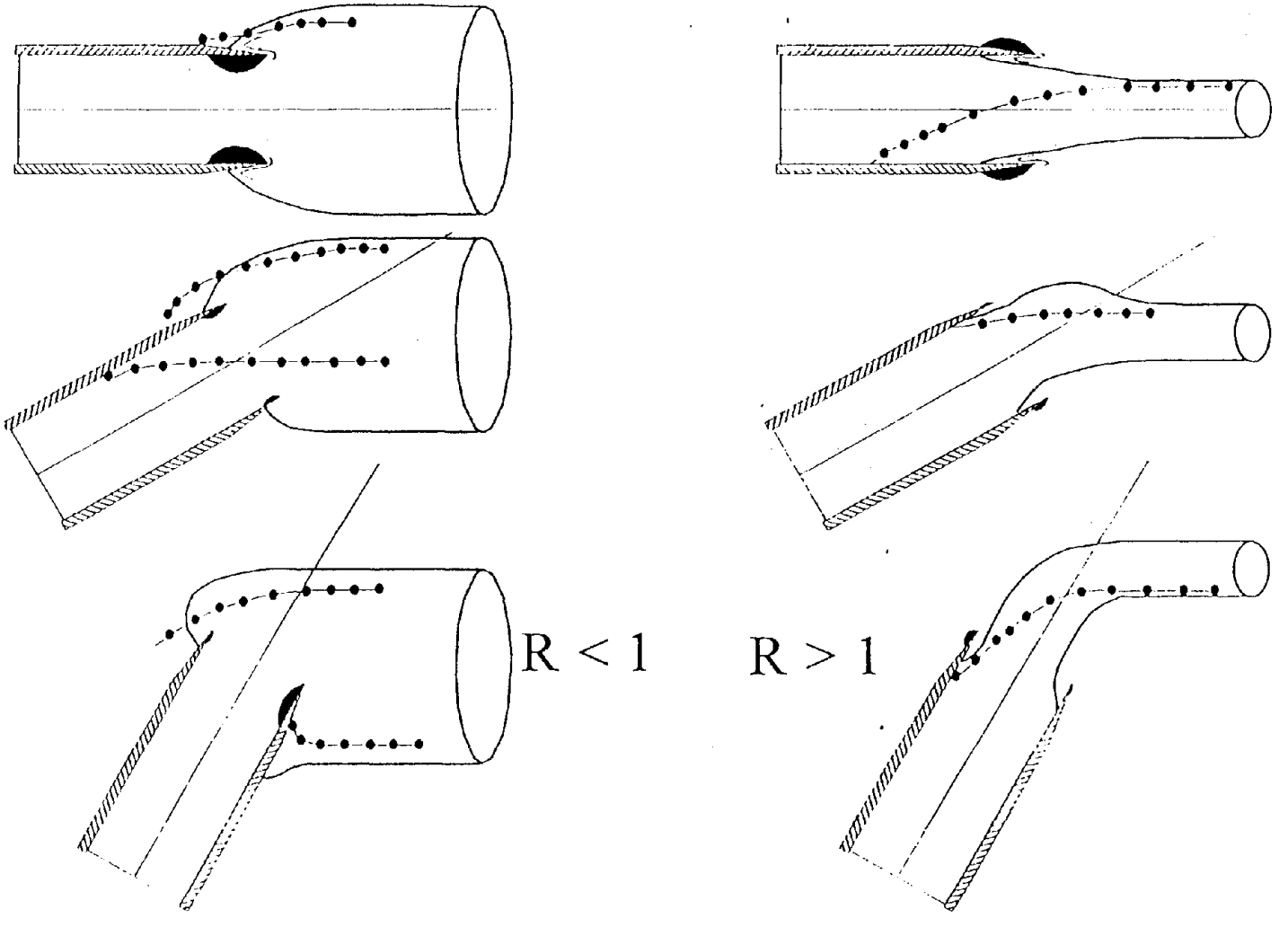

Figure 5.5 Schematic of the Limiting Streamlines and Particle Trajectories for Thin-Walled Probes at $R < 1$ and $R > 1$

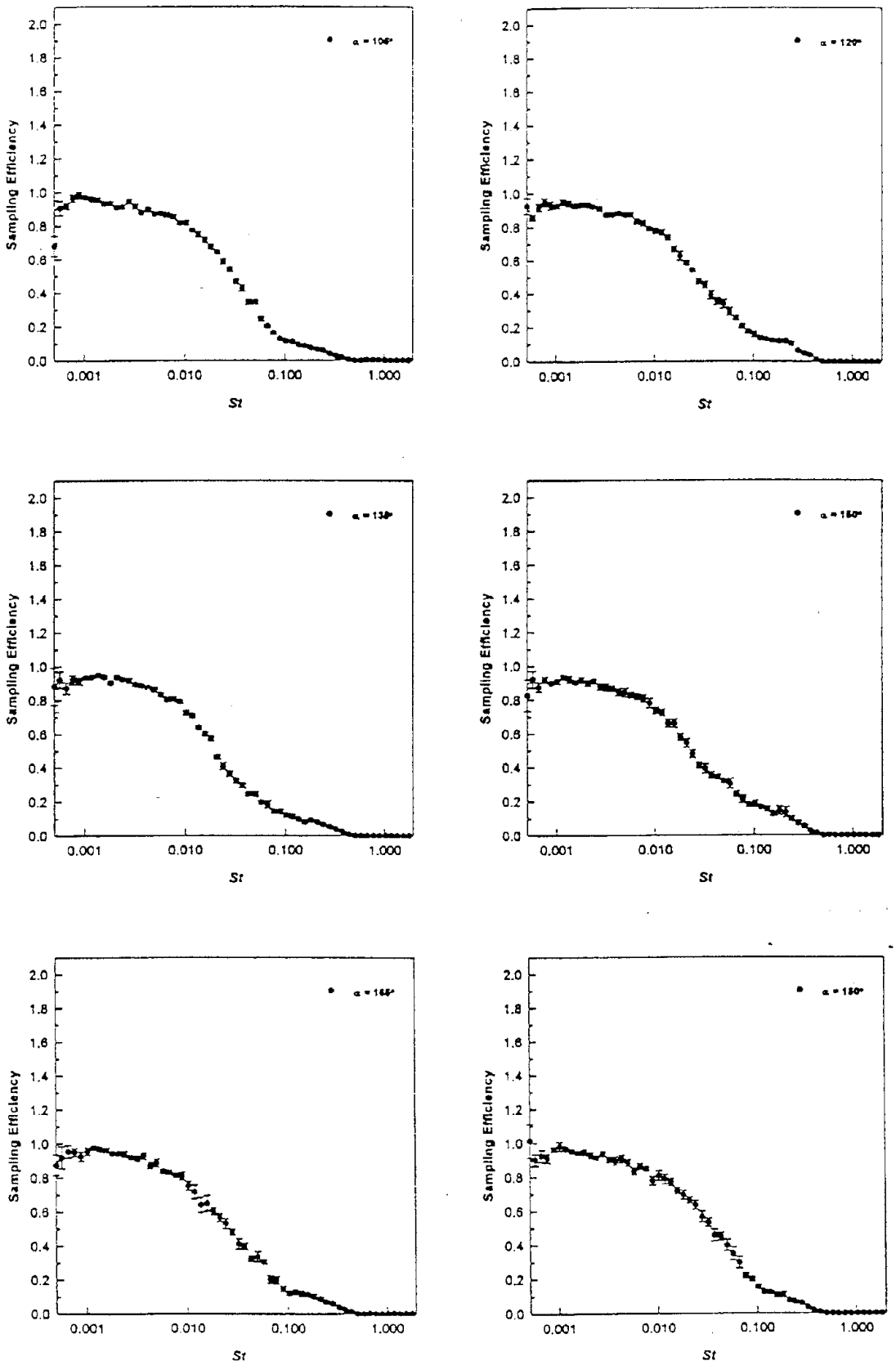

Figure 5.6 Sampling Efficiency Versus *St* for Thin-Walled Probes in Horizontal Plane for Angles Greater than 90°

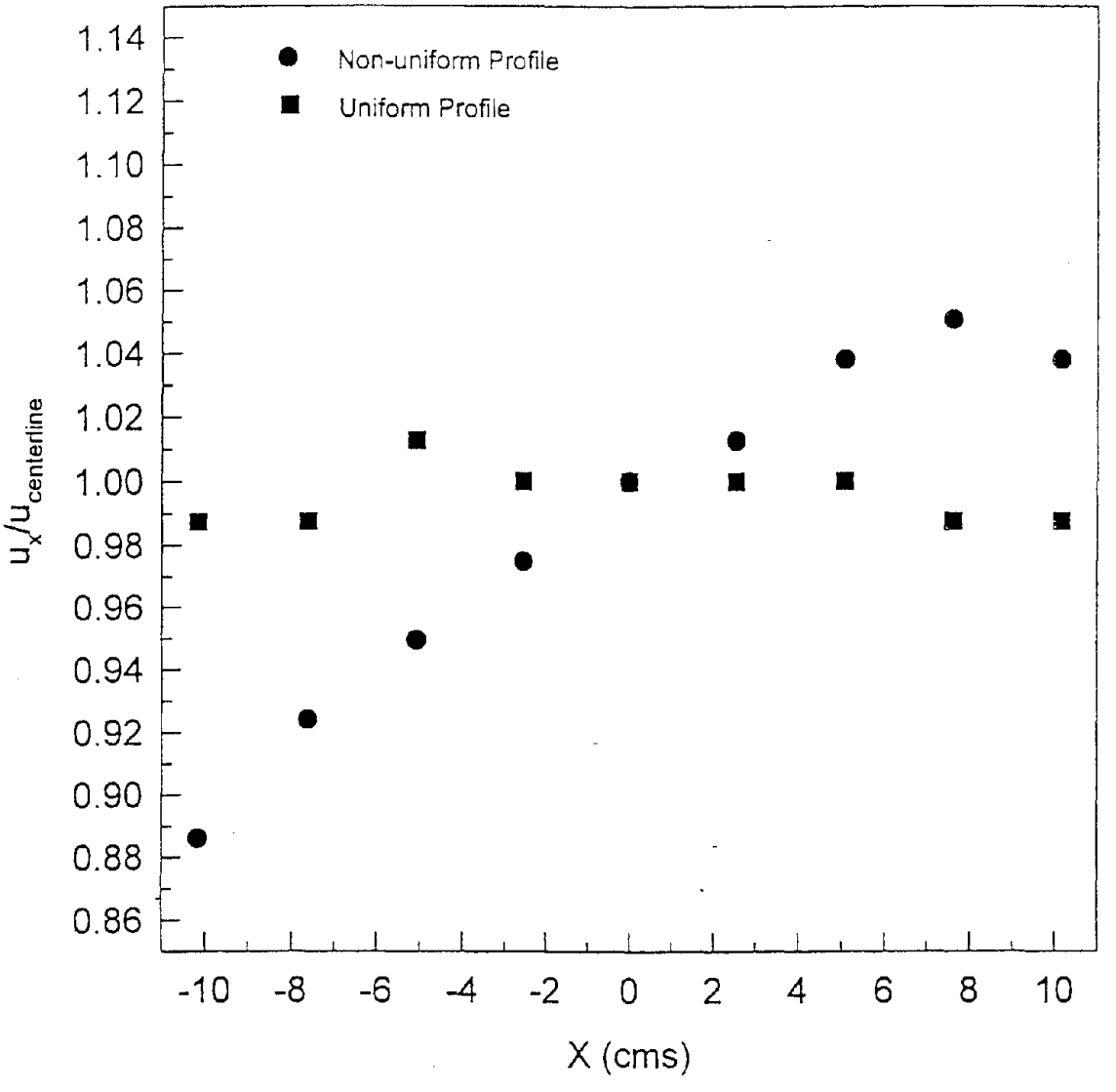

Figure 6.1 Velocity profiles in the test section along the X-axis

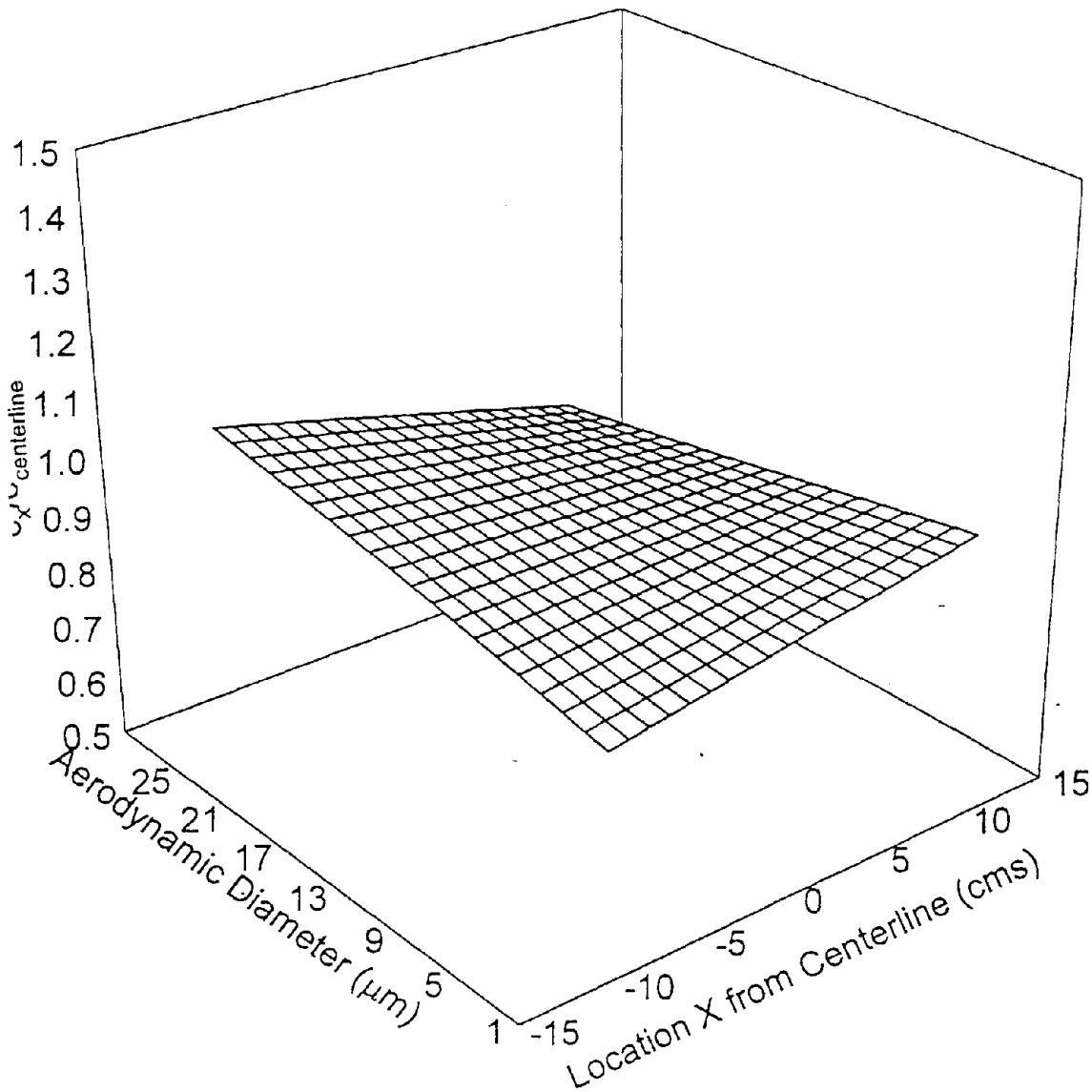

Figure 6.2 Concentration profiles in the test section along the x & y-axes

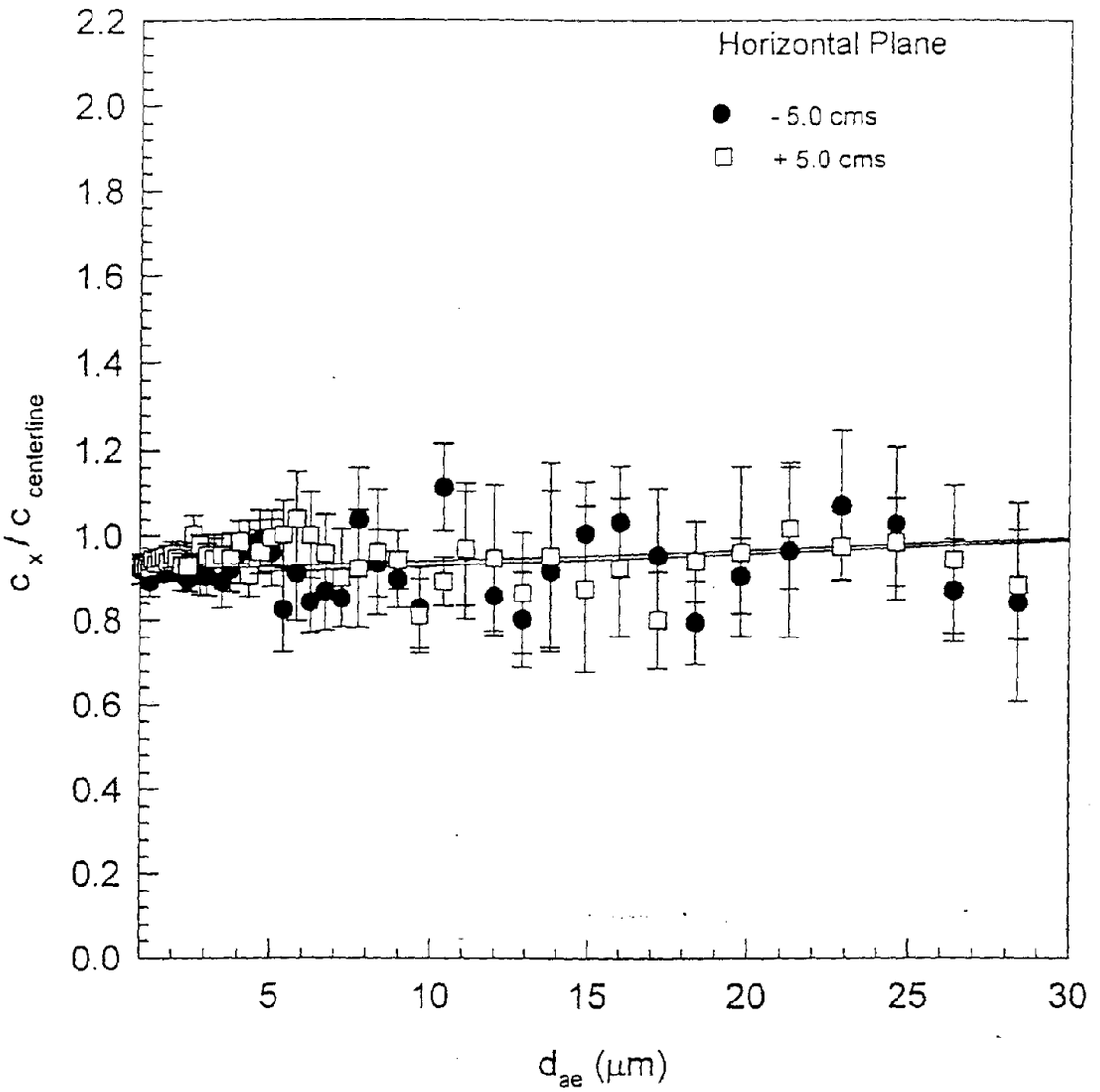

Figure 6.3 Aerosol concentration profile at 5 cm from the centerline for the case of uniform velocity profile

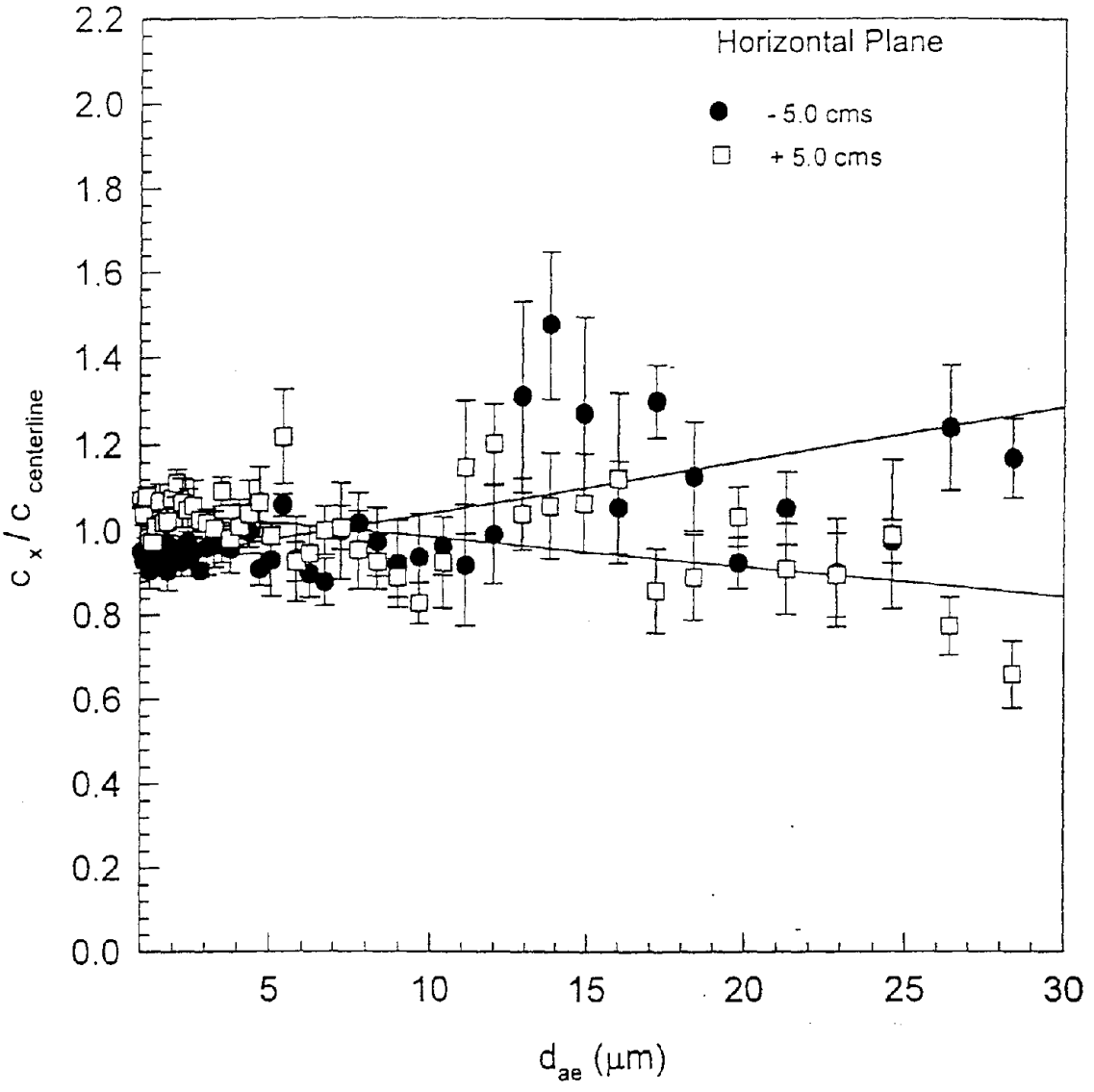

Figure 6.4 Aerosol concentration profile at 5 cm from the centerline for the case of non-uniform velocity profile

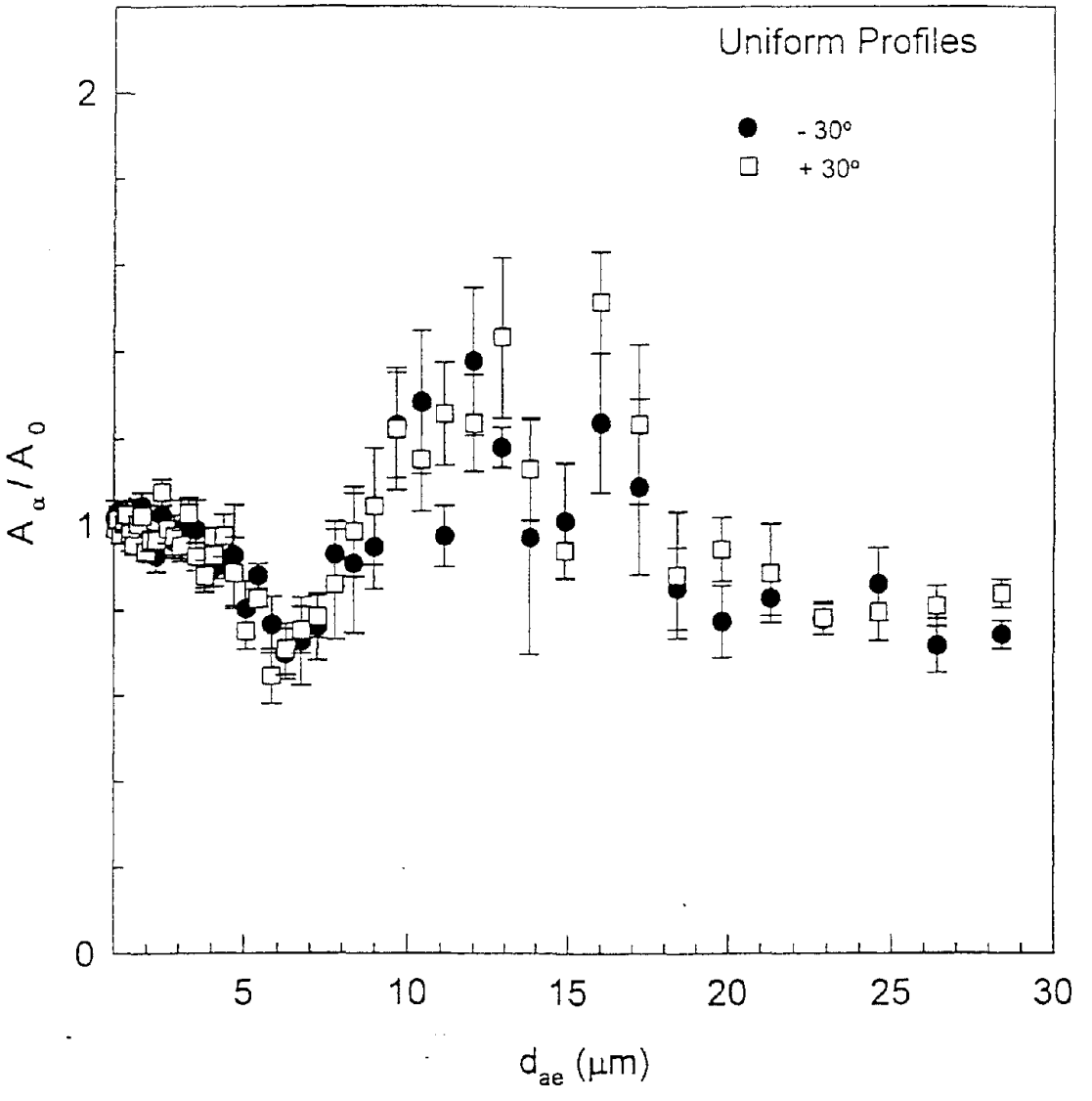

Figure 6.5 Sampling efficiency for $\alpha = 30°$ for the case of uniform velocity and concentration profiles

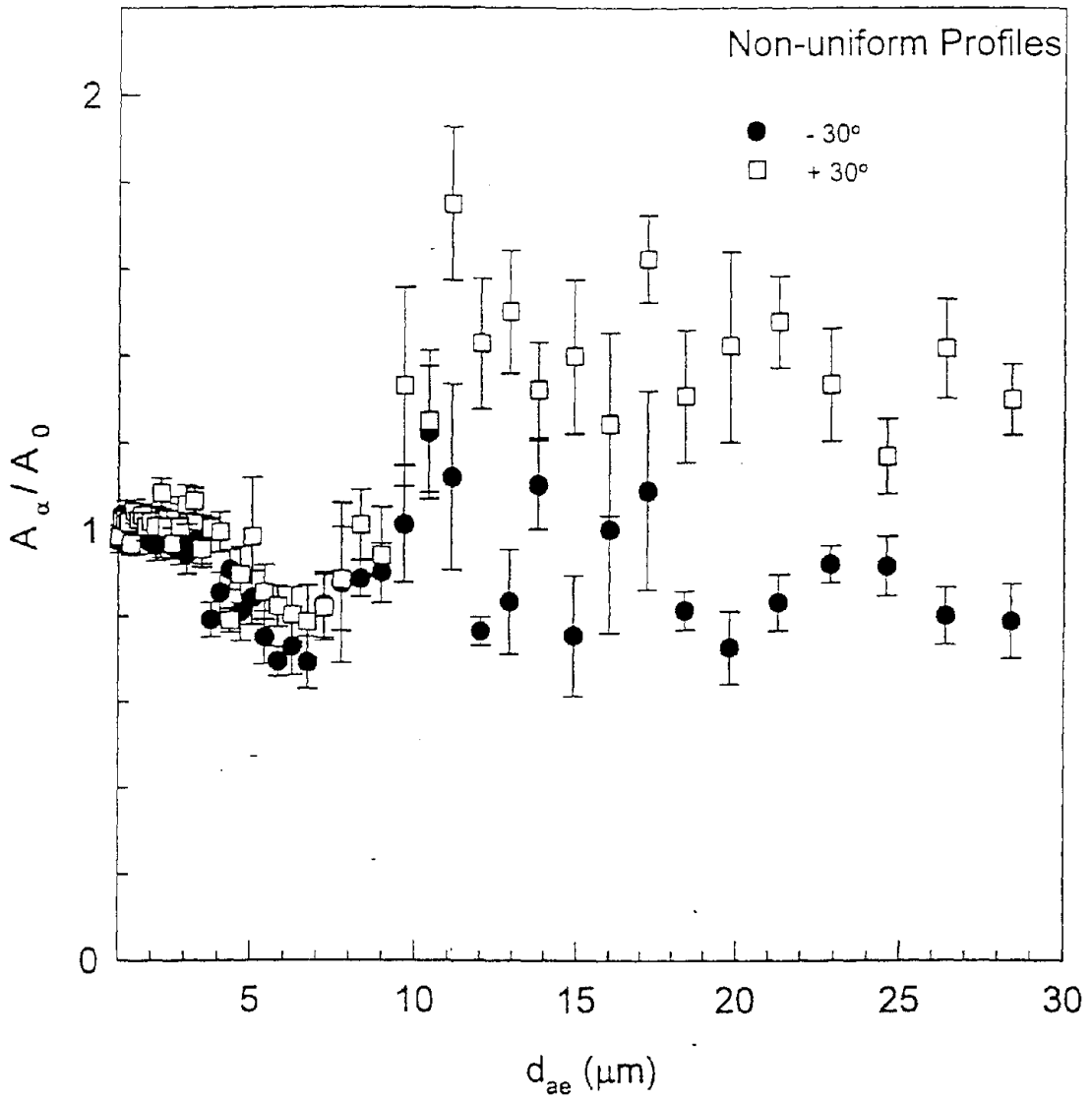

Figure 6.6 Sampling efficiency for $\alpha = 30°$ for the case of non-uniform velocity and concentration profiles

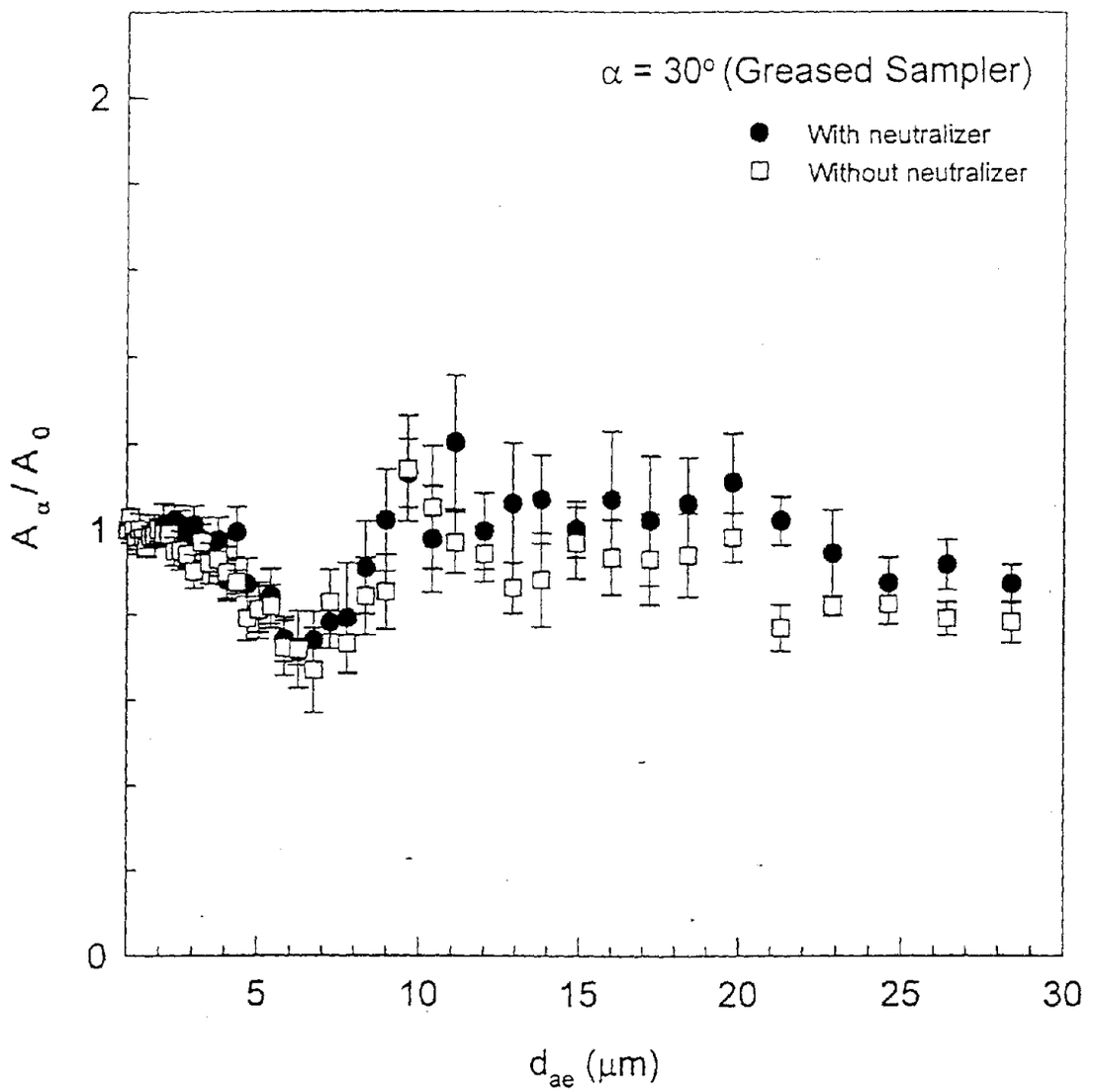

Figure 6.7 Effect of electrostatic charge on the sampling efficiency

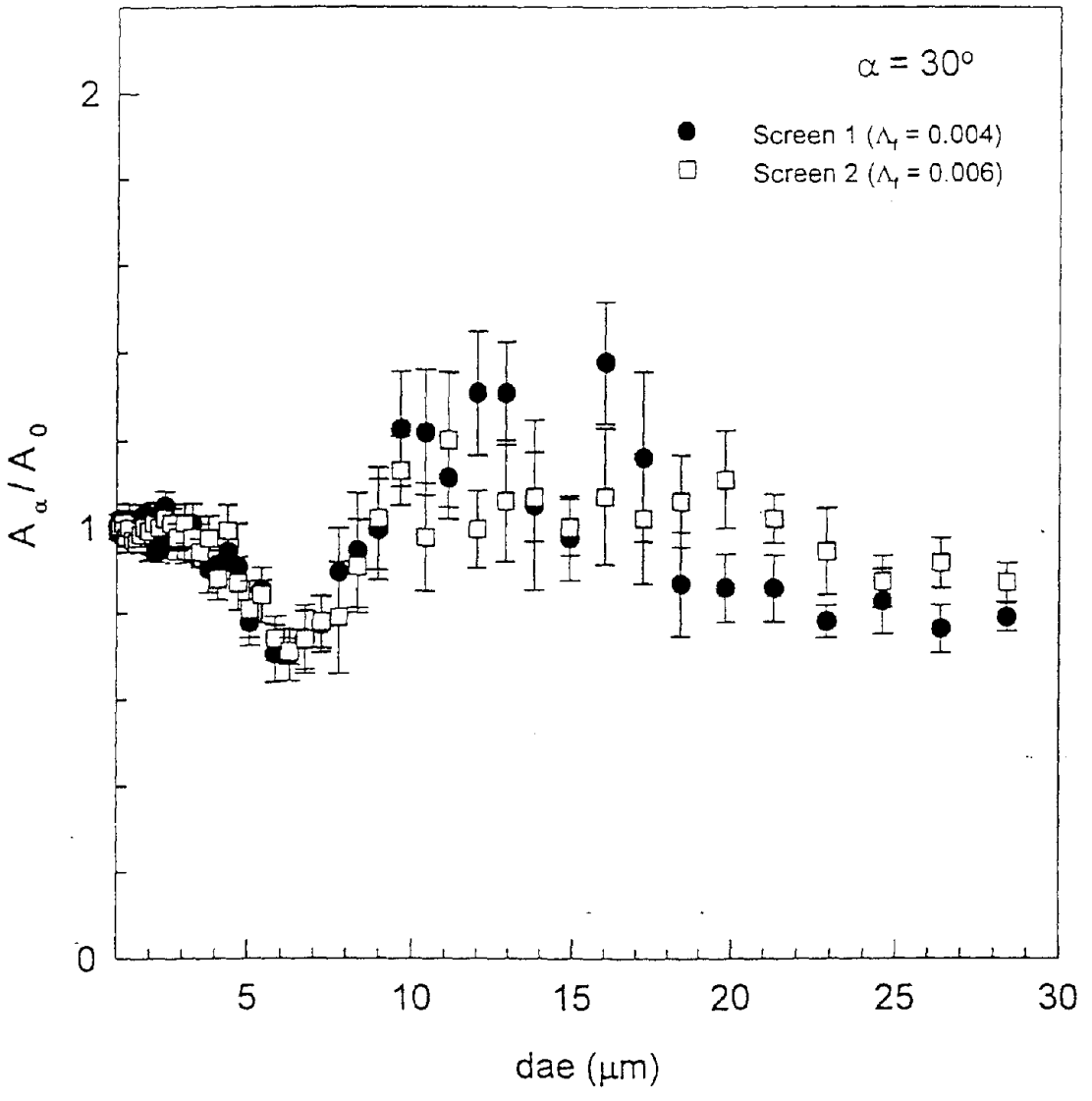

Figure 6.8 Effect of freestream turbulence on sampling efficiency

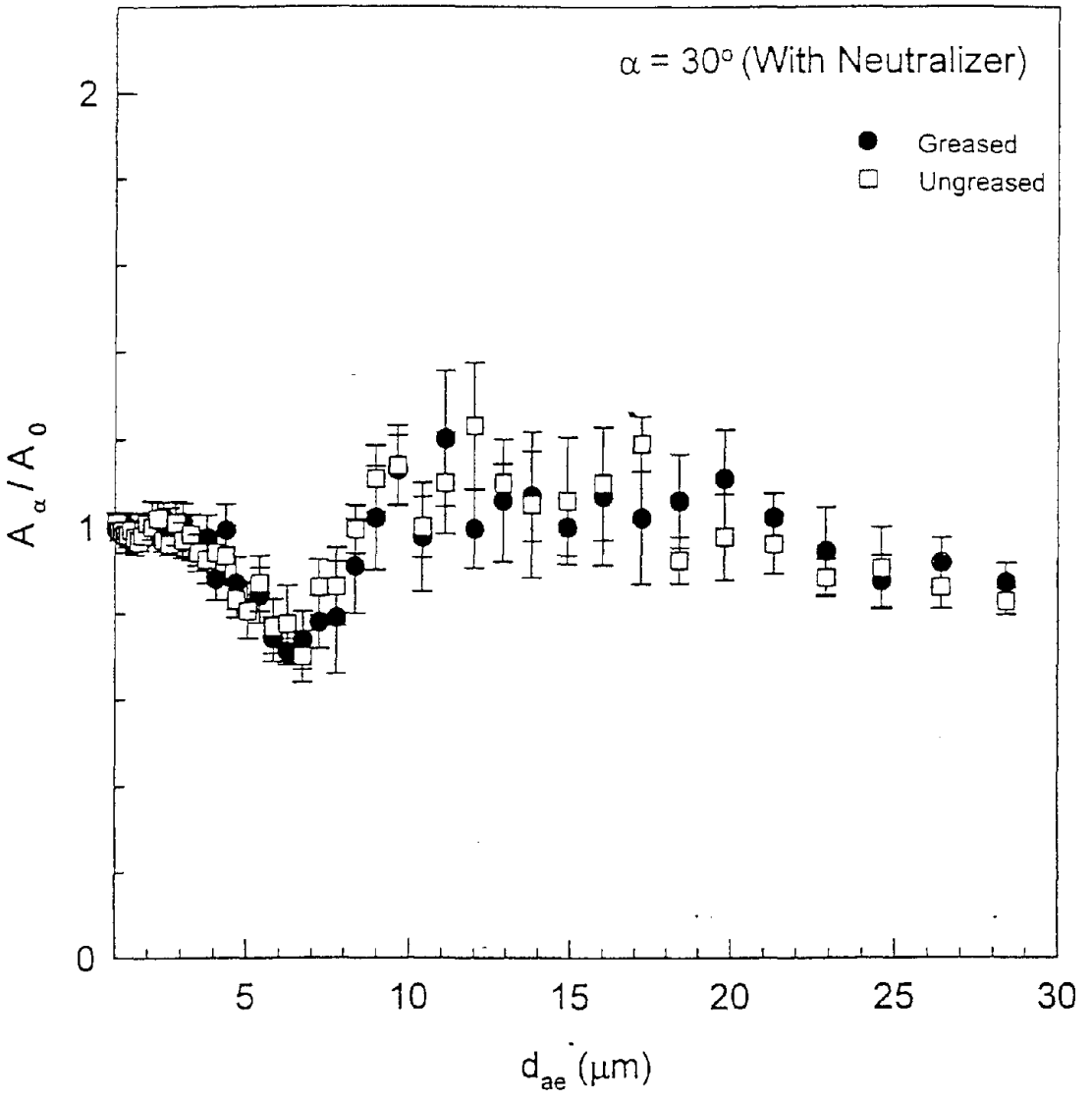

Figure 6.9 Effect of particle bounce on the sampling efficiency

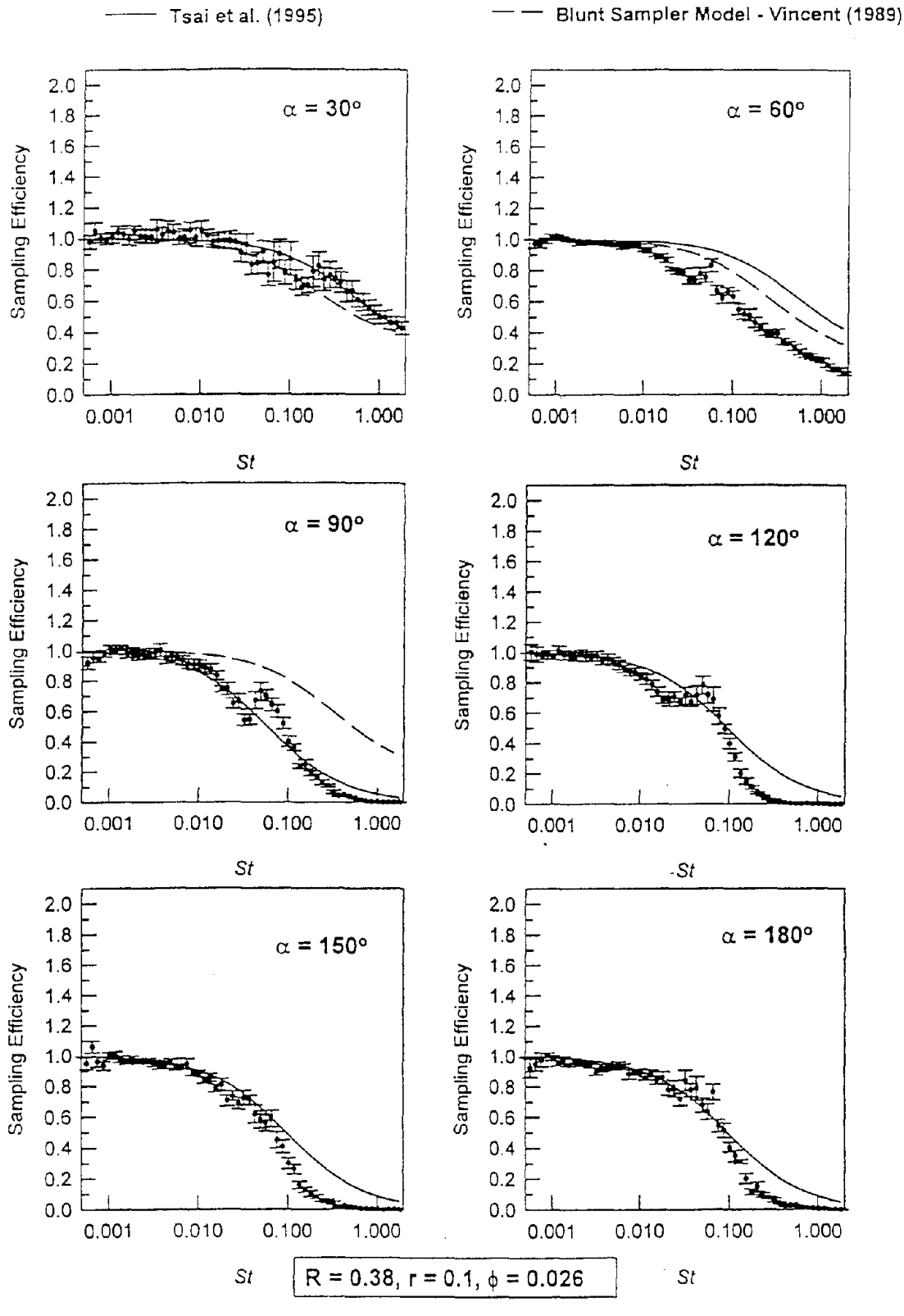

Figure 6.10 Plot of Sampling Efficiency versus *St* at Different Orientations from the Freestream for the Spherical Sampler for $R = 0.38$ and $r = 0.1$

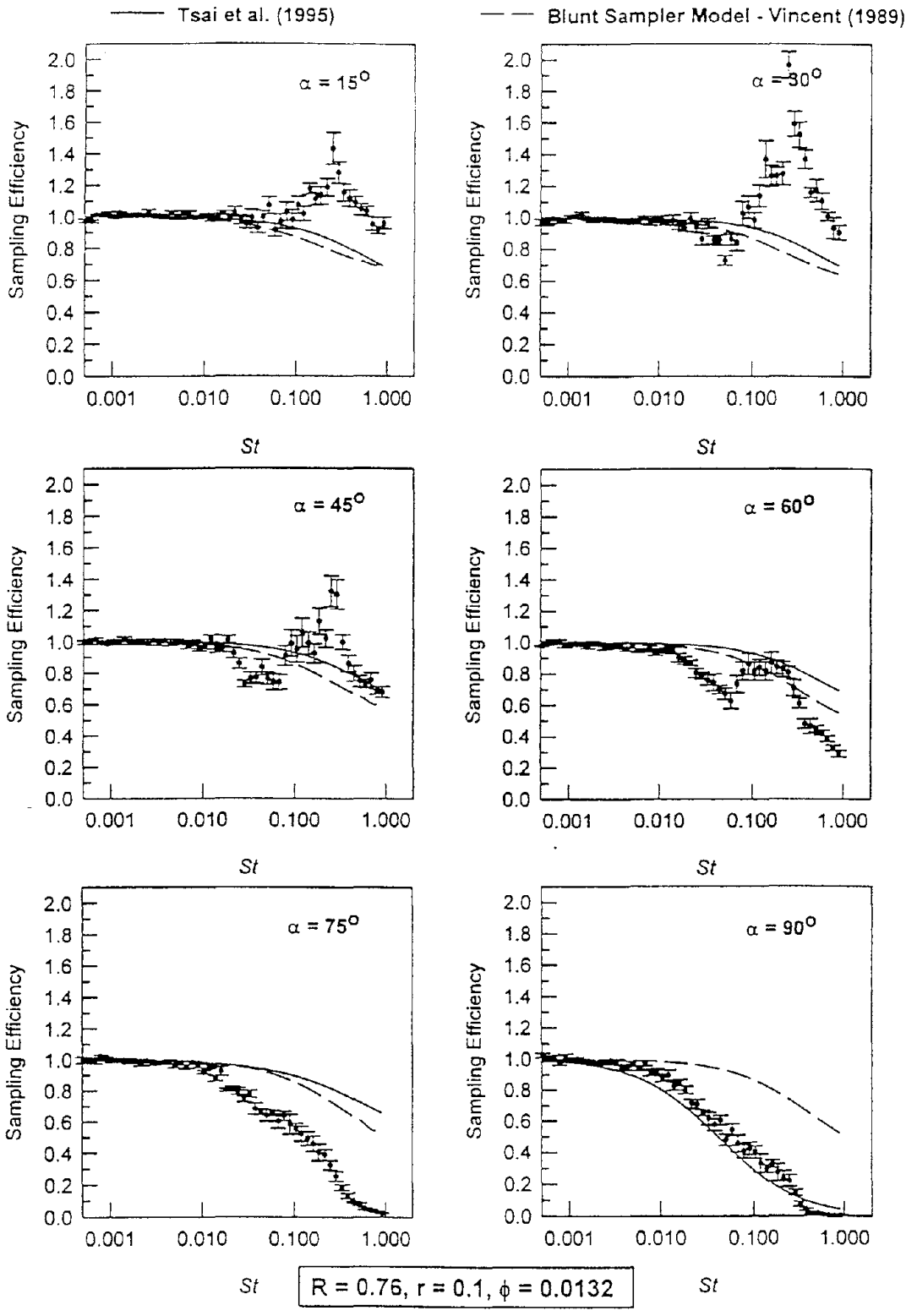

Figure 6.11(a) Plot of sampling efficiency versus *St* at different orientations from the freestream for $R = 0.76$ and $r = 0.1$

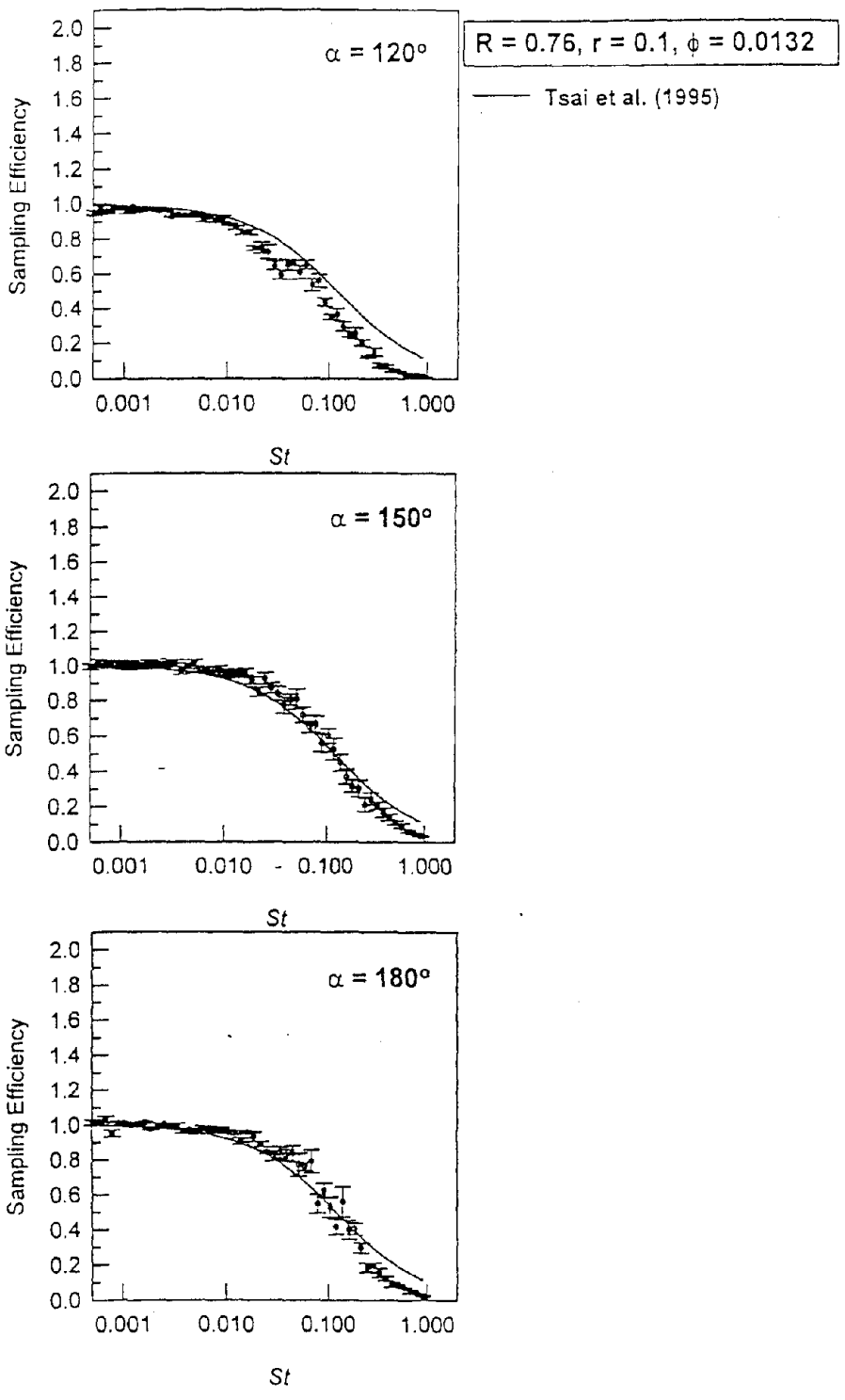

Figure 6.11(b) Plot of sampling efficiency versus St at different orientations from the freestream for $R = 0.76$ and $r = 0.1$

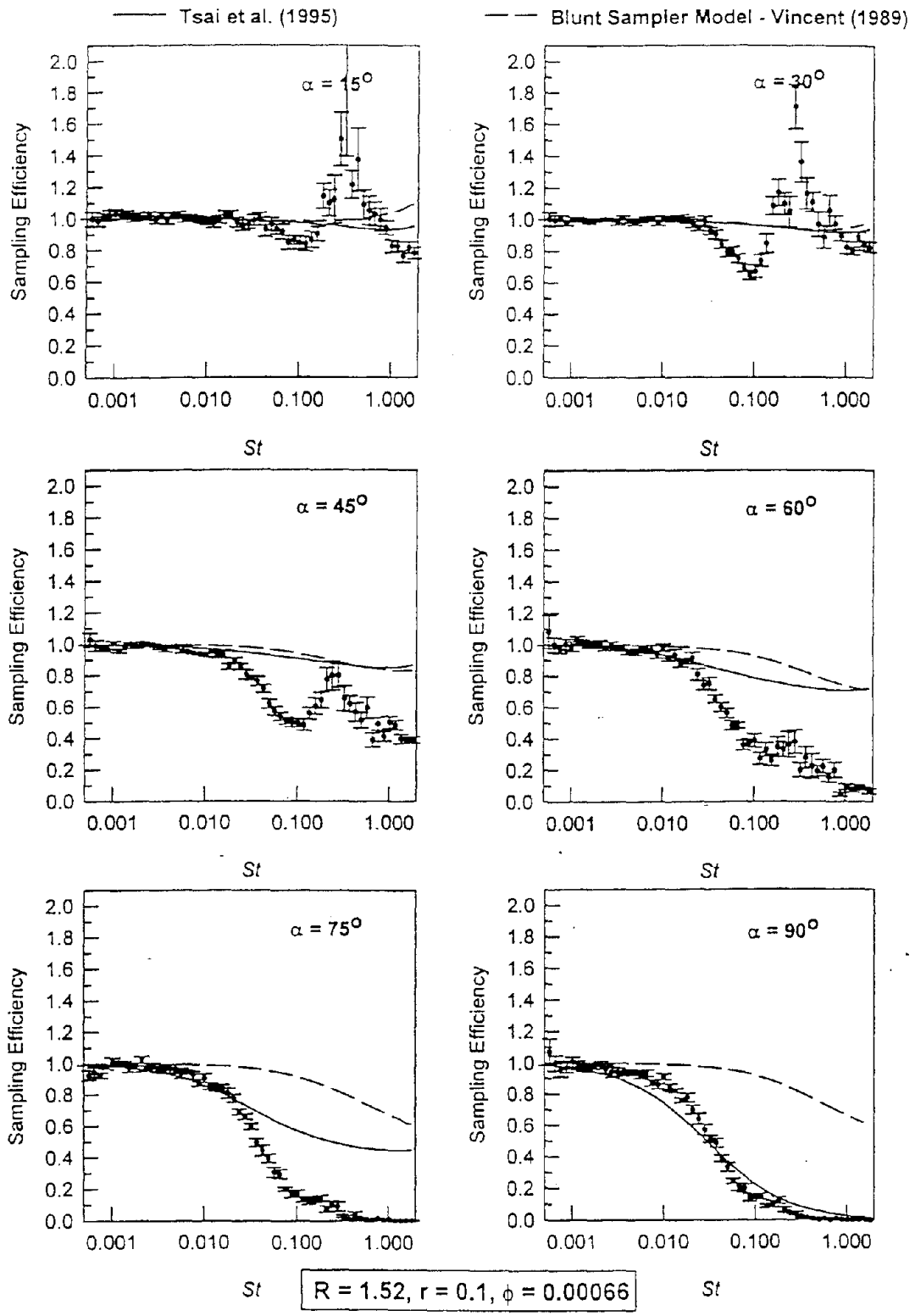

Figure 6.12(a) Plot of sampling efficiency versus *St* at different orientations from the freestream for $R = 1.52$ and $r = 0.1$

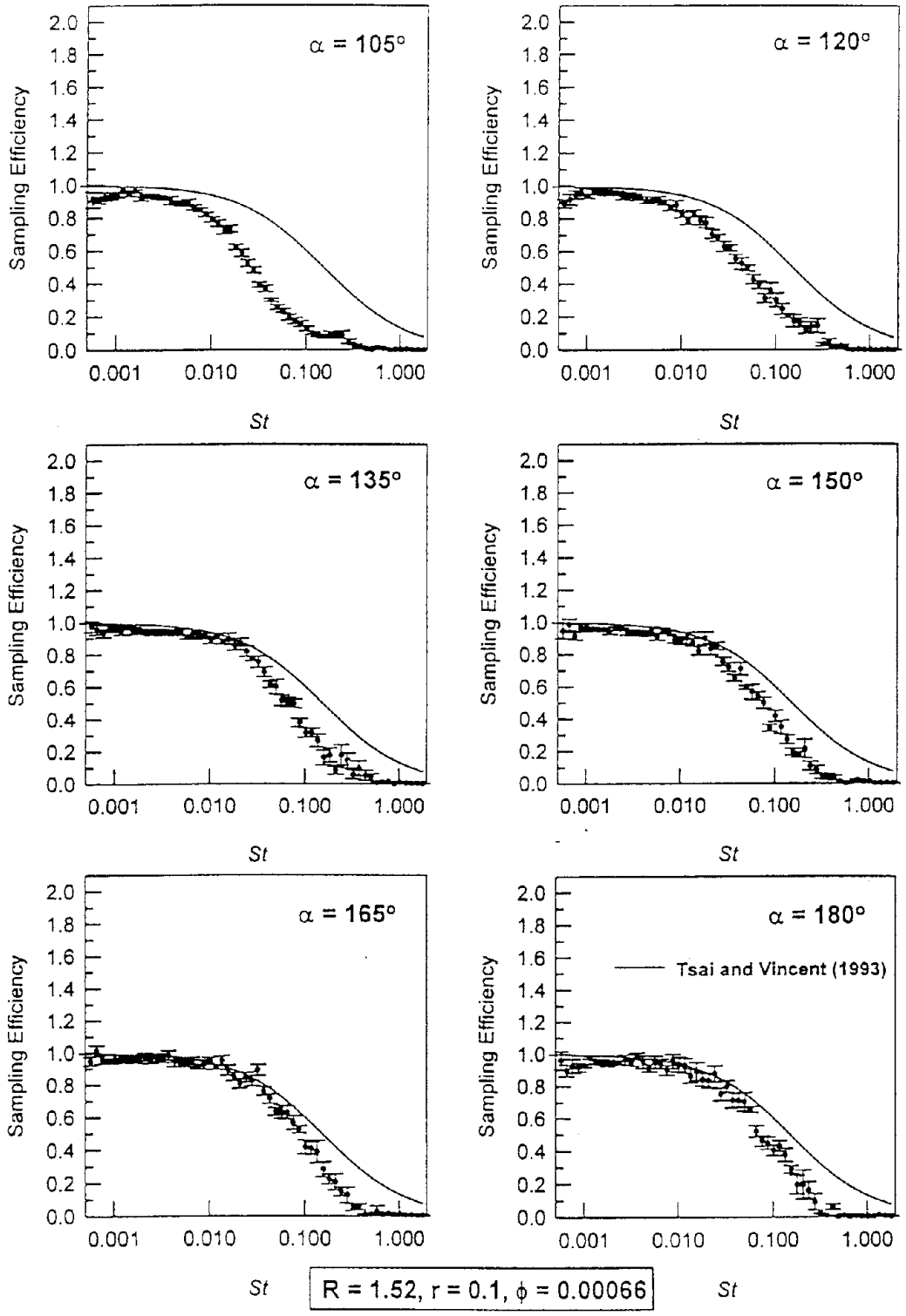

Figure 6.12(b) Plot of sampling efficiency versus St at different orientations from the freestream for $R = 1.52$ and $r = 0.1$

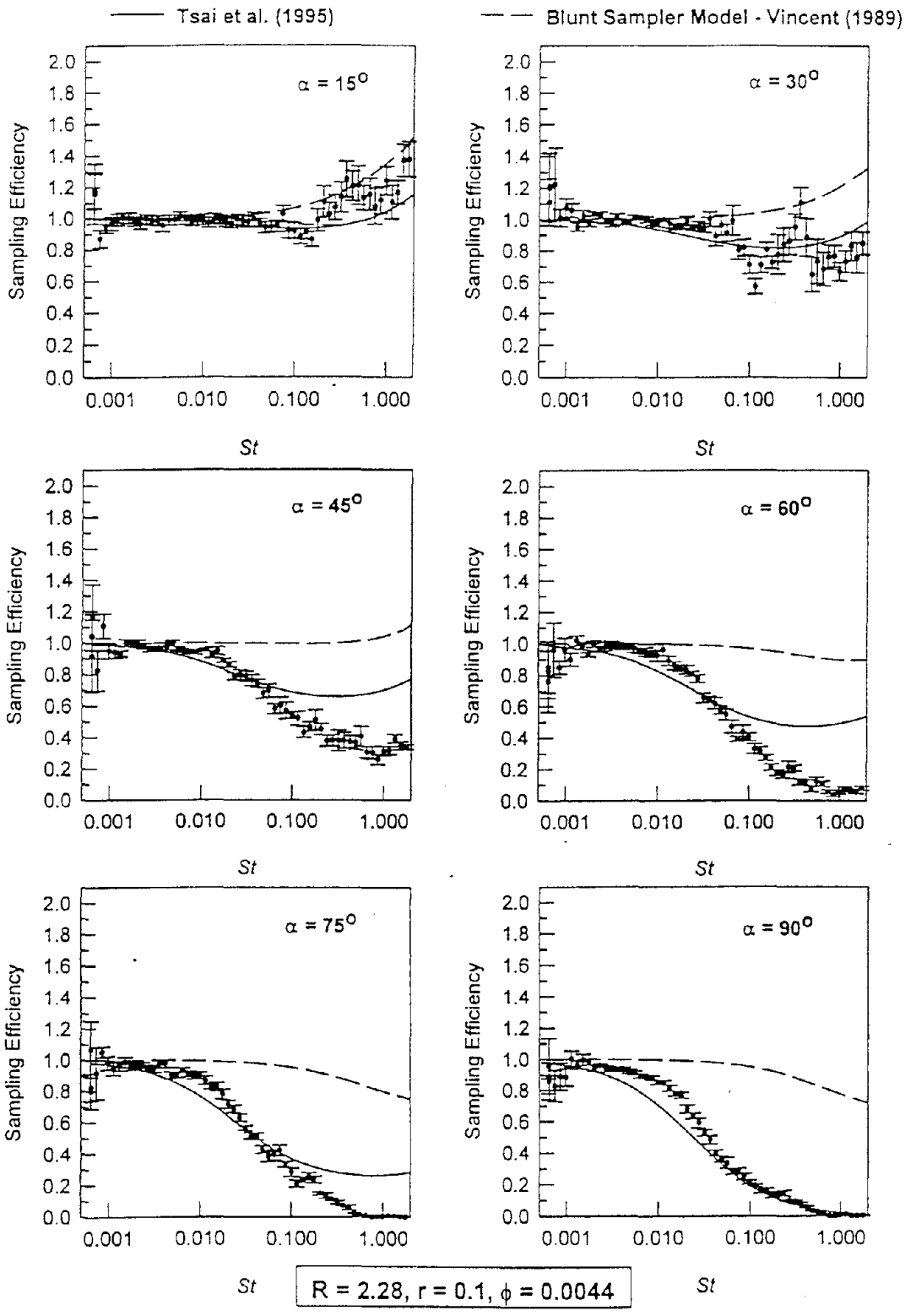

Figure 6.13(a) Plot of sampling efficiency versus *St* at different orientations from the freestream for $R = 2.28$ and $r = 0.1$

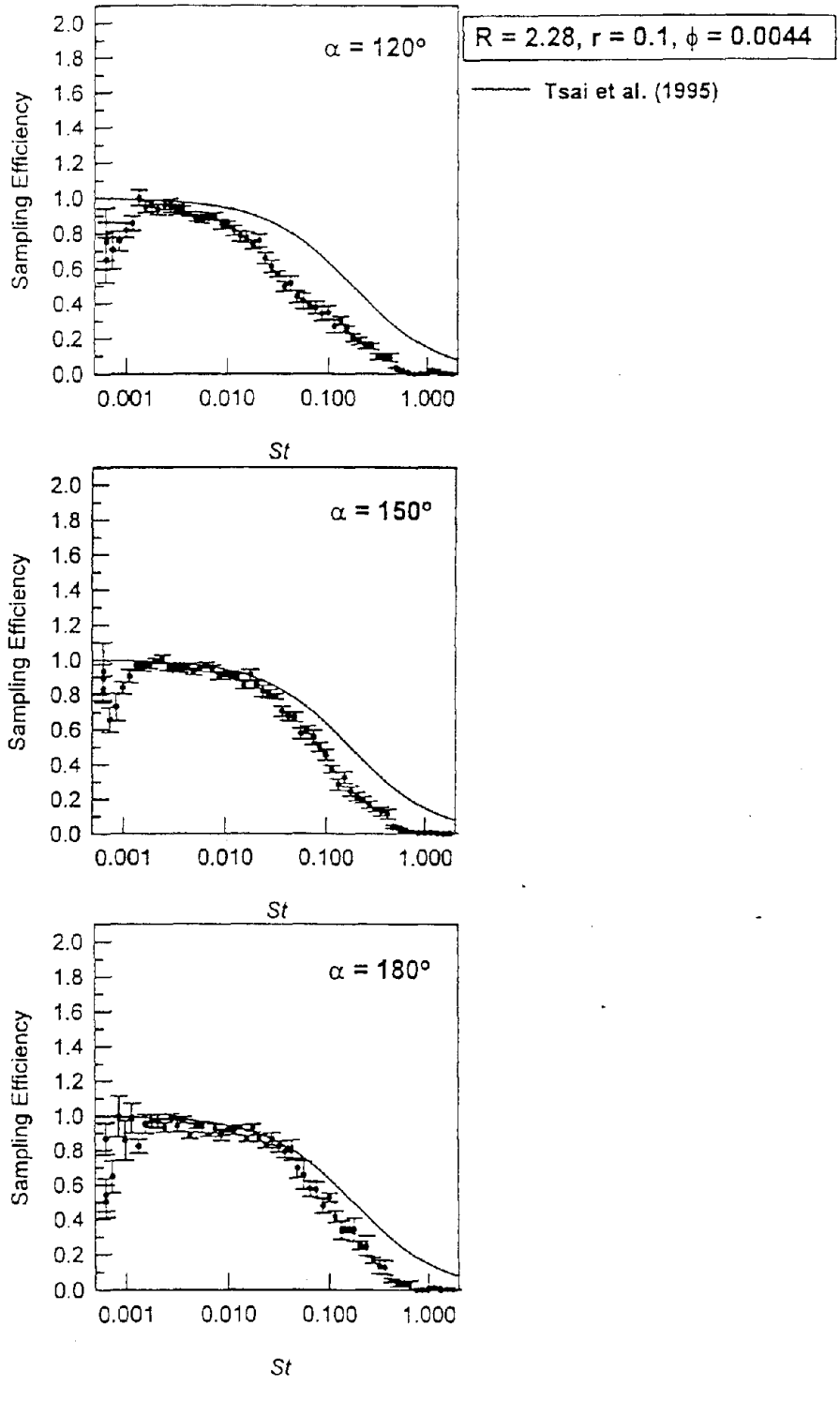

Figure 6.13(b) Plot of sampling efficiency versus St at different orientations from the freestream for $R = 2.28$ and $r = 0.1$

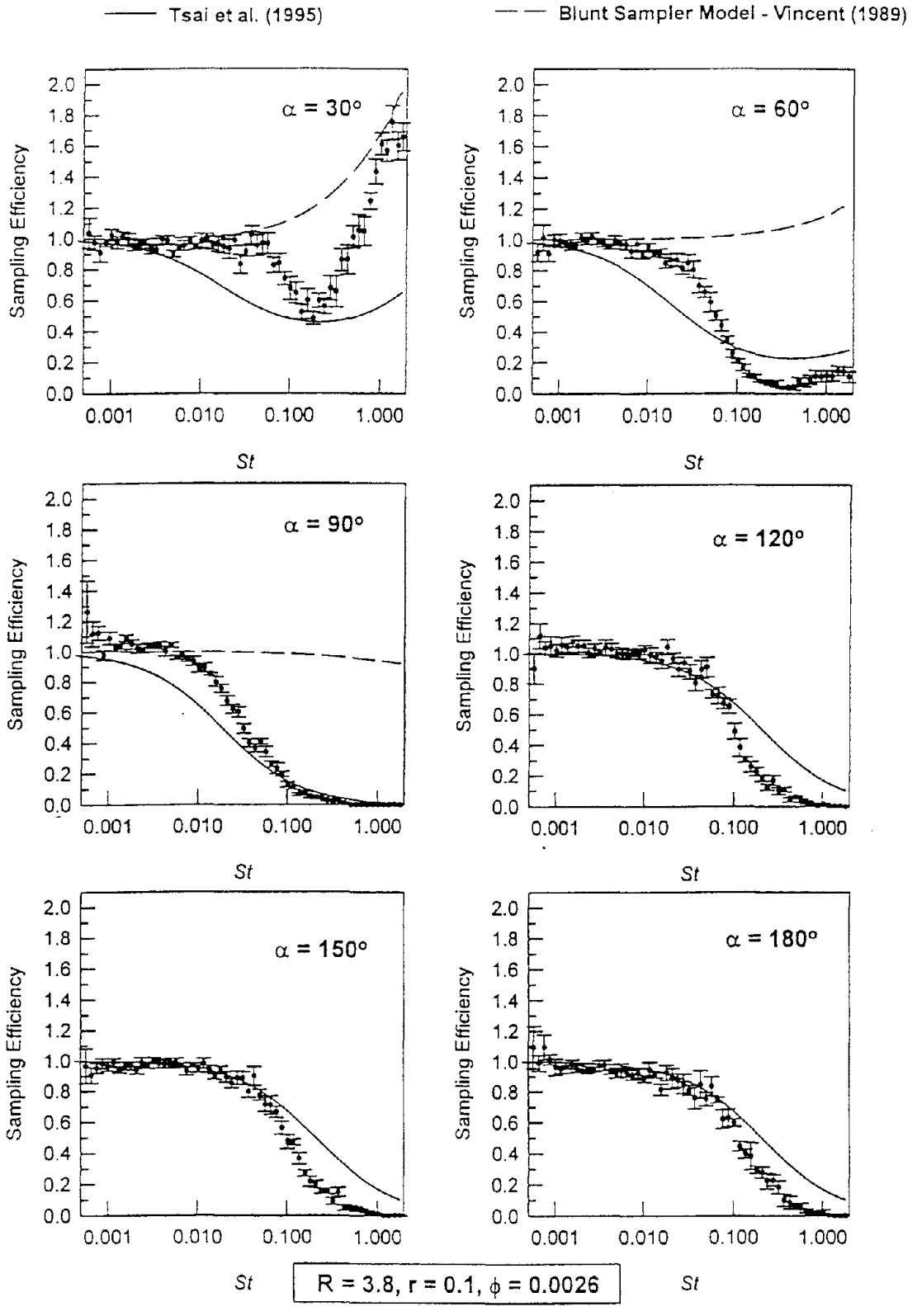

Figure 6.14 Plot of sampling efficiency versus *St* at different orientations from the freestream for $R = 3.8$ and $r = 0.1$

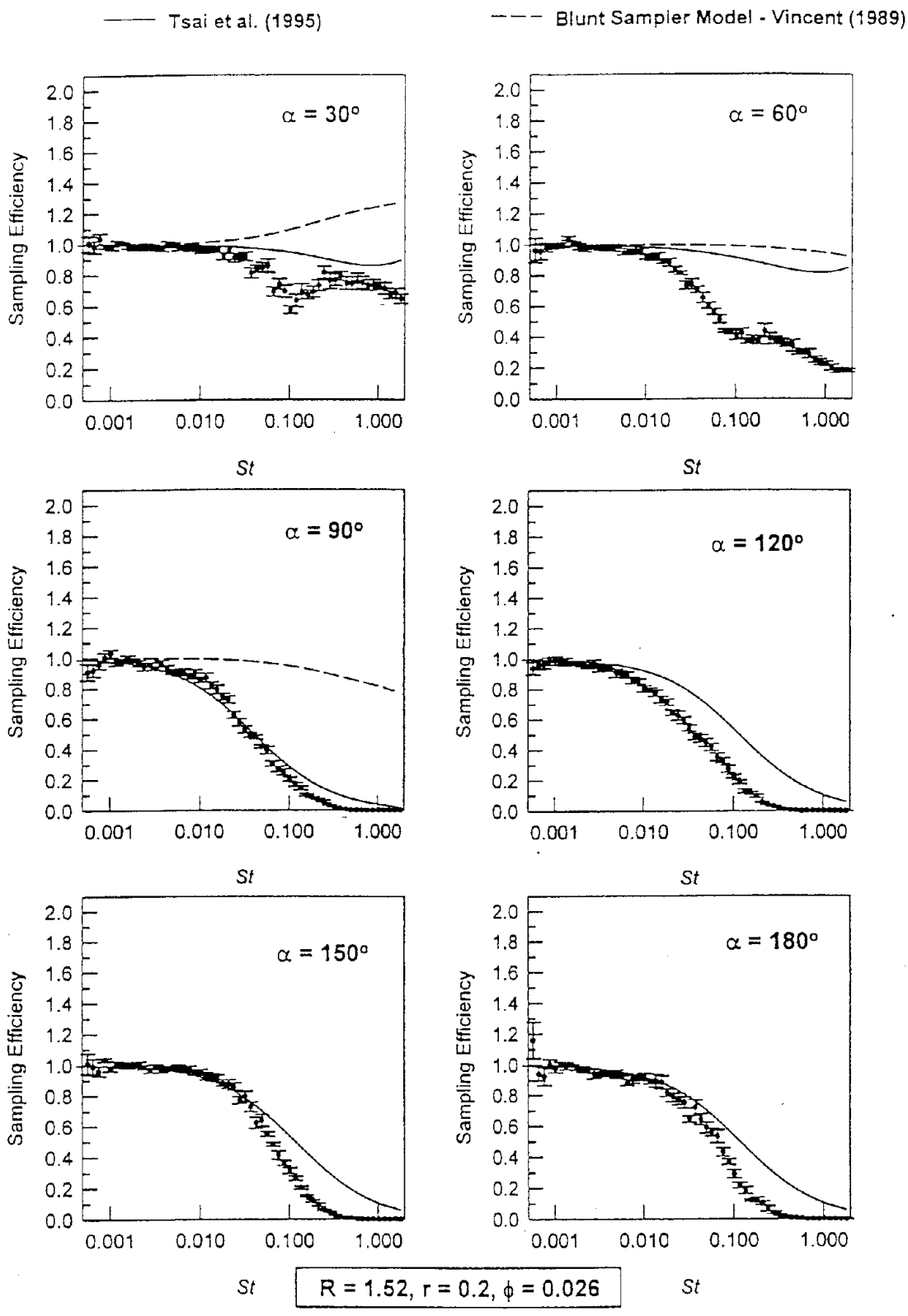

Figure 6.15 Plot of sampling efficiency versus *St* at different orientations from the freestream for $R = 1.52$ and $r = 0.2$

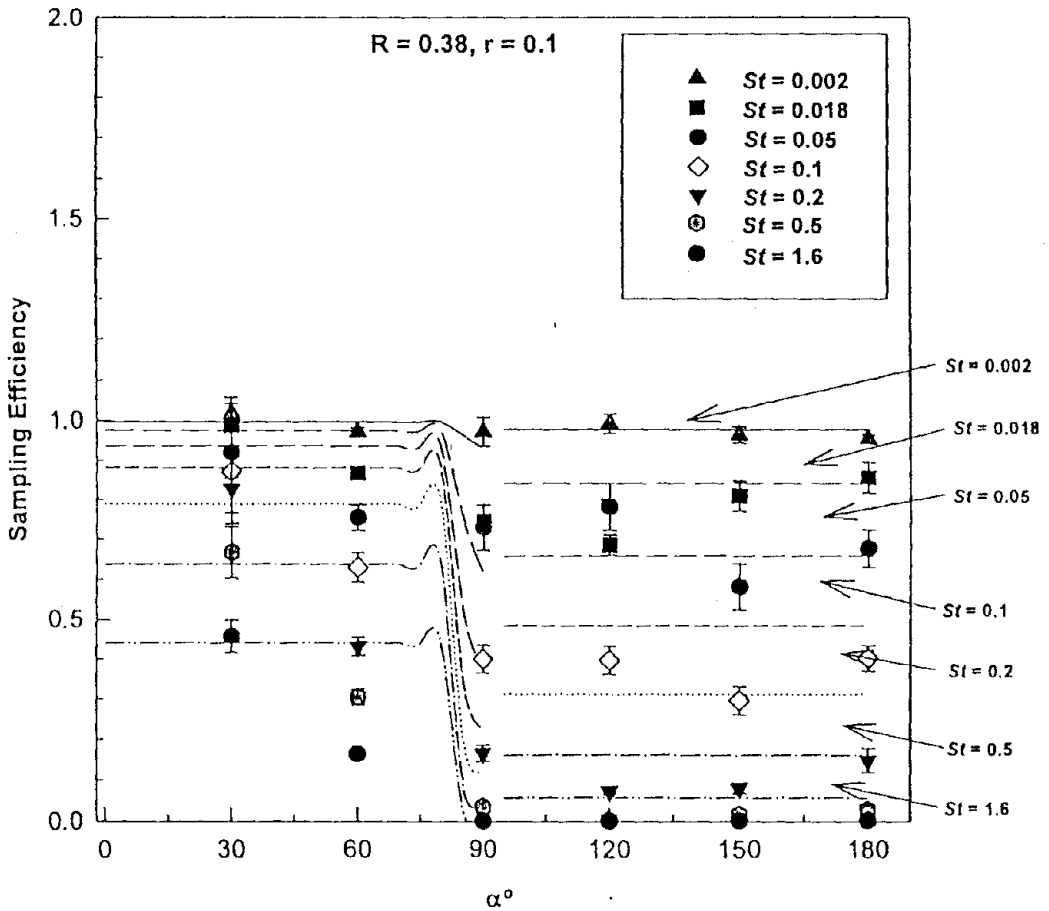

Figure 6.16 Effect of Orientation on the Sampling Efficiency of Spherical Sampler Along the Horizontal Plane for $R = 0.38$ and $r = 0.1$ Compared with Theory (Tsai *et al.*, 1995)

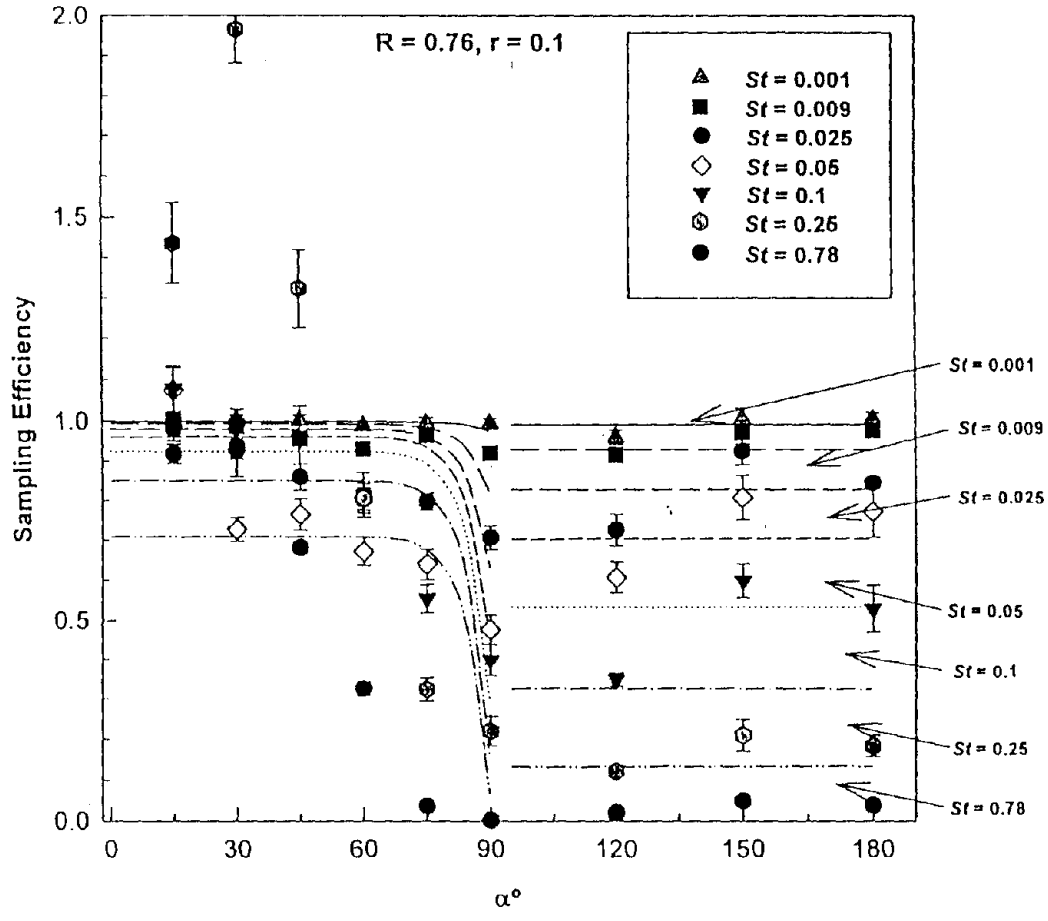

Figure 6.17 Effect of Orientation on the Sampling Efficiency of Spherical Sampler Along the Horizontal Plane for $R = 0.76$ and $r = 0.1$ Compared with Theory (Tsai *et al.*, 1995)

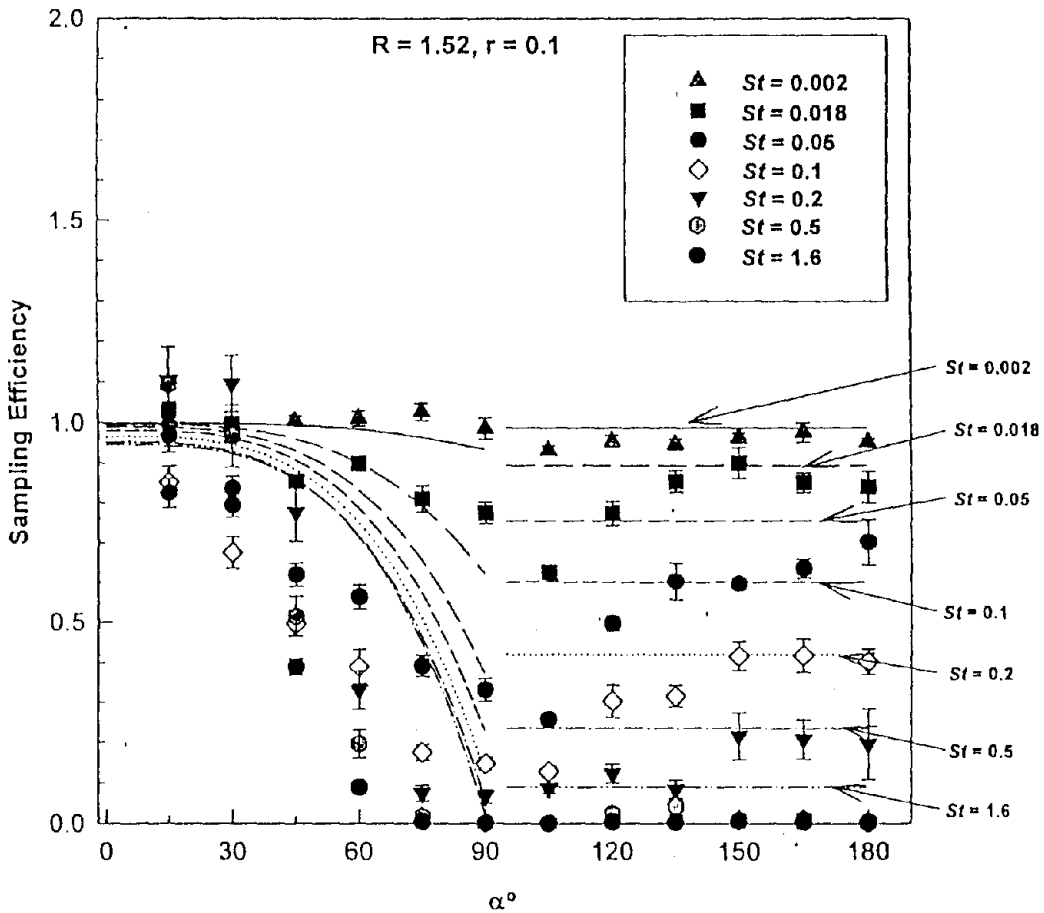

Figure 6.18 Effect of Orientation on the Sampling Efficiency of Spherical Sampler Along the Horizontal Plane for $R = 1.52$ and $r = 0.1$ Compared with Theory (Tsai *et al.*,1995)

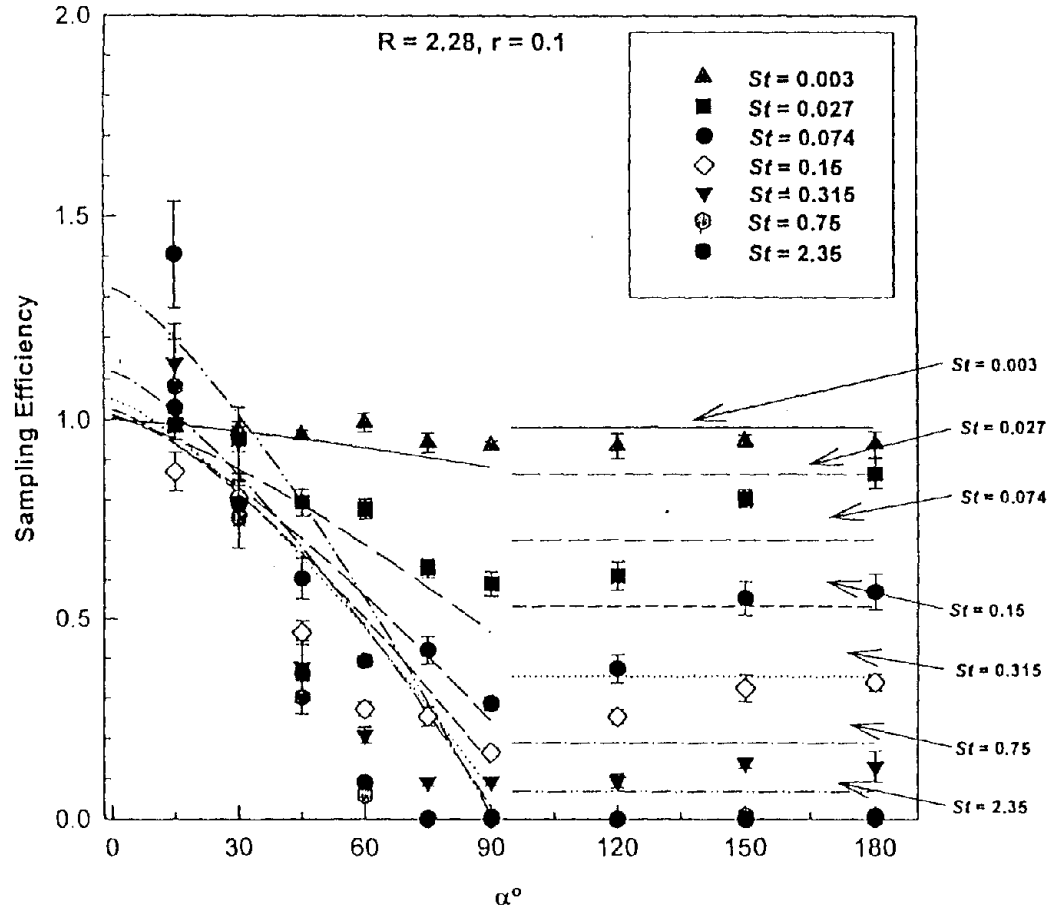

Figure 6.19 Effect of Orientation on the Sampling Efficiency of Spherical Sampler Along the Horizontal Plane for $R = 2.28$ and $r = 0.1$ Compared with Theory (Tsai *et al.*,1995)

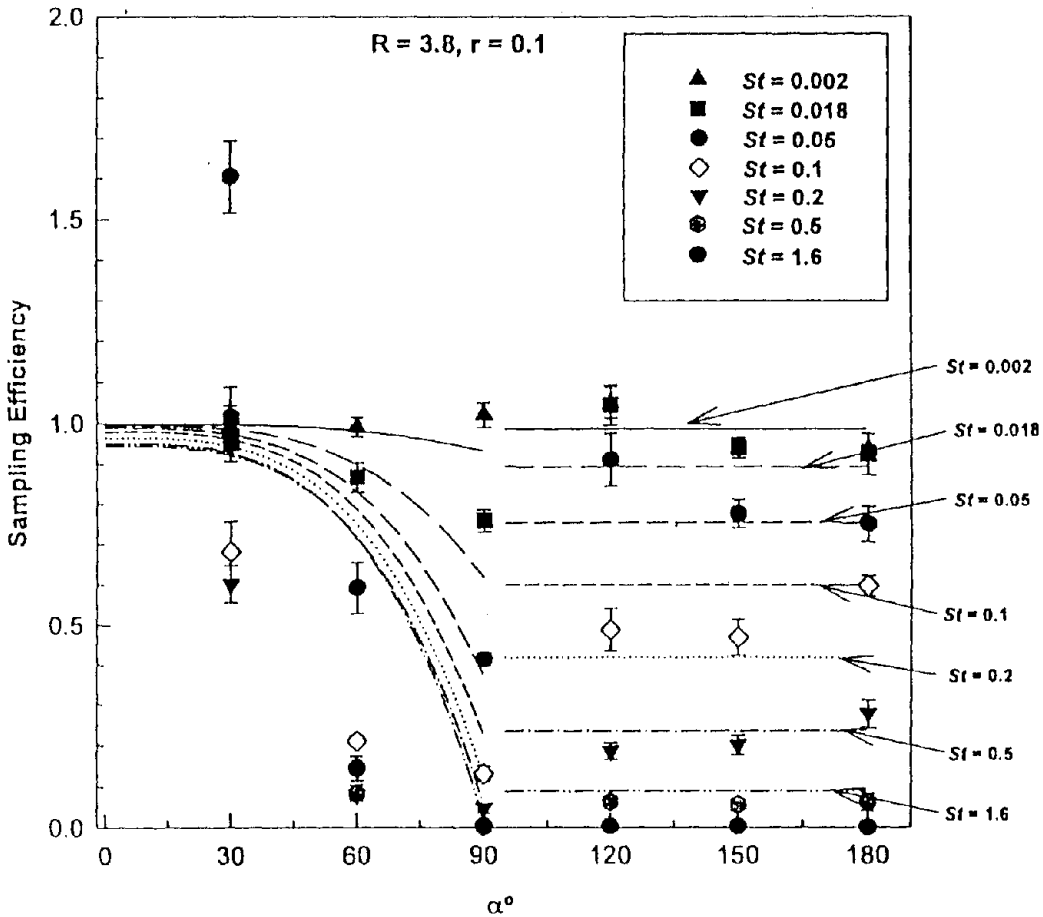

Figure 6.20 Effect of Orientation on the Sampling Efficiency of Spherical Sampler Along the Horizontal Plane for $R = 3.8$ and $r = 0.1$ Compared with Theory (Tsai *et al.*, 1995)

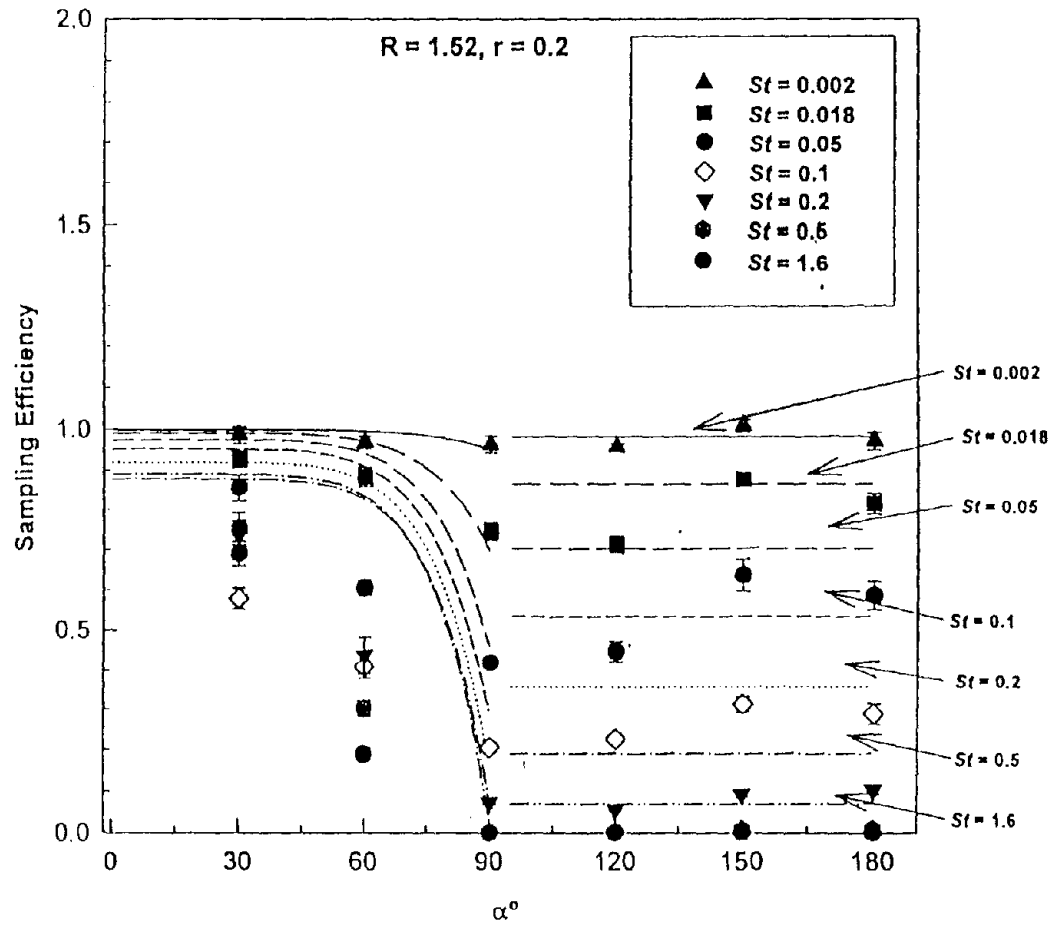

Figure 6.21 Effect of Orientation on the Sampling Efficiency of Spherical Sampler Along the Horizontal Plane for $R = 1.52$ and $r = 0.2$ Compared with Theory (Tsai *et al.*, 1995)

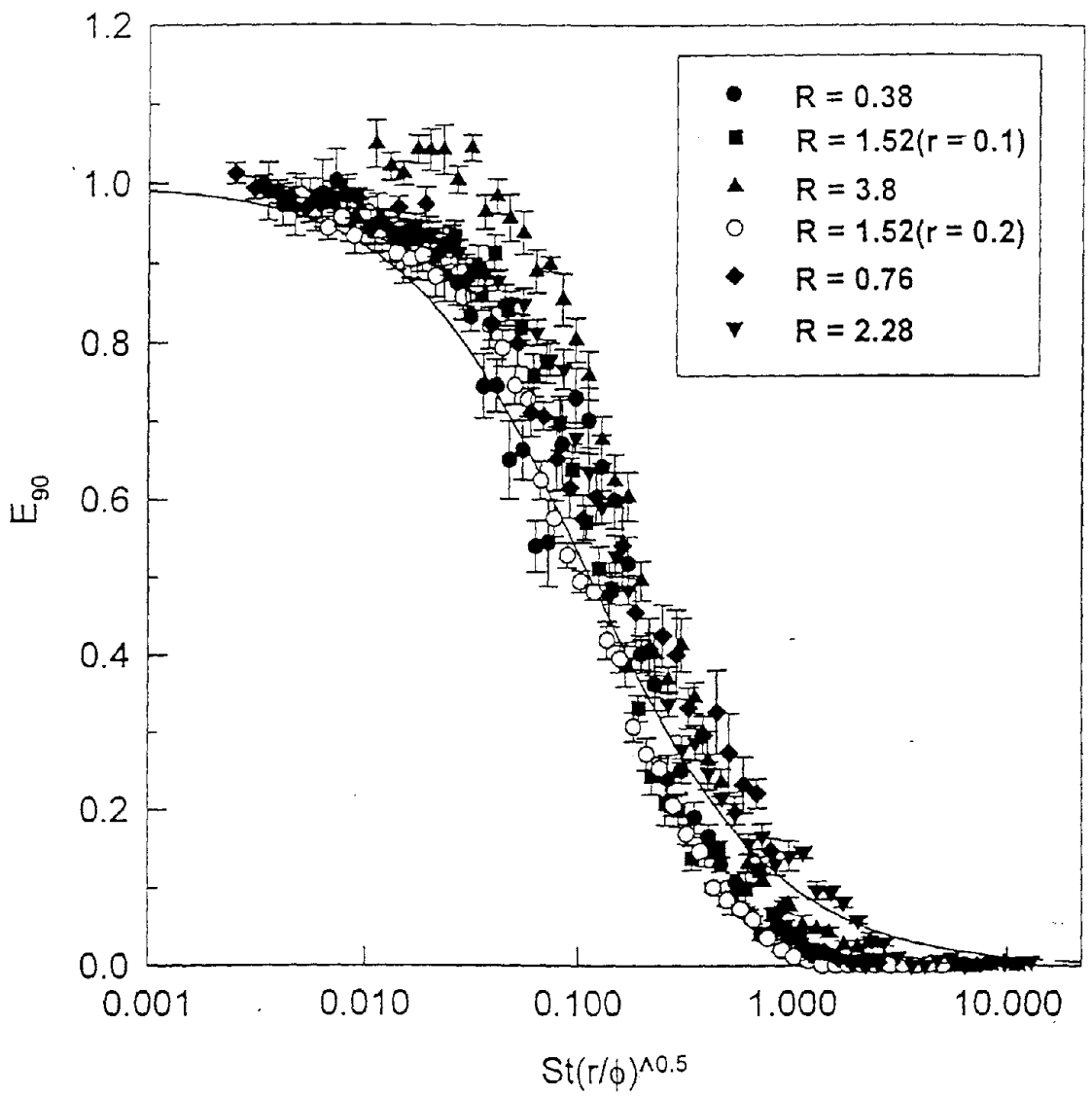

Figure 6.22 Comparison of sampling efficiency versus $St(r/\phi)^{\frac{1}{2}}$ for all spherical sampler data at $\alpha = 90°$

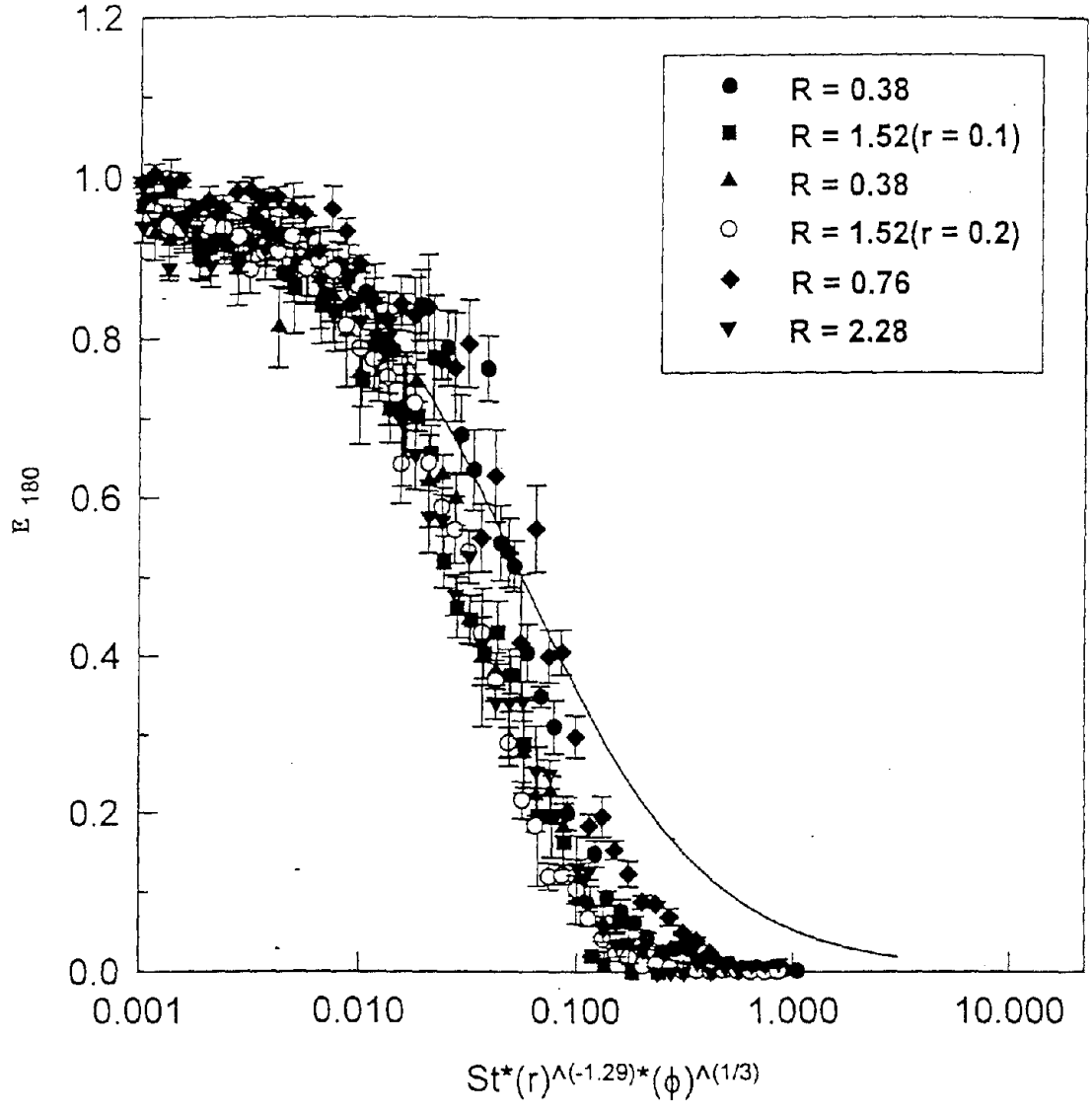

Figure 6.23 Comparison of sampling efficiency versus $St\, r^{-1.29}\phi^{1/3}$ for all spherical sampler data at $\alpha = 180°$

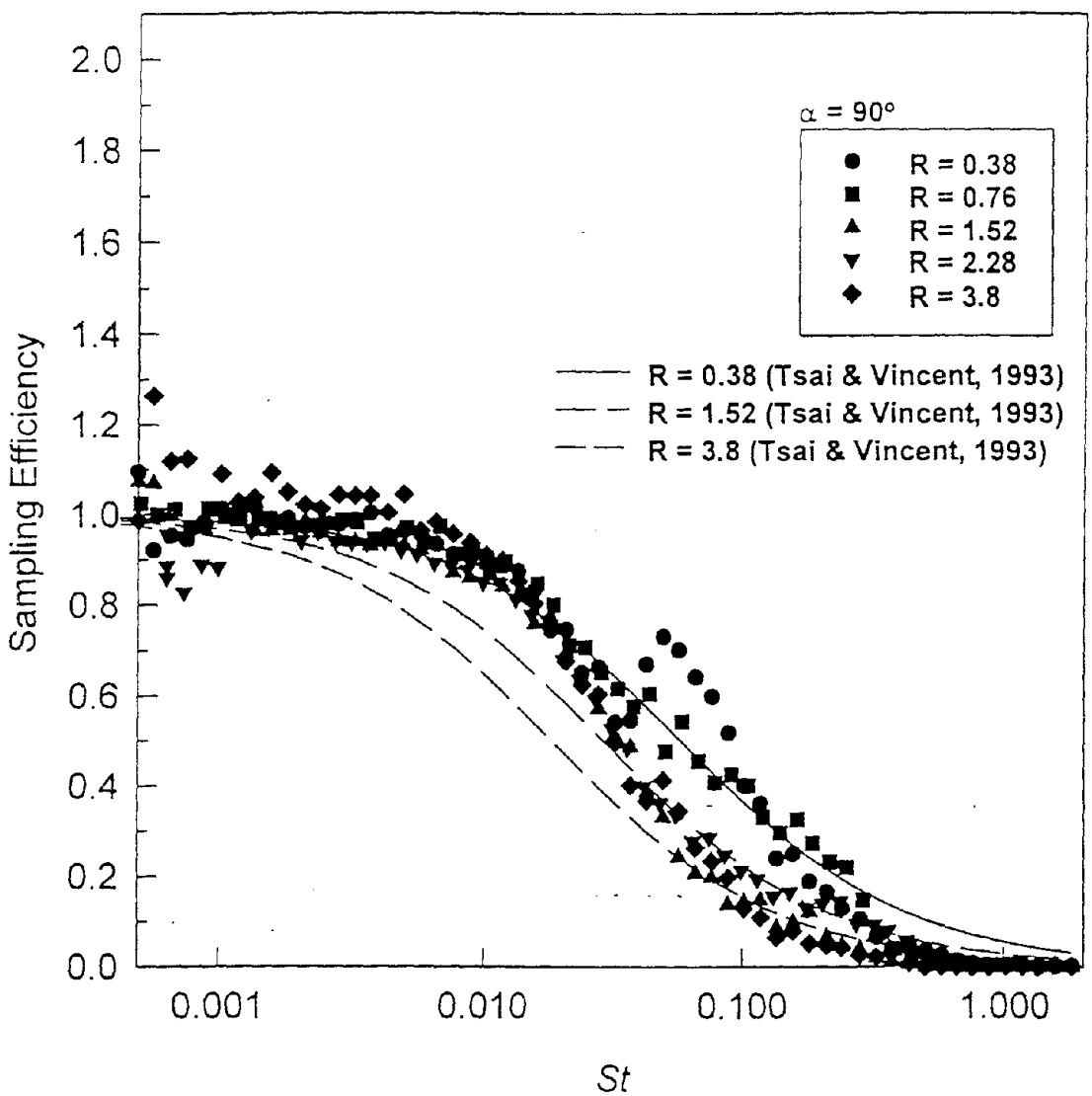

Figure 6.24 Comparison of sampling efficiency at $\alpha = 90°$ versus St at different values of R

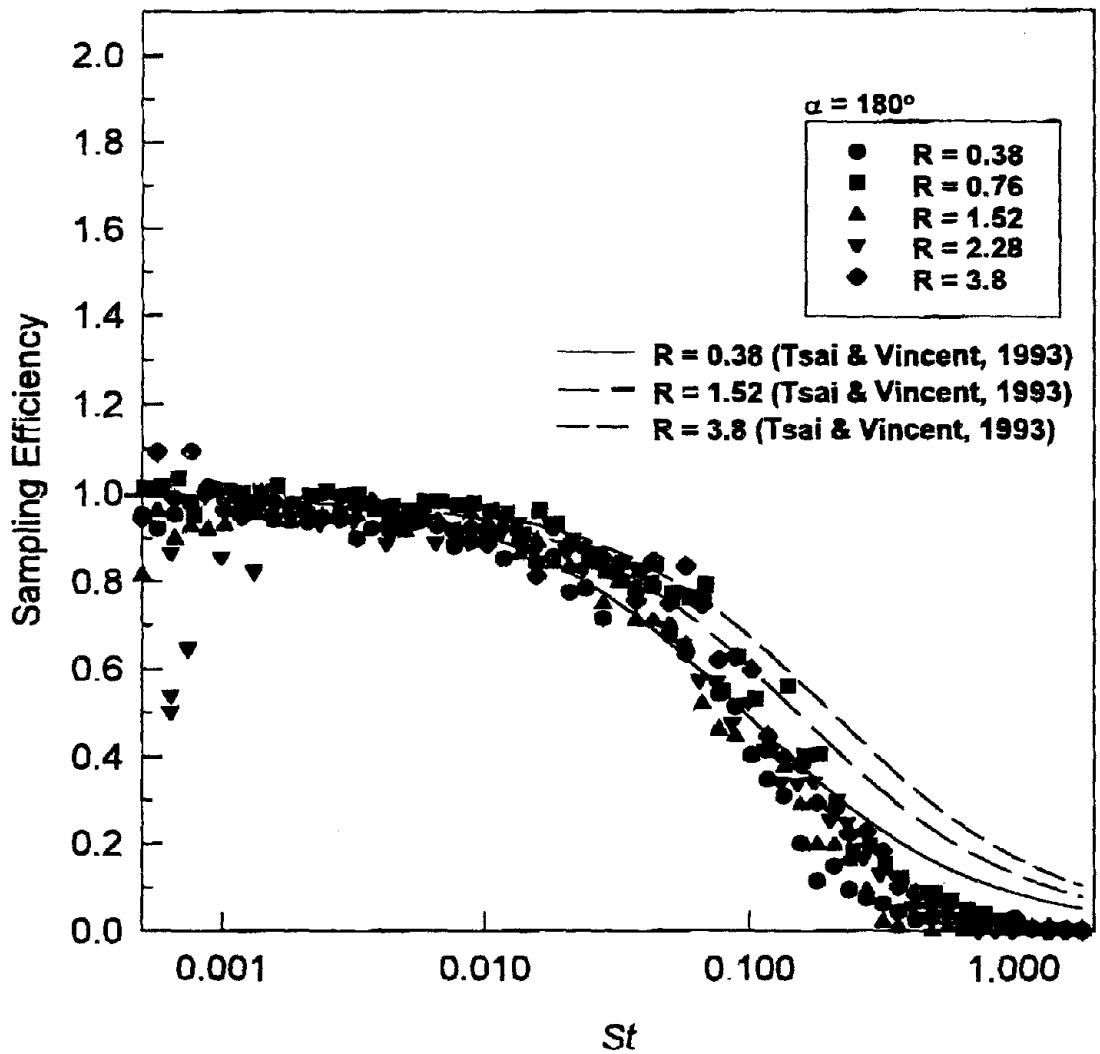

Figure 6.25 Comparison of sampling efficiency at $\alpha = 180°$ versus St at different values of R

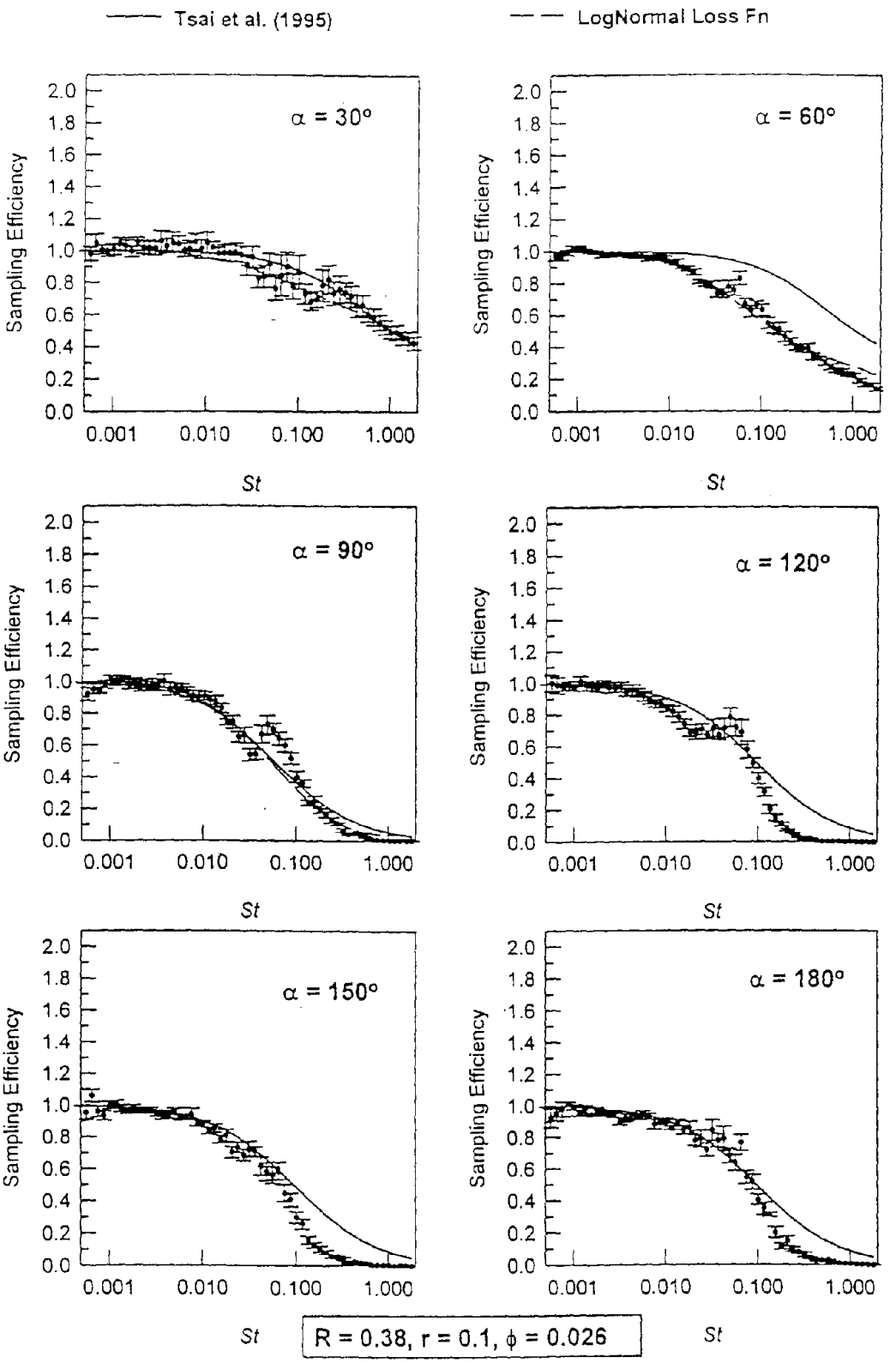

Figure 6.26 Comparison of Experimental Data with the New Model (up to $\alpha = 90°$) and the Tsai *et al.* Model for the Spherical Sampler Along the Horizontal Plane for $R = 0.38$ and $r = 0.1$

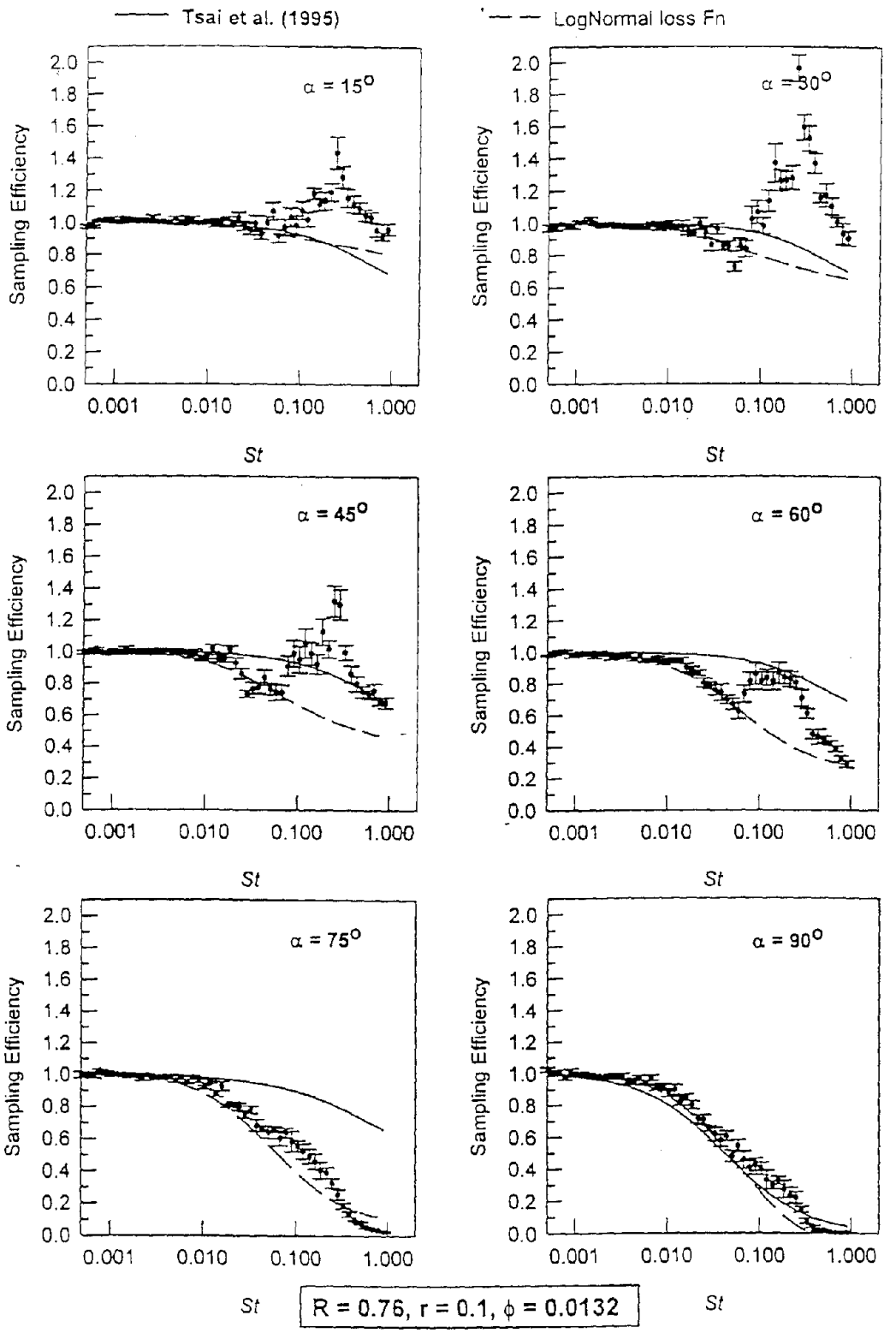

Figure 6.27 Comparison of Experimental Data with the New Model (up to $\alpha = 90°$) and the Tsai *et al.* model for the Spherical Sampler Along the Horizontal Plane for $R = 0.76$ and $r = 0.1$

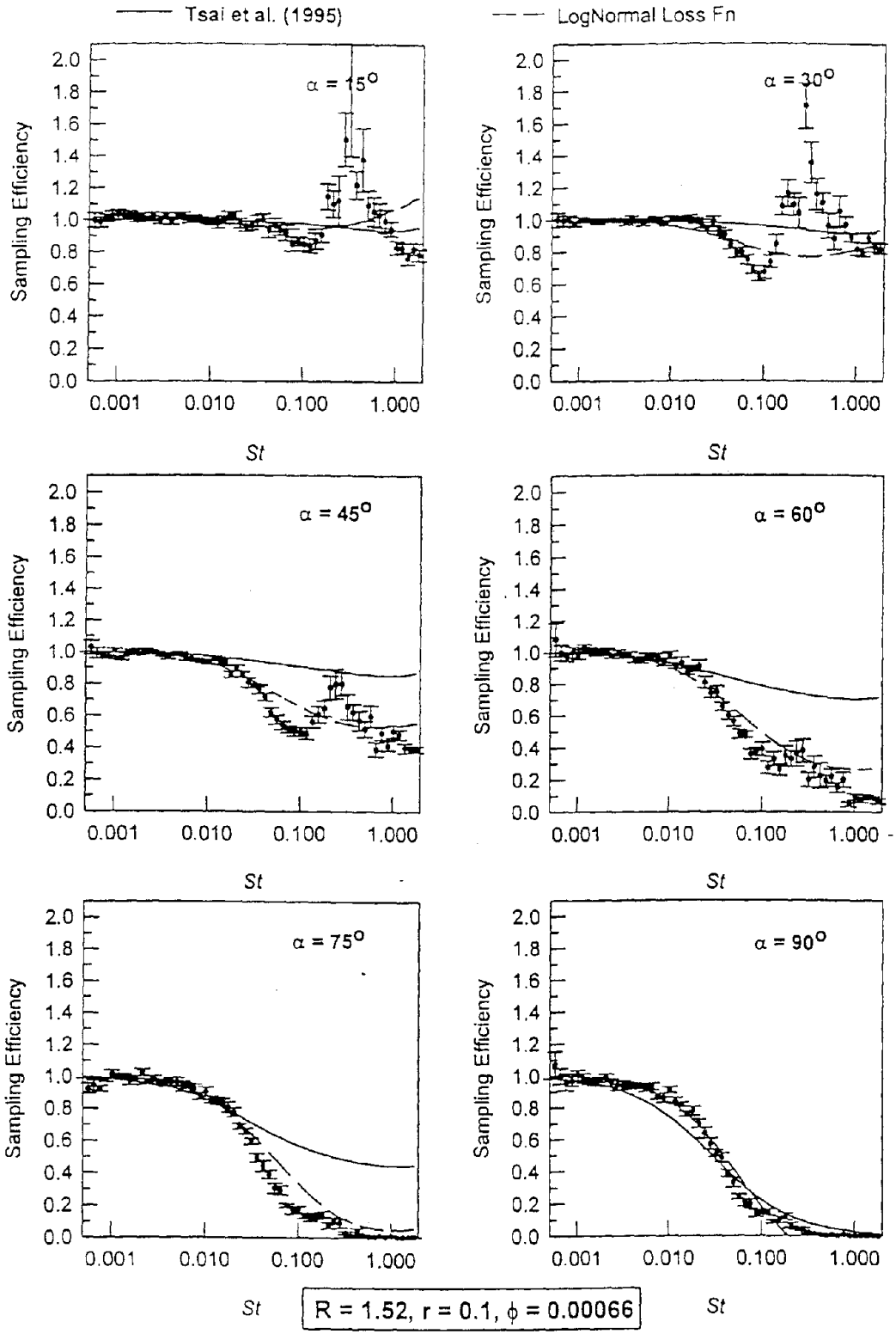

Figure 6.28. Comparison of Experimental Data with the New Model (up to $\alpha = 90°$) and the Tsai *et al.* Model for the Spherical Sampler Along the Horizontal Plane for $R = 1.52$ and $r = 0.1$

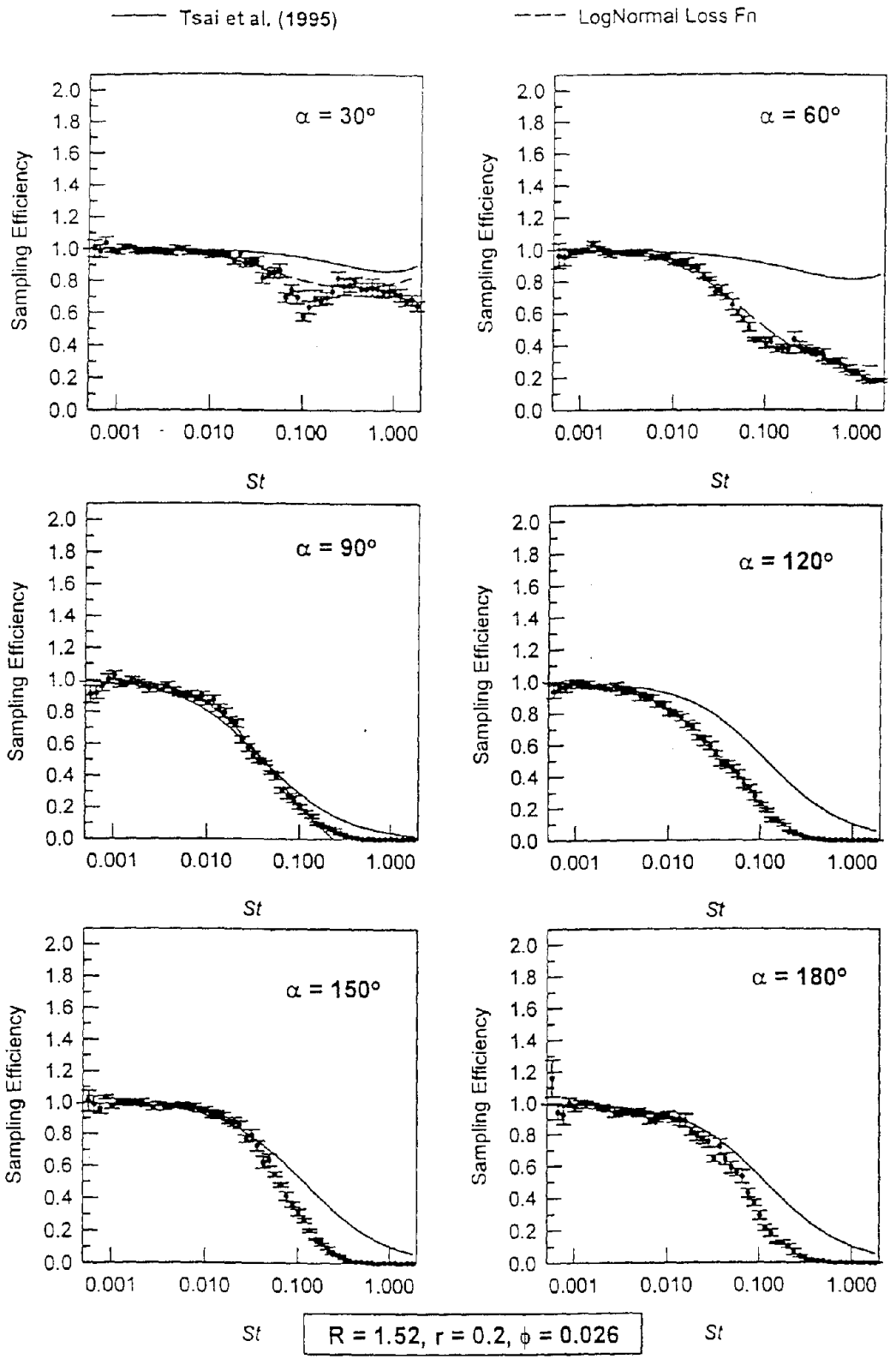

Figure 6.29. Comparison of Experimental Data with the New Model (up to $\alpha = 90°$) and the Tsai *et al.* Model for the Spherical Sampler Along the Horizontal Plane for $R = 1.52$ and $r = 0.2$

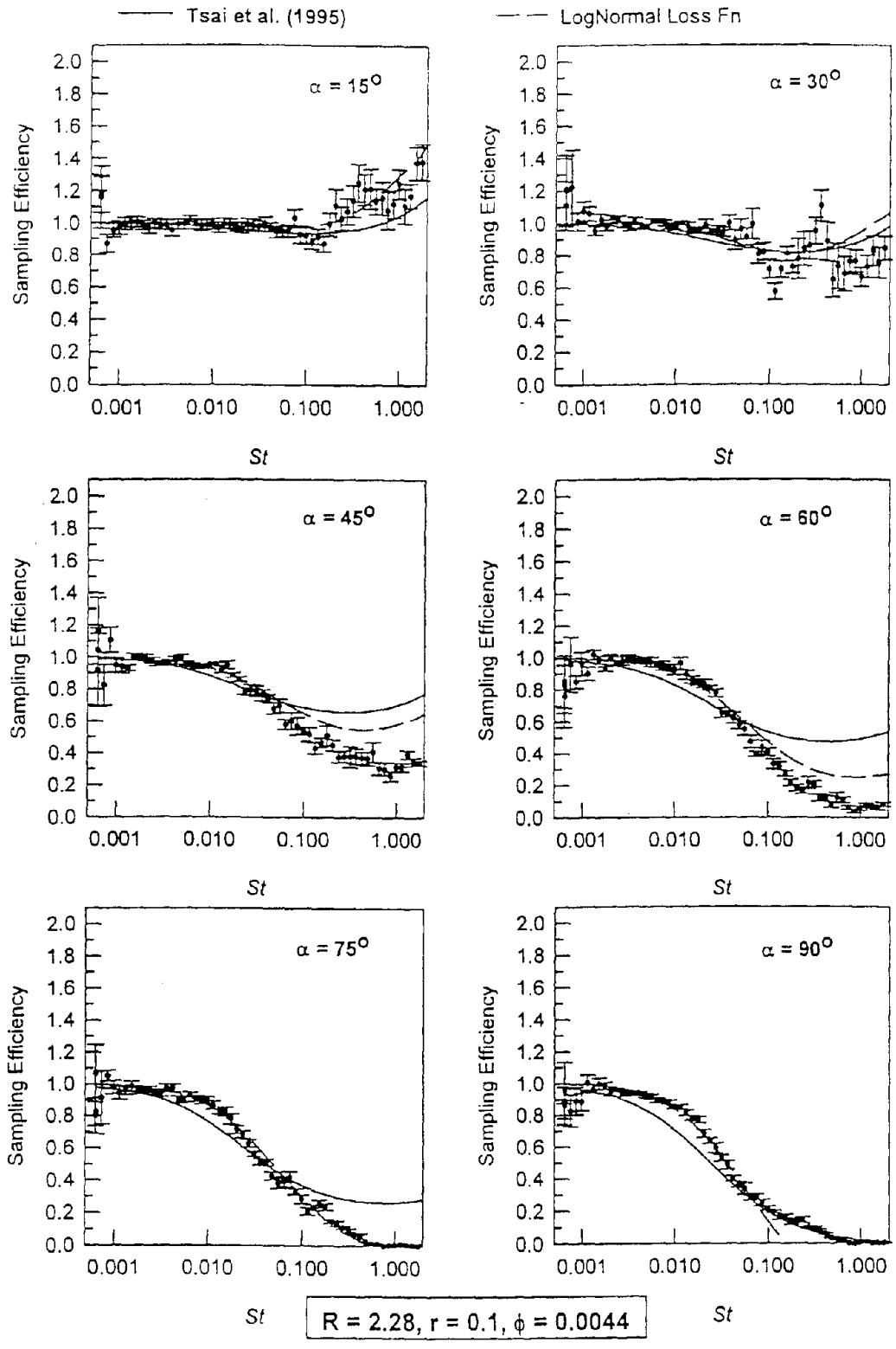

Figure 6.30 Comparison of Experimental Data with the New Model (up to $\alpha = 90°$) and the Tsai *et al.* Model for the Spherical Sampler Along the Horizontal Plane for $R = 2.28$ and $r = 0.1$

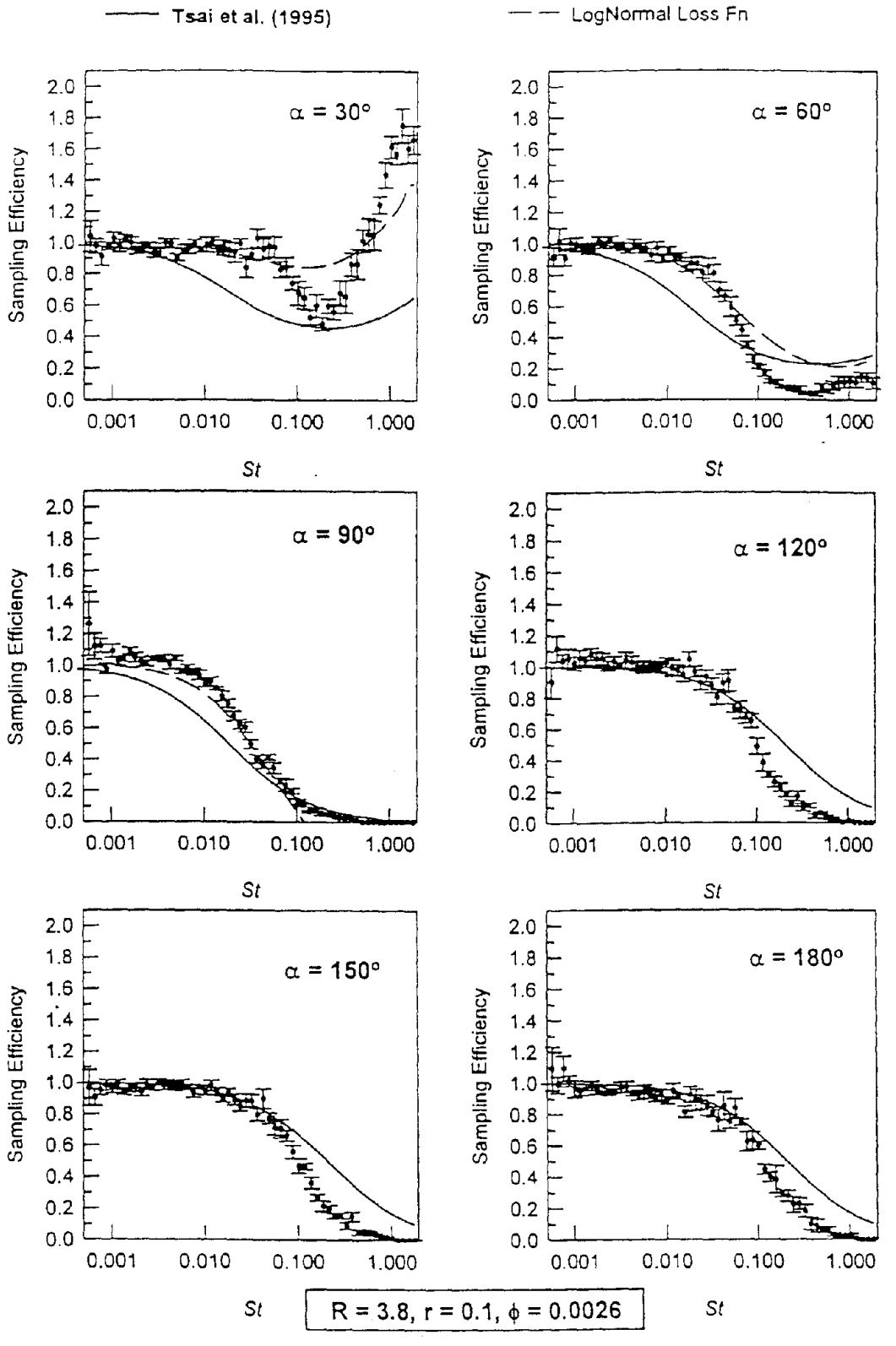

Figure 6.31 Comparison of Experimental Data with the New Model (up to $\alpha = 90°$) and the Tsai et al. Model for the Spherical Sampler Along the Horizontal Plane for $R = 3.8$ and $r = 0.1$

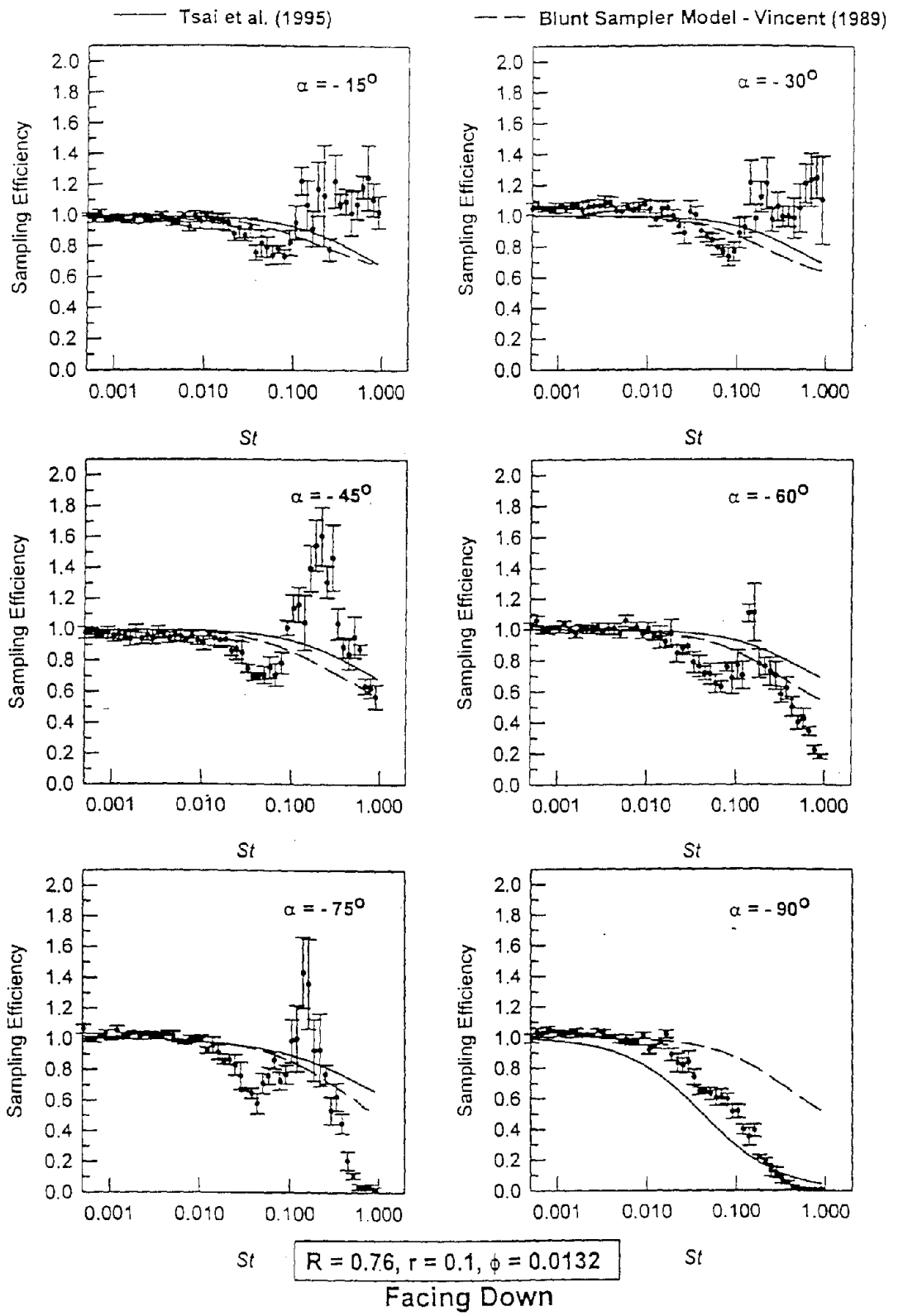

Figure 7.1a Plot of Sampling Efficiency versus *St* for Spherical Sampler at Different Orientations in the Vertical Plane, Facing Down for $R = 0.76$ and $r = 0.1$

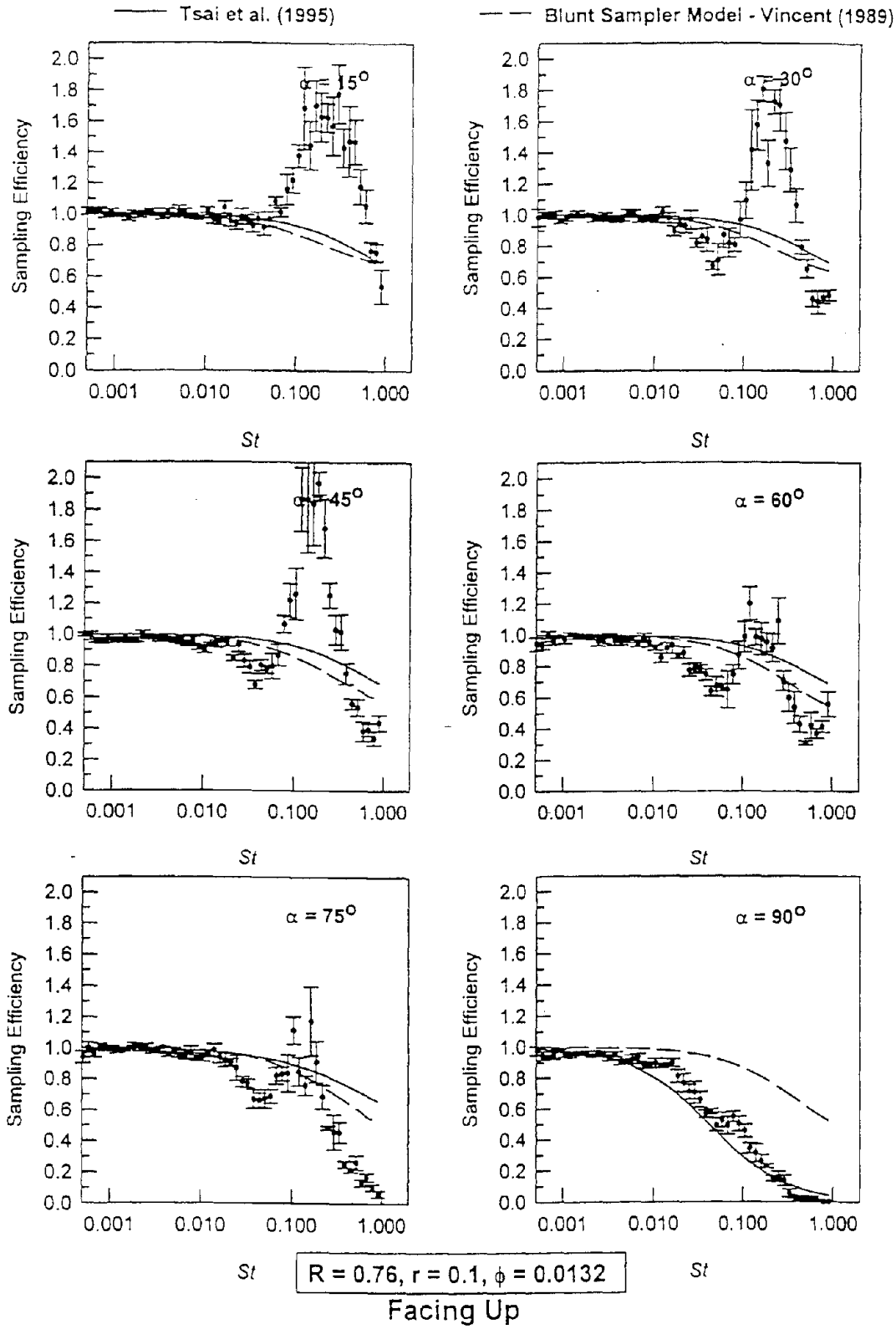

Figure 7.1b Plot of Sampling Efficiency versus *St* for Spherical Sampler at Different Orientations in the Vertical Plane, Facing Up for $R = 0.76$ and $r = 0.1$

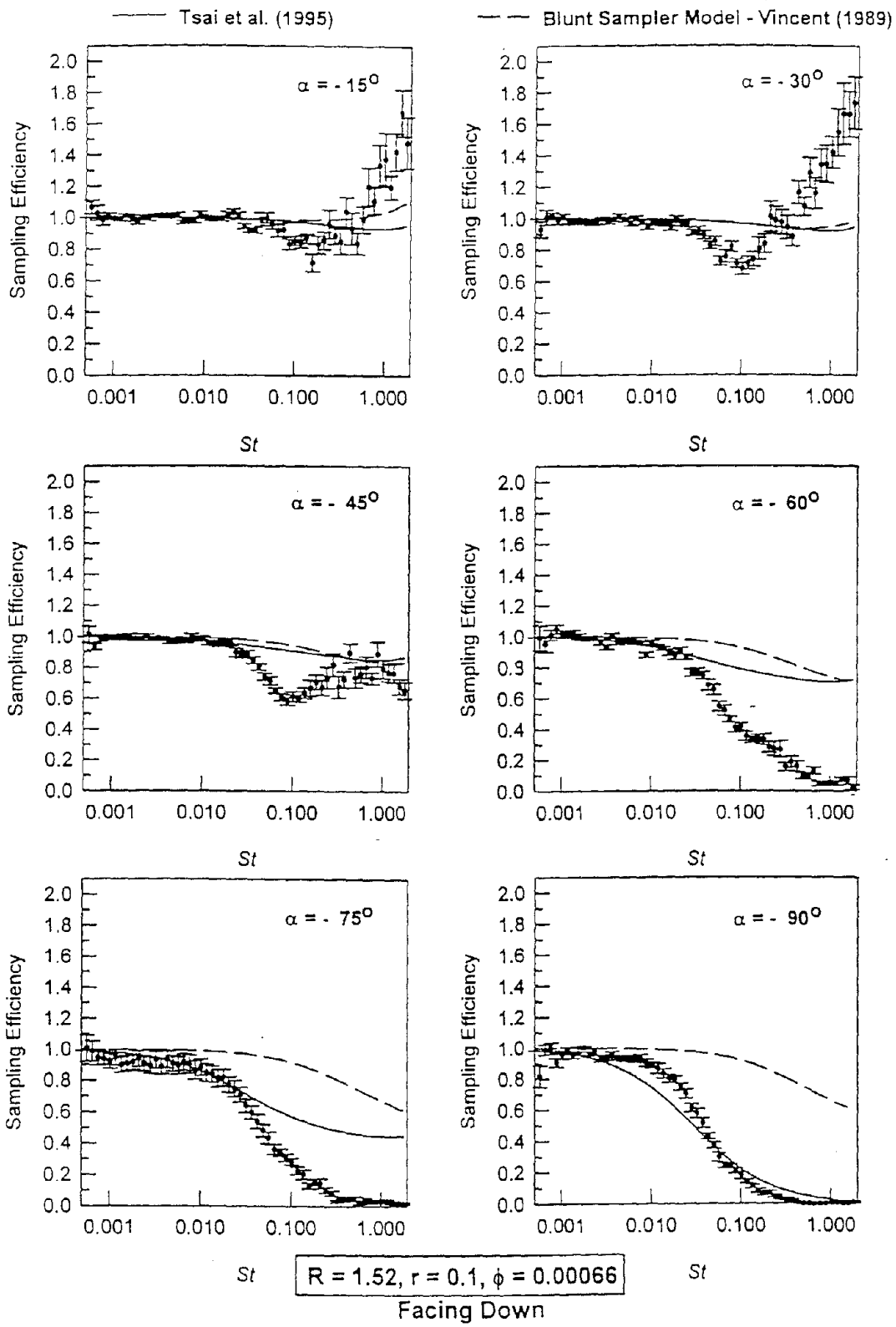

Figure 7.2a Plot of Sampling Efficiency versus *St* for Spherical Sampler at Different Orientations in the Vertical Plane, Facing Down for $R = 1.52$ and $r = 0.1$

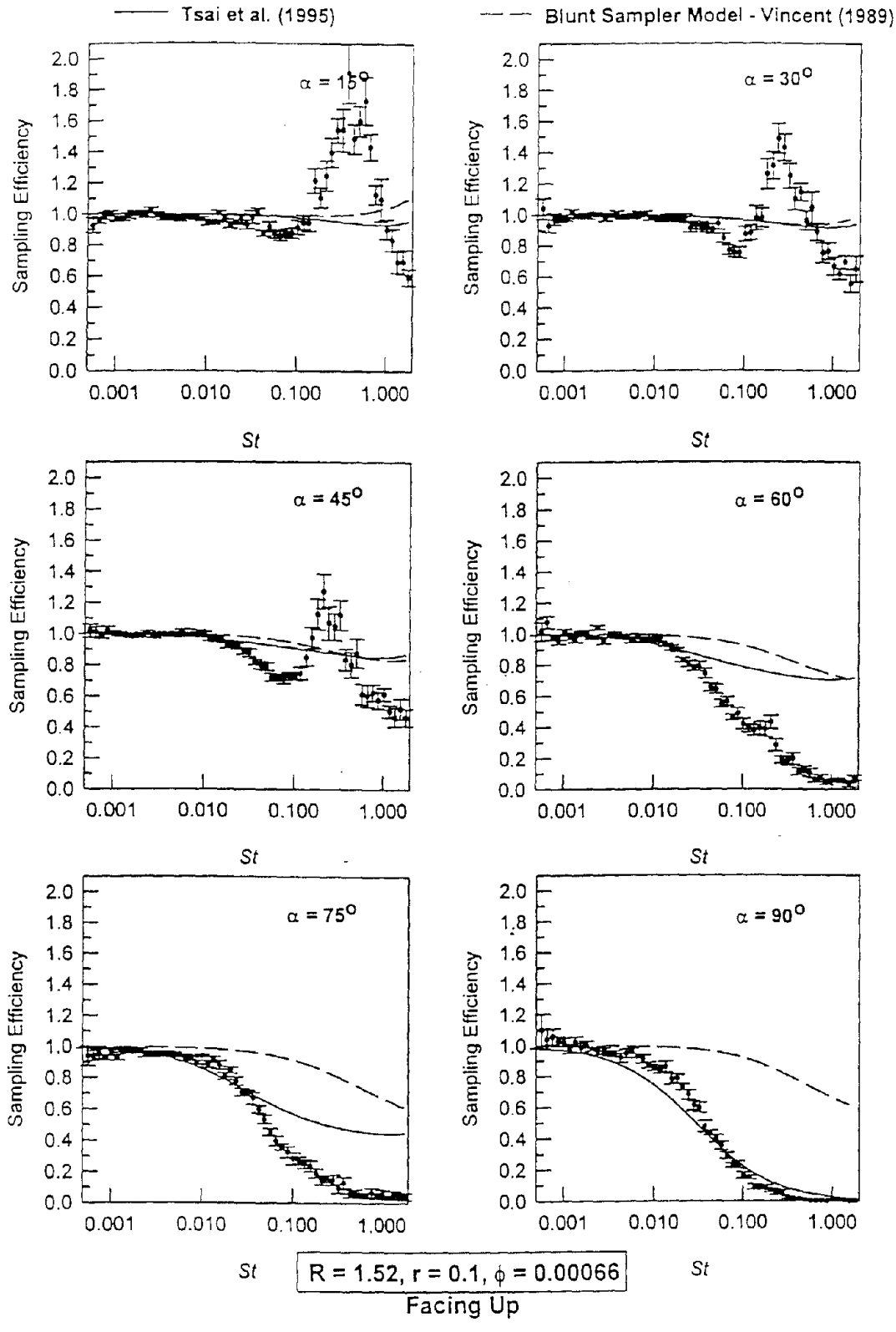

Figure 7.2b Sampling Efficiency versus *St* for Spherical Sampler at Different Orientations in the Vertical Plane, Facing Up for $R = 1.52$ and $r = 0.1$

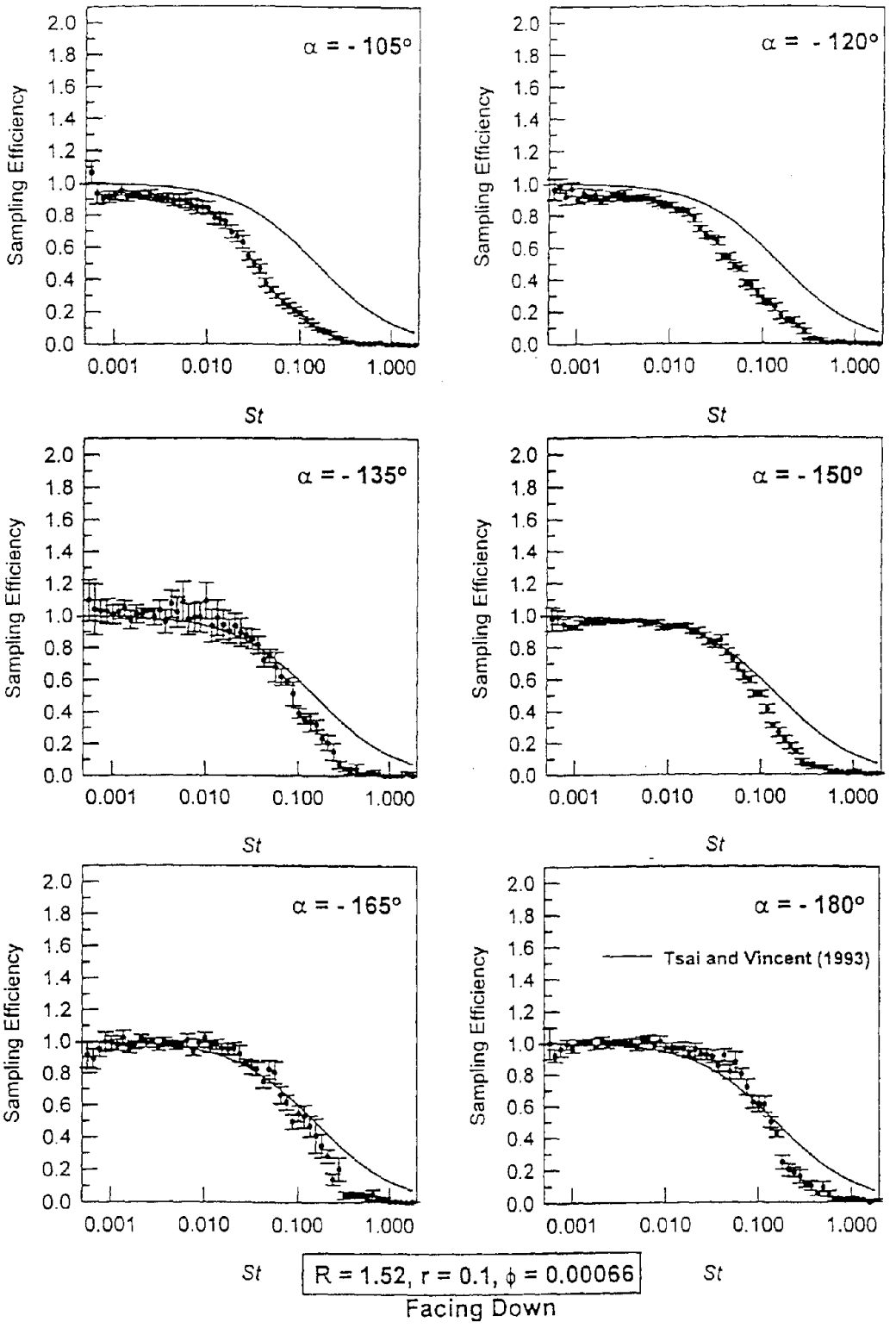

Figure 7.3a Sampling Efficiency versus *St* for Spherical Sampler at Different Orientations in the Vertical Plane, Facing Down for R = 1.52 and r =0.1

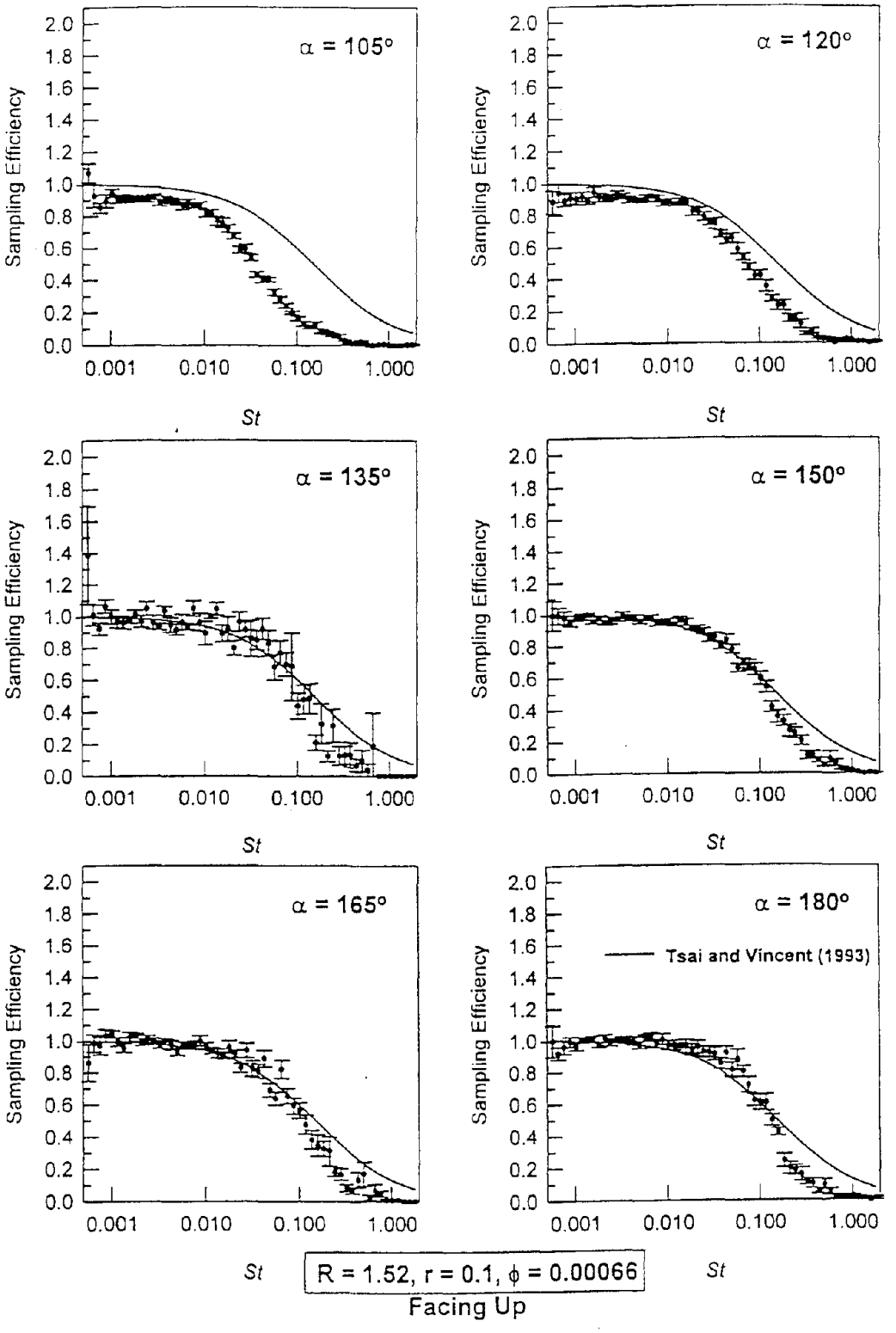

Figure 7.3b Sampling Efficiency versus St for Spherical Sampler at Different Orientations in the Vertical Plane, Facing Up for R = 1.52 and r =0.1

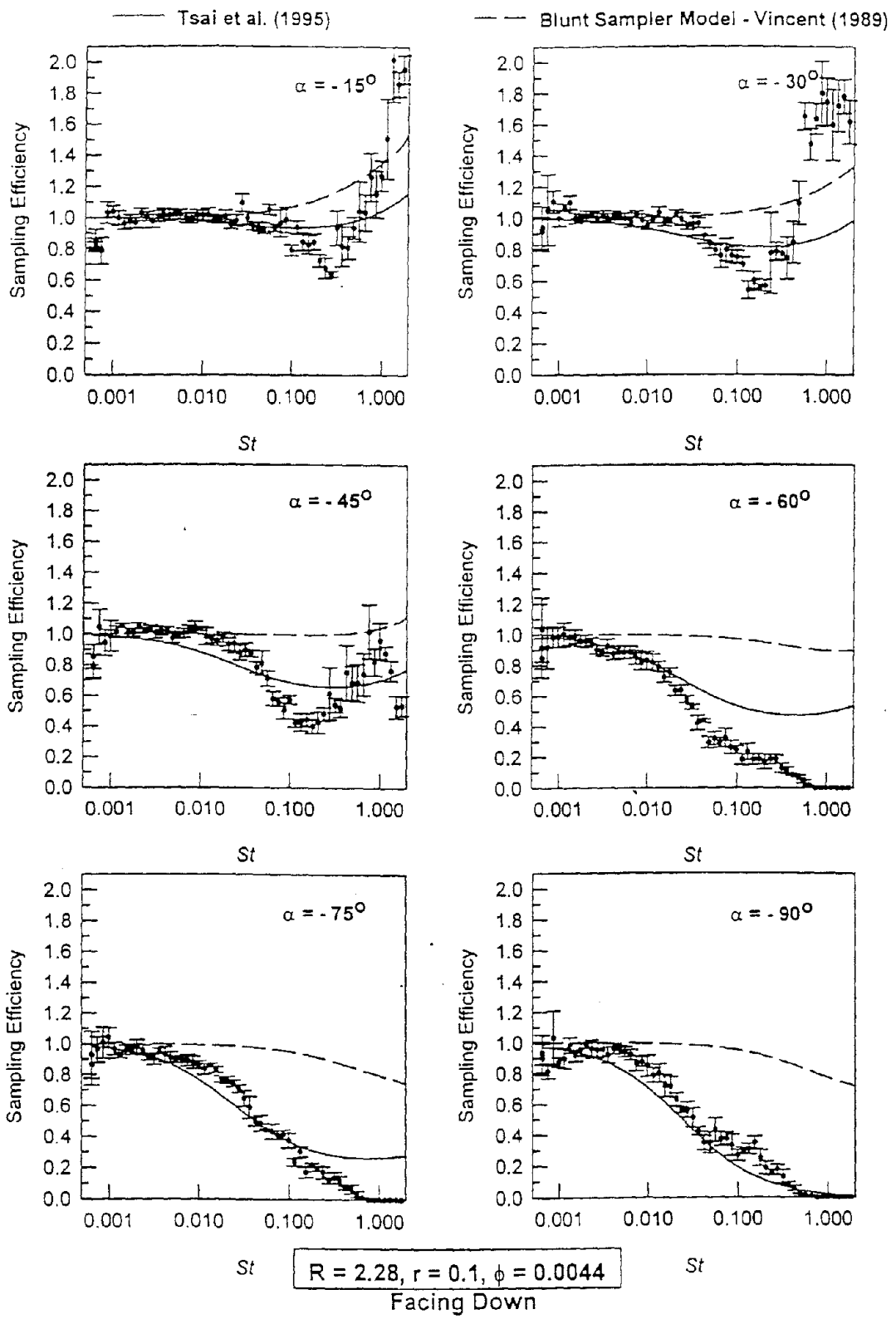

Figure 7.4a Sampling Efficiency versus *St* for Spherical Sampler at Different Orientations in the Vertical Plane, Facing Down for $R = 2.28$ and $r = 0.1$

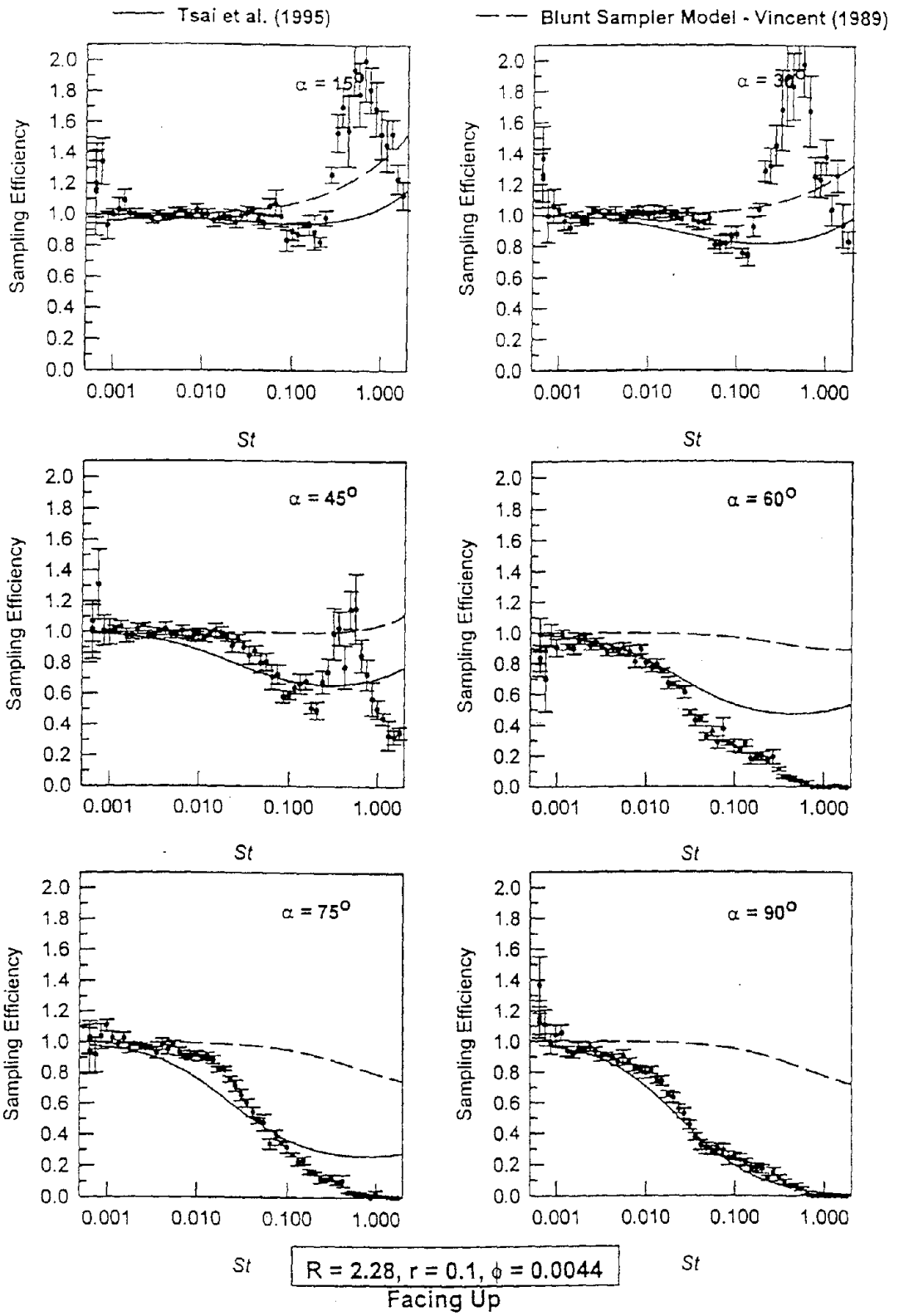

Figure 7.4b Sampling Efficiency versus *St* for Spherical Sampler at Different Orientations in the Vertical Plane, Facing Up for $R = 2.28$ and $r = 0.1$

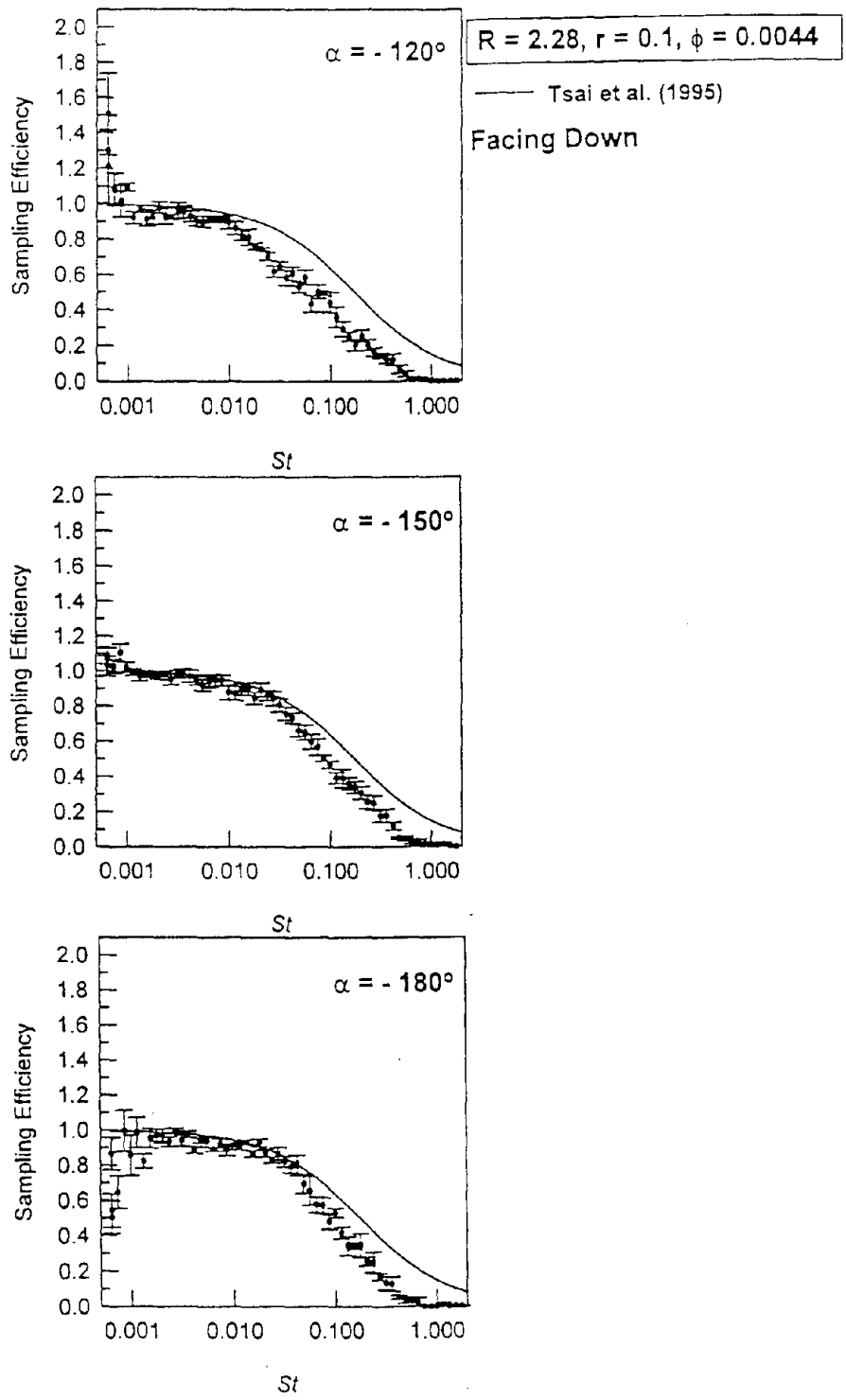

Figure 7.5a Plot of Sampling Efficiency Versus *St* for Spherical Sampler at Different Orientations in the Vertical Plane, Facing Down for $R = 2.28$ and $r = 0.1$

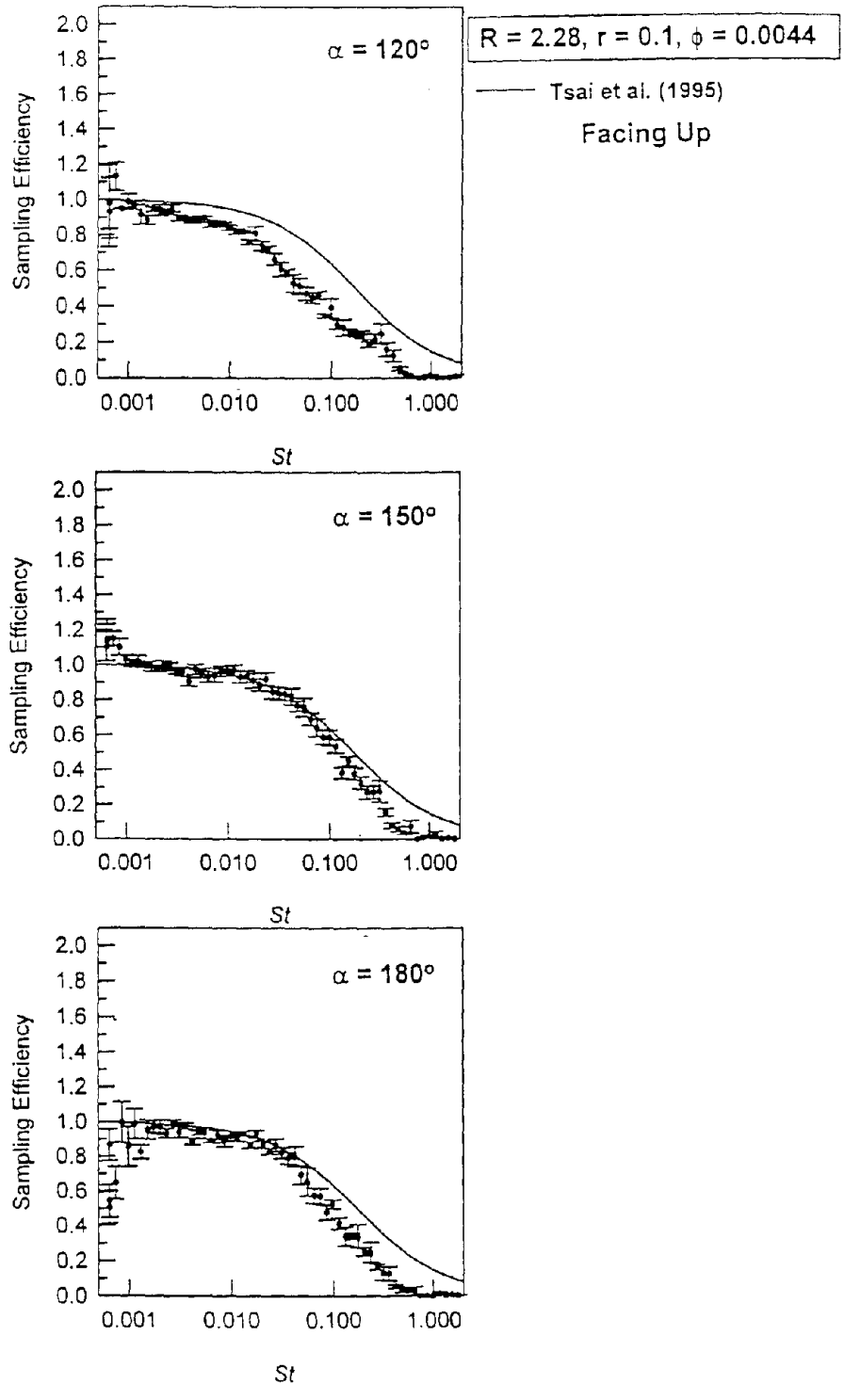

Figure 7.5b Plot of Sampling Efficiency versus *St* for Spherical Sampler at Different Orientations in the Vertical Plane, Facing Up for $R = 2.28$ and $r = 0.1$

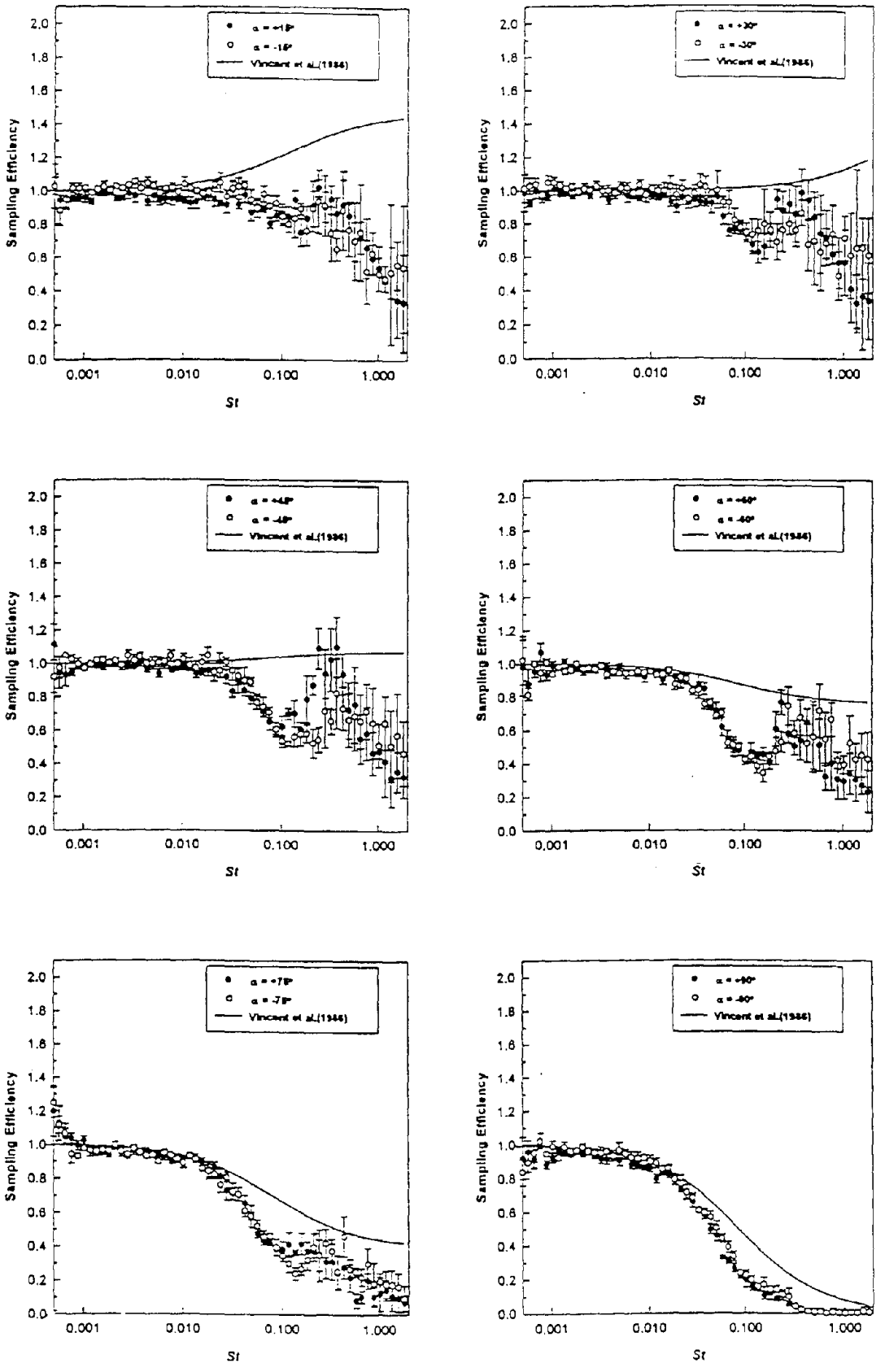

Figure 7.6a Sampling Efficiency Versus St for Thin-Walled Probes in the Vertical Plane for Angles up to 90°

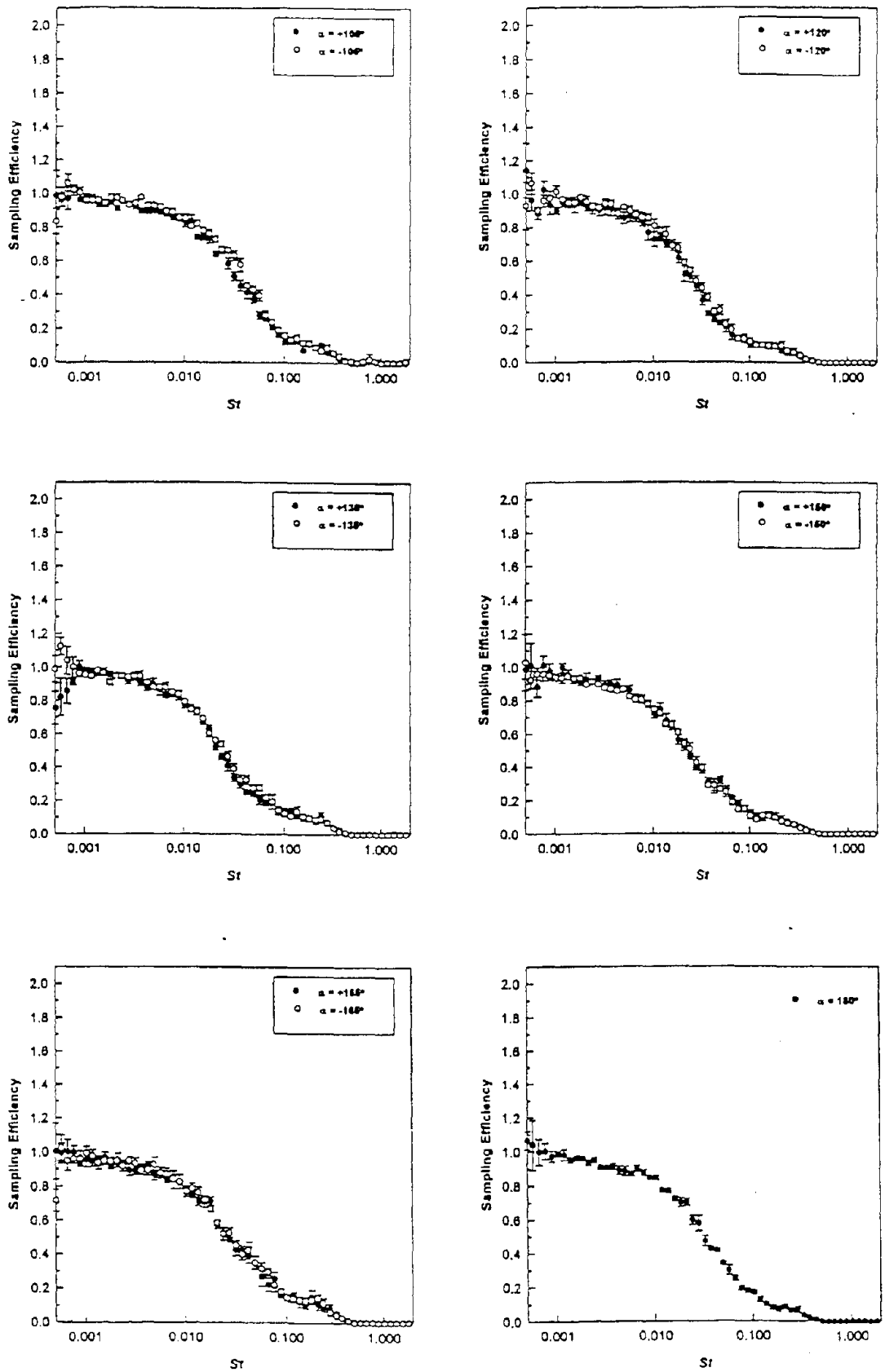

Figure 7.6b Sampling Efficiency Versus St for Thin-Walled Probes in the Vertical Plane for Angles Greater than 90°

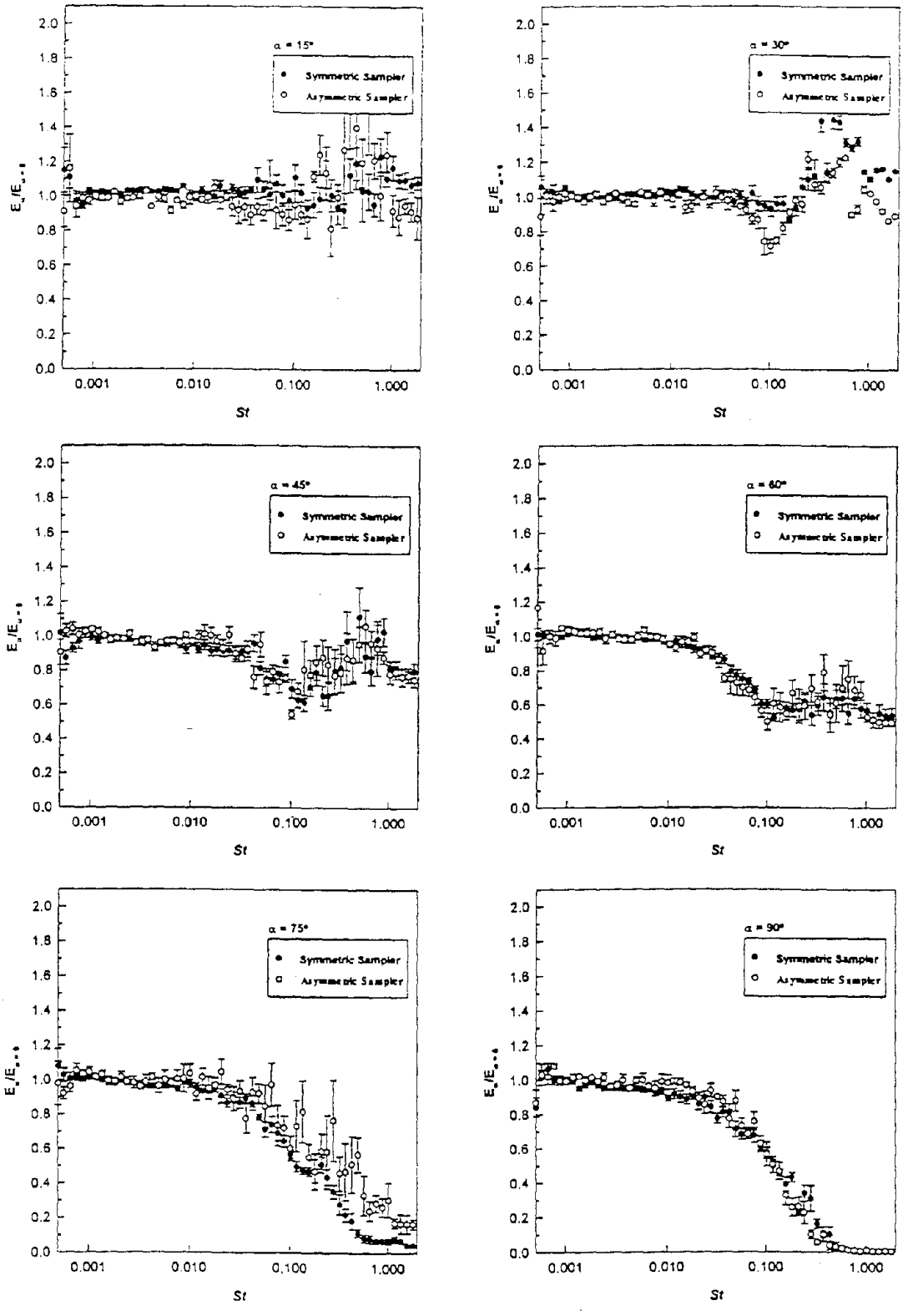

Figure 8.1a Sampling Ratio versus *St* for Symmetric and Asymmetric Samplers for Angles up to 90°

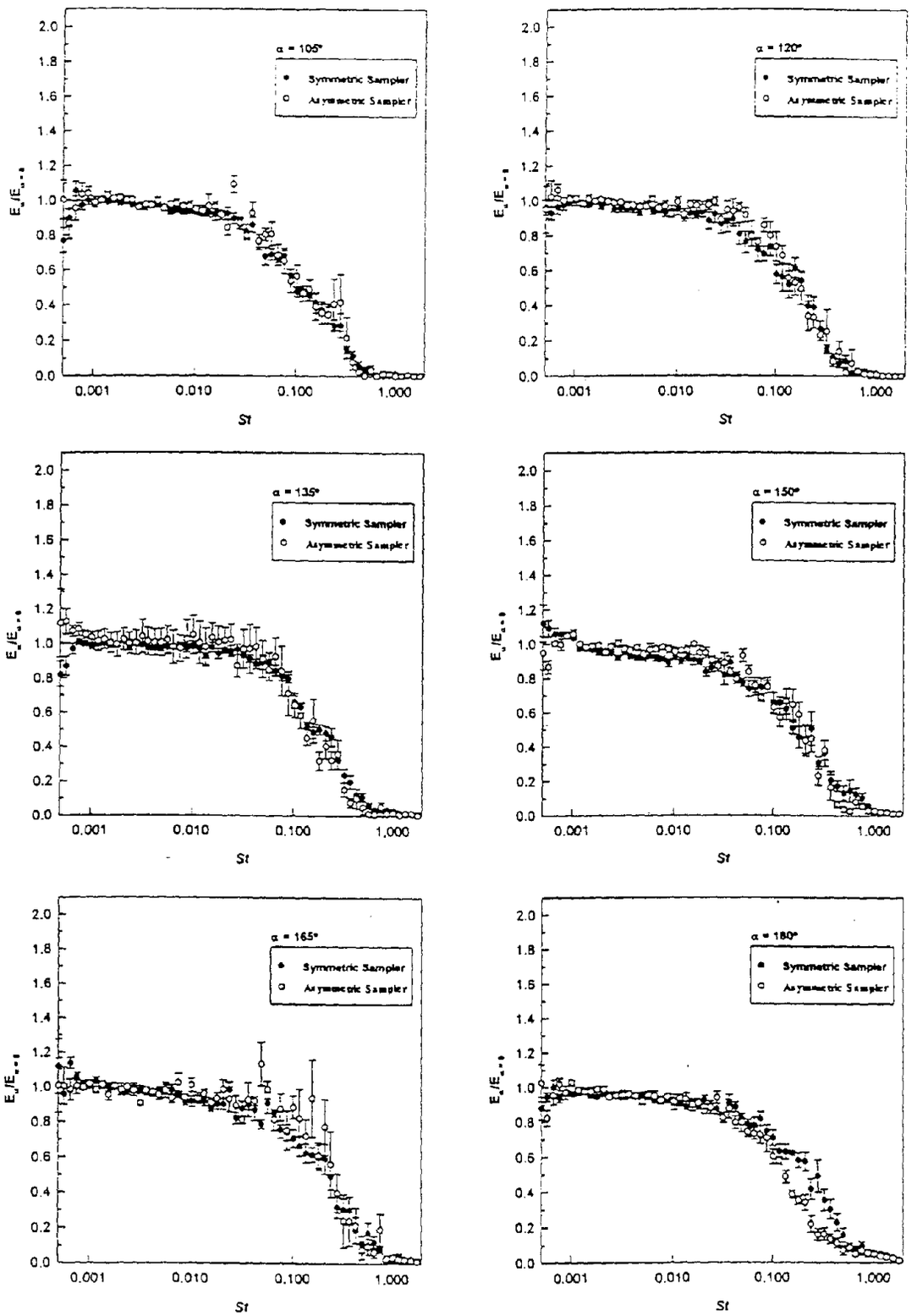

Figure 8.1b Sampling Ratio versus *St* for Symmetric and Asymmetric Samplers for Angles Greater than 90°

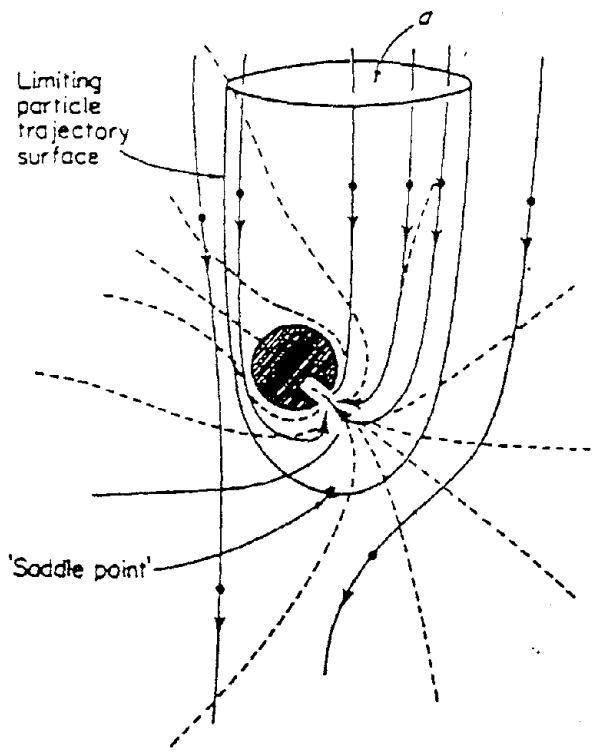

Figure 9.1 The limiting particle trajectory surface enclosing the area, a, for a sampler of arbitrary shape and orientation in calm air (Taken from Vincent, 1989)

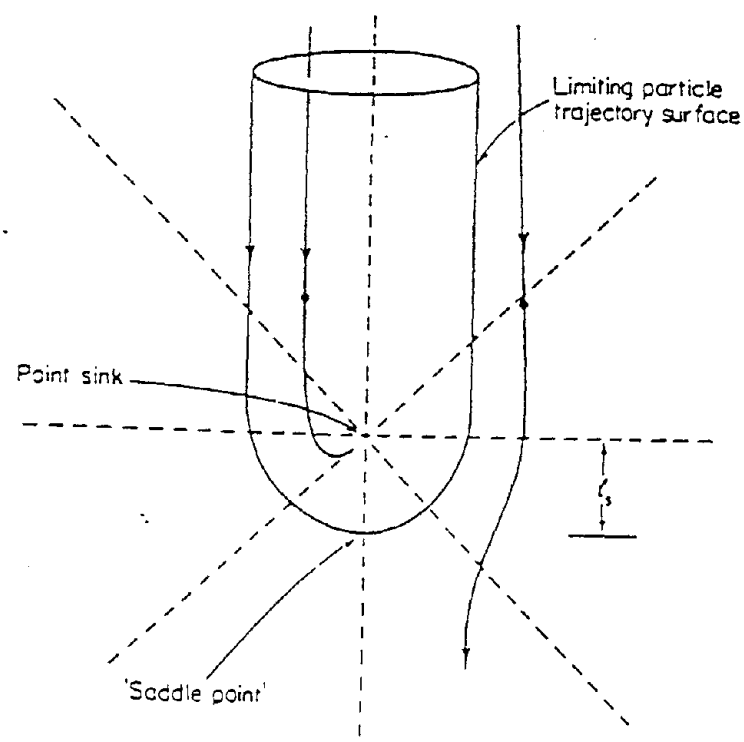

Figure 9.2 The limiting particle trajectory near a point sink in calm air (Taken from Vincent, 1989)

Figure 9.3 Schematic of experimental apparatus

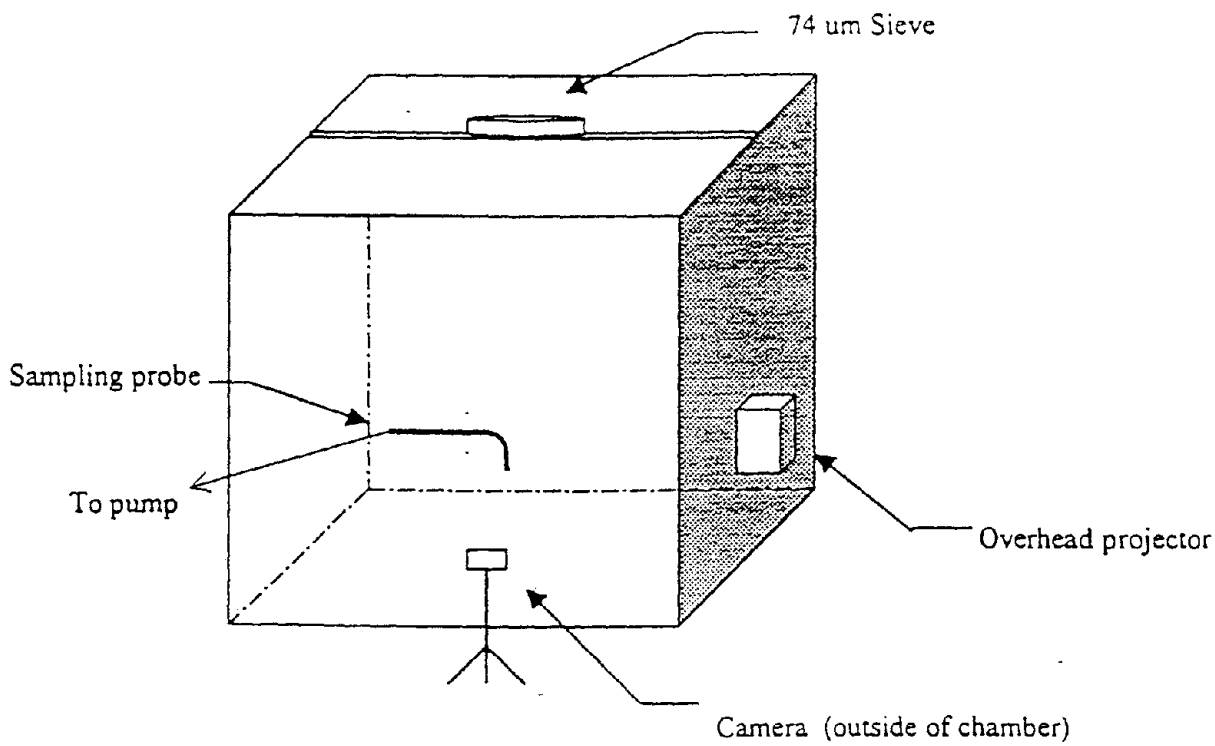

Figure 9.4 Aspiration of Particles into a Thin-walled Probe in Calm Air

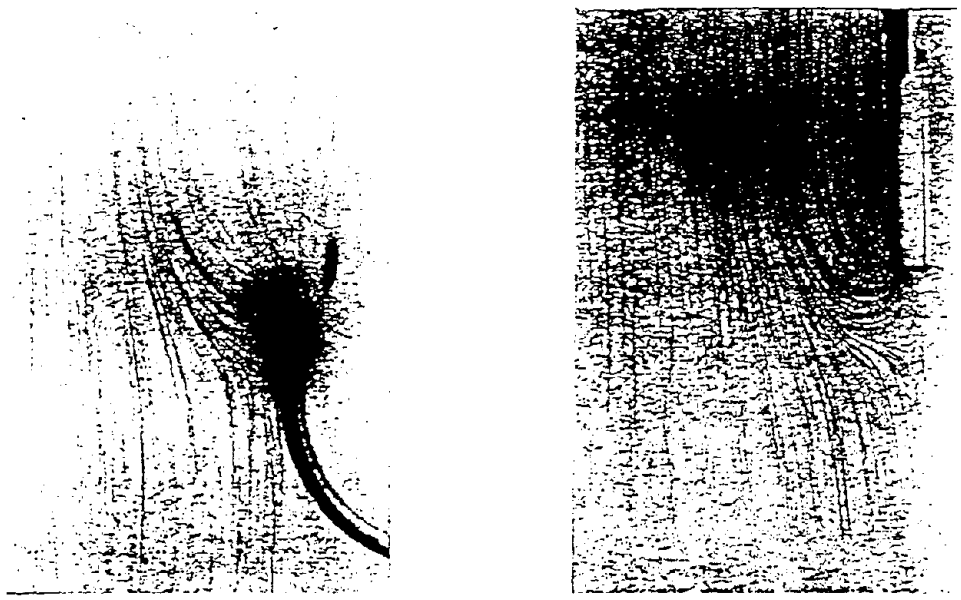

Upwards-facing Probe

Downwards-facing Probe

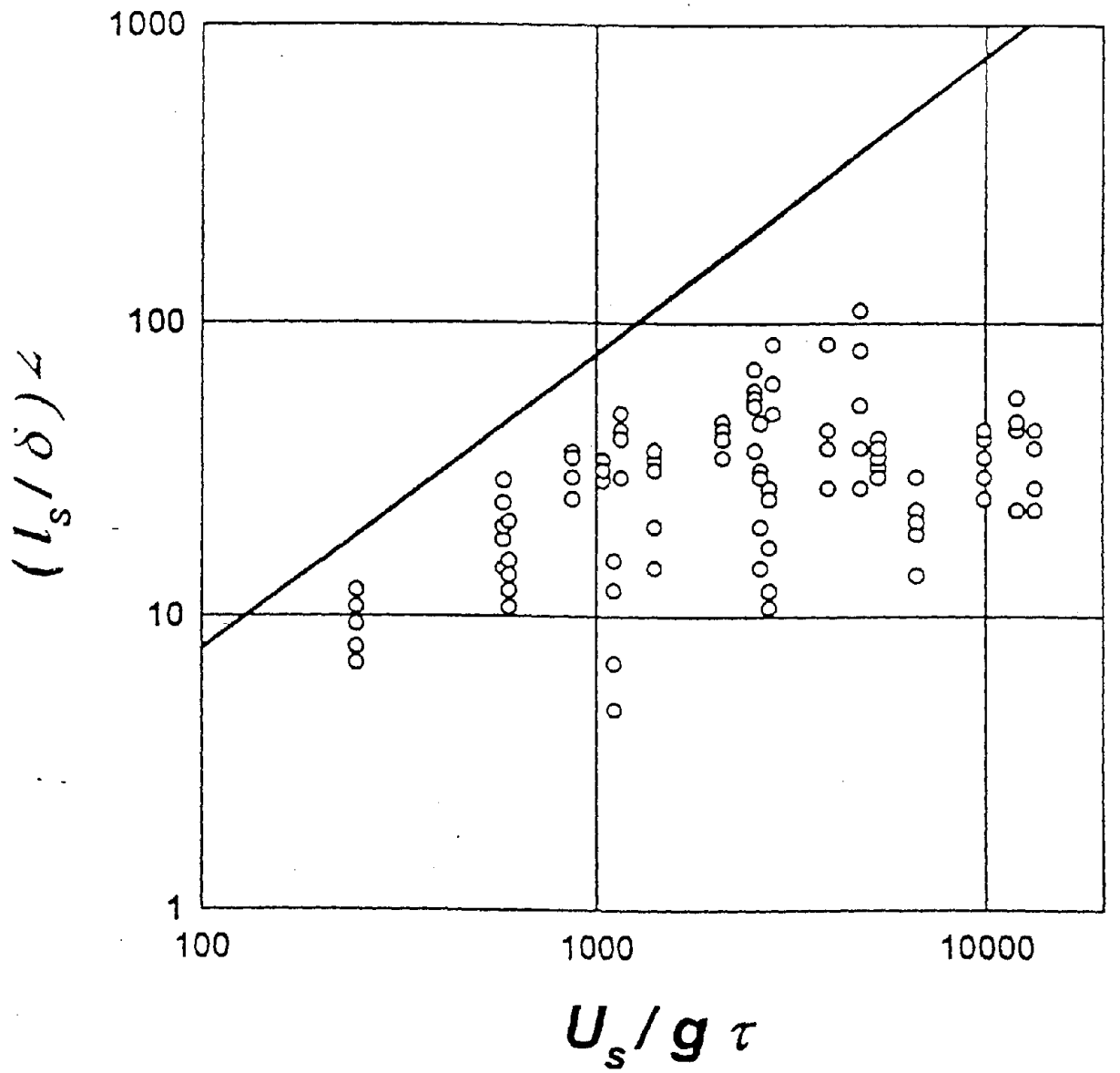

Figure 9.5 Comparison of the experimental sampling parameter data with the predicted line

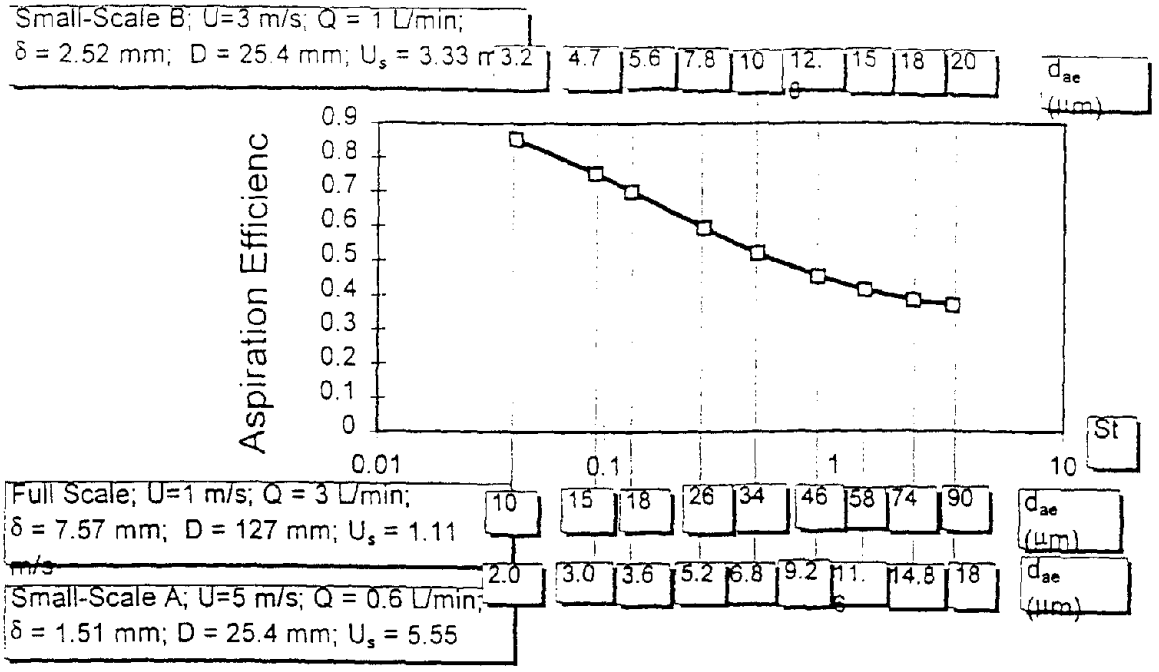

Figure 10.1. Two scaled-down (5:1) sampler designs and experimental conditions dimensionally equivalent to the 3 Lpm IOM static inhalable aerosol sampler (tested at full-scale in a wind tunnel at a windspeed of 1 m/s).

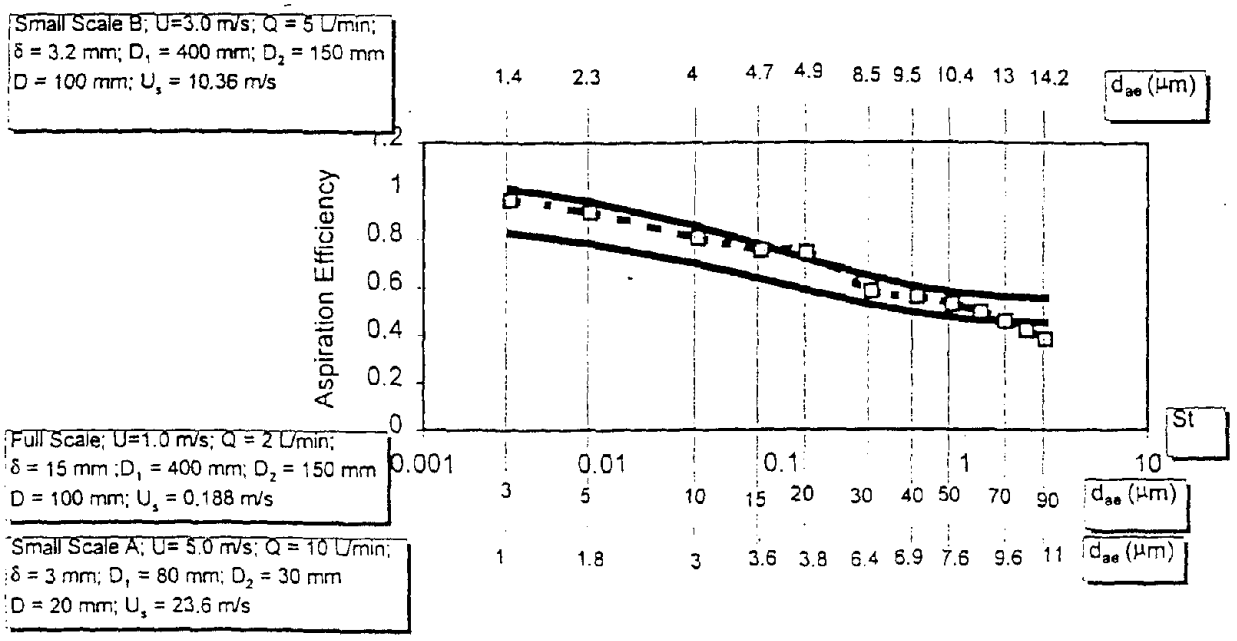

Figure 10.2. Two scaled-down (5:1) sampler designs and experimental conditions dimensionally equivalent to the 2 Lpm IOM personal inhalable aerosol sampler (tested at full-scale in a wind tunnel at a windspeed of 1 m/s)